2013

Classical Antifolates: Synthesis of 5-Substituted, 6-Substituted and 7-Substituted Pyrrolo[2,3-d]Pyrimidines as Targeted Anticancer Therapies

Yiqiang Wang

CLASSICAL ANTIFOLATES: SYNTHESIS OF 5-SUBSTITUTED, 6-SUBSTITUTED AND 7-SUBSTITUTED PYRROLO[2,3-*d*]PYRIMIDINES AS TARGETED ANTICANCER THERAPIES

A Dissertation

Submitted to the Graduate School of Pharmaceutical Sciences

Duquesne University

In partial fulfillment of the requirements for

the degree of Doctor of Philosophy

By

Yiqiang Wang

May 2013

Name: Yiqiang Wang

Dissertation: CLASSICAL ANTIFOLATES: SYNTHESIS OF 5-SUBSTITUTED, 6-SUBSTITUTED AND 7-SUBSTITUTED PYRROLO[2,3-*d*]PYRIMIDINES AS TARGETED ANTICANCER THERAPIES

Degree: Doctor of Philosophy

Date Feb 06, 2013

APPROVED & ACCEPTED

Aleem Gangjee, Ph.D. (Committee Chair)
Professor of Medicinal Chemistry
Mylan School of Pharmacy Distinguished Professor
Graduate School of Pharmaceutical Sciences
Duquesne University, Pittsburgh, Pennsylvania

APPROVED

Marc W. Harrold, Ph.D. (Committee Member)
Professor of Medicinal Chemistry
Graduate School of Pharmaceutical Sciences,
Duquesne University, Pittsburgh, Pennsylvania

APPROVED

Patrick T. Flaherty, Ph.D. (Committee Member)
Associate Professor of Medicinal Chemistry
Graduate School of Pharmaceutical Sciences,
Duquesne University, Pittsburgh, Pennsylvania

APPROVED

David J. Lapinsky, Ph.D. (Committee Member)
Assistant Professor of Medicinal Chemistry
Graduate School of Pharmaceutical Sciences,
Duquesne University, Pittsburgh, Pennsylvania

APPROVED

Lawrence H. Block, Ph.D. (Committee Member)
Professor emeritus of Pharmaceutics
Graduate School of Pharmaceutical Sciences,
Duquesne University, Pittsburgh, Pennsylvania

APPROVED

Douglas J. Bricker, Ph.D.
Dean of Mylan School of Pharmacy, Professor of Pharmacology-Toxicology
Graduate School of Pharmaceutical Sciences,
Duquesne University, Pittsburgh, Pennsylvania

ABSTRACT

CLASSICAL ANTIFOLATES: SYNTHESIS OF 5-SUBSTITUTED, 6-SUBSTITUTED AND 7-SUBSTITUTED PYRROLO[2,3-*d*]PYRIMIDINES AS TARGETED ANTICANCER THERAPIES

By

Yiqiang Wang

May 2013

Dissertation supervised by Professor Aleem Gangjee, Ph.D.

This dissertation comprises an introduction, background and current research progress in the area of classical antifolates as the targeted anticancer therapies.

Mammalian cells have a sophisticated folate uptake and retention system. Transport into the cell is usually facilitated by one or more of three folate transporters: reduced folate carrier (RFC), the membrane folate receptor (FR), and the proton coupled folate transporter (PCFT). The expression of RFC in both normal and tumor cells presents a potential obstacle to antitumor selectivity. Thus, it is of interest to design targeted antifolates that are substrates for transporters other than RFC to restrict drug transport into normal tissues selectivity. This rationale provides the foundation to develop targeted agents that can be selectively transported into tumors by FRs and PCFT over RFC, with potent intracellular targets inhibition.

At the same time, it has been of interest not only to design potent antifolates against specific enzymes such as dihydrofolate reductase (DHFR), thymidylate synthase (TS), glycinamide- ribonucleotide formyl transferase (GARFTase) and amino-imidazole-carboxamide-ribonuleotide formyl transferase (AICARFTase) but also to design and synthesize single agents that have potent multiple inhibitory activity against these enzymes. This strategy is particularly promising in anticancer chemotherapy against the multiple drug resistant cancers. Such a single agent could act at more than one active site and provide "combination chemotherapy" benefits.

In this study, twelve series of classical 5-, 6- and 7-substituted pyrrolo[2,3-*d*]pyrimidines were designed and synthesized. Extensive structure modifications of the pyrrolo[2,3-*d*] pyrimidine scaffold were investigated to determine selective transport *via* FR or/and PCFT and tumor targeted antifolates with GARFTase or multiple folate metabolizing enzyme inhibition.

The design strategies employed include: variation of the side chain substitution position (5-,6- and 7-substituted); variation of the side chain length (n=1-6); isosteric replacement of the 1,4-disubstituted phenyl ring with 1,2- and 1,3- disubstituted phenyl ring and 2,5- disubstituted thiophenyl ring; replacement the *L*-glutamate with variation at the α and γ carboxylic acids.

As a part of this study, a total of one hundred and fifty six new compounds (including new intermediates) were synthesized and separated. Of these, twelve series consisting of forty two classical antifolate final compounds were submitted for biological evaluation. In addition, bulk synthesis of some potent final compounds (**2**, 2.0 g; **161**, 500 mg; **175**, 1.0 g; **166**, 500 mg; **194**, 500 mg) was carried out to facilitate *in vivo* evaluation.

During the synthesis of the target compounds, several synthetic improvements were achieved successfully including:

1. α-Bromo ketones instead of α-chloro ketones were synthesized to react with 2,4-diamino-6-hydroxypyrimidine to selectively afford pyrrolo[2,3-*d*]pyrimidines without side product furo[2,3-*d*]pyrimidines.

2. Instead of using the reported reaction condition to get 72% yield in the hydrogenation of **235**, a 10% Pd/C, 5 h condition was employed to get a complete transformation (100% yield of **236**) without any partial reduction. The troublesome separation of **236** was avoided.

More importantly, a new Heck coupling of the thiophene iodide **301** and allyl alcohols to synthesize aldehydes in one step was discovered. The reaction condition is mild (45 ^{o}C) with a good yield (65%) and the labile ester group of **301** is tolerated at this condition. In addition, the reaction is fast (2 h) and easy to handle (no argon protection needed). Due to its potential use in analog synthesis of clinically used antifolates such as RTX and PMX, this mild conditioned and easy to handle Heck coupling reaction is highly attractive.

During this study, the SAR of folate transporters (RFC, FR and PCFT) and GARFTase inhibitors were extensively explored. The 6-substituted straight chain compound **166** (n=7) was extremely potent against KB tumor cells (IC_{50}=1.3 nM, about 80-fold more potent than clinically used PMX) without any RFC activity. The intracellular enzyme target of **166** was subsequently identified as GARFTase. The 5-substituted phenyl compound **175** (n=4) showed AICARFTase as the primary target with potent KB tumor cell inhibition (IC_{50}=7.9 nM, about 8-fold more potent than PMX) and

also indirectly activated AMPK cell signaling pathway *via* ZMP accumulation which transmits an inhibitory signal to the mTOR complex leading to tumor cell apoptosis. Both of these compounds were selected for animal study to determine the antitumor activity against human tumor xenograft in mice. Due to their potent antitumor activities, these two compounds serve as leads for future structural optimization.

DEDICATION

Dedicated To My Family For Their Love And Support

ACKNOWLEDGEMENT

I would like to thank all of those who contributed to this work. In particular I am most grateful to my supervisor, Professor Dr. Aleem Gangjee, for his guidance and support which made this dissertation possible. I am indebted to him not just for his scientific guidance but also for his encouragement, day after day, financial support and his friendship.

I would like to thank my dissertation committee: Drs. Marc W. Harrold, Patrick T. Flaherty, David J. Lapinsky, Lawrence H. Block and Aleem Gangjee for their advice and support. I wish to thank Dr. Larry H. Matherly at Barbara Ann Karmanos Cancer Institute, Wayne State University School of Medicine and Dr. Roy L. Kisliuk at Tufts University School of Medicine for evaluating all the compounds for enzyme inhibitory activity and antitumor activity. I wish to express my sincere appreciation to Nancy Hosni and Jackie Farrer in the office of pharmacy school for their help and assistance. I would like to give thanks to all my colleagues in the Graduate School of Pharmaceutical Sciences for their help and stay with me at Duquesne University. I would like to thank the Graduate School of Pharmaceutical Sciences for the financial support.

Finally, I would like to express my love and gratitude to my beloved family for their understanding & endless love, through the duration of my studies.

TABLE OF CONTENTS

LIST OF TABLES

Page

LIST OF FIGURES

Page

LIST OF SCHEMES

Page

LIST OF ABBREVIATIONS

AICA	Aminoimidazole-4-carboxamide
AICAR	Aminoimidazole-4-carboxamide ribosyl-5-phosphate
AICARFTase	Aminoimidazole-4-carboxamide ribosyl-5-phosphate Formyl Transferase
AIDS	Acquired immunodeficiency syndrome
ALL	Acute lymphoblastic leukemia
AML	Acute myelogenous leukemia
AMP	Adenosine monophosphate
AMPK	AMP-activated protein kinase
AMT	Aminopterin
ARDS	Acute respiratory distress syndrome
ATIC	5-Amino-4-imidazolecarboxamide ribonucleotide formyltransferase/IMP cyclohydrolase
ATP	Adenosine-5'-triphosphate
CAM	Chorioallantoic membrane
CNS	Central nervous system
DHFR	Dihydrofolate reductase
DMAP	4-Dimethylamino pyridine
DMF	*N*,*N*-dimethyl formamide
DMSO	Dimethyl sulfoxide
DNA	Deoxyribonucleic acid

dATP	2’-Deoxyadenosine-5’-triphosphate
dGTP	2’-Deoxyguanosine-5’-triphosphate
dTDP	2’-Deoxythymidine-5’-diphosphate
dTMP	2’-Deoxythymidine-5’-monophosphate
dTTP	2’-Deoxythymidine-5’-triphosphate
dUMP	2’-Deoxyuridine-5’-monophosphate
dUTP	2’-Deoxyuridine-5’-triphosphate
E. coli	*Escherichia coli*
EDX	10-Ethyl-l0-deaza aminopterin
FA	Folic acid
FGAR	Formyl glycinamide ribonucleotide
FH_2	7,8-Dihydrofolate
FH_4	5,6,7,8-Tetrahydrofolate
FPGH	Folylpolyglutamate hydrolase
FPGS	Folyl poly-γ-glutamate synthetase
FR	Folate receptor
FdUMP	5-Fluoro-2’-deoxyuridine-5’-monophosphate
5-FU	5- Fluorouracil
GAR	Glycinamide ribosyl-5-phosphate
GARFTase	Glycinamide ribonucleotide formyl transferase
GDP	Guanosine diphosphate
GPI	Glycosylphosphatidylinositol
GTP	Guanosine triphosphate

IMP	Inositol monophosphate
L. casei	*Lactobacillus casei*
LMX	Lometrexol
LV	Leucovorin
MAC	*Mycobacterium Avium Complex*
MFS	Major facilitator superfamily
MRP	Multidrug resistance protein
MTHFR	Methylene tetrahydrofolate reductase
MTX	Methotrexate
NADPH	Nicotinamide adenine dinucleotide phosphate
NCI	National cancer institute
NMR	Nuclear magnetic resonance
NRTI	Nucleoside reverse transcriptase inhibitors
NSCLC	Non-small cell lung cancer
PABA	Para-amino benzoic acid
PCFT	Proton coupled folate transporter
PDB	Protein data bank
PDDF	N^{10}-propargyl-5,8-dideazafolate
Pgp	P-glycoprotein
Piv	Pivaloyl (trimethyl acetyl)
PMX	Pemetrexed
PPRP	Phosphoribosylpyrophosphate
PteGlu	Pteroylglutamic Acid

PTX	Piritrexim
Rh	Recombinant human
rl	Rat liver
RNA	Ribonucleic acid
RFC	Reduced folate carriers
RTX	Raltitrexed
SCID	Severe combined immunodeficient
SHMT	Serine hydroxymethyl transferase
T. gondii	*Toxoplasma gondii*
TLC	Thin layer chromatography
TMP	Trimethoprim
TMQ	Trimetrexate
TNP-351	*N*-[4-[3-(2,4-Diamino-7*H*-pyrrolo[2,3-*d*]pyrimidin-5-yl)propyl]benzoyl-L-glutamic acid.
TS	Thymidylate Synthase

I. BIOCHEMICAL REVIEW

Folic acid (Figure 1), a water-soluble vitamin of the B-complex group, was first reported by Mitchell and coworkers[1] in 1941 by isolating this growth factor from spinach leaves and naming it folic acid. The structure of folic acid consists of three moieties: a hetero-bicyclic pteridine, a *p*-aminobenzoic acid (PABA) and a glutamic acid (Figure 1), and thus folic acid is also called pteroylglutamic acid. Its structure probably does not occur in nature as such, but it can be regarded as the parent compound of a group of naturally occurring folates which are designated as the B9 vitamin family.

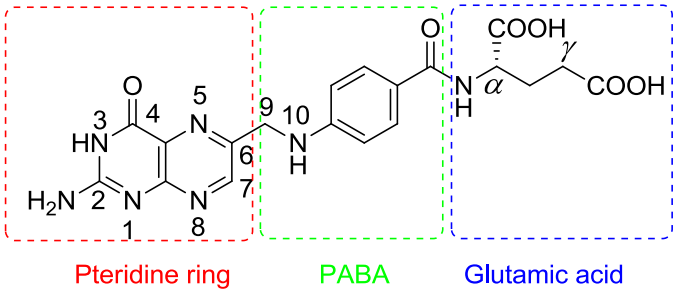

Figure 1 Structure of folic acid illustrating the three principle moieties.

Folic acid in its various cofactor forms plays a crucial role in the biosynthesis of nucleic acid precursors and resultantly in deoxyribonucleic acid (DNA) synthesis and cell replication.[2-4] Compounds that closely resemble FA and inhibit the function of enzymes involved in folate metabolism are termed antifolates. These antifolates represent an important class of antimetabolites and are used as chemotherapeutic agents.[5-9]

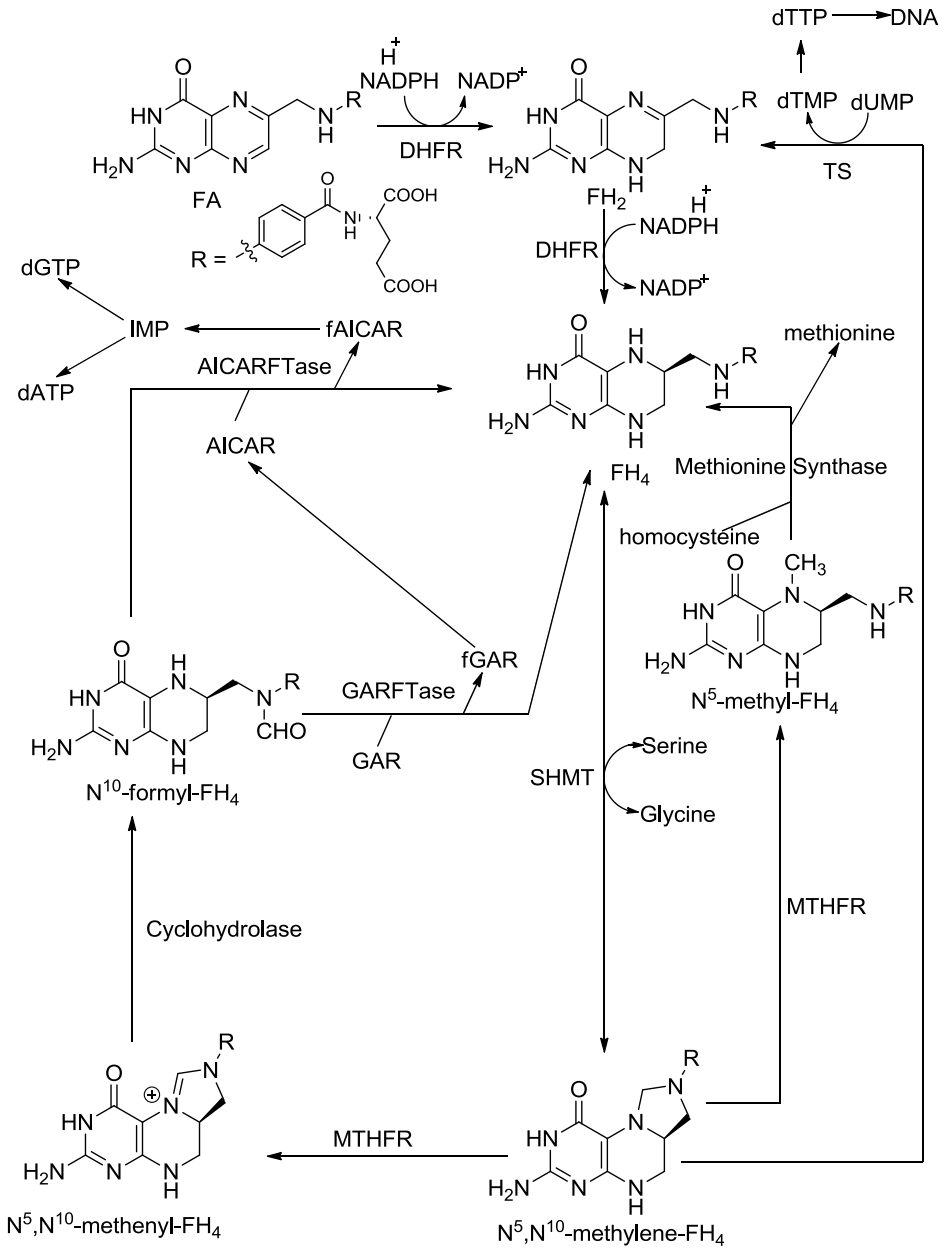

Figure 2 Folates and their roles in the biosynthesis of nucleic acid precursors and amino acids. Note: TS: Thymidylate Synthase; DHFR: Dihydrofolate Reductase; SHMT: Serine Hydroxymethyltransferase; MTHFR: Methylenetetrahydrofolate Reductase; GARFTase: Glycinamide-ribonucleotide Formyl Transferase; AICARFTase: Amino-imidazole-carboxamide-ribonuleotide Formyl Transferase; AICAR: Aminoimidazole-4-carboxamide

ribosyl-5-phosphate; dTMP: 2'-Deoxythymidylate 5'-monophosphate; dUMP: 2'-Deoxyuridylate-5'-monophosphate; dTMP: 2'-Deoxythymidylate 5'-triphosphate; GAR: Glycinamide Ribosyl-5-phosphate; DNA: Deoxyribonucleotide; IMP: Inositol monophosphate.

1. FOLATE METABOLISM

Folic acid exists in several oxidative states, each of which is essential to the role of the cofactor in metabolism. Intracellular reduction of the pyrazine portion of the pteridine ring, catalyzed by a NADPH (nicotinamide adenine dinucleotide phosphate)-specific dihydrofolate reductase (DHFR) leads to the formation of 7,8-dihydrofolate (FH_2) followed by 5,6,7,8-tetrahydrofolate (FH_4) (Figure 2).[10] Folic acid is poorly taken up into mammalian cells by a reduced folate carrier (RFC) system which is ubiquitously expressed and present on the cell surface. The principal mechanism of folic acid (FA) uptake is *via* the proton coupled folate transporter (PCFT) in the intestines.[11-13] Tetrahydrofolate functions as the coenzyme in the utilization of single-carbon units and is the central component of the folate metabolism. The metabolism of amino acids (glycine, serine, methionine, and histidine), nucleic acid synthesis (purine nucleotide and the 5-methyl group of thymine) and formation of formylmethionyl-tRNA are all dependent on FH_4 (Figure 2). FH_4 is capable of carrying single carbon units in various oxidation states including methyl, methylene, and formyl groups. The oxidative levels of these single carbon units correspond to methanol, formaldehyde, and formic acid, respectively. These single carbon units may be attached to the N^5- and/or N^{10}- positions. The biologically

relevant cofactor forms of FA include 5-methyltetrahydrofolate (N^5-CH_3-FH_4), 5,10-methylenetetrahydrofolate (N^5,N^{10}-CH_2-FH_4), 5-formyltetrahydro-folate (N^5-CHO-FH_4), 10-formyltetrahydrofolate (N^{10}-CHO-FH_4), and 5-formiminotetra-hydrofolate (N^5-CH=NH-FH_4) (Figure 2).

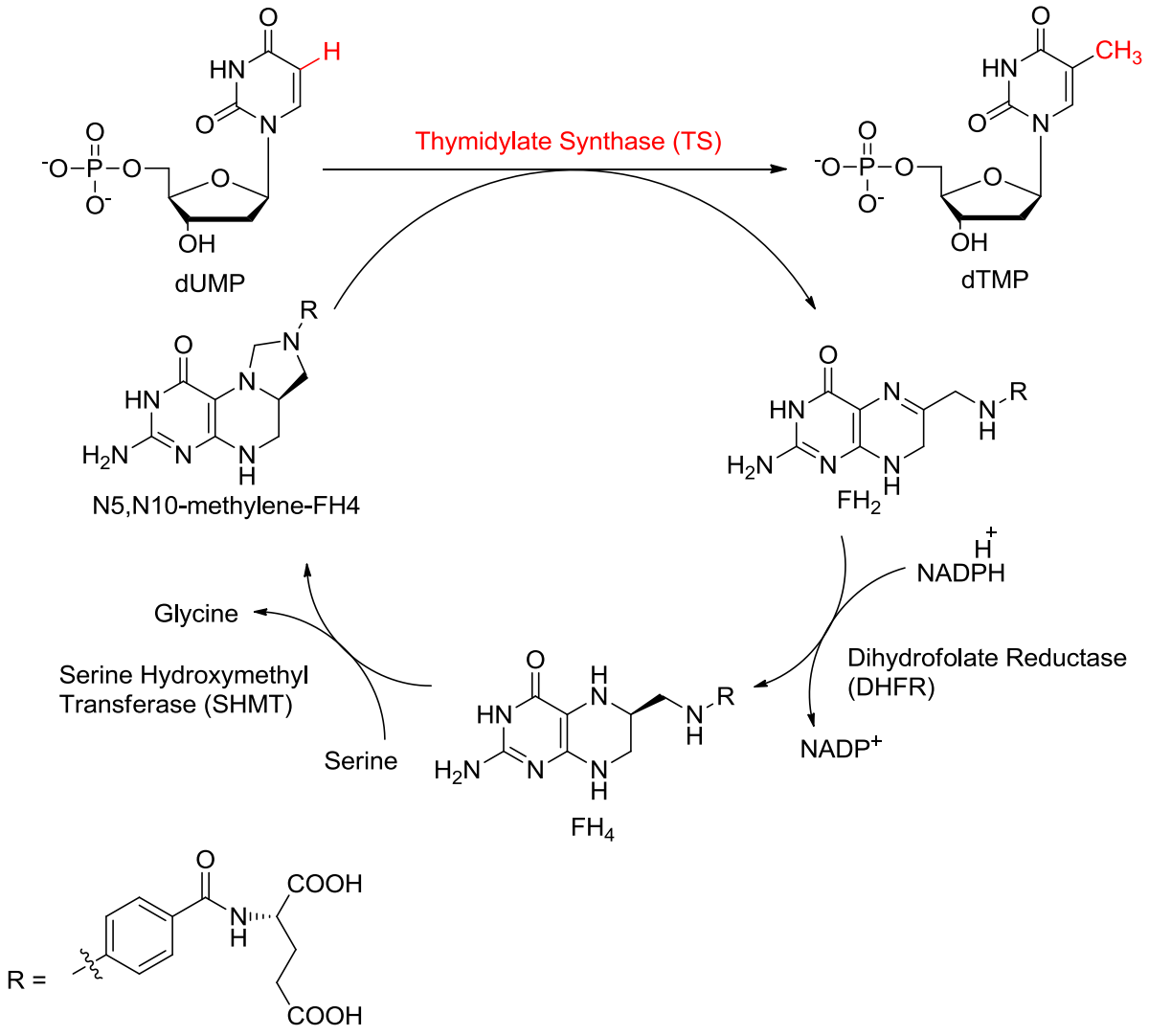

Figure 3 Thymidylate synthase (TS) catalyzed biosynthesis of dTMP from dUMP.

A number of enzymes are involved in folate-dependent reactions by using different derivatives of FH_4 in one-carbon transfer reactions (Figure 2). (i) 5,10-

methylene tetrahydrofolate (N^5,N^{10}-CH_2-FH_4) provides one carbon for the synthesis of thymidylate from deoxyuridylate mediated by thymidylate synthase (TS), an initial step in the synthesis of precursors for DNA. (ii) N^{10}-CHO-FH_4 provides two carbons sequentially for the synthesis of the purine ring in reactions mediated by glycinamide-ribonucleotide formyl transferase (GARFTase) and amino-imidazole-carboxamide-ribonuleotide formyl transferase (AICARFTase). (iii) N^5-CH_3-FH_4 provides one carbon for the vitamin B-12 dependent synthesis of methionine from homocysteine mediated by methionine synthetase, which is followed by the synthesis of *S*-adenosylmethionine.

TS is unique among enzymes that utilize FH_4 cofactor in that N^5,N^{10}-CH_2-FH_4 acts as the source of the methyl group as well as the reductant, by concerted transfer of its methylene moiety and the 6-hydrogen atom in the form of hydride to form the 5-methyl group of dTMP (Figure 3). This represents the sole *de novo* source of dTMP in dividing cells. Hence, inhibition of TS, in the absence of salvage, leads to "thymineless death".[14] "Thymineless death" is observed in mammalian cells when severe deoxythymidine-triphosphate (dTTP) depletion takes place due to 5-fluorouracil (5-FU) or methotrexate (MTX) treatment.[15] The dTTP depleted mammalian cells irreversible lose colony-forming ability and undergo cell death.[14] This phenomenon underlies the mechanism of several antibacterial, antimalarial and anticancer agents, such as Sulfamethoxazole, Trimethoprim, Methotrexate and Fluorouracil.[14, 16-18] The phenomenon was first reported by Barner and Cohen[19, 20] in 1954 that thymine requiring mutants of the *E. coli* bacterium lost viability when grown in a medium lacking thymine but containing other essential nutrients. The phenomenon was commonly attributed to "unbalanced growth" when cells continued fundamental processes of RNA transcription, protein synthesis and metabolism

in the absence of DNA replication.[20] This effect is unusual in that the deprivation of many other nutritional requirements such as amino acids or vitamins has a biostatic, but not lethal effect.[21, 22] Studies on numerous tumor cells have indicated that thymine starvation has both direct and indirect effects. The direct effects include both single- and double-strand DNA breaks.[23] The former may be repaired effectively, but the latter will lead to cell death. Depletion of dTTP in mammalian cells induces apoptosis, although the mechanism underlying this process remains to be elucidated.[24-26] Methotrexate and 5-FU cause a decrease in dTTP levels and a concomitant increase in dUTP, which is incorporated into DNA. This leads to extensive DNA damage as a result of the active process of excision repair at the many uracil-containing sites in DNA, and thus triggers a DNA-damage-induced apoptosis.[15]

During TS catalyzed dTMP biosynthesis, N^5,N^{10}-CH_2-FH_4 is oxidized to FH_2 and is converted back to FH_4 by dihydrofolate reductase (DHFR) which maintains the intracellular reduced folate pool. Thus inhibition of DHFR leads to a partial depletion of the intracellular reduced folate pool and consequently limits cell growth.[27] Both human TS and human DHFR are crucial enzymes for cell growth and both continue to represent attractive chemotherapeutic targets.[28, 29]

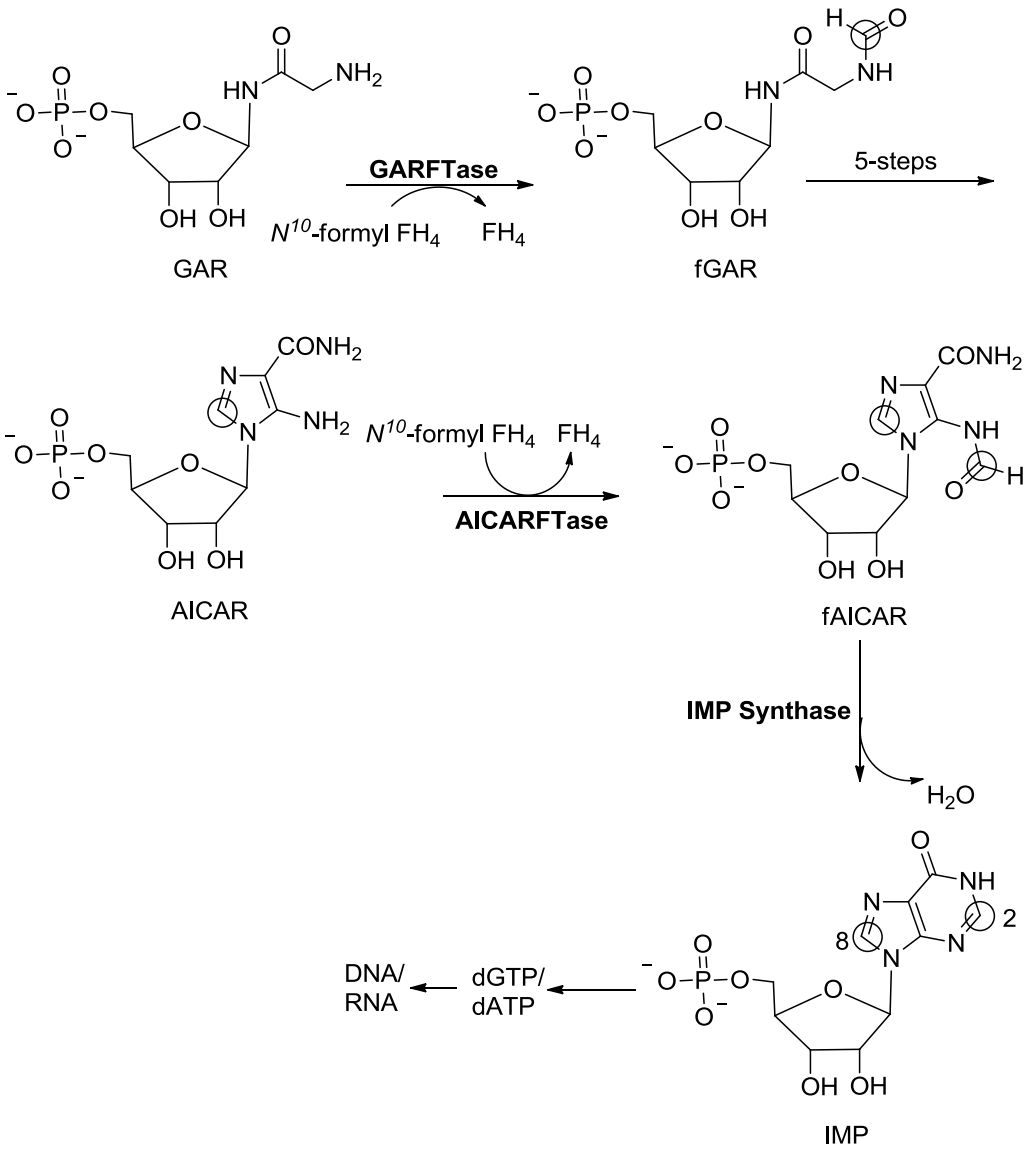

Figure 4 GARFTase and AICARFTase functions in *de novo* synthesis of Purines.[30]

Two other folate related enzymes in the *de novo* biosynthesis of purine nucleotides are β-Glycinamide-ribonucleotide transformylase (GARFTase) and Amino-imidazolecarboxamide ribosyl-5-phosphate formyl transferase (AICARFTase) utilizing the cofactor, N^{10}-CHO-FH_4 to transfer one carbon units (Figure 4).[30] These carbons comprise the C-8 carbon and C-2 carbon of purine nucleotides. GARFTase catalyzes the third in the series of ten reactions required for purine synthesis (Figure 4), the conversion

of glycinamide ribosyl-5-phosphate (GAR) to formyl-glycinamide ribosyl-5-phosphate (fGAR), utilizing N^{10}-formyl-FH_4. GARFTase occurs in mammals as one enzyme in a trifunctional protein, which catalyzes the second and the fifth steps of this pathway in addition to the third step. The fGAR formed is converted further to amino-imidazolecarboxamide ribosyl-5-phosphate (AICAR). AICARFTase is responsible for the catalysis of the last two steps in *de novo* biosynthesis of purine. AICARFTase utilizes N^{10}-CHO-FH_4 cofactor and converts AICAR to formyl-amino-imidazolecarboxamide ribosyl-5-phosphate (fAICAR). fAICAR continues along the purine biosynthetic pathway leading to the formation of inosine-5'-monophosphate (IMP), the precursor of adenosine-5'-triphosphate (ATP) and guanosine-5'-triphosphate (GTP) necessary for ribonucleic acid (RNA) synthesis and of 2'-deoxyadenosine-5'-triphosphate (dATP) and 2'-deoxyguanosine-5'-triphosphate (dGTP) necessary for DNA synthesis.[28]

Mammalian cells have been discovered to have sophisticated folate uptake and retention systems due to the importance of folate in the maintenance of one carbon metabolism.[28, 31] Transport into the cell is usually facilitated by one of three carrier systems: reduced folate carrier (RFC), the membrane folate receptor (FR), and the proton coupled folate transporter (PCFT). The reduced form of FA including N^5-CH_3-FH_4 and N^{10}-CHO-FH_4 are actively taken up into the cell by the RFC system.[32] FR, however, has a higher affinity for the oxidized form of the folate cofactor than the reduced form. PCFT is primarily responsible for FA uptake from the diet via the intestines at relatively low pH in the jejunum.[11-13]

Once transported inside the cell, the cofactors are converted to the poly-γ-

glutamyl species by the enzyme folylpoly-γ-glutamate synthetase (FPGS), which adds glutamic acid residues to the gamma carboxylic acid *via* amide bonds. Usually 4-8 glutamate residues are added to the γ-carboxylic acid group of the cofactor or reduced folate. The polyglutamylated folates usually have higher binding affinity to some folate dependent enzymes (e.g. TS) and have increased intracellular retention time, because of their polyanionic nature.[31, 33, 34]

Folylpolyglutamate hydrolase (FPGH)[35] is an enzyme found in the lysosomes, which catalyzes the hydrolysis of folates polyglutamates back to their monoglutamate form. Through an ATP dependent process, folate monoglutamates can be effluxed from the cell *via* multidrug resistance protein (MRP) including P-glycoprotein (Pgp).[36]

Folate metabolism has been recognized for a long time as an attractive target for cancer chemotherapy because of its crucial role in the biosynthesis of nucleic acid precursors.[37-40] Antimetabolites that interfere with this folate metabolism pathway are known as antifolates and are clinically useful as antimicrobial, antifungal, antiprotozoal, and antitumor agents.[5, 7, 41, 42]

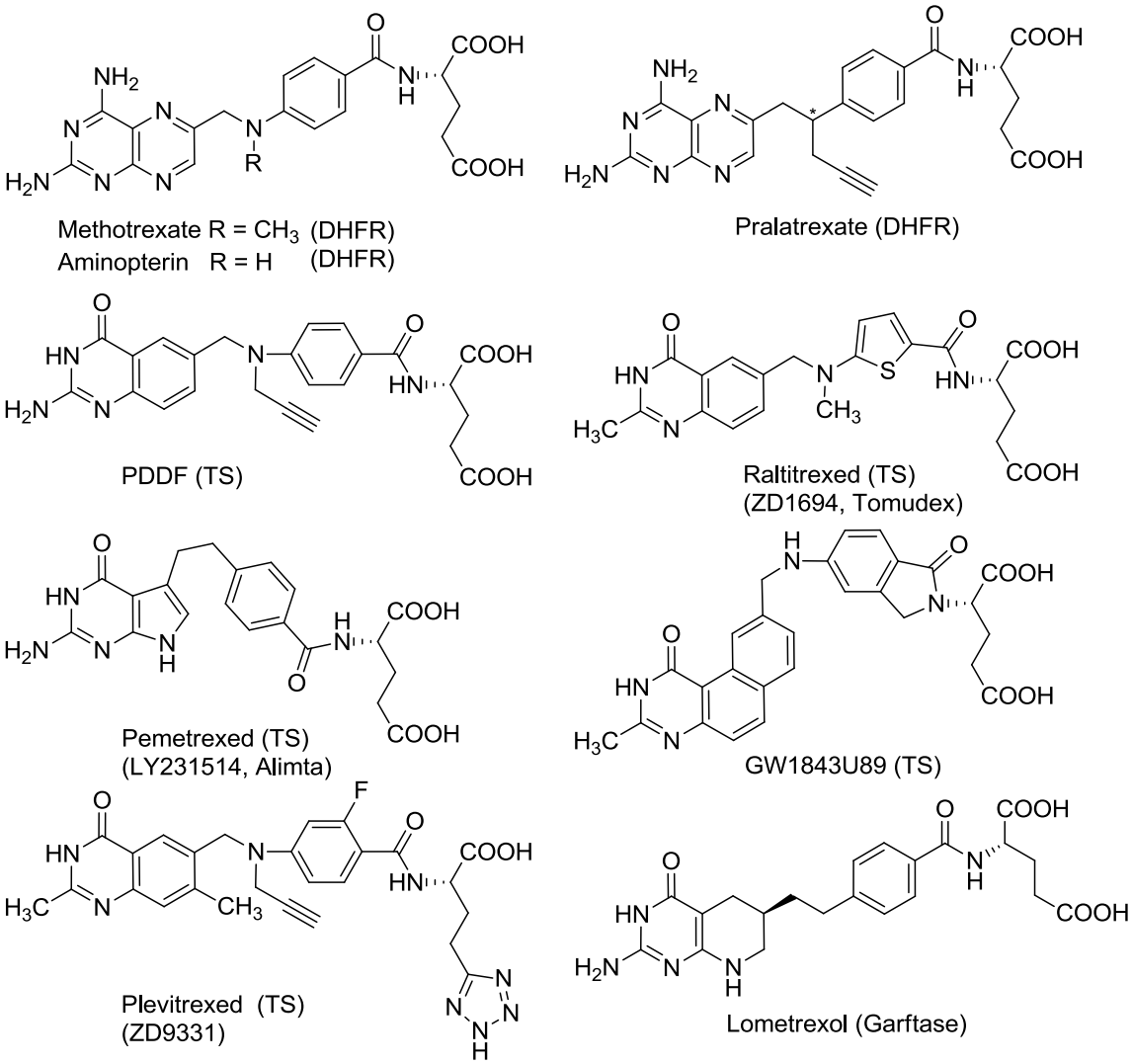

Figure 5 Representatives of classical antifolates and their principal target(s).

Based on their mechanism of transportation and the ability to undergo polyglutamylation, antifolates are classified into two types: classical antifolates and nonclassical antifolate.[43] Classical antifolates contain an intact *L*-glutamate side chain , while nonclassical antifolates contain a lipophilic side chain.[44, 45] As shown in Figure 5, representatives of classical antifolates include methotrexate (MTX), aminopterin (AMT), pralatrexate, N^{10}-propargyl-5,8-dideazafolate (PDDF), raltitrexed (RTX, ZD1694, Tomudex), pemetrexed (PMX, LY231514, Alimta), GW1843, plevitrexed (ZD9331) and

lometrexol (LMX). This group of antifolates closely resembles the structure of endogenous folates and their metabolites. Classical antifolates are actively taken up into cells by folate transporter systems.[32, 33]

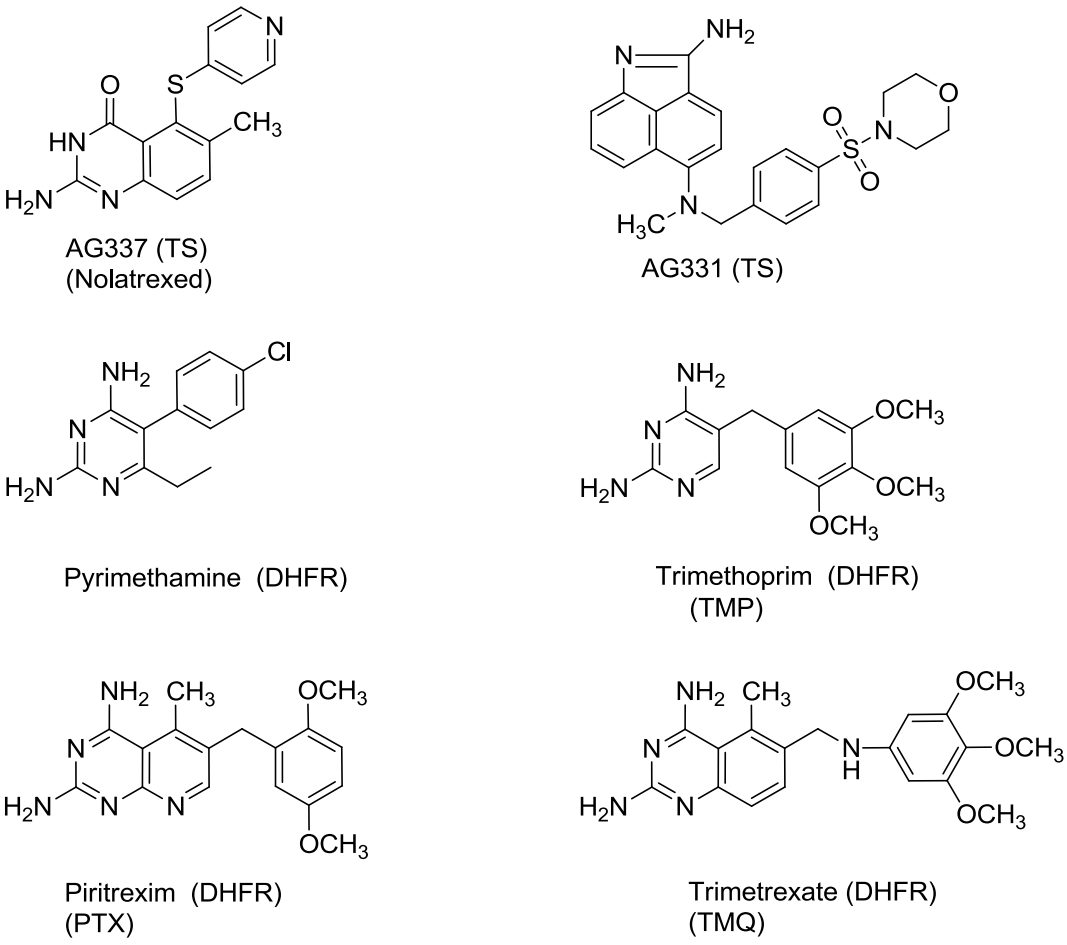

Figure 6 Representatives of nonclassical antifolates and their principal target(s).

The nonclassical antifolates are represented by structures shown in Figure 6: AG337 (nolatrexed, thymitaq), AG331, pyrimethamine, trimethoprim (TMP), piritrexim (PTX) and trimetrexate (TMQ). Nonclassical antifolates are not taken up by the folate active transport systems (RFC, FR and PCFT) and are presumably taken up by passive and/or facilitated diffusion.[32, 33]

2. Membrane transport of folates

Mammalian cells are unable to synthesize folates *de novo*, therefore, internalization of extracellular folates is essential. Natural folates are hydrophilic anionic molecules which show only minimal capacities to cross biological membranes by passive diffusion alone. Accordingly, three major folate uptake systems have been discovered to facilitate absorbtion and membrane translocation of these essential cofactors.[46-48] As mentioned above, the reduced folate carrier (RFC) is the major transport system for folates in mammalian cells and tissues at physiologic pH. Folate receptors (FRs) α and β are glycosylphosphatidylinositol (GPI)-anchored proteins that transport folates by receptor-mediated endocytosis.[49] Finally, the proton-coupled folate transporter (PCFT) functions optimally at acidic pH.[10, 50-52]

2.1. The Reduced Folate Carrier (RFC)

The ubiquitously expressed RFC is the major transport system in mammalian cells and tissues for folates except FA. RFC is also the major transporter of antifolates used for cancer chemotherapy such as MTX, PMX, and RTX (Figure 5), and that the effectiveness of these agents is closely linked to levels and activity of this transport system in both tumors and normal tissues.[53, 54]

2.1.1. Structure of RFC

Goldman and coworkers[55] first reported the functional properties of RFC for murine leukemia cells in 1968. RFC (SLC19A1), a member of the major facilitator superfamily (MFS) of transporters, is characterized by its anion exchange property. Human RFC (hRFC) is comprised of 591 amino acids and is 64-66% conservation with rodent RFCs. RFC is an integral membrane protein characterized by 12 transmembrane domains (TMDs) and cytoplasmic-oriented amino and carboxyl termini.[56-59] hRFC is *N*-glycosylated at an *N*-glycosylation consensus site in the first extracellular loop (EL) connecting TMD1 and TMD2 (Asn58).[60] A large loop domain that connects TMD6 and TMD7 is poorly conserved between species and can be replaced by a nonhomologous segment from the SLC19A2 carrier.[61] When separate TMD1-TMD6 and TMD7-TMD12 RFC half-molecules are coexpressed in human RFC-null cells, they are targeted to the cell plasma membrane surface and restore RFC transport activity.

2.1.2. RFC distribution

RFC is the major folate cofactor transporter in mammals and transports folates into cells of peripheral tissues from blood.[62] In human tissues, the highest hRFC transcript levels were recorded in placenta and liver, with significant hRFC levels in kidney, leukocytes, lung, bone marrow, intestine, and portions of the central nervous system (CNS) and brain.[63] RFC is essential for tissue development since targeting both RFC alleles is embryonic lethal.[64] In at least some tissues (e.g., small intestine), mouse RFC is responsive to dietary folates supply such that increased RFC transcripts and proteins were

detected under conditions of dietary folate deficiency.[65] However, the significance of this result in intestine is unclear since RFC is unlikely to be active at the acid pH of the gut and PCFT is the major intestinal transporter for uptake of dietary folates.

2.1.3. Transport mechanism of RFC

RFC is a secondary active anionic exchanger that transports reduced folates *via* counter-transport with organic anions.[4] RFC is the major transport system for reduced folates in mammalian cells and tissues. Its physiologic substrate is 5-methyl THF, the major circulating folate form.[4] As an integral transmembrane protein, RFC has a high affinity (~50-100-fold) for reduced folates (Ki ~1-5 μM) and a low affinity for FA (Ki ~ 200 μM). Transport by RFC is characterized by a neutral pH optimum and significantly decreased transport activity below pH 7.[4, 48, 50]

Only small transmembrane chemical gradients were generated by RFC. However, folates are negatively charged by preserve of the two glutamate carboxyl groups which are ionized at physiological pH. When considered within the context of the membrane potential, RFC actually produces a substantial electrochemical potential difference for folates across cell membranes.[55] RFC function is not directly linked to ATP hydrolysis and it is neither Na^+ nor H^+ dependent, which is unique.[66, 67] Instead, RFC-mediated transport is highly sensitive to the transmembrane anion gradient, in particular, the organic phosphate gradient. [66, 67] Organic phosphates are highly concentrated in cells where they are synthesized by ATP-dependent reactions and are largely retained. Their resulting asymmetrical distribution across cell membranes is the driving force for RFC-mediated uphill transport of folates into cells.[67]

2.1.4. RFC in antifolate chemotherapy

Classical antifolates such as MTX, RTX, and PMX (Figure 5) are all actively transported into mammalian cells by RFC as the major transporter.[54, 68] Membrane transport of antifolates such as MTX is critical to antitumor activity since this provides sufficient intracellular drug to sustain maximal inhibition of targeted enzymes (e.g. DHFR and TS) and for synthesis of polyglutamate derivatives required for high affinity binding to some intracellular enzymes and for sustained drug effects as plasma antifolate levels decline. However, the loss of active transport of MTX in drug resistance tumors has been reported as early as 1962 in MTX resistant L5178 murine leukemia cells.[69] Since then, impaired transport has emerged as one of the dominant modes of tumor resistance to classical antifolate inhibitors such as MTX.[70, 71]

Impaired transport (RFC) that results in a loss of sensitivity to standard doses of antifolate should be circumvented to some extent by increasing extracellular concentrations of drug. The increase forces the drug into tumor cells expressing mutated or low levels of RFC, and involves alternate uptake routes or passive diffusion, to a sufficient extent to inhibit intracellular enzymes and/or to support polyglutamate synthesis. However, the elevated extracellular antifolate concentration always results in severe toxicity due to the lack of selectivity of uptake into the tumor cells compared normal cells.

2.2. The folate receptors (FRs)

The FRs are a family of proteins with high affinity folate binding and represent

another mode of folate uptake into mammalian cells. They bind folic acid, reduced folates, many antifolates and folate conjugates with high (low nanomolar) affinities.

2.2.1. Structure of FRs

Human FRs are encoded by three distinct genes, designated α, β and γ localized to chromosome 11q13.3-q13.5.[72] FRs α, β and γ are homologous proteins (68-79% identical amino acid sequences) and contain from 229 to 236 amino acids with two (β, γ) or three (α) *N*-glycosylation sites.[73] Compared to RFC, FRα and β are cell surface glycosyl phosphatidylinositol (GPI)-anchored glycoproteins, while FRγ lacks a signal for GPI anchor attachment and is a secretory protein of unknown function.[49]

2.2.2. FRs distribution

FRα is predominantly expressed on the apical (luminal) surface of polarized mammalian epithelial cells where it is not in contact with the circulating folate.[74] Among normal tissues, FRα is widely expressed at the brush-border membrane of the choroid plexus, retinal pigment epithelium, proximal tubules in kidney, fallopian tubes, uterus and placenta.[49] The unusual polarized expression of FRα appears to protect normal tissues from FR-targeted cytotoxic agents in the circulation.[75] FRβ is expressed in placenta, spleen, thymus and in $CD34^+$ monocytes and hematopoeitic cells.[76-79] In normal bone marrow and peripheral blood cells, expression of FRβ is restricted to the

myelomonocytic lineage (e.g. mature neutrophils) and was reported to be nonfunctional.[80]

FRα has been reported to be overexpress in malignant tissues, such as non-mucinous adenocarcinomas of ovary, uterus and cervix, and ependymal brain tumors.[49] FRα levels positively correlate with tumor stages and grades.[81] FRβ malignant expression has been reported to involve a substantial fraction of chronic myelogenous leukemia and acute myelogenous leukemia (AML) cells, but not Acute Lymphoblastic Leukemia (ALL).[80, 82] Both FRα and FRβ in malignant tissues seem to be functional, prompting the use of folic acid and pteroyl moieties for tumor targeting of toxins, liposomes, imaging and cytotoxic agents. [75, 82, 83]

2.2.3. Transport mechanism of FRs

Membrane-bound FRs mediate folate internalisation *via* a non-classical receptor-mediated endocytosis.[84-87] This process is initiated when a folate molecule binds to a folate receptor on the cell surface, followed by invagination of the plasma membrane at that site and the formation of a vesicle (endosome) that migrates along microtubules in the cytoplasm to the perinuclear endosomal compartment where it is acidified to a pH of 6.0-6.5. The decrease in pH results in dissociation of the folate from the folate receptor complex.[88] Folate ligand is then exported into the cytoplasm by a process requiring a transendosomal pH gradient.[86, 87, 89, 90]

FRs offer a potential means of selective tumor targeting, given their restricted pattern of tissue expression and function as discussed above. Importantly, FR*α* is reported to be overexpressed in a number of carcinomas including up to 90% of ovarian cancers.[81,

[91] FRα in normal tissues (unlike tumors) is reported to be inaccessible to the circulation, which ensured the targeting safety without toxicity to normal tissues. FRβ is expressed in a wide range of myeloid leukemia cells, while FRβ in normal hematopoetic cells differs from that in leukemia cells in its inability to bind folate ligand.[80]

2.3. The proton-coupled folate transporter (PCFT)

PCFT, a new folate carrier (SLC46A1) was discovered in 2006.[10] Two other members of this family (SLC46A2 and SLC46A3) were also reported recently.[51, 52]

PCFT as a high-affinity folate transporter is a proton-folate symporter that functions optimally at acidic pH by coupling the flow of protons down an electrochemical concentration gradient to the uptake of folates into cells.[10, 50-52] Like RFC, PCFT is major facilitator superfamily (MFS) protein. However, human PCFT (hPCFT) shares only ~14% amino acid identity with hRFC.[48, 50] Although PCFT can transport heme, its primary role appears to be intestinal absorption of dietary folates and plays a major role in *in vivo* folate homeostasis.[92, 93]

2.3.1. Structure of PCFT

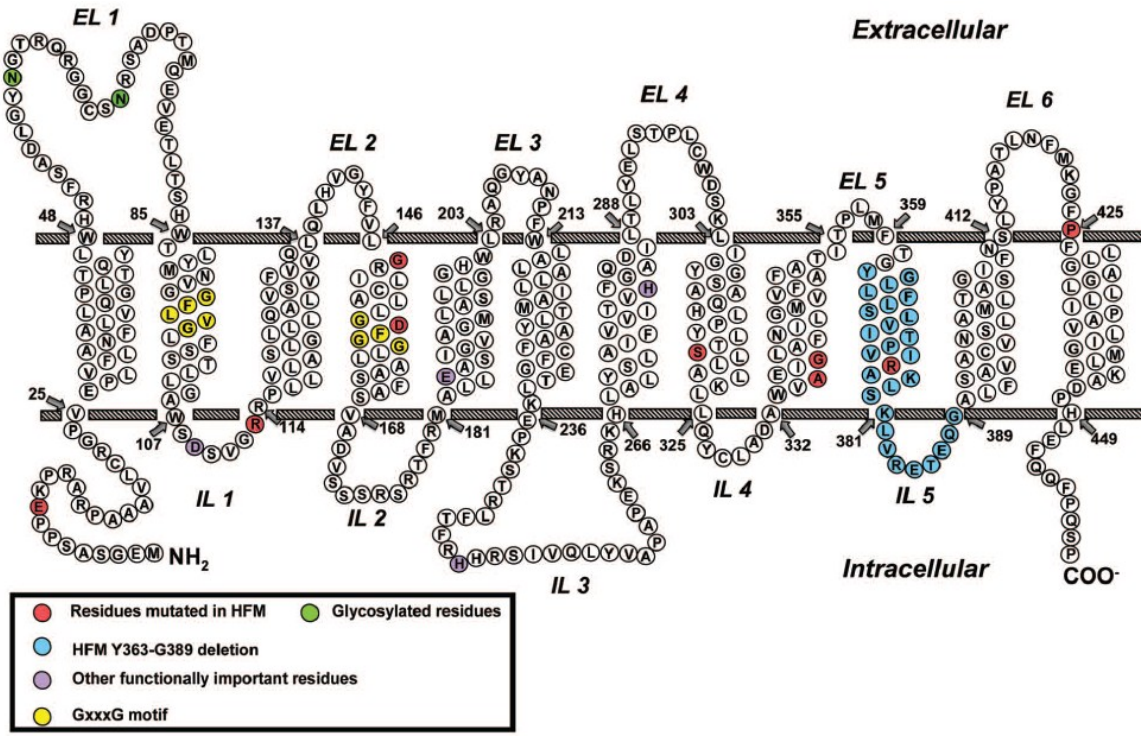

Figure 7 Human PCFT structure.[56]

The gene that encodes human PCFT (SLC46A1) is located on chromosome 17q11.2. and consists of five exons. hPCFT is comprised of 459 amino acids with a molecular mass of 49.8 kDa. It is predicted to include 12 TMDs with N- and C-termini oriented to the cytoplasm (Figure 7). This structure has been validated by immunofluorescence analysis of hemagglutin (HA)-tagged hPCFT molecules.[94, 95] The loop domain between the first and second TMDs must be extracellular because the two putative *N*-glycosylation consensus sites in this region are glycosylated. *N*-glycosylation does not appear to be required for either PCFT trafficking or function.[94]

2.3.2. PCFT expression patterns in human tissue

PCFT is expressed in many normal tissues including small intestine, colon, liver, kidney, placenta, retina and brain. Within the intestine and colon, high levels of PCFT are expressed in apical brush-border membranes in the proximal jejunum and duodenum. However, PCFT levels decrease sharply in other segments of the intestine and colon.[10] PCFT is also found in the choroid plexus.[96]

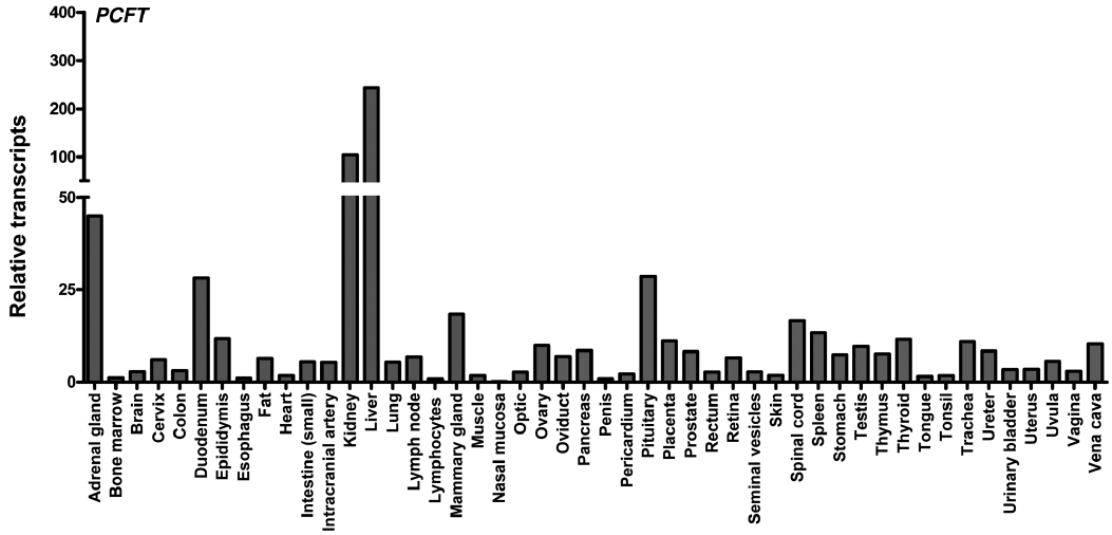

Figure 8 PCFT transcript expression in human normal tissues.[56]

In normal human tissues, elevated hPCFT levels were measured in kidney, liver, placenta, and spleen, with modest levels in most tissues and undetectable levels in bone marrow and colon (Figure 8).[56] For a number of human tissues, hPCFT proteins were detected by immunohistochemistry with hPCFT-specific antibody. These results substantiate and demonstrate that while hPCFT is expressed in normal human tissues, its levels are more limited than for hRFC.[56] While PCFT in the upper gastrointestinal tract is involved in absorption of dietary folates, the physiologic role of PCFT in tissues not normally associated with low pH microenvironments is not clear yet. PCFT may still

conceivably contribute to folate internalization in such tissues by virtue of localized acidification or at sufficiently elevated levels to transport 5-methyl THF and related folates.[48] However, at comparatively neutral pHs characterizing most tissues, RFC is much more efficient at delivering reduced folates than PCFT.[97]

2.3.3. Transport mechanism of PCFT

Folate transport mediated by human, mouse and rat PCFTs is electrogenic indicating there is a net translocation of positive charges as each folate molecule is transported.[51, 98-100] PCFT functions as a folate-proton symporter: the downhill flow of protons *via* PCFT is coupled with the uphill flow of folates into cells. A transvesicular pH gradient results in increased unidirectional folate transport and substantial transmembrane folate concentration gradients from the low-pH to the high-pH compartment, which is consistent with a proton-coupled process.[101] A distinguishing characteristic of PCFT involves its acidic pH optimum: for PCFT, transport is maximal at pH 5-5.5. As the pH increases above pH 5.5, transport decreases dramatically; above pH 7, activity is not detectable.[48, 50]

This leads to an important cancer chemotherapy hypothesis that selective transport *via* PCFT could afford targeted therapy access solid tumors. The internal pH of solid tumors is often acidic,[102, 103] which favors PCFT transport. Actually, PCFT was identified in 29 of 32 solid human tumor cell lines[104] and high levels of human PCFT (hPCFT) transcripts were reported in a broad range of human tumors. Whereas the role of hPCFT in antifolate activity and tumor selectivity is still under investigation, transport of classic antifolates by PCFT has been described previously.[97]

2.3.4. FRs and PCFT specific anticancer chemotherapy

The expression of RFC in both normal and tumor cells presents a potential obstacle to antitumor selectivity. Further, loss of RFC is frequently associated with antifolate resistance. Thus, it is of interest to design targeted antifolates that are substrates for transporters other than RFC with limited expression and/or transport into normal tissues compared with tumors. This rationale provided the impetus to develop targeted agents that are selectively transported into tumors by FRs and PCFT over RFC, with potent intracellular targets inhibition.[56]

a. Folate-conjugated cytotoxins

Folate-conjugated cytotoxins, liposomes, radionuclides, or cytotoxic antifolates have been used to target FRs.[105-108] Unfortunately, for most folate-based anticancer agents such as classical antifolates (including MTX, RTX and PMX), tumor selectivity is lost, since substrates are shared between FRs and the ubiquitously expressed RFC. One strategy for selectively tumor cell targeting *via* FRs involves prodrug conjugates in which folate or pteroate is covalently linked to cytotoxins such as mitomycin C[18] that, upon internalization, are selectively cleaved to release cytotoxic drug. While these drug conjugates are not likely to be RFC substrates, the success of this tumor targeting approach could be significantly compromised by inefficient cleavage and release of the cytotoxic moiety, resulting in decreased chemotherapeutic activity. Alternatively, premature cleavage of the drug conjugates (prior to tumor internalization) could decrease selectivity and increase toxicity to normal proliferative tissues. Additionally, use of folic acid conjugates could ultimately release free folic acid within the tumor which could

function as a nutrient for the tumor. However, if a FR targeted ligand were itself cytotoxic without RFC activity, selective tumor targeting would ensue.[109]

b. FRα-targeted TS inhibitor BGC638 and BGC945

Jackman and colleagues[110, 111] introduced a new generation of TS-targeted therapeutics to include the FRα-targeted agents BGC638 and BGC945, both cyclopenta[*g*]quinazoline analogs, neither of which are RFC or FPGS substrates. BGC945 demonstrated superior *in vitro* efficacy over BGC638 with FRα-expressing tumors. BGC945 was tested *in vivo* in mice with human KB tumor xenografts and treated with 5-[125I]-iodo-2'-deoxyuridine. [110, 111] It was established that BGC945 was a selective TS inhibitor toward FRα-expressing tumors. BGC945 was licensed by Onyx Pharmaceuticals with the name ONX 0801 and in 2009, a phase I clinical trial was initiated in the UK. No further information on these compounds is currently available.

c. FRα- and PCFT-targeted Garftase inhibitors

Gangjee and coworkers[109, 112, 113] recently reported novel 6-substituted classical pyrrolo[2,3-*d*]pyrimidine and thieno[2,3-*d*]pyrimidine as cytotoxic antifolates with varying lengths of the carbon bridge region (Table 1 shows only the three- and four-carbon bridge analogs), that are characterized by selective FR and/or PCFT transport over RFC transport.

Pyrrolo[2,3-*d*]pyrimidines and thieno[2,3-*d*]pyrimidines as FR and/or PCFT specific anticancer agents (Table 1)

Structure	Compound	Biological Activity (IC_{50})		Ref.
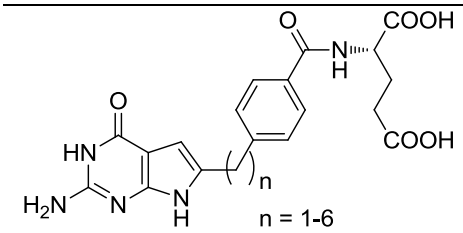	**1** n = 3	hGARFTase	2.44 μM	[101]
		KB	1.7 nM	
		IGROV1	2.2 nM	
	2 n = 4	hGARFTase	0.15 μM	
		KB	1.9 nM	
		IGROV1	3.6 nM	
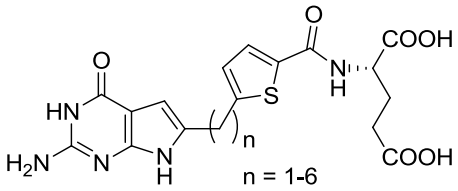	**3** n = 4	hGARFTase	0.06 μM	[105]
		KB	0.55 nM	
		IGROV1	0.97 nM	
	4 n = 5	hGARFTase	3.31 μM	
		KB	3.17 nM	
		IGROV1	176 nM	
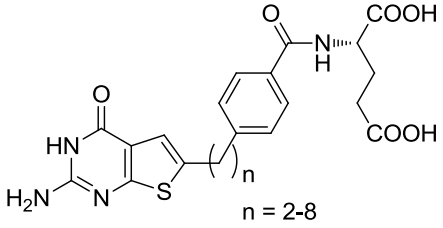	**5** n = 3	hGARFTase	8.52 μM	[104]
		KB	23 nM	
		IGROV1	4.7 nM	
	6 n = 4	hGARFTase	5.51 μM	
		KB	4.9 nM	
		IGROV1	5.9 nM	

1. SAR of 2-amino-4-oxo-6-substituted-pyrrolo[2,3-*d*]pyrimidines and thieno[2,3-*d*]pyrimidine with different side chain aromatic rings in whole cell assay as GARFTase inhibitors with selectivity for FRs and/or PCFT over RFC.[101,104,105]

For all these series, the three- and four-carbon bridge analogs were discovered the most active toward FR and PCFT-expressing human tumors (KB and IGROV1) and the cytotoxicity was primarily due to potent inhibition of GARFTase, although for the thieno[2,3-*d*]pyrimidine antifolates, a secondary target, most likely AICARFTase, was also implied at higher concentration.[109, 112-114]

The biological results for these analogs establish the remarkable potency against tumor cell proliferation, resulting from FR- and/or PCFT-mediated cellular uptake, and inhibition of GARFTase. Significant *in vivo* antitumor activity was recorded for the thieno[2,3-*d*]pyrimidine compound **6** with severe combined immunodeficient (SCID) mice bearing both early and more importantly advanced stage KB tumors.

2. SAR of 2-amino-4-oxo-6-substituted-pyrrolo[2,3-d]pyrimidines with different side chain aromatic rings in whole cell assay as GARFTase inhibitors with selectivity for FRs and/or PCFT over RFC.[115] (Figure 9)

None of the isomers (**2-3** and **7-10**) are substrates for RFC. For FRα, replacement of the side chain phenyl (**2**, IC_{50} of 6.3 nM for FRα-expressing RT16 cells) with a thiophene (**3**, IC_{50} of 1.8 nM for FRα-expressing RT16 cells) or furan ring (**7**, IC_{50} of 0.16 nM for FRα-expressing RT16 cells) favors binding and transport by FRα.

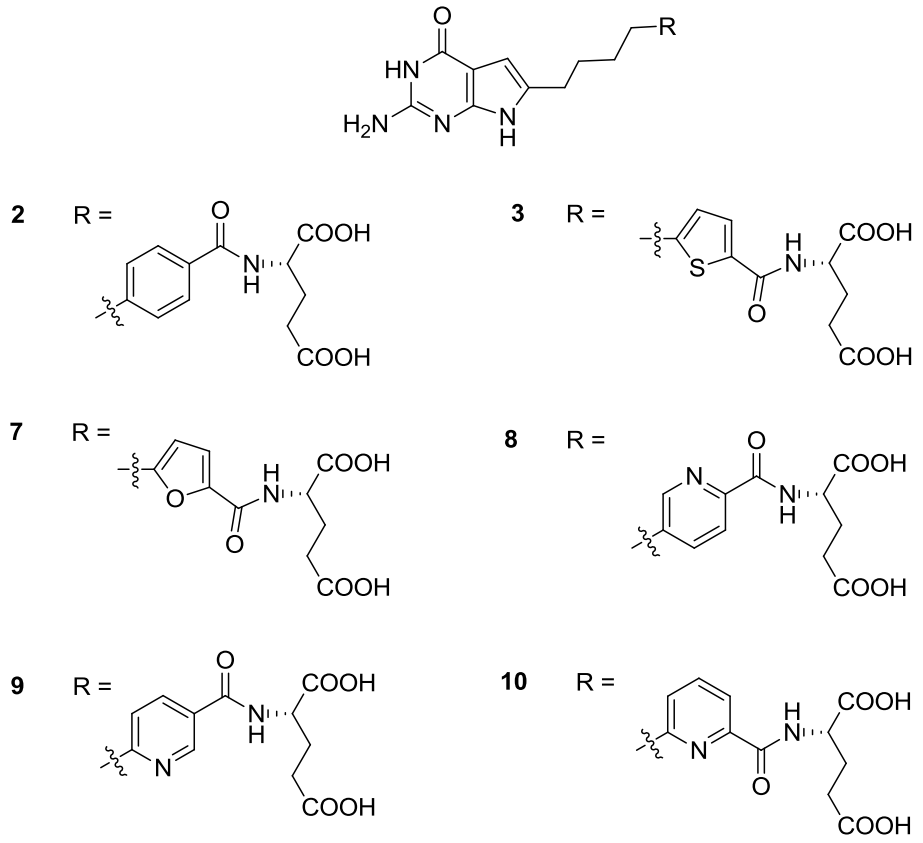

Figure 9 Structures of 2-amino-4-oxo-6-substituted-pyrrolo[2,3-d]pyrimidines with different side chain aromatic rings.[115]

The relative position of the carbon bridge and *L*-glutamate is important for the pyridine side chain (**8**, **9** and **10**, IC_{50} of 8.5 nM, 1.27 nM and 215 nM for FRα-expressing RT16 cells, respectively). For FRβ, replacement of the side chain phenyl (**2**, IC_{50} of 10 nM for FRβ-expressing D4 cells) with a thiophene (**3**, IC_{50} of 0.57 nM for FRβ-expressing D4 cells) or furan ring (**7**, IC_{50} of 0.92 nM for FRβ-expressing D4 cells) favors binding and transport by FRβ as well. For PCFT, replacement of the side chain phenyl (**2**, IC_{50} of 213 nM for hPCFT-expressing R2/hPCFT4 cells) with a thiophene (**3**, IC_{50} of 43.4 nM for hPCFT-expressing R2/hPCFT4 cells) favors binding and transport by PCFT, whereas, a furan side chain (**7**, IC_{50} of 439 nM for hPCFT-expressing R2/hPCFT4

cells) decreases the binding and transport by PCFT. The relative position of the carbon bridge and L-glutamate is also important for the pyridine side chain (**9**, IC_{50} of 66.8 nM for hPCFT-expressing R2/hPCFT4 cells; **8** and **10** are not transported by PCFT), hence, the position of the pyridine nitrogen is important in the regioisomers.

3. SAR of 2-amino-4-oxo-6-substituted-pyrrolo[2,3-*d*]pyrimidines with a thienoyl side chain in whole cell assay as GARFTase inhibitors with selectivity for FRs and/or PCFT over RFC.[116] (Figure 10)

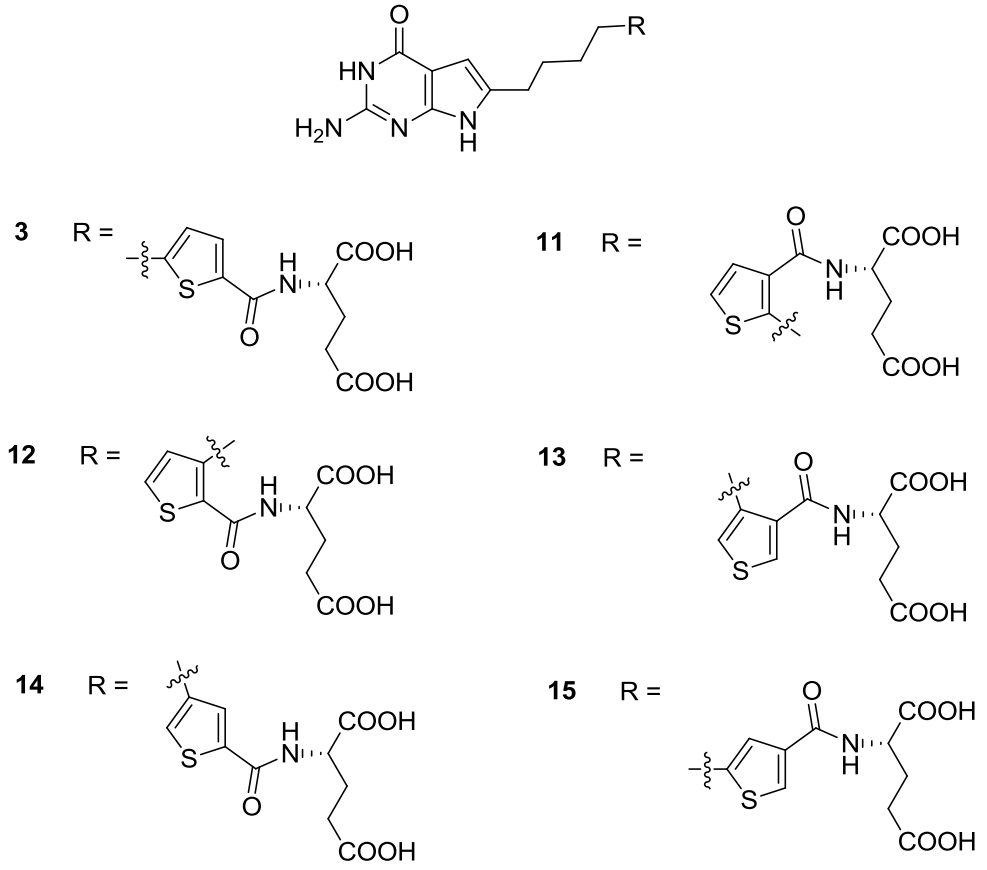

Figure 10 Structures of 2-amino-4-oxo-6-substituted-pyrrolo[2,3-*d*]pyrimidines with a thienoyl side chain.[116]

None of the regioisomers (**11-15**) are substrates for RFC. Analogs with a 1,3-disubstituted relationship (**14** and **15**) of the 4-carbon bridge and the *L*-glutamate demonstrate better activity toward KB tumor cells (IC_{50} of 0.14 nM and 0.13 nM, respectively), which is about 2-fold more potent than **3**. Analogs with a 1,2-disubstituted relationship (**11**, **12** and **13**) of the 4-carbon bridge and the *L*-glutamate show substantially decreased yet moderate activity toward KB (IC_{50} of 171 nM, 267 nM and 25nM, respectively). Compounds **14** and **15** also showed a significantly high level of FRα and PCFT activity (IC_{50} of 2.53 nM and 2.56 nM for FRα-expressing RT16 cells; IC_{50} of 35 nM and 64 nM for hPCFT-expressing R2/hPCFT4 cells), which is equipotent to **3** (IC_{50} of 2 nM for FRα-expressing RT16 cells; IC_{50} of 43.4 nM for hPCFT-expressing R2/hPCFT4 cells). In contrast, compounds **11** and **12** are inactive toward FRα-expressing RT16 cells and hPCFT-expressing R2/hPCFT4 cells. Compound **13**, however, shows weak inhibitory activity of FRα (IC_{50} of 147 nM for FRα-expressing RT16 cells). Hence, for both FRα and PCFT transport, 1,3-disubstituted relationship between the carbon bridge domain and *L*-glutamate moiety is important to maintain binding and transport of this series.

Although the 6-substituted pyrrolo[2,3-*d*]pyrimidine antifolates exhibit near exclusive selectivity for FR and hPCFT over hRFC, it is important to better identify structure-activity relationships for substrate binding and transport for each of these carriers. Indeed, while it has been possible to identify cytotoxic folate analogs with selective membrane transport by FRs over RFC, to date no compounds have been identified with hPCFT transport selectivity without substantial FR uptake. Furthermore, it

is not yet certain whether it might be beneficial to develop exclusive hPCFT-selective substrates without FR transport, as long as hRFC transport is limited.[56]

3. Glycinamide-ribonucleotide transformylase (GARFTase)

GARFTase (EC 2.1.2.2) was first discovered and partially characterized from pigeon liver by pioneer investigators Warren and Buchanan.[117] GARFTase catalyzes the transfer of the formyl group from N^{10}-CHO-FH_4 to the primary, side-chain amino group of glycinamide ribonucleotide (GAR) to yield formylglycinamide ribonucleotide (FGAR) and tetrahydrofolate (Figure 4), ultimately resulting in the incorporation of C-8 into inosinic acid (IMP) as summarized above in the folate metabolism section. It is the third step and the first of two folate-dependent formyl transfers in the *de novo* purine biosynthetic pathway. The critical role that purine nucleotides play as precursors to RNA and DNA led to that inhibition of *de novo* purine biosynthesis might be a viable approach for cancer chemotherapy.[5, 118] The validation of this hypothesis was demonstrated when 5,10-dideazatetrahydrofolate (DDATHF), a potent antitumor agent, was determined to be the inhibition of GARFTase and consequently of *de novo* purine biosynthesis.[119] GARFTase continues to be of interest because of its function in catalyzing the formyl transfer,[120, 121] its role in the synthesis of DNA precursor purines,[122] its key mechanistic features of the reaction,[123-126] and as an important target for chemotherapeutic drug design.[127-137]

3.1. Structure of GARFTase

hGARFTase is located at the C-terminus of a trifunctional enzyme with a molecular mass of more than 110 kDa, which is also responsible for catalyzing the second (glycinamide ribonucleotide synthetase) and fifth (aminoimidazole ribonucleotide synthetase) reactions of *de novo* purine biosynthesis.[138] The crystal structure of hGARFTase has been reported at pH 4.2 (1.7 Å), at pH 8.5 (2 Å), at pH 8.5 in the binary complex with the substrate *β*-GAR (2.2 Å)[126] and at pH 7 in a binary complex with the co-substrate analog inhibitor 10-trifluoroacetyl-5,10-dideaza-acyclic-5,6,7,8-tetrahydrofolic acid (10-CF_3CO-DDACTHF) (2 Å)[139] and a series of other folate inhibitors.[133]

3.2. Catalytic Mechanism of GARFTase

Kinetic studies of the *E. coli* GARFTase[120] and of the human GARFTase[140] and murine GARFTase[141] domains suggest a sequential mechanism in which the formyl group is transferred by a direct nucleophilic attack of the GAR amino group on the formyl carbon of the co-substrate, leading to the formation of a tetrahedral intermediate. Formation of this intermediate and its transformation to product require proton transfers. It has been proposed that a " fixed" water molecule, rather than the invariant amino acids in the active site, mediates the proton transfer between substrate and cofactor, but this has not been verified by experiments.

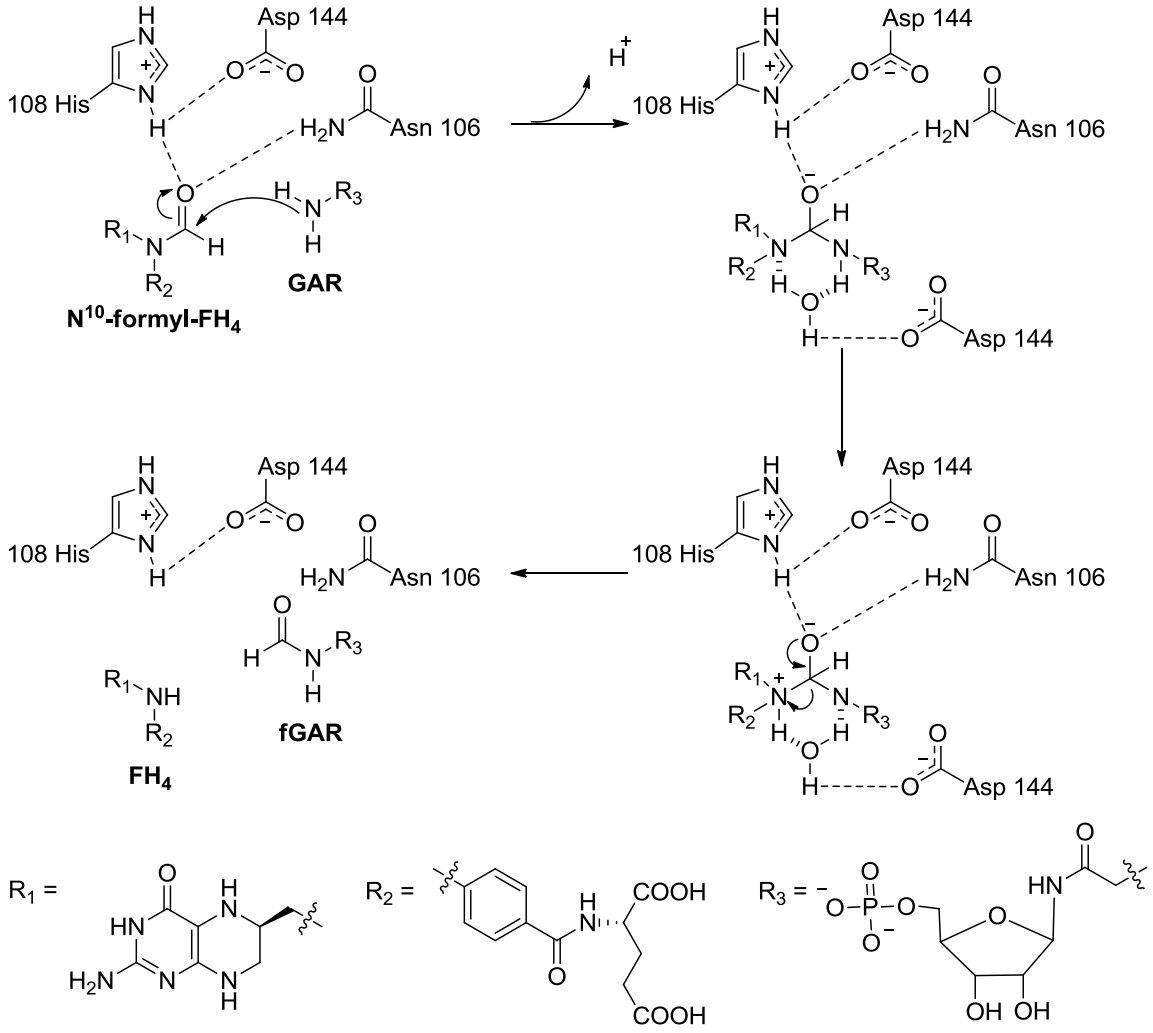

Figure 11 A proposed mechanism of GARFTase.[121]

A proposed GARFTase mechanism is shown in Figure 11.[121] As the cofactor N^{10}-CHO-FH_4 binds to the active site, Asp144 forms a salt bridge to the imidazolium of His108 and the formyl group is positioned to form hydrogen bonds to Asn106 and the protonated imidazolium group of His108. The nucleophilic amino group of GAR then attacks the activated formyl group to form a tetrahedral intermediate. A proton transfer from GAR to the N^{10} of folate is mediated by a catalytic water molecule, followed by the breakdown of the tetrahedral intermediate to form products. The positioning of this water

molecule may be assisted by a hydrogen bond to the carboxylic acid group of Asp144. (To simplify the figure, Asp144 is shown twice in Figure 7; it actually spans from the N^1 of His108 to the bound H_2O molecule.)

3.3. Binding of Inhibitors

An X-ray crystal structure (1.98 Å) of hGARFTase was reported by Zhang *et al.*[139] in a binary complex with the co-substrate analog inhibitor 10-CF_3CO-DDACTHF (Table 2) at pH 7 (PDB ID 1NJS). The cofactor binding pocket of hGARFTase is located at the interface between the N-terminal mononucleotide binding domain and the C-terminal half of the structure and consists of three parts: the pteridine binding cleft, the benzoylglutamate region, and the formyl transfer region.

Pteridine Binding Cleft. The diaminopyrimidinone ring of 10-CF_3CO-DDACTHF is deeply buried in the active site cleft at the same location as the quinazoline ring of 10-formyl-5,8,10-trideazafolic acid (10-formyl-TDAF) in the *E. coli* GARFTase complex (PDB entry 1C2T). The connecting chain from the diaminopyrimidinone ring to the *L*-glutamate, composed of single carbon bonds, is longer than its counterpart in 10-formyl-TDAF, due to the removal of the fused benzene ring, which makes it more flexible when adapting to the binding site to optimize the gem-diol interactions with the protein. The diaminopyrimidinone ring of 10-CF_3CO-DDACTHF is tilted about 15 ° relative to the quinazoline ring of 10-formyl-TDAF, facilitating N_2 within hydrogen bonding range (3.1 Å) of the backbone carbonyl oxygen of Glu141. The diaminopyrimidinone ring conserves all of the key interactions observed with the quinazoline ring of 10-formyl-TDAF, and

provides additional key hydrogen bonds with the enzyme. Several hydrophobic residues (Leu85, Ile91, Leu92, Phe96, and Val97) encircle a deep cavity holding the heterocycle. The diaminopyrimidinone ring forms six hydrogen bonds to the main chain amides and carbonyls of Arg90, Leu92, Ala140, Glu141, and Asp144, and two hydrogen bonds to ordered waters (W18 and W70). In the quinazoline ring of 10-formyl-TDAF, the N^8 nitrogen has been proposed to play a key role in recognition and interaction with folate-binding enzymes and forms one end of an H-bond donor−acceptor−donor array. While its replacement with carbon does not preclude its binding to GARFTase, its presence appears to contribute to substrate recognition by the folate transport system and/or FPGS. The diaminopyrimidinone ring of 10-CF_3CO-DDACTHF, however, preserves this N^8 nitrogen and forms hydrogen bonds to the carbonyl oxygen of Arg90 (2.8 Å) and an ordered solvent molecule W70 (2.7 Å).

Glutamate Tail. In the 10-CF_3CO-DDACTHF complex, the PABA moiety is located in a hydrophobic pocket sandwiched between the side chains of Ser118 and Ile91. The carbonyl group is in the same plane as the phenyl ring. The glutamate tail is almost perpendicular to the PABA plane and parallel to the aliphatic stem of the diaminopyrimidinone ring. In contrast to its flexibility in *E. coli* GARFTase complex structures, the glutamate moiety is solvent-exposed, but exhibits a remarkably well-ordered structure in the complex structure of 10-CF_3CO-DDACTHF with human GARFTase. A salt bridge (2.7 Å) is formed between the α-carboxylate and Arg64 so that the γ-carboxylate points to the solvent. Additional interactions observed include a hydrogen bond between the Ile91 backbone amide and the α-glutamate carboxylate (2.8 Å).

Formyl Transfer Region and the Gem-Diol Structure. Key interactions for tight binding of 10-CF_3CO-DDACTHF to hGARFTase are found in the formyl transfer region. Strong electron density next to the ketone oxygen indicates that the ketone is hydrated to a gem-diol, similar to the 10-formyl-TDAF and β-GAR complex with the *E. coli* GARFTase (PDB ID 1C2T). The gem-diol forms extensive interactions with the formyl transfer region, especially with two essential residues Asp144 and His108. The Asp144 carboxylate forms hydrogen bonds (2.5 and 2.7 Å) to each of the hydroxyl groups of the gem-diol. N^3 in the imidazole ring of His108 also forms hydrogen bonds with both hydroxyl groups of the gem-diol [OA1 (2.7 Å) and OA2 (3.1 Å)]. Additionally, OA2 also forms a potential hydrogen bond (3.0 Å) with the backbone carbonyl oxygen of Gly117.

3.4. GARFTase Inhibitors

Three classes of GARFTase inhibitors are reviewed and listed in Table 2, Table 3 and Table 4.

3.4.1. 5,6,7,8-Tetrahydropyrido[2,3-*d*]pyrimidines and 7,8-dihydro-pyrimido[5,4-*b*][1,4]thiazines as GARFTase inhibitors (Table 2)

Structure	Compound	Biological Activity	Ref.
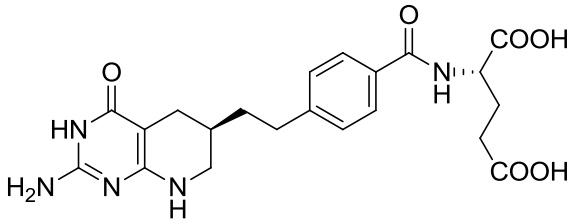	Lometrexol (DDATHF)	hGARFTase (K_i) 6 nM	[142]
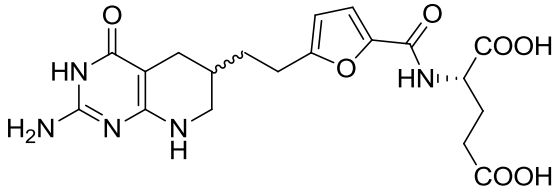	LY-222306 (6-*R*,*S*)	hGARFTase (K_i) 0.77 nM CCRF-CEM (IC_{50}) 27 nM	[143]
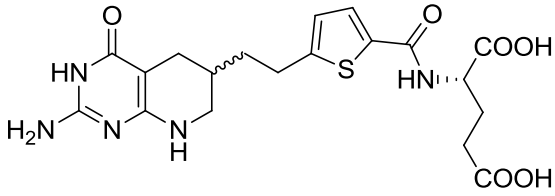	LY-254155 (6-*R*,*S*) LY-309887 (6-*R*)	hGARFTase (K_i) 2.1 nM CCRF-CEM (IC_{50}) 27 nM	[144]
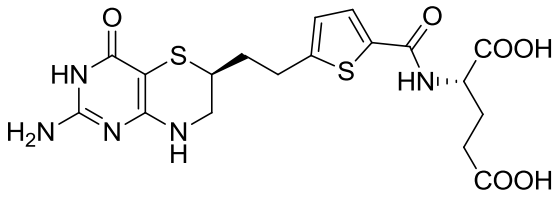	AG-2034	hGARFTase (K_i) 28 nM CCRF-CEM (IC_{50}) 2.9 nM	[145]
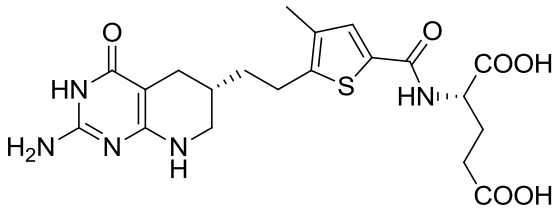	AG-2037 (pelitrexol)	hGARFTase (K_i) 0.5 nM	[146]

Lometrexol. The first GARFTase inhibitor in clinical trials, the 6-(*R*)-isomer (the same configuration found in natural tetrahydrofolates of 5,10-dideazatetrahydrofolic acid) of DDATHF, termed lometrexol (LMTX, Table 1), was synthesized by E.C. Taylor at

Princeton and Chuan (Joe) Shih at Eli Lilly in 1985.[147] This discovery established GARFTase and the purine *de novo* biosynthetic pathway as valid targets for antineoplastic intervention. LMX is structurally analogous to THF except that the 5- and 10- nitrogens of THF are replaced by carbons. LMTX is a poor inhibitor of both TS and DHFR, but a potent inhibitor of GARFTase (K_i = 6 nM) and a substrate for FPGS.[148] In CCRF-CEM cells with impaired RFC function, polyglutamylation of LMTX by FPGS is so extensive as to effectively negate the impact of the loss of RFC and the resistant phenotype.[149] In phase I clinical trials, patients treated with LMTX without folic acid coadminstration developed severe and cumulative dose-limiting myelosuppression and mucositis.[150] The cumulative toxicity of LMTX is believed to be due in part to its ability to be transported by both the RFC and FRs, resulting in toxic cellular levels.[151] When LMTX was administered with folic acid, there was a reduction in clinical toxicity, permitting a 10-fold dose escalation over that without folate supplementation.[152]

While LMTX is an excellent substrate for FRs,[32] it is primarily transported into tumors and normal tissues by RFC, whereupon it is extensively polyglutamylated by FPGS and inhibits GARFTase, leading to ATP and GTP depletion and potent antitumor activity with preclinical models in vitro and in vivo.[119, 153]

LY-309887. Unexpected cumulative toxicity with LMTX led to a search for a second-generation antimetabolite with a more favorable toxicological, biochemical and pharmacological profile. Habeck *et al*.[143] reported a novel class of classical antifolates that replaced the 1',4'-phenyl group of LMTX with a 2',5'-furan (LY-222306) and a 2',5'-thiophene (LY-254155) (Table 1) in 1994. Both LY-222306 and LY-254155

(mixtures of diastereomers) were found to be potent inhibitors of CCRF-CEM cell growth (IC_{50} = 27 and 2.3 nM, respectively) and human GARFTase (K_i = 0.77 and 2.1 nM, respectively). Further resolution of LY-254155 into its two diastereomers provided LY-309887 (6*R*-2',5'-thienyl-5,10-dideazatetrahydrofolic acid, Table 1), which was more potent than LMTX at inhibiting tumor growth in the murine C3H mammary tumor model and several tumor xenografts.[144, 153] LY-309887 displayed a 9-fold more inhibitory potency against GARFTase compared to LMTX. In preclinical models, LY-309887 was more potent than LMTX against two pancreatic xenografts and in the human LX-1 lung carcinoma model. However, in two preliminary reports of phase I studies with LY-309887, all patients received concurrent folic acid but still suffered from cumulative toxicity, suggesting that, like LMTX, cumulative toxicity and lack of selective transport into tumors remains a toxic property of LY-309887 as well.[154, 155]

AG-2037. AG-2037 (pelitrexol) is in phase II clinical development (Table 1) for patients with metastatic adenocarcinoma of the colon or rectum that failed prior fluorouracil and leucovorin calcium therapy.[156] Its configuration at C-6 is reversed compared to LMTX and the thiophene is methylated at the 4-position of AG-2037. AG-2037 is a potent inhibitor of GARFTase (K_i = 0.5 nM) and exhibits significant antiproliferative effects against tumor cells both *in vitro* and *in vivo*.[157] Several phase I studies have been completed that indicate that AG-2037 is well tolerated and its maximum tolerated dose in phase II studies have been determined.[158]

3.4.2. Pyrimidines as GARFTase inhibitors (Table 3)

Structure	Compound	Biological Activities	Ref.
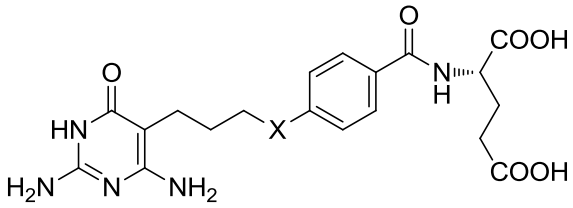	7-DM-DDATHF X = CH_2	CCRF-CEM (IC_{50}) 0.13 μM	[159]
	5-DACTHF X = NH	hog liver GARFTase (IC_{50}) 2.6 μM	[160]
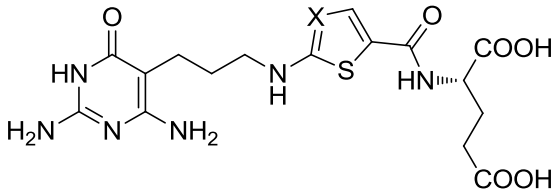	X = CH	hog liver GARFTase (IC_{50}) 2.06 μM	[161]
	X = N	hog liver GARFTase (IC_{50}) 0.14 μM	[161]
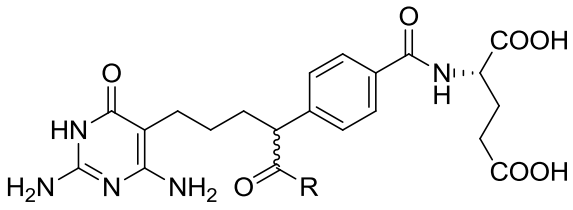	10-CHO-DDACTHF R = H	hGARFTase (K_i) 14 nM CCRF-CEM (IC_{50}) 60 nM	[134]
	10-CF_3CO-DDACTHF R = CF_3	rhGARFTase (K_i) 15 nM CCRF-CEM (IC_{50}) 16 nM	[162]
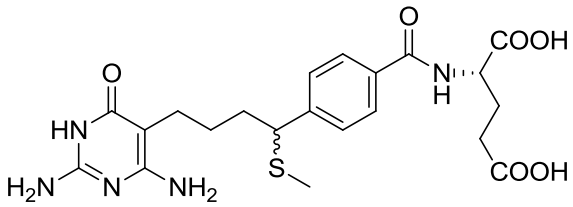	(10*R*)-CH_3S-DDACTHF	rhGARFTase (K_i) 210 nM CCRF-CEM (IC_{50}) 80 nM	[163]
	(10*S*)-CH_3S-DDACTHF	rhGARFTase (K_i) 180 nM CCRF-CEM (IC_{50}) 50 nM	[163]
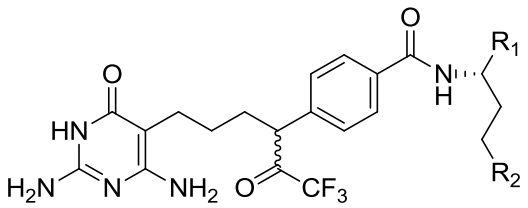	α-CH_2-10-CF_3CO-DDACTHF R_1=$COONH_2$ R_2=COOH	hGARFTase (K_i) 4.8 μM CCRF-CEM (IC_{50}) inactive	[164]

γ-CH_2-10-CF_3CO-DDACTHF R_1=COOH R_2=$COONH_2$	hGARFTase (K_i) 56 nM CCRF-CEM (IC_{50}) 300 nM	[164]
γ -Tetrazole-10-CF_3CO-DDACTHF R_1=COOH R_2=tetrazole	hGARFTase (K_i) 130 nM CCRF-CEM (IC_{50}) 40 nM	[165]

7-DM-DDATHF. During the development of GARFTase inhibitors, open-chain analogs of LMTX were synthesized and evaluated by Boger *et al*..[159, 166] These analogs avoided the C-6 stereocenter of LMTX and were therefore less challenging to synthesize. 7-Desmethylene-DDATHF (7-DM-DDATHF) (Table 2) is approximately 8-fold less potent than LMTX against human leukemia CCRF-CEM cells (IC_{50} = 130 nM *vs.* 16 nM). 7-DM-DDATHF is also a FPGS substrate and its polyglutamated conjugates are more potent inhibitors of GARFTase than the parent compound. These results demonstrated the removal of the annulated tetrahydropyridine ring of LMTX had minimal effect on binding to GARFTase. A similar compound 5-DACTHF (Table 2) was reported by Kelley *et al*.[167] in 1990. 5-DACTHF showed an IC_{50} of 2.6 μM against hog liver GARFTase and slight inhibition of AICARFTase (IC_{50} = 200 μM in L1210 cells).

10-CF_3CO-DDACTHF. The synthesis and evaluation of 10-formyl-5,10-dideaza-acyclic-5,6,7,8-tetrahydrofolic acid (10-CHO-DDACTHF, Table 2), an acyclic analog of

LMTX bearing a nontransferable C-10 formyl group, was also reported.[168] 10-CHO-DDACTHF showed potent inhibition against cell growth (IC_{50} = 60 nM, CCRF-CEM) and hGARFTase (K_i = 14 nM), but suffered from instability due to a facile oxidative deformylation. By combining the 2,4-diaminopyrimidone core of 10-CHO-DDACTHF with a more stable trifluoromethyl ketone moiety, 10-(Trifluoroacetyl)-5,10-dideaza-acyclic-5,6,7,8-tetrahydrofolic acid (10-CF_3CO-DDACTHF, Table 2) was discovered.[139] It is a potent inhibitor of tumor cell proliferation, with an IC_{50} of 16 nM against CCRF-CEM cells, which represents a 10-fold improvement over LMTX. This compound specifically inhibits recombinant hGARFTase (K_i = 15 nM), and is stable, displaying no competitive oxidative deacylation.

10-CH_3S-DDACTHF. 10-CH_3S-DDACTHF was also reported to be potent, exhibiting an IC_{50} of 100 nM against CCRF-CEM cells.[169] A follow-up asymmetric synthesis of (10*R*)- and (10*S*)- diastereomers of 10-CH_3S-DDACTHF was reported in 2008.[170] Both diastereomers are potent and selective inhibitors of rhGARFTase (10*R*, K_i = 210; 10*S*, K_i = 180 nM) and effective inhibitors of cell growth (IC_{50} = 80 and 50 nM, respectively, against CCRF-CEM cells), which is dependent on intracellular polyglutamation by FPGS but not transported by the RFC.

***γ-$CONH_2$-10-CF_3CO-DDACTHF and γ-tetrazole-10-CF_3CO-DDACTHF* (Table 2).** The glutamic acid portion of 10-CF_3CO-DDACTHF was further explored in the development of GARFTase inhibitors. As summaried previously, folates and many

antifolates are polyglutamylated by FPGS after entering cells. FPGS attaches additional glutamates to the γ-carboxylic acid of folates and antifolates. Polyglutamation of folates and antifolates increases their affinity to target enzymes (e.g. TS and GARFTase) and makes them less susceptible to cellular efflux, providing a long-lived cellular supply of the molecules. However, this long-term enhanced intracellular accumulation of antifolates, which results from their polyglutamation, contributes to their cumulative toxicity. Therefore, GARFTase inhibitors that do not undergo polyglutamylation while maintaining potent enzyme binding is considered to be attractive. Amide analog γ-$CONH_2$-10-CF_3CO-DDACTHF (Table 2) exhibited potent inhibitory activity against rhGARFTase (K_i = 56 nM) and purine-sensitive cytotoxic activity (IC_{50} = 300 nM, CCRF-CEM), whereas α-$CONH_2$-10-CF_3CO-DDACTHF showed decreased affinity (K_i = 4.8 μM) and was inactive in cellular functional assays.[17148] Another potent nonpolyglutamatable analog γ-tetrazole-10-CF_3CO-DDACTHF (Table 2) exhibited purine-sensitive cytotoxic activity (IC_{50} = 40 nM) and was a selective inhibitor of hGARFTase (K_i = 130 nM).[172] As anticipated, both γ-$CONH_2$-10-CF_3CO-DDACTHF and γ-tetrazole-10-CF_3CO-DDACTHF are not dependent on FPGS for activity, and hence not susceptible to resistance caused by FPGS.

3.4.3. Pyrrolo[2,3-*d*]pyrimidines and thieno[2,3-*d*]pyrimidines

Gangjee and coworkers[109, 112, 113] recently described novel 6-substituted classical pyrrolo[2,3-*d*]pyrimidine and thieno[2,3-*d*]pyrimidine as cytotoxic antifolates with varying lengths of the carbon bridge region (Table 1), that are characterized by selective

FR and PCFT transport over RFC transport. For every series, the three- and four-carbon bridge analogs were the most active toward FR-expressing human tumors (KB and IGROV1) and the cytotoxicity was primarily due to potent inhibition of GARFTase, although for the thieno[2,3-*d*]pyrimidine antifolates, a secondary target, most likely AICARFTase, was also implied at higher concentration. [50-51]

The 6-substituted classical pyrrolo[2,3-*d*]pyrimidine with a thiophene side chain, compound **3** is much more potent *in vitro* compared with the most potent of the previously published pyrrolo[2,3-*d*]pyrimidine **2** and the thieno[2,3-*d*]pyrimidine **6**, both of which contain a benzoyl ring in the side chain (Table 1). Significant *in vivo* antitumor activity was demonstrated for compound **3** with severe combined immunodeficient (SCID) mice bearing both early and more importantly advanced stage KB tumors.

4. Aminoimidazole-4-carboxamide ribonucleotide transformylase (AICARFTase)

Aminoimidazole-4-carboxamide ribonucleotide transformylase (AICARFTase) catalyzes the penultimate reaction in the de novo purine biosynthetic pathway, producing formyl-AICAR (FAICAR) from AICAR using N^{10}-formyltetrahydrofolate (N^{10}-CHO-FH_4) as the formyl donor. It exists as one domain of a bifunctional enzyme that also contains IMP cyclohydrolase (IMP CHase) that catalyzes the final reaction of the pathway (Figure 4). Because of the large demand for purines by cancer cells, AICARFTase has been targeted by antifolate inhibitors in chemotherapy along with GARFTase.[173, 174]

4.1. Structure of AICARFTase

AICARFTase is highly conserved from *E. coli* to human but has no sequence homology with other folate-dependent enzymes, such as GARFTase.[175] Thus, folate-based inhibitors of GARFTase do not usually inhibit AICARFTase because of differential interactions within the two active sites.[176] For example, lometrexol potently inhibits GARFTase but not AICARFTase.[119, 177]

Ian A. Wilson and coworkers[174, 176, 178-180] have previously reported several crystal structures of human and avian ATIC (the bifunctional enzyme, aminoimidazole-4-carboxamide ribonucleotide (AICAR) transformylase (AICARFTase)/IMP cyclohydrolase (IMPCH)) in both unliganded and complexed forms. The ATIC forms an intertwined symmetrical homodimer (each monomer being composed of 393 residues) with the IMPCH domain at the N terminus (residues 1–199) and the AICARFTase domain at the C terminus (residues 200–593). The IMPCH active sites are contained within each monomer of the dimer, but the AICARFTase active site is located at the dimer interface with key active-site residues being contributed from both monomers.

4.2. AICARFTase catalytic mechanism

Because both transformylases (GARFTase and AICARFTase) catalyze a similar chemical reaction, that is a transfer of a formyl group from the same cofactor, they were anticipated to have similar catalytic mechanisms. However, evidences implied that two enzymes might operate differently.[173] (1) The amino acid sequence homology between the two transformylases is quite low. Although a similar grouping of amino acids (His, Asp, and Asn) that acts as a catalytic triad in GARFTase was also found in AICARFTase,

these amino acids are not the catalytic residues as revealed by mutation analysis.[181] (2) The transformylation of AICAR by N^{10}-formyldihydrofolate (N^{10}-CHO-FH_2; kinetically equivalent to N^{10}-CHO-FH_4) is an unfavorable reaction with a K_{eq} of 0.024.[182] AICARFTase is found as a domain of the bifunctional enzyme throughout all species characterized to date from *E. coli* to human, an arrangement that couples the unfavorable formation of FAICAR with the highly favorable cyclization reaction catalyzed by IMP CHase.[173] (3) Previous studies on substrate analogues revealed that the amide moiety in AICAR is essential for formyl transfer, and its conformation is important in the binding to the enzyme active site. Wilson and coworkers[182] proposed that the amide assists in the required proton shuttling from the 5-amino group to the N^{10} of the folate in the tetrahedral transition state. (4) A partially refined crystallographic structure of the bifunctional enzyme has indicated that Lys266 and His267 are two potentially important catalytic residues in the active site.[173] Site-directed mutation of these residues to alanine were found to abolish the transformylase activity of the mutants, although they still retain binding affinity for AICAR.[183]

The catalytic mechanism of AICARFTase was evaluated with pH dependent kinetics, site-directed mutagenesis, and quantum chemical calculations.[173] The result indicated that the amide-assisted mechanism is concerted such that the proton transfers from the 5-amino group to the formamide are simultaneous with nucleophilic attack by the 5-amino group. Because this process does not lead to a kinetically stable intermediate, the intramolecular proton transfer from the 5-amino group through the 4-carboxamide to the formamide proceeds in the same transition state. Collectively, these experimental and theoretical analyses lead to a proposed mechanism for AICARFTase catalysis shown in

Figure 12.

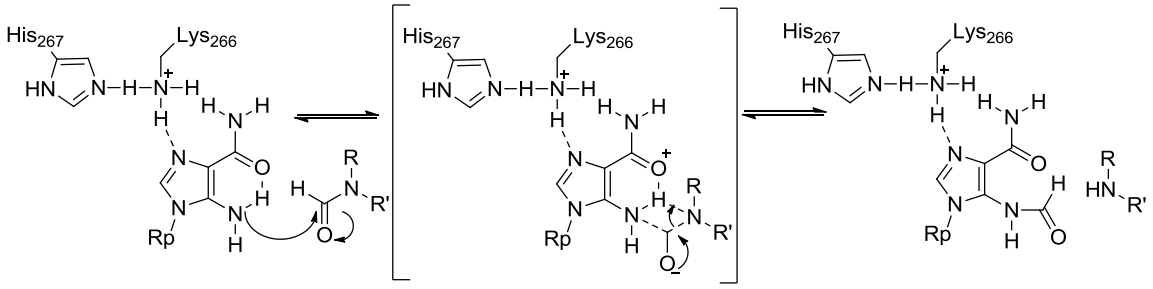

Figure 12 A proposed mechanism of AICARFTase.[173]

In this proposed mechanism, Lys266, with the aid of His267, acts as a general acid catalyst to interact with the N3 of the imidazole ring of AICAR. His267 aids Lys266 to be in the right position for a hydrogen-bonding interaction. The 4-carboxamide mediates proton shuttling from the 5-amino to 4-carboxamide and then to the nitrogen of the leaving group with simultaneous nucleophilic attack of the 5-amino group on the formyl group of folate cofactor. The first proton transfer is facilitated by the intramolecular hydrogen bond in the ground-state AICAR and the protonated 4-carboxamide species is only present transiently. The theoretical results suggest that protonation of the nitrogen of the leaving group is critical in the aminolysis reaction between AICAR and the formyl group rather than the nucleophilic attack on the carbonyl group. The central role assigned to proton transfer compensates for the weak nucleophilicity of the AICAR 5-amino group.

4.3. Binding of AICARFTase inhibitors

AICARFTase is unique among folate-binding enzymes for several reasons:[184] (1) Its most striking features are its “oxyanion hole” consisting of Lys266, Arg451, and its backbone amide in the center of the active-site cleft, and an additional helix dipole

consisting of residues 450-468 with its N-terminus pointing toward the “oxyanion hole”.

A.

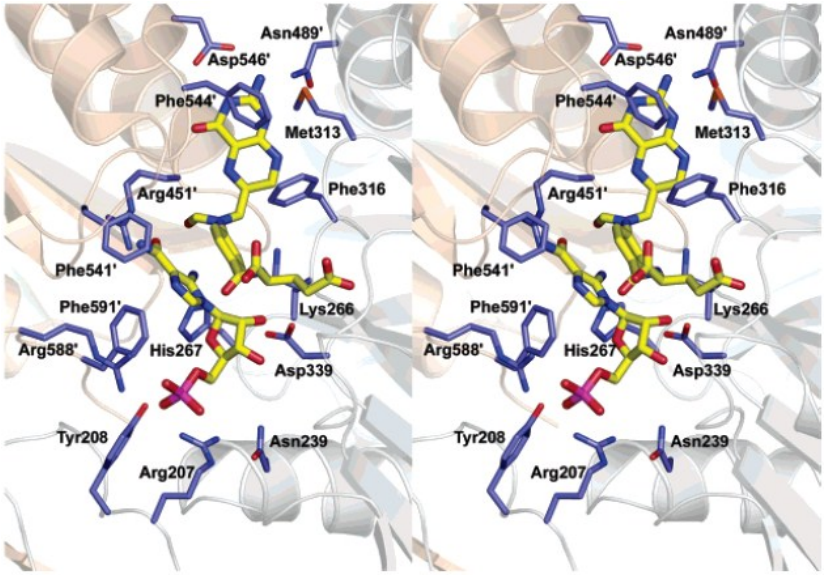

B.

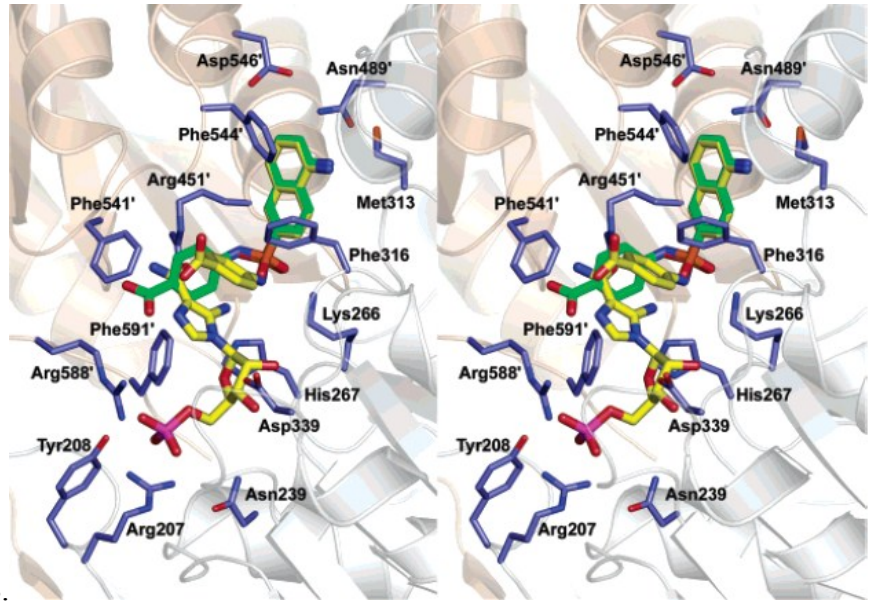

Figure 13 Stereoview of folate cofactor and selected inhibitors binding to AICARFTase active site (PDB 1P4R).[184] (A) AICARFTase active site. The lower ligand is the native AICAR substrate identified by X-ray crystallography. The upper ligand is the folate cofactor docked *via* AutoDock. (B) NSC37173 binds to the active site. The lower ball-and-stick ligand is the crystallographic AICAR binding position. The upper ball-and-stick

ligand is the docked position of NSC37173 with AICAR present. The green stick model is the docked position of NSC37173 without AICAR present (empty active site).

Considering the weak nucleophilicity of the 5-amino group of AICAR and the overall reaction direction favoring the reactants, this "oxyanion hole" is very likely to be particularly important for the stabilization of the transition state during the formyl transfer. Some AICARFTase inhibitors found in the virtual screening have either an "electron-rich" linker [-(O=)S(=O)-NH-, -(O=)S(=O)-O-, -C(=O)-NH-, or -C(=O)-O-] or an "electron-rich" terminal group (-SO3-) or both.[184] This feature appears to be the most critical "hot spot" for future inhibitor design and is consistent with the crystal structures of ATIC complexed with the sulfonyl-containing antifolates.[175] (2) The second important feature of the AICARFTase active site is its aromatic system composed of residues Phe316, Phe591, Phe544, and Phe541, which play a critical role in anchoring and orienting the substrate AICAR and folate cofactor for binding and catalysis.

As shown in the crystal structures and docking studies of the folate cofactor and NSC37173 (PDB 1P4R) (Figure 13), the aromatic stacking of Phe591, the imidazole of AICAR, the benzene of the folate, and Phe316 essentially "locate and orient" the enzyme-substrate-cofactor ternary complex for catalysis. Again, all of the inhibitors identified contain at least one aromatic moiety that mostly binds into the pterin binding pocket and stacks with Phe544, or more frequently, have two aromatic moieties linked by an "electron rich" linker. The second aromatic moiety interacts with Phe316 or Phe541 depending on the "perturbation" from the rest of the inhibitors. Effective utilization of an aromatic system seems the second principle for AICARFTase inhibitor design. The above

two features may play a defining role in developing useful pharmacophores and in selecting useful novel scaffolds.[184] (3) Unlike TS, DHFR, or GARFTase, AICARFTase does not undergo significant conformational change upon ligand binding.[184] The most noticeable changes are for Arg207 side chain moving in for phosphate/sulfate binding, the Phe544/Phe316 side-chain rotations for aromatic modulation, and a slight "closing-in" of the Pro543-Phe544-Arg545-Asp546 loop for a more constricted pterin pocket. From a drug designer's view, a more predictive behavior of the designed ligands and a more reliable free energy assessment should be expected with this type of "pre-formed" active site. However, the role of sequestered structural waters is difficult to predict.

4.4. AICARFTase inhibitors

a. BW1540 and BW2315

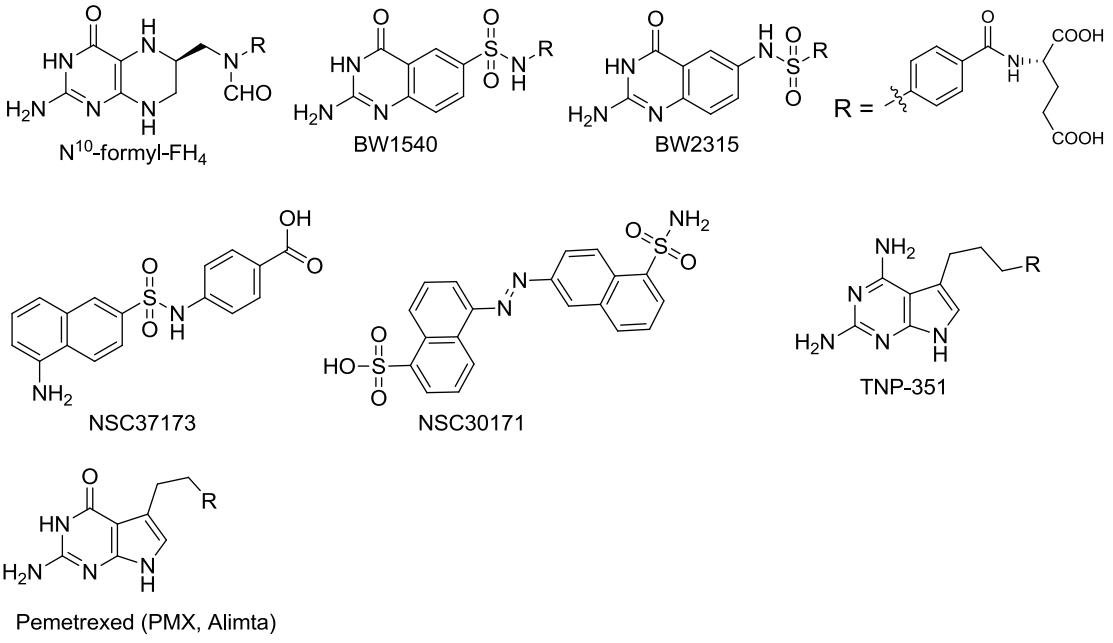

Figure 14 AICARFTase inhibitors.

Compared with the number of relatively potent inhibitors of GARFTase summarized before, specific inhibitors of AICARFTase have been scarce. However, Burroughs Wellcome (Research Triangle Park, NC) had designed and synthesized two antifolates that are specific (nM) for human AICARFTase, as compared with other folate-dependent enzymes, GARFTase, DHFR, and TS.[175] These compounds are both sulfamido-bridged 5,8-dideazafolate analogs identified as BW1540U88UD (BW1540) and BW2315U89UC (BW2315) (Fig. 14) that differ only in the disposition of the imido and sulfonyl groups within the bridge region. BW1540 and BW2315 have approximate K_i values against human ATIC of 8 and 6 nM, respectively, whereas the K_i values against GARFTase, DHFR and TS are within the micromolar range, except for BW1540, which showed low nanomolar inhibition against DHFR.[175] Cytotoxicity assays against human colon cell lines yielded an approximate IC_{50} of 0.7–3 μM for BW1540 and 1–5 μM for BW2315 respectively. BW1540 and BW2315 were co-crystallized at 2.55 and 2.60 Å with human ATIC in the presence of substrate AICAR to elucidate their mechanism of inhibition. It was found both of these compounds bound to the AICARFTase active site of ATIC and the sulfonyl groups dominate inhibitor binding and orientation through interaction with the proposed oxyanion hole. These agents then appear to mimic the anionic transition state and now implicate Asn431 in the reaction mechanism along with previously identified key catalytic residues Lys266 and His267. Moreover, interaction of the sulfonyl oxygens with the oxyanion hole of the AICARFTase active site suggests that it is the driving force behind the high affinity for these sulfonyl-containing antifolates (The K_m of 10-f-THF is 100 μM[185], whereas the K_i values for BW1540 and BW2315 are 8 and 6 nM, respectively.[175] Thus, these two antifolates bind more strongly to the

AICARFTase active site, by at least 1000-fold, than the natural co-factor N^{10}-formyltetrahydrofolate. This effect is probably due to the sulfonyl groups mimicking the oxyanion of the transition state perhaps with a stronger interaction.

b. NSC37173 and NSC30171

Virtual screening of the human AICAR transformylase active site by use of AutoDock against the NCI diversity set, a library of compounds with nonredundant pharmacophore profiles, has revealed NSC30171, which had nanomolar inhibition (K_i = 154 nM, IC_{50} = 600 nM), and NSC37173 (IC_{50} = 4.1 μM) against human AICARFTase.[184] The human AICARFTase /BW1540 complex (PDB 1P4R) was selected as the docking template. NSC30171 was picked out via NSC37173 similarity searching. Enzymatic testing revealed that it is the most potent inhibitor found through virtual screening of this series of compounds (K_i = 154 nM and IC_{50} = 600 nM). Docking with and without AICAR substrate in the active site strongly indicates that this nonfolate competes with AICAR substrate for the AICAR binding site. Key interactions with the AICARFTase active site residues appear to be the electrostatic and H-bonding interactions between its sulfate and the enzyme "oxyanion hole", and the aromatic stacking of the NSC30171 naphthalene ring with the Phe590 benzyl ring.

c. TNP-351

TNP-351, characterized by a pyrrolo[2,3-*d*]pyrimidine ring, exhibits potent antitumor activities against mammalian solid tumors.[186] The mechanism of action of TNP-351 was evaluated using methotrexate-resistant CCRF-CEM human lymphoblastic

leukemia cell lines as well as partially purified FPGS, AICARFTase, and GARFTase from parent CCRF-CEM cells. TNP-351 was found to significantly inhibit the growth of L1210 and CCRF-CEM cells in culture, with the doses effective against 50% of the cells (ED_{50} values) being 0.79 and 2.7 nM, respectively. The methotrexate-resistant CCRF-CEM cell line, which has an impaired methotrexate transport, showed less resistance to TNP-351 than to methotrexate. Inhibitory activities of TNP-351 and its polyglutamates-G_n (n=1–6) for AICARFTase were found to be significantly enhanced with increasing glutamyl chain length (inhibition constants (K_i): G_1, 52 μM; G_6, 0.07 μM). Neither TNP-351 nor its polyglutamates were very potent GARFTase inhibitors.

d. Pemetrexed (PMX, Alimta)

Pemetrexed (PMX) is currently in widespread clinical use as the first line therapy of mesothelioma and non–small cell lung cancer (NSCLC) and is also currently being evaluated for the treatment of a variety of other solid tumors in the US.[187, 188] In 2009, PMX was approved in combination with cisplatin as a first-line treatment of patients with locally advanced or metastatic NSCLC, the first drug ever approved for this purpose.[188] Thymidylate synthase (TS) was identified originally as the primary intercellular target[189] of PMX. However, it was clear from the start that PMX is a multitargeted antifolate that inhibit DHFR, GARFTase and AICARFTase in addition to TS.[188]

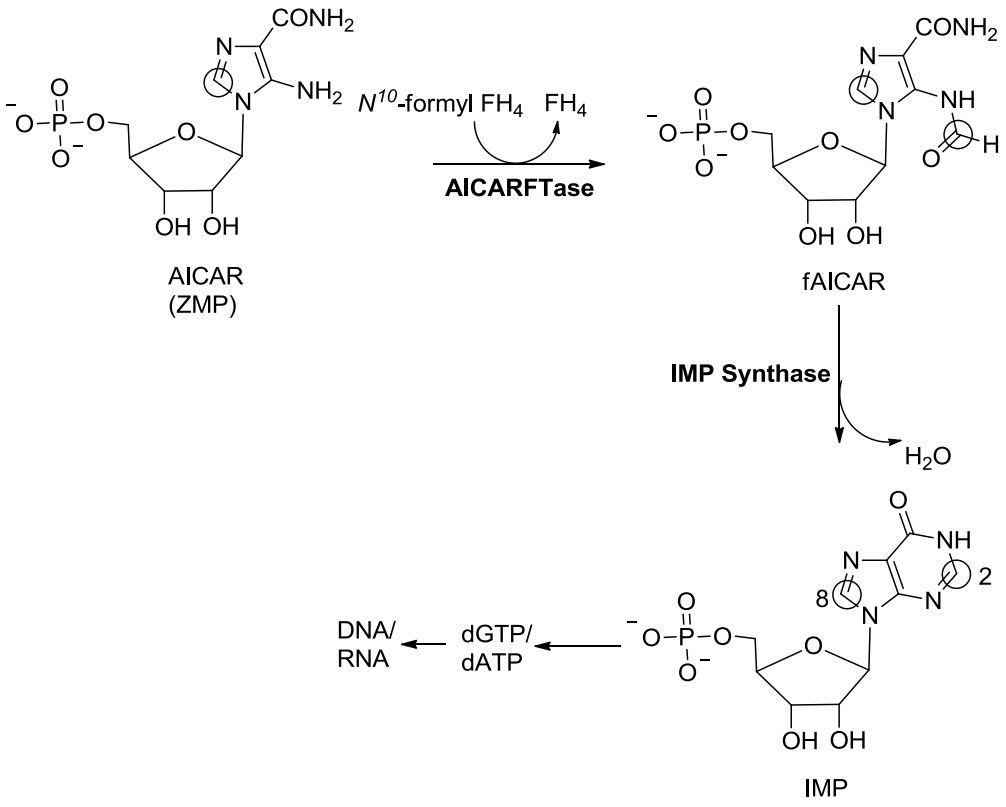

Figure 15 The folate-dependent steps of de novo purine synthesis and the site of entry of AICAR into the pathway.[190]

Although GARFTase was originally suggested to be an important secondary target of PMX, R.G. Moran and colleagues[190, 191] suggested that AICARFTase (pemetrexed, K_i = 3 μM; polyglutamate pemetrexed, K_i = 0.26 μM against human AICARFTase) was likely a more important target for PMX than originally envisaged in the absence of TS. The substrate of the AICARFTase reaction, ZMP, accumulated in intact pemetrexed-inhibited tumor cells (ZMP is an AMP mimetic and activator of AMPK) by AICARFTase inhibition. The ZMP accumulation causes an activation of AMP-activated protein kinase, which causes phosphorylation of AMPK target proteins and the subsequent inhibition of the mammalian target of rapamycin (mTOR) and

hypophosphorylation of the downstream targets of mTOR that control initiation of protein synthesis and cell growth. (Figure 15)

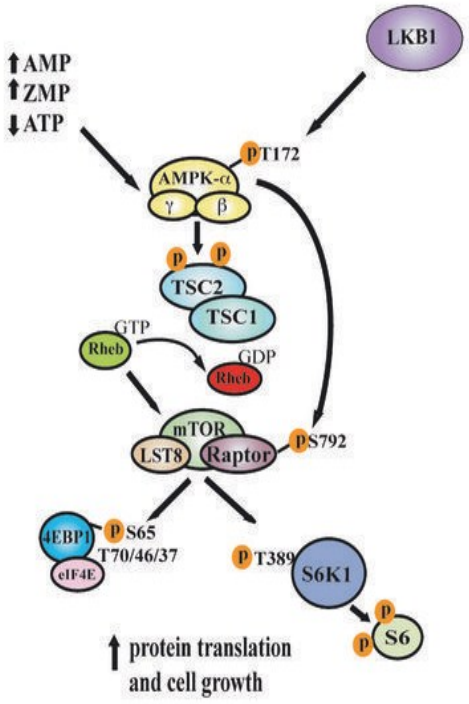

Figure 16 Effects of PMX on activation of AMPK and inhibition of mTOR. Schematic diagram showing activation of AMPK by either AMP or ZMP that result in inhibition of mTOR and its downstream targets.[190]

It was also suggested that the activity of pemetrexed against human cancers is a reflection of its direct inhibition of folate dependent target proteins combined with prolonged inhibition of the mTOR pathway secondary to accumulation of ZMP. (Figure 15)[190, 191] Pharmacologic inhibition of mTOR with direct inhibitors is currently of substantial interest for cancer therapy, and current mTOR inhibitors have shown activity against human lung cancers.[192, 193] Perhaps this indirect inhibition of pemetrexed to the mTOR pathway explains the activity of pemetrexed in lung cancers, an unusual pattern

for classical antifolates. However, whether AMPK activation offers a therapeutic advantage over direct mTOR inhibitors remains an open question. Although downstream effects on mTORC1 are involved in pemetrexed action, the spectrum of effects is not confined to mTORC1-dependent processes, and AICARFTase inhibitors represent a unique class of anticancer agents different from the rapamycin analogs.

5. Dihydrofolate reductase (DHFR)

Dihydrofolate reductase (DHFR) (EC 1.5.1.3) is a universal enzyme found in almost all organisms including: *Pneumocystis jirovecii* (*P. jirovecii*), *Toxoplasma gondii* (*T. gondii*), *Mycobacterium avium* complex (MAC) and cancer. DHFR inhibitors play a very important role in the treatment of cancer, as exemplified by MTX (Figure 5) in neoplastic diseases.

Aminopterin (AMT) (Figure 5), is the first 2,4-diamino antifolate in the treatment of acute lymphoblastic leukemia (ALL). MTX, the N^{10}-methyl analog of AMT, is widely used in clinical alone and in combination in the treatment of various forms of cancer, such as lymphoma, germ cell tumors, breast cancer and head and neck cancer.[194] Both AMT and MTX differ from FA by the substitution of a 4-amino group for the 4-oxo group of the pteridine ring. This minor modification transforms the normal substrate into a very tight-binding inhibitor of DHFR. AMT and MTX have a highly basic 2,4-diaminopyrimidine moiety *in vitro* and *in vivo* in the pteridine ring which is protonated and forms an ionic bond with the active site of the DHFR enzyme at the Glu30 and accounts, in part, for the high affinity of these compounds for DHFR.[195] X-ray crystal structure demonstrates a different binding mode for MTX compared to the normal

substrate. While MTX was successful in cancer treatment, tumor resistance to MTX has developed. Two of the most common MTX resistance mechanisms are identified: decreased MTX transport (RFC) into tumor cells[196-198] and an increase in DHFR due to gene amplification.[198, 199] Other mechanisms include: decreased retention due to defective polyglutamylation (FPGS),[200-202] decreased binding of MTX to DHFR because of DHFR mutation, increased translational of DHFR and increased breakdown of MTX polyglutamates.[203, 204]

5.1. Structure of DHFR

The first crystal structure of a DHFR enzyme was reported by Matthews in 1977.[205] Since then, X-ray crystal structures have been reported for complexes of the protein from various species (bacteria, avian and mammalian). The homology among vertebrate DHFR is 75-90% while only 25-40% in bacterial DHFR.[206, 207]

DHFR is a monomeric protein containing 159-250 amino acids with a molecular weight in the range of 18000-22000 Daltons. It has a α/β structure with the core made up of eight-stranded β-sheet consisting of seven parallel strands, and one antiparallel strand present at the C-terminal. It contains at least four α-helices. Vertebrate DHFRs usually contain longer sequences (30 amino acid residues) with the additional amino acid residues accommodated in eight insertions into the loop regions connecting the elements of the secondary structure. The DHFR active site is located in a hydrophobic pocket (with the exception of Asp27 (E. coli DHFR) for bacterial enzyme or Glu30 in vertebrate DHFR) is 15 Å deep, which cuts across one face of the enzyme. The hydrophobic nature

of the active site indicates that hydrophobic and van der Walls interactions play an important role in cofactor or inhibitor binding. This hydrophobic pocket serves as a binding site for the substrate or the antifolates and the nicotinamide portion of NADPH. The polarity of the substrate binding site is complementary to the folate or inhibitors.[208] The pteridine ring and the glutamate side chain portions of the folate/antifolate are surrounded by backbone carbonyls and polar side chains, while the benzoyl moiety of the folate forms hydrophobic interactions with the side-chains of surrounding non-polar hydrophobic residues.[208]

5.2. Catalytic mechanism of DHFR

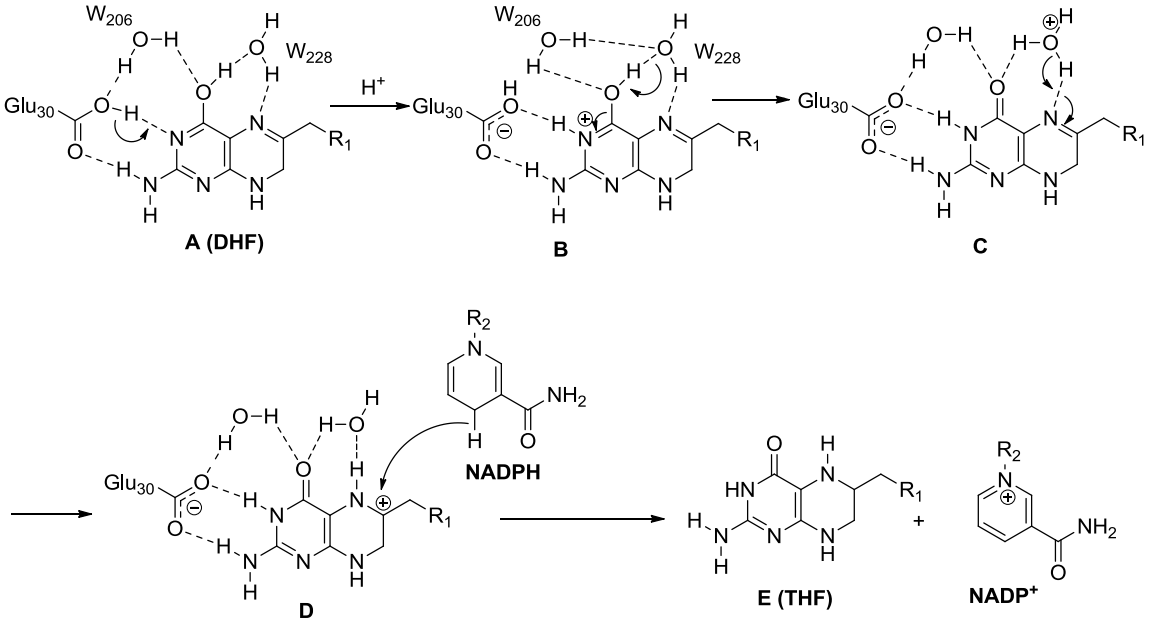

Figure 17 The catalytic mechanism of human DHFR.[209, 210]

As shown in Figure 17, there is an indirect proton transfer from Glu30 residue to the N5 atom of the substrate.[209] In addition, W206 stabilizes Glu30 whereas W228 and W206 serve as a hydrogen atom channel from the Glu30 to the N5 of the pterin ring.[209]

5.3. Ligand (inhibitor or cofactor) binding to DHFR

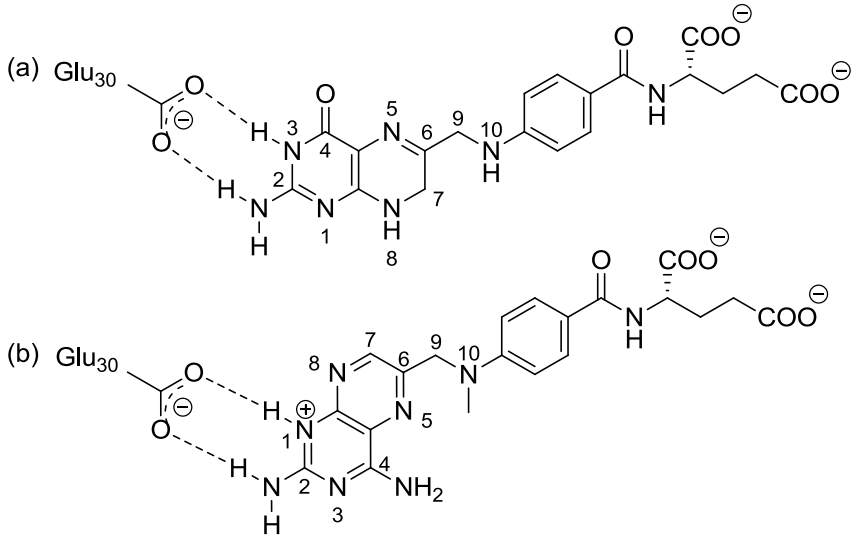

Figure 18 Interaction of Glu30 with (a) dihydrofolate and (b) MTX in the active site of human DHFR.[208, 211]

MTX binds to DHFR in a conformation that the *para*-aminobenzoyl moiety is almost perpendicular to the pteridine moiety as observed in various crystal structures.[208, 211] A variety of evidence (spectroscopic,[212, 213] calorimetric,[213] theoretical and NMR[214]) strongly identified that N^1 of MTX is protonated in the crystal structures. The Glu30 in human DHFR is ionized and forms an ionic bond with the protonated N^1 of MTX (Figure

18). In addition to the ionic bond, the two oxygen atoms of Glu30 form hydrogen bonds with the 2-amino group and N^1. This ionic (or salt bridge) bonding has been noted as a hallmark of all known potent DHFR inhibitors. It should also be noted that all DHFR inhibitors with a 2,4-diamino pyrimidine moiety such as pteridines, pyridopyrimidines, and quinazolines are bound in the similar mode as MTX. In contrast to the pyrimidine portion of the pteridine ring of MTX, the pyrazine portion is not directly bonded to DHFR. The *para*-aminobenzoyl moiety of MTX is surrounded by hydrophobic residues in the DHFR active site. The α-carboxylate of the L-glutamate is involved in a reinforced ionic bond with the protonated guanidinium moiety of a conserved Arg57, while the γ-carboxylate is nonspecific in its binding to the enzyme.[208, 211]

Nonclassical antifolates also bind to DHFR using the same type of ionic bond as classical antifolate MTX. Lipophilic nonclassical antifolates have limited success as anticancer agents because of their low therapeutic selectivity and difficulty in pharmaceutical formulation related to solubility.[215, 216]

5.4. DHFR inhibitors

MTX[217] (Figure 5) was first synthesized in 1949 and is still, together with the antibacterial drug TMP, the DHFR inhibitor most often used in clinic. The most common use of MTX is as an anticancer drug, but the drug is widely used as an anti-inflammatory and immunosuppressive agent with activity against autoimmune disorders.[218]

The drug exists as a highly polar anion at physiological pH and enters the cells by

the energy-dependent RFC. Inside the cell the molecule is polyglutamylated, which leads to altered properties.

Intrinsic and acquired resistance to MTX limits its efficacy in clinic. Resistance has been attributed to several different mechanisms including a reduced level of cellular uptake of the drug,[219] and an increase in DHFR levels involved in folic acid metabolism. As mentioned, MTX is transported into cells by RFC. Consequently, the poor ability to transport the drug into the cell can be a source of natural resistance.[220, 221] Major limitations, besides the resistance with MTX treatment, are bone marrow toxicity, gastrointestinal ulceration, and kidney and liver damage. In high doses, given intermittently, the adverse effect on the bone-marrow can be relieved by the periodic administration of leucovorin (LV), circumventing the MTX mediated blockade of tetrahydrofolic acid production (LV 'rescue' procedure).[222, 223]

Pralatrexate (Figure 5) was identified in 1990s.[224] It was of interest in developing antifolates with greater therapeutic selectivity that could be more effectively internalized into tumors (transported into the cells through RFC) and would be more toxic to cancer cells than normal cells. This led to the discovery of pralatrexate, which was approved as a treatment for relapsed or refractory peripheral T-cell lymphoma by FDA in 2009.[225]

Lipophilic nonclassical antifolates have been developed in an attempt to circumvent the mechanisms of resistance, such as decreased active transport, decreased polyglutamylation, DHFR mutations. These nonclassical antifolates differ from the traditional classical analogs by increased potency, greater lipid solubility, or improved cellular uptake. Although they are effective inhibitors, problems still remain with respect

to the toxicity due to the lack of selectivity for tumors.

6. Thymidylate synthase (TS)

Thymidylate synthase (TS) is present in almost all living organisms including bacteria, DNA viruses and protozoa.[226] TS is a macromolecular homodimeric enzyme that catalyzes the reductive methylation of dUMP to dTMP which is further phosphorylated to thymidine-5'-diphosphate (dTDP) and thymidine-5'-triphosphate (dTTP). The dTTP formed is utilized by DNA polymerase and is incorporated into DNA. The TS catalyzed reaction is a key step in DNA biosynthesis and the only *de novo* biosynthetic pathway to dTMP. TS inhibition results in a thymineless state, which prevents the growth of actively dividing cells.[227-229] This effect is probably due to increased DNA fragmentation resulting from dTTP depletion, which increases misincorporation of 2'-deoxyuridine-5'-triphosphate (dUTP). TS has long been regarded as an important target in cancer chemotherapy, and antimetabolites have been developed that inhibit at both the dUMP as well as the folate cofactor (antifolates) binding site.

6.1. Structure of TS

Thymidylate synthase (TS) enzymes are highly conserved evolutionary both in terms of structure and mechanism.[226] The active Thymidylate synthase (TS) enzyme is a homodimer consisting of two identical subunits of about 35000 Dalton each, and contains about 316 amino acids. The primary structure of TS from thirty species is highly conserved: approximately 27 amino acids are completely conserved.[226] The crystal structures of PMX and RTX with human TS have also been obtained.[230, 231] Several

crystal structures of TS complexed with substrates and inhibitors have also been reported.[232-236] These crystal structures are important in understanding both the mechanism and inhibition of TS and provide useful insights for structure based rational drug design.

6.2. Catalytic mechanism of TS

Binding of substrate and cofactor to Thymidylate synthase (TS) proceeds in an ordered fashion with sequential binding of substrate (dUMP) followed by cofactor (N^5,N^{10}-CH_2-THF), which induces a conformational change to form a noncovalent ternary complex (TS-dUMP-cofactor).[237] The substrate dUMP is activated at the C5 position by a nucleophilic attack on the C6 of the uracil ring of dUMP by a catalytic sulfhydryl moiety Cys195 of human TS which results in the formation of a Michael-type adduct **16** (Figure 19).

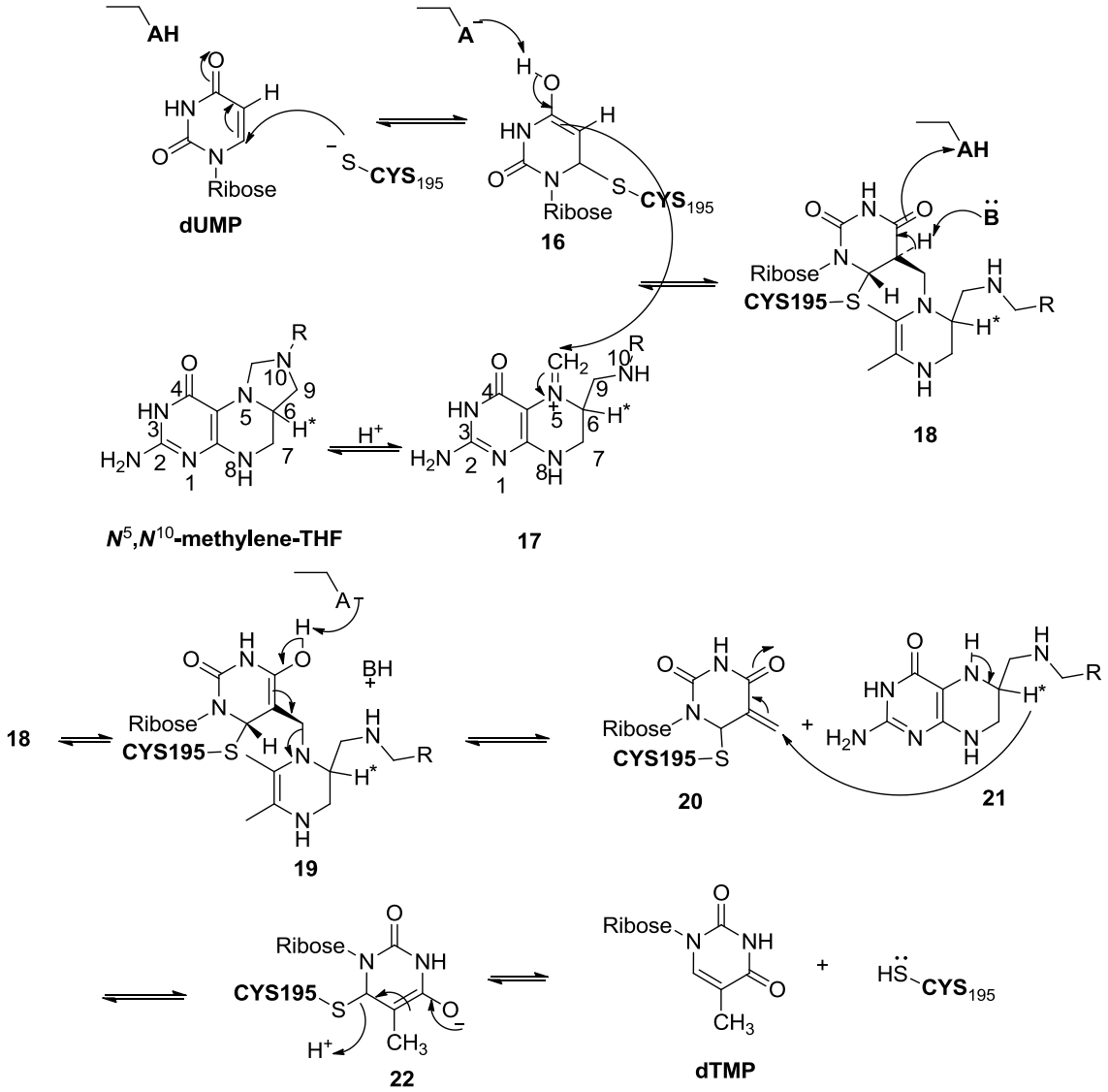

Figure 19 The catalytic mechanism of human TS.[237]

N^{10} protonation changes the cofactor from an inactive tricyclic form to the active bicyclic form **17** in which the cofactor N^5,N^{10}-CH_2-FH_4 is in the iminium ion form at N^5. This results in the transformation of the noncovalent ternary complex into an unstable covalent ternary complex. The activated C5 of Michael-type adduct is then

trapped by the N^5-iminium ion of the reduced cofactor to form intermediate **18**. The proton at the C5-position of dUMP is abstracted by a yet unidentified base in the active site. The enzymatic reaction is completed by the reduction of the methylene of **20** *via* hydride transfer from C6 of the reduced cofactor **21**, which is simultaneously oxidized at the N^5–C6 bond to form FH_2. At the same time β-elimination of the sulfhydryl anion from C6 in **22** occurs to reform the double bond affording the product, dTMP which is then released from the active site.

6.3. Binding of TS inhibitors.

The crystal structure of the ternary complex of human TS with dUMP and PMX has been solved at 1.9 Å resolution. PMX is a 6-5 fused TS inhibitor with the pyrrolo[2,3-*d*]pyrimidine instead of 6-6 fused pteridine or quinazoline rings of other antifolates (Figure 20).[231] The ternary structure of human TS-dUMP- PMX reveals that PMX is anchored in the active site by aromatic stacking between the fused pyrrolo[2,3-*d*]pyrimidine ring system and the dUMP pyrimidine ring. In addition to the hydrogen bond between the donor exocyclic amino group (N^{10}) of PMX to Ala312 O, there is another between the donor amino group (N^3) of PMX and the O of Asp218.

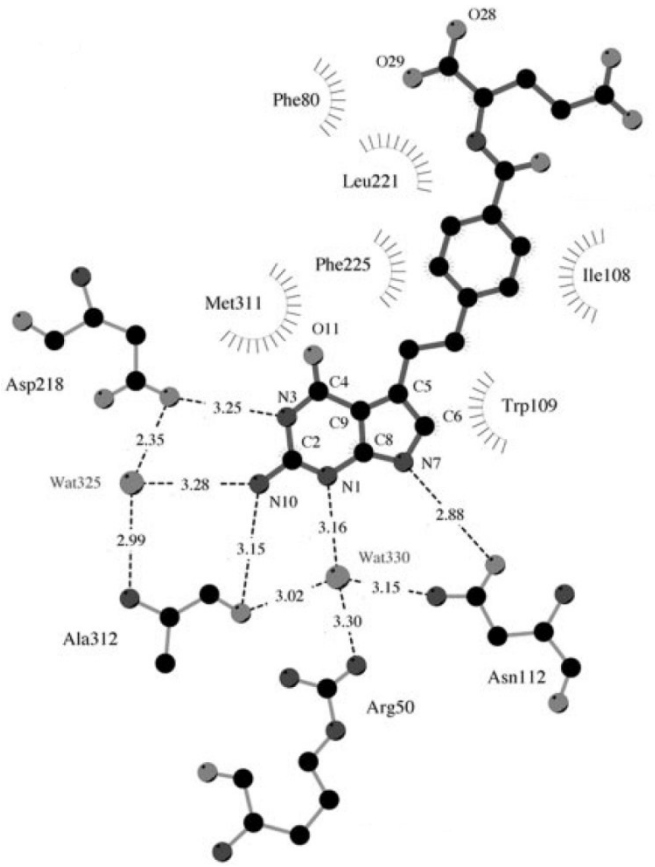

Figure 20 The interactions in the complex of hTS-dUMP-PMX.[231]

A conserved water molecule (Wat330) donates a hydrogen bond to the acceptor N^1 of the pyrrolo[2,3-*d*]pyrimidine ring, and donates another to either the Ala312 O atom or to Val313 O. Wat330 is surrounded in a tetrahedral arrangement by these two acceptors and two hydrogen bond donors (Arg50 -NH, and Asn112 -NH), enabling the water molecule to completely satisfy its hydrogen bonding potential. An additional specific hydrogen bond is also observed between the donor N^7 H of PMX and O atom of Asn112.

The PABA ring of PMX is surrounded by hydrophobic side-chains: Ile108, Leu221, Phe225 and Met311. This hydrophobic environment provides several favorable interactions important to the tight binding of folate-based inhibitors. The negatively

charged glutamic acid tail occupies a shallow, positively charged groove on the enzyme surface. The Glu carboxyl group interacts with the highly conserved Lys77 –N atom, and may form water-mediated hydrogen bonds to this group, as in other TS inhibitors.

6.4. TS inhibitors

PDDF[238, 239] (Figure 5) was the first quinazoline TS inhibitor to be tested clinically. Although PDDF was active in phase I, it resulted unpredictable and unacceptable renaltoxicity and hepatotoxicity which resulted in a discontinuation of any further clinical studies. The poor solubility, largely attributed to the presence of the 2-amino group in PDDF, probably caused the drug to precipitate within the renal tubules.

RTX[240] (Figure 5), the third generation analog of PDDF, was found to be more water soluble at low pH and has no significant renal toxicity. RTX is a TS inhibitor and is a good substrate for FPGS. Once polyglutamylated, RTX is more than 100-fold more potent as an inhibitor of TS than the monoglutamylated drug. RTX is currently approved for clinical use in Europe and Japan.

PMX[241] (Figure 5), an antifolate originally developed as a TS inhibitor, is a multitargeted agent, which possesses a 6-5 fused pyrrolo[2,3-*d*]pyrimidine instead of the more common 6-6 fused pteridine or quinazoline ring structure. Preliminary studies[187, 242] revealed that PMX polyglutamates are not only potent inhibitors of TS but also of AICARFTase , DHFR and GARFTase. PMX has been approved by FDA for the treatment of malignant pleural mesothelioma in combination with cisplatin and recently in non small lung cancer in the United States and has provided a renewed interest in the

development of classical antifolates as antitumor agents.

Plevitrexed[243] (Figure 5) is classical compound that does not depend on FPGS for its activity, however it uses the RFC system for its entry into the cell. This compound resulted from a series of studies aimed at developing water-soluble, nonpolyglutamylatable TS inhibitors.

7. Multiple targeted antifolates in combinational anticancer chemotherapy

It has been of interest not only to design potent antifolates against specific enzymes of DHFR, TS, GARFTase and AICARFTase but also to design and synthesize single agents that have potent multiple inhibitory activity against these enzymes.[244, 245] This strategy is particularly promising in anticancer chemotherapy against the multiple drug resistant cancers. Such a single agent could act at more than one active site and provide "combination chemotherapy" benefits including: circumvent the pharmacokinetic problems of multiple agents, avoid of drug-drug interactions, used at lower doses to alleviate toxicity, devoid of overlapping toxicities, and most importantly delay or prevent cancer drug resistance.[246-248] Other advantages of such single agents are in the reduced cost and increased patient compliance. In addition, the clinical success of pemetrexed provides a good example of multiple targeted antifolates used in combinational anticancer chemotherapy. [244, 245, 249, 250]

As summarized before, PMX is a multitargeted antifolate (MTA) that inhibit DHFR, GARFTase and AICARFTase in addition to TS, which is the primary intracellular target.

The clinical success of pemetrexed has generated renewed interest in the design of single agents that function as multitargeted inhibitors against more than one target.

It has been our long-standing goal to design and synthesize single agents that are potent multitargeted inhibitors against folate metabolism enzymes.

II. CHEMICAL REVIEW

The chemistry related to the present work is reviewed and includes synthetic approaches to the following heterocyclic systems and relevant reactions:

1. Synthesis of pyrrolo[2,3-*d*]pyrimidines
2. Sonogashira coupling in antifolate synthesis
3. Heck coupling reaction in one-step aldehyde synthesis

1. Synthesis of pyrrolo[2,3-*d*]pyrimidines

A large quantity of literature has been disclosed for the synthesis of pyrrolo[2,3-*d*]pyrimidines because of their application as deazapurine analogs. The synthetic strategies to this 6-5 bicyclic ring system have three general classifications from:

1. furan precursors
2. pyrimidine precursors
3. pyrrole precursors

1.1. From furan precursors

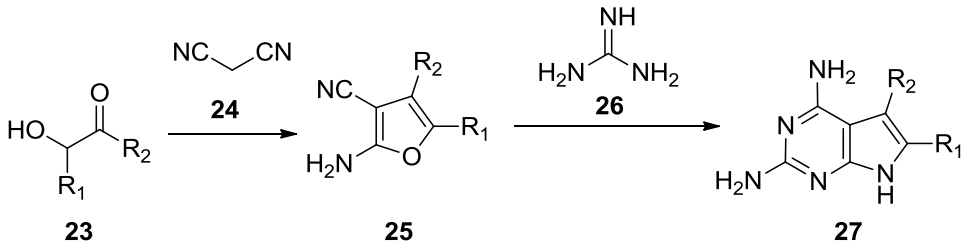

Scheme 1 Synthesis of 2,5,6-trisubstitutedpyrrolo[2,3-*d*]pyrimidines **27**.

Taylor and coworkers[251] reported a general method to 2,5,6-trisubstituted-4-amino-pyrrolo[2,3-*d*]pyrimidines **27** in 1995 (Scheme 1). Condensation of appropriate α-hydroxyketones **23** with malonodinitrile **24** afforded the corresponding 2-amino-3-cyanofurans **25** which on cyclization with amidines **26** afforded the corresponding 2,4-diamino-pyrrolo[2,3-*d*]pyrimidines **27** by an unexpected ring transformation/ring annulation sequence.

1.2. From pyrimidines precursors

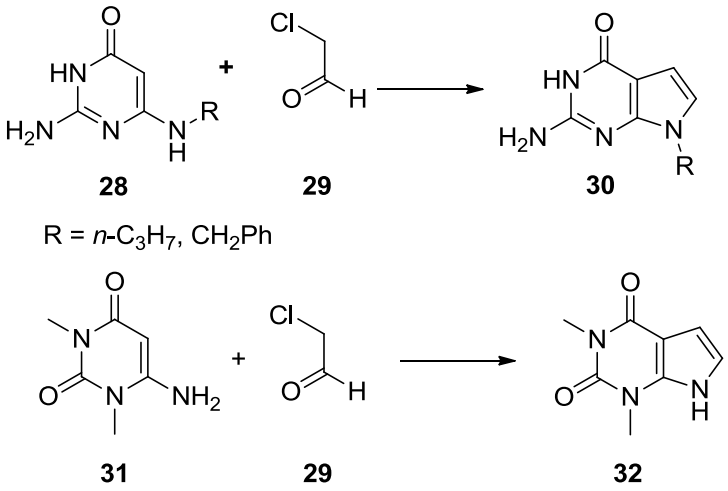

Scheme 2 Synthesis of pyrrolo[2,3-*d*]pyrimidines **30** and **32**.

Noell and Robins[252] first reported in 1964 the synthesis of pyrrolo[2,3-*d*]pyrimidines **30** and **32** by the reaction of chloroacetaldehyde **29** with 2-amino-6-alkylamino-4-hydroxypyrimidines **28** and 6-amino-1,3-dimethyluracil, **31** respectively (Scheme 2).

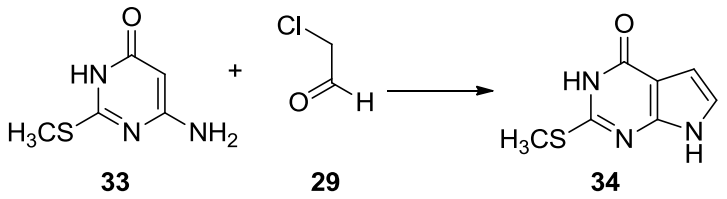

Scheme 3 Synthesis of pyrrolo[2,3-*d*]pyrimidine **34**.

In the same report, Noell and coworkers[252] also reported the synthesis of pyrrolo[2,3-*d*]pyrimidine **34** from 2-methylthio-6-amino-4-pyrimidone **33** and chloroacetaldehyde **29** (Scheme 3).

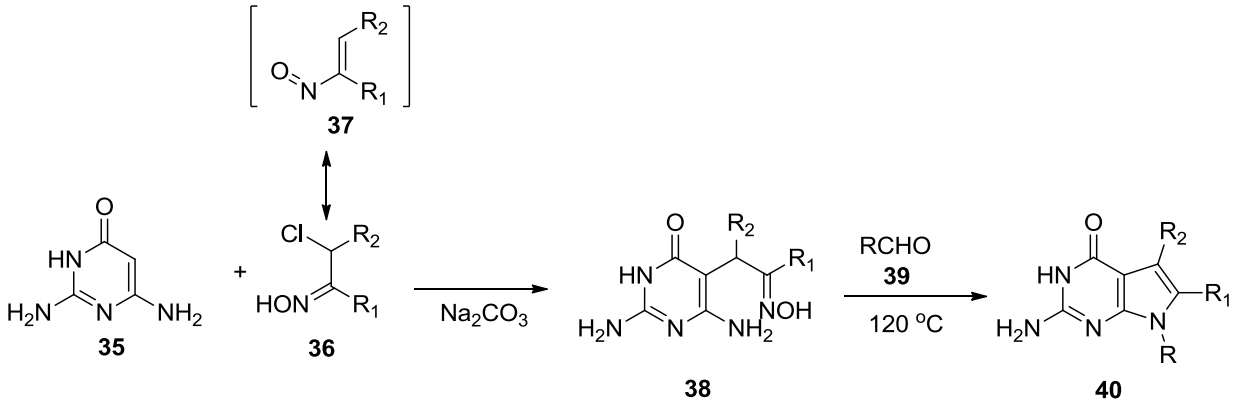

Scheme 4 Synthesis of pyrrolo[2,3-*d*]pyrimidines **40**.

Gibson *et al*.[253] reported in 1998 a synthetic approach to prepare 2-amino-4-oxo-pyrrolo[2,3-*d*]pyrimidines **40** (Scheme 4). In this report, 2,6-diamino-4-hydroxypyrimidine **35** was reacted with a biselectrophile, an oxime **36**, in the presence of a weak base (sodium carbonate, sodium acetate, or triethylamine) to afford the C-5 alkylated pyrimidine derivatives **38**. No side products resulting from substitution at any other position were isolated. Cyclization of pyrimidine derivatives **38** at 120 °C under acid-catalyzed transoximation with benzaldehyde or acetaldehyde **39** afforded substituted

pyrrolo[2,3-*d*]pyrimidines **40**.

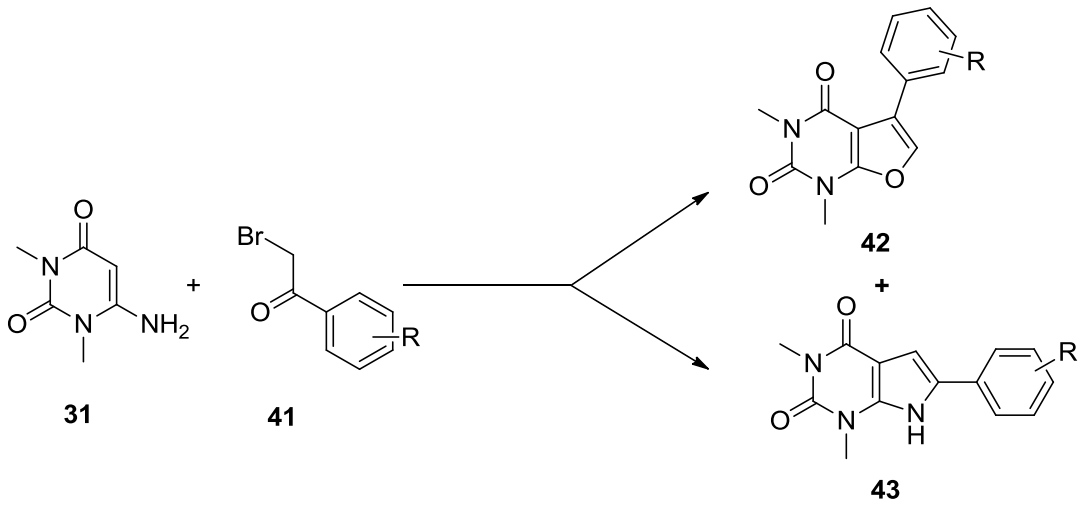

Scheme 5 Synthesis of furo[2,3-*d*]pyrimidines **42** and pyrrolo[2,3-*d*]pyrimidines **43**.

Fumio *et al*.[254] reported in 1973 that the reaction of 6-amino-1,3-dimethyluracil **31** with phenacyl bromides **41** in DMF afforded 1,3-dimethyl-6-phenylpyrrolo[2,3-*d*]pyrimidines **43** in 69-74% yields (Scheme 5). The reaction of **31** and **41** in acetic acid afforded 1,3-dimethyl-5-phenylfuro[2,3-*d*]pyrimidine-2,4(1*H*,3*H*)-diones **42** as a by-product.

Secrist and Liu[255] provided a detailed study of the reaction of 2,6-diamino-4-hydroxypyrimidine **35** with various α-halo aldehydes and ketones (Scheme 6) in 1978. They reported that the cyclization occurred *via* two different modes to produce either the pyrrolo[2,3-*d*]pyrimidine and/or the furo[2,3-*d*]pyrimidine. Thus α-halo ketones, chloroacetone **44** and 3-bromo-2-butanone **45**, afforded both the furo[2,3-*d*]pyrimidine **47** and the pyrrolo[2,3-*d*]pyrimidine **46**, whereas **45** afforded only the pyrrolo[2,3-*d*]pyrimidine **46** on reaction with **35**. It was concluded that a critical electron density is

necessary at the C5 of the pyrimidine nucleus for it to react with the α-carbon atom of the α-halo aldehydes or ketones to afford exclusively pyrrolo[2,3-*d*]pyrimidines.

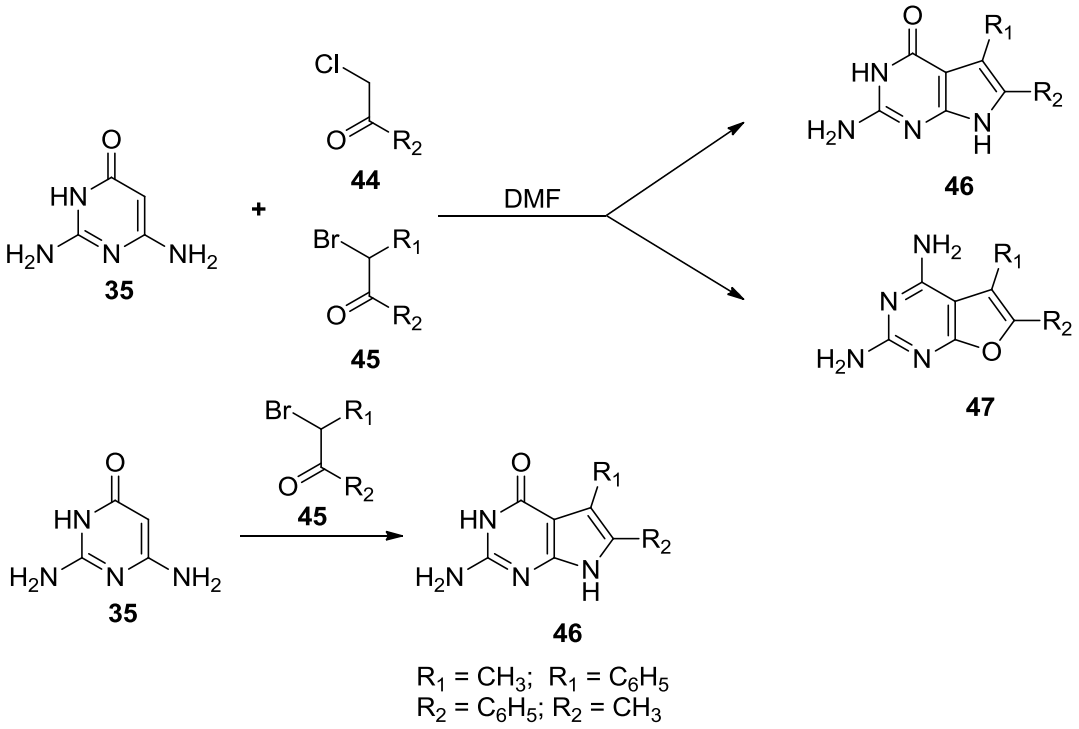

Scheme 6 Synthesis of pyrrolo[2,3-*d*]pyrimidines **46** and furo[2,3-*d*]pyrimidines **47**.

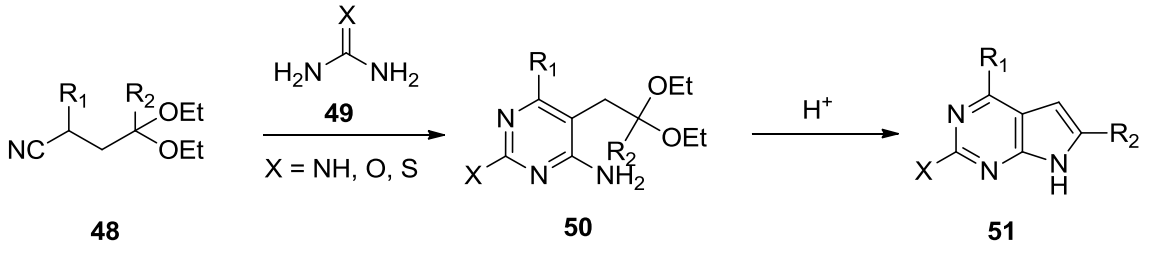

Scheme 7 Synthesis of pyrrolo[2,3-*d*]pyrimidines **51**.

Davoll and coworker[256] reported in 1960 the synthesis of various pyrrolo[2,3-

d]pyrimidines **51** (Scheme 7) by an acid mediated cyclization of suitable pyrimidine 5-acetone or acetaldehyde side-chains onto the neighboring amino group. The pyrimidines were obtained from the acetals ethyl(2,2-diethoxyethyl)acetate **48**, or 2,2-diethoxyethylmalonodinitrile, or their ketal derivatives respectively and cyclization with guanidine, urea or thiourea **49**.

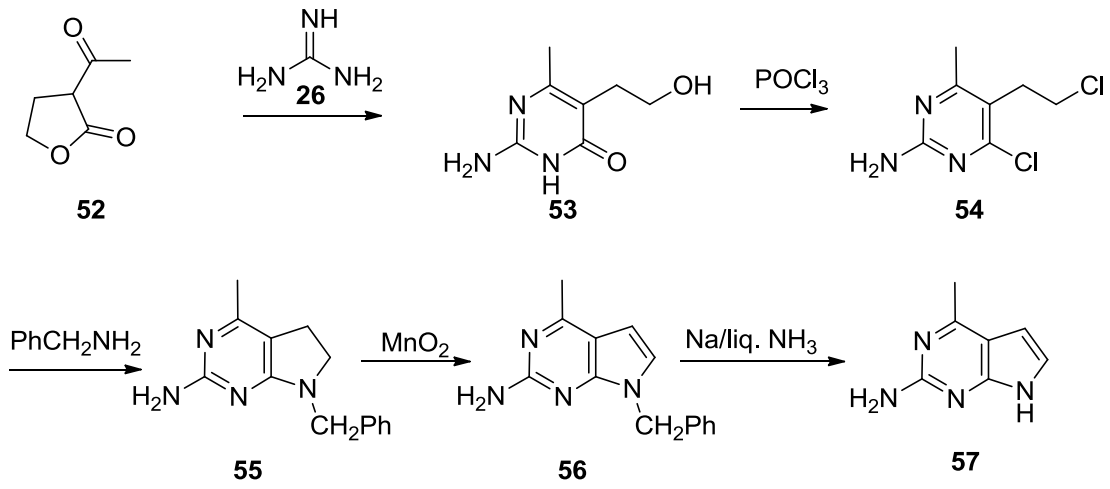

Scheme 8 Synthesis of 2-amino-4-methyl pyrrolo[2,3-*d*]pyrimidine **57**.

Gangjee and coworkers[257] reported in 2000 the synthesis of 2-amino-4-methyl-pyrrolo[2,3-*d*]pyrimidine **57** (Scheme 8) *via* a novel ring closure method. The synthesis started with condensation of 2-acetylbutyrolactone **52** with guanidine carbonate **26** to afford the substituted pyrimidine **53**. Chlorination with $POCl_3$ provided the dichloro compound **54** which was in turn condensed with benzylamine to afford 2-amino-4-methyl-7-(*N*-benzyl)piperidinyl[2,3-*d*]pyrimidine **55**. Oxidative aromatization of this compound with MnO_2 provided the N^7-benzylated compound **56**. Compound **57** was afforded following debenzylation of **56** with metallic sodium in ammonia.

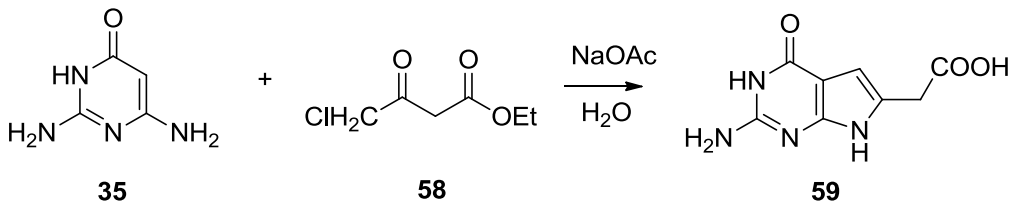

Scheme 9 Synthesis of 2-(2-amino-4-oxo-4,7-dihydro-1*H*-pyrrolo[2,3-*d*]pyrimidin-6-yl)acetic acid **59**.

Gangjee and coworkers[258] reported in 2001 the synthesis of 2-(2-amino-4-oxo-4,7-dihydro-1*H*-pyrrolo[2,3-*d*]pyrimidin-6-yl)acetic acid **59** from the condensation of 2,6-diaminopyrimidin-4(1*H*)-one **35** with ethyl 4-chloro-3-oxobutanoate **58** in the presence of sodium acetate (Scheme 9).

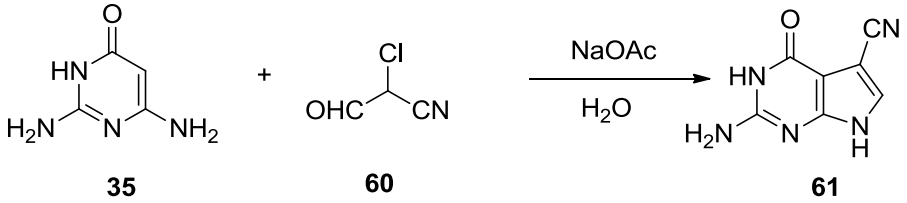

Scheme 10 Synthesis of 2-amino-4-oxo-4,7-dihydro-1*H*-pyrrolo[2,3-*d*]pyrimidine-5-carbonitrile **61**.

In another report of 2001, Gangjee and coworkers[259] also reported the synthesis of 2-amino-4-oxo-4,7-dihydro-1*H*-pyrrolo[2,3-*d*]pyrimidine-5-carbonitrile **61** (Scheme 10) from the condensation of compound **35** with 2-chloro-3-oxopropanenitrile **60** under basic conditions.

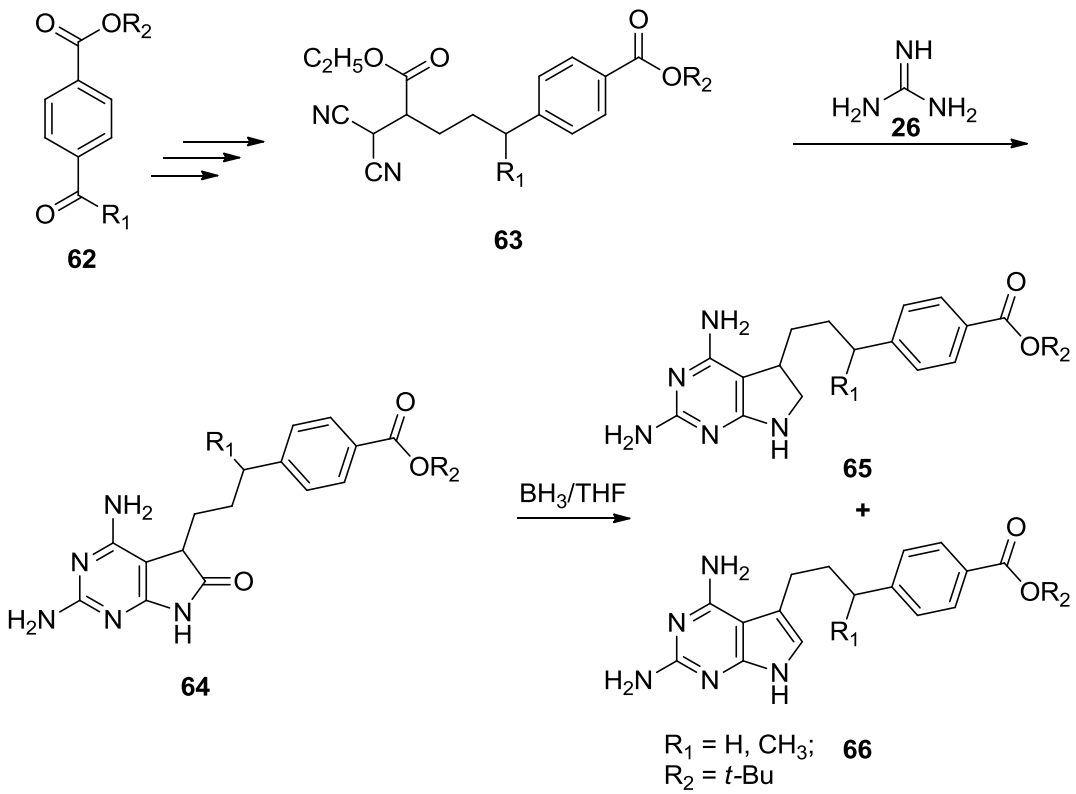

Scheme 11 Synthesis of 2,4-diamino-5-arylalkyl substituted pyrrolo[2,3-*d*]pyrimidine **66**.

Miwa and coworkers[260] reported in 1991 the synthesi of a series of 2,4-diamino-5-arylalkyl substituted classical pyrrolo[2,3-*d*]pyrimidine antifolates (Scheme 11). In this report, the ring system was constructed by the condensation of guanidine **26** and the malonodinitrile derivative **63**. The resulting lactam **64** was subjected to borane reduction to provide the pyrrolo[2,3-*d*]pyrimidine intermediate **66** along with its 5,6-dihydro analog **65**, which were separated by flash chromatography in 45% and 46% yields, respectively.

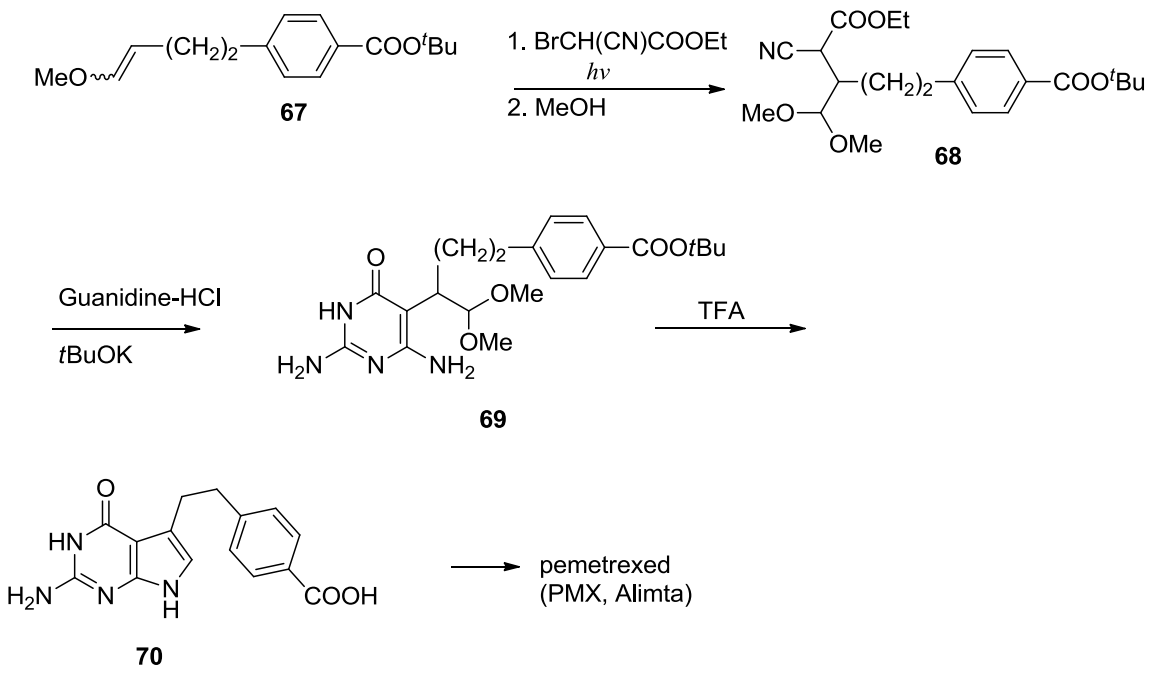

Scheme 12 Synthesis of 5-substituted pyrrolo[2,3-*d*]pyrimidine **70**.

Miwa and coworkers[260] reported in 1993 a synthesis of pemetrexed utilizing the spontaneous cyclization of 6-amino-5-pyrimidylacetaldehyde for the synthesis of pemetrexed (Scheme 12). The synthesis of the acetal protected aldehyde **68** was a photo-initiated free radical addition of ethyl bromocyanoacetate to the corresponding enol ether **67**. The reaction of the enol ether **67** with ethyl bromocyanoacetate in methanol under UV irradiation regioselectively afforded the acetal functionalized ethyl cyanoacetate **68**. Condensation of **68** and guanidine at reflux provided the acetal protected 6-amino-5-pyrimidylacetaldehyde **69**. Acid catalyzed deprotection of the dimethyl acetal and *t*-butyl moieties of **69** afforded 4-[2-(2-amino-4-oxo-pyrrolo[2,3-*d*]pyrimidin-5-yl)-ethyl]-benzoic acid **70**. Conversion of acid **70** to pemetrexed involved a standard peptide coupling with diethyl *L*-glutamate and final saponification.

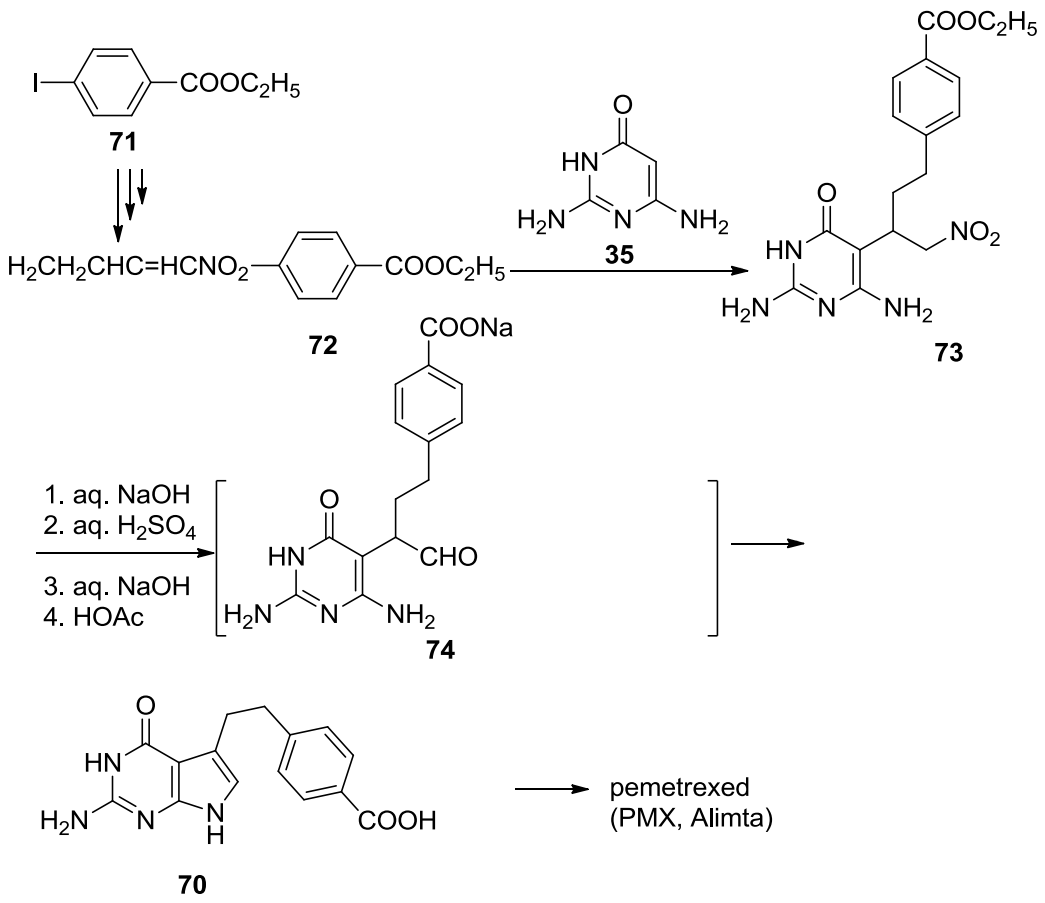

Scheme 13 Synthesis of PMX from 6-amino-5-pyrimidylacetaldehydes **74**.

Taylor and coworker[261] reported in 1999 a concise synthesis of PMX (Scheme 13) which involved the spontaneous cyclization of 6-amino-5-pyrimidylacetaldehydes **74** which was generated utilizing the Nef reaction with compound **73** onto the adjacent amino group. 2,4-Diamino-6-oxo-pyrimidine, **35** was known to form Michael adducts at its unsubstituted C-5 position.[262-266] The synthesis of **60** thus involved a Michael addition reaction between **35** and the Michael acceptor **72**, which was synthesized in three steps that involved a palladium-catalyzed cross-coupling[267] between methyl 4-iodobenzoate **71** and allyl alcohol, aldol condensation with nitromethane followed by dehydration with methanesulfonyl chloride in the presence of triethylamine.[268] As expected, the

condensation afforded the nitro derivative **73** in high yield. Compound **73** was then converted to 4-[2-(2-amino-4-oxo-7*H*-pyrrolo[2,3-*d*]pyrimidin-5-yl]ethylbenzoic acid **70** by the Nef reaction in a one-pot, five-step procedure. Conversion of acid **70** to pemetrexed involved a standard peptide coupling with diethyl L-glutamate using 2-chloro-4,6-dimethoxy-1,3,5-triazine as the activating agent in presence of *N*-methylmorpholine and final saponification.

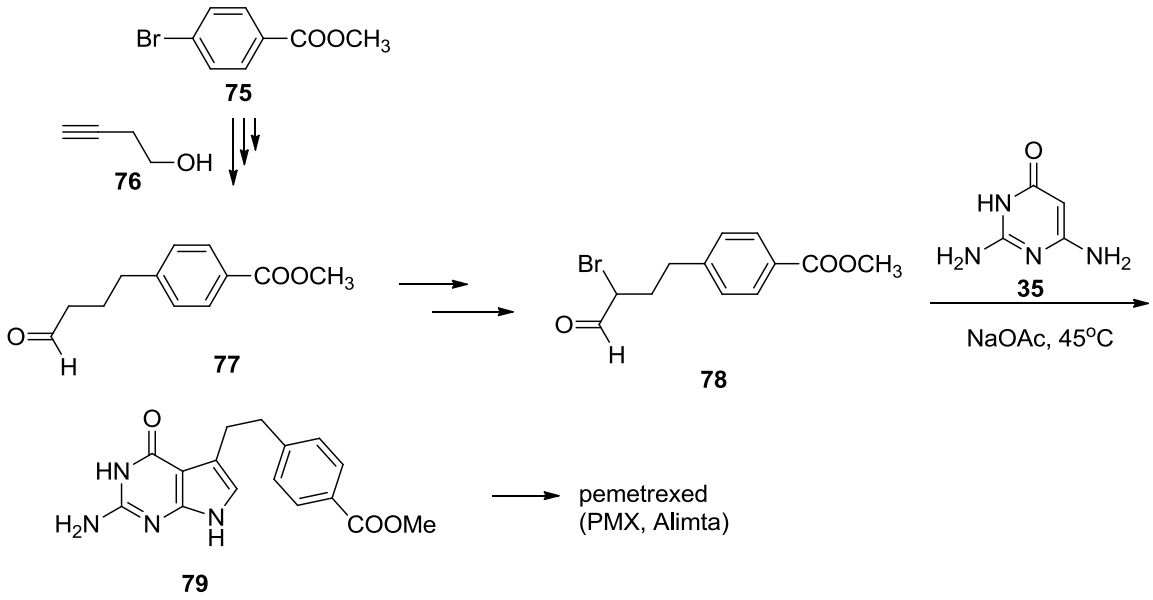

Scheme 14 Synthesis of PMX from α-bromo aldehyde **78**.

Barnett and coworker also reported[269] in 1999 a practical synthesis of PMX (Scheme 14) which involved the cyclization of 2-bromo-4-arylbutanal **78** with 2,4-diamino-6-oxo-pyrimidine **35** regioselectively provided 5-substituted pyrrolo[2,3-*d*]pyrimidine **79** as shown in Scheme 14. The key intermediate α-bromo aldehyde **78** was synthesized from aryl bromide **75** and alkyne **76** with Sonogashira coupling followed by reduction of the triple bond, oxidation to aldehyde and corresponding bromination of the aldehyde **78**.

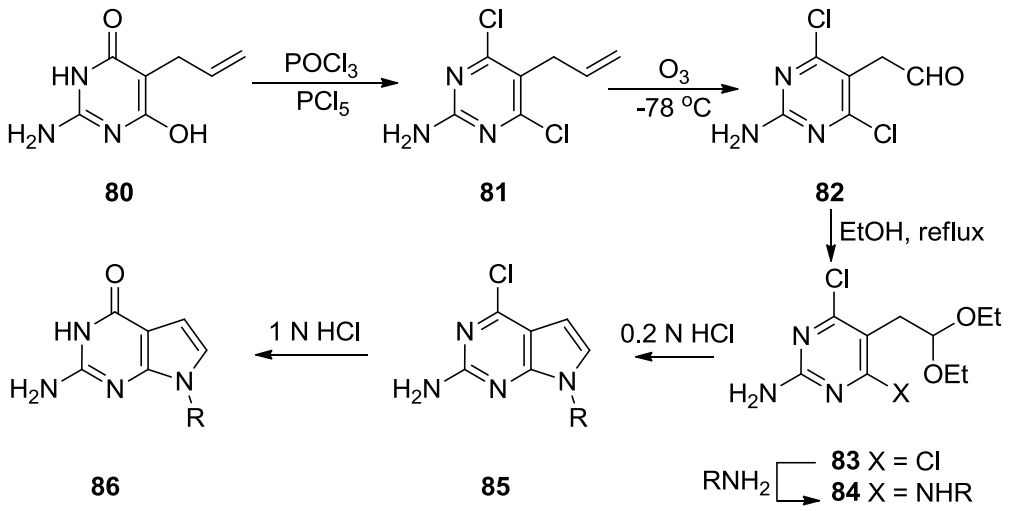

Scheme 15 Synthesis of 7-substituted pyrrolo[2,3-*d*]pyrimidines **86**.

Legraverend and coworkers[270] reported in 1985 the synthesis of pyrrolo[2,3-*d*]pyrimidines **86** from 2-amino-4,6-dichloro-5-(2,2-diethoxyethyl)pyrimidine **83** (Scheme 15). Thus, 5-allyl-2-amino-4,6-dihydroxypyrimidine **80**, prepared by the reaction of guanidine hydrochloride with diethyl allylmalonate, was converted to the 4,6-dichloro derivative **81** by reacted with $POCl_3$, and diethylaniline in the presence of PCl_5. The (2-amino-4,6-dichloropyrimidin-5-yl)acetaldehyde **82** was afforded from **81** by ozonolysis of the allyl group (Scheme 15). The diethylacetal **83** was prepared from its aldehyde **82** by using standard methods. The acetal **83** was cyclized to 2-amino-4-chloro-7-alkyl-7*H*-pyrrolo-[2,3-*d*]pyrimidine **85** by reacted with dilute aqueous HCl at room temperature. Final compound **86** was then obtained by hydrolysis of the 4-chloro group of **85** using 1 N HCl at 100 °C.

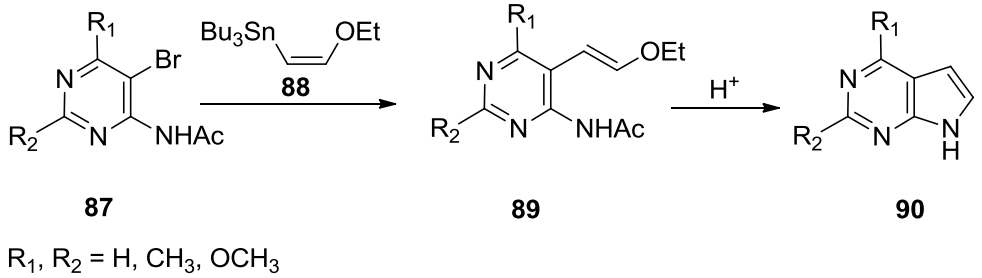

87 **89** **90**

R_1, R_2 = H, CH_3, OCH_3

Scheme 16 Synthesis of pyrrolo[2,3-*d*]pyrimidines **90**.

Sakamoto and coworkers[271] reported in 1993 the synthesis of pyrrolo[2,3-*d*]pyrimidines **90** by utilizing an intramolecular cyclization of protected 5-acetaldehyde pyrimidines **89** (Scheme 16). Compounds **89** were synthesized by palladium (0) catalyzed coupling of the appropriate 2,4-disubstituted-5-bromo-6-acetamido pyrimidine **87** with (*Z)*-1-ethoxy-2-(tributylstannyl)ethane **88**. The same methodology was also applicable for the synthesis of pyrrolo[3,2-*d*]pyrimidines, except that, 5-acetylamino-4-iodopyrimidine was used as the starting material.

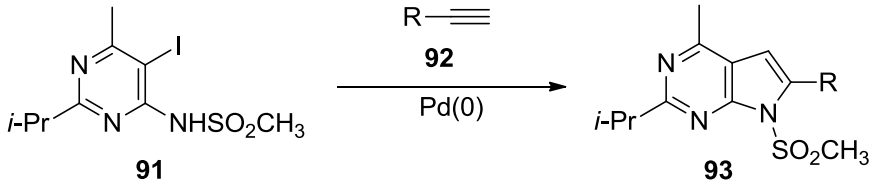

91 **93**

Scheme 17 Synthesis of 4-methyl pyrrolo[2,3-*d*]pyrimidines **93**.

Kondo *et al*.[272] reported the synthesis of 4-methyl pyrrolo[2,3-*d*]pyrimidine **93** *via* a palladium(0) catalyzed cross-coupling of terminal acetylenes **92** with *N*-(5-halo-4-pyrimidinyl)methane sulfonamides **91** (Scheme 17).

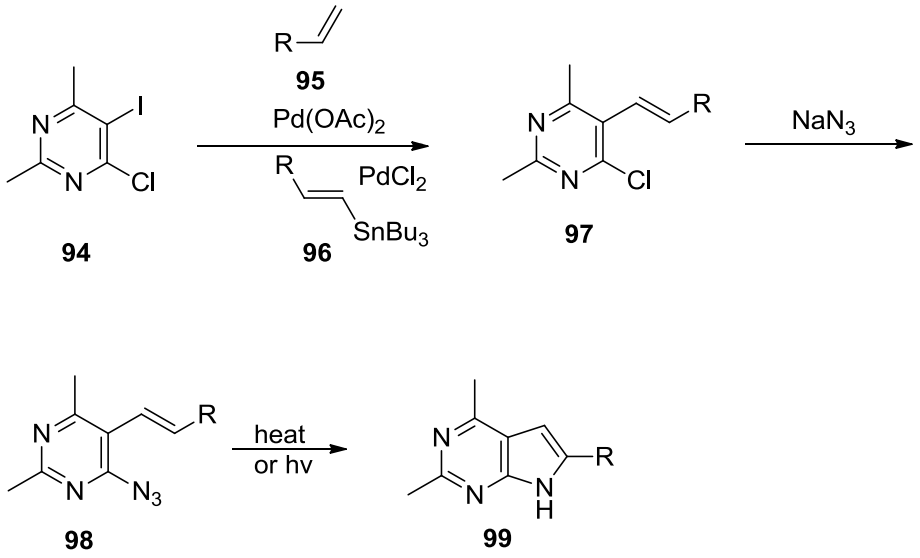

Scheme 18 Synthesis of 2,4-dimethyl pyrrolo[2,3-*d*]pyrimidines **99**.

In the same report, Kondo and coworkers[272] also reported the synthesis of 2,4-dimethyl pyrrolo[2,3-*d*]pyrimidine **99** *via* a photoinduced or thermal cyclization of 4-azidopyrimidines **98** containing an olefinic functionality at the 5-position (Scheme 18). Intermediates **98** were obtained by a palladium catalyzed cross-coupling between the 5-iodopyrimidine **94** and appropriate stannanes **95**, followed by nucleophilic displacement of the 4-chloro in pyrimidine **97** in the presence of sodium azide.

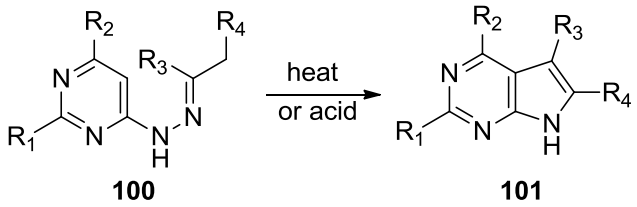

Scheme 19 Synthesis of pyrrolo[2,3-*d*]pyrimidines **101** *via* Fischer indole cyclization.

Another report employed the Fischer indole cyclization of 4-pyrimidinylhydrazones **100** (Scheme 19) to afford the pyrrolo[2,3-*d*]pyrimidine ring

system **101**.[273-277] The applicability of the Fischer-indole cyclization to the synthesis of pyrrolo[2,3-*d*]pyrimidines, however, is limited by the high reaction temperature and the steric constraints for the [3,3] sigmatropic rearrangement involved in the mechanism.

1.3. From Pyrroles

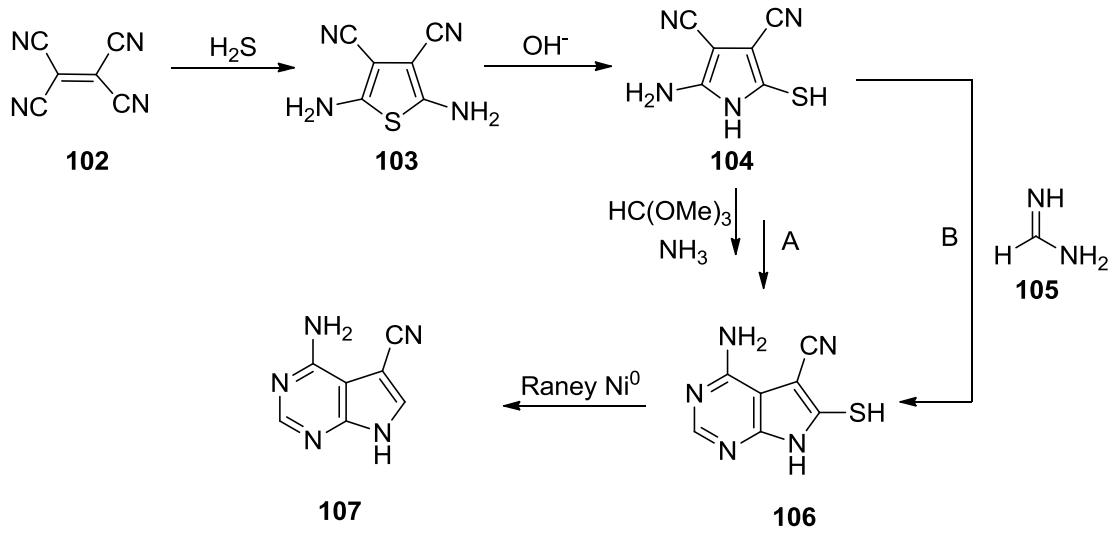

Scheme 20 Synthesis of 4-amino-5-cyanopyrrolo[2,3-*d*]pyrimidine **107**.

Taylor and coworkers[278] reported in 1965 the synthesis of 4-amino-5-cyano-pyrrolo[2,3-*d*]pyrimidine **107** (Scheme 20) starting from the tetracyanoethylene **102** *via* 2-mercapto-3,4-dicyano-5-aminopyrrole **104**.[279] Reaction of **104** with triethylorthoformate followed by ammonia (as shown in route A) resulted in the formation of a formamidine intermediate which then cyclized to **106**. The mercapto group of **106** could be removed by Raney nickel to afford **107**. Formamidine acetate **105** also condensed with **104** to give **106** but in lower yields as shown in route B.

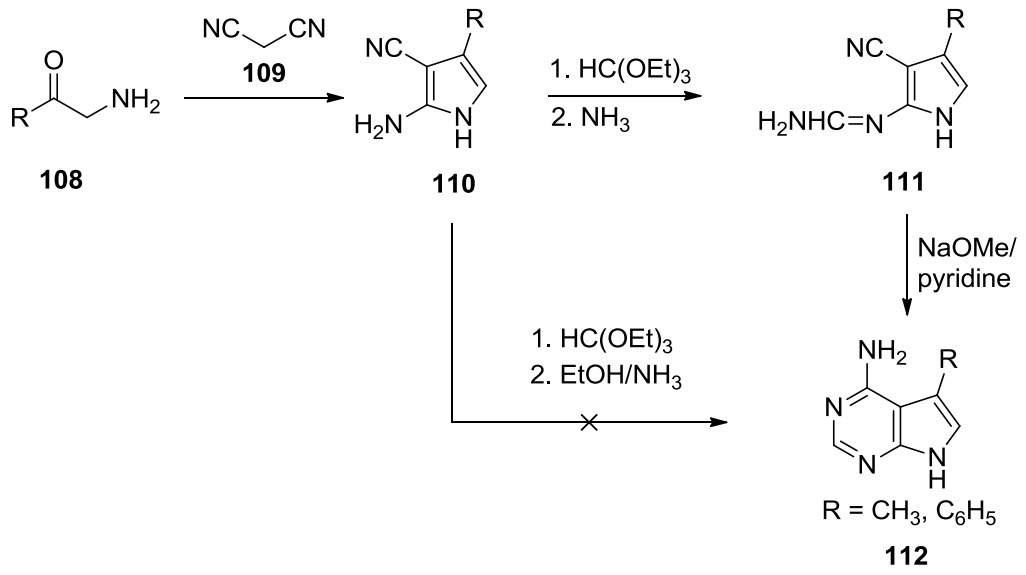

Scheme 21 Synthesis of 4-amino-5-substituted pyrrolo[2,3-*d*]pyrimidines **112**.

In the same report, Taylor and coworkers[278] also reported synthesized 4-amino-5-methyl-pyrrolo[2,3-*d*]pyrimidine **112** (R = CH_3, C_6H_5) (Scheme 21) from 2-amino-3-cyano-5-substituted pyrroles **111** which were obtained from malonodinitrile **109** and the appropriate *α*-aminoketones **108**. Treatment of pyrrole **110** with triethylorthoformate followed by ammonia resulted in a failure to afford the desired pyrrolo[2,3-*d*]pyrimidine **110**. The fact that pyrroles **110** did not cyclize to pyrrolo[2,3-*d*]pyrimidine **112** in ethanolic ammonia was attributed to the absence of the second nitrile.

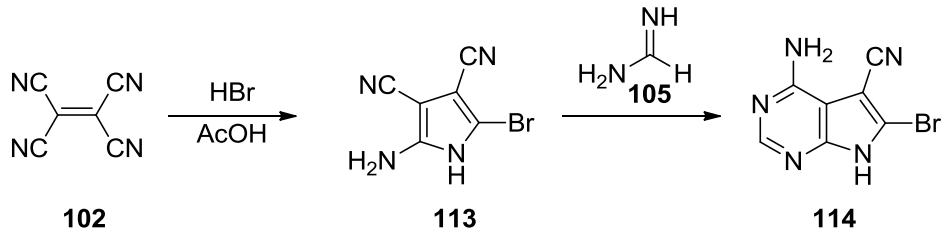

Scheme 22 Synthesis of 5,6-disubstitutedpyrrolo[2,3-*d*]pyrimidine **114**.

Tolman and coworkers[280] reported in 1968 the synthesis of pyrrolo[2,3-*d*]pyrimidine **114** by cyclization of 2-amino-5-bromo-3,4-dicyanopyrrole **113** with formamidine acetate **91a** (Scheme 22). Ramasamy and coworkers[281] also utilized the pyrrole **105** to form the pyrrolo[2,3-*d*]pyrimidine ring system for use in nucleoside synthesis. Swayze and coworkers [282] reported the synthesis of the versatile pyrrole **113** in an efficient one-step reaction from tetracyanoethylene **102**. On controlled addition of HBr in acetic acid, **113** undergoes an intramolecular self-condensation to afford **114**.

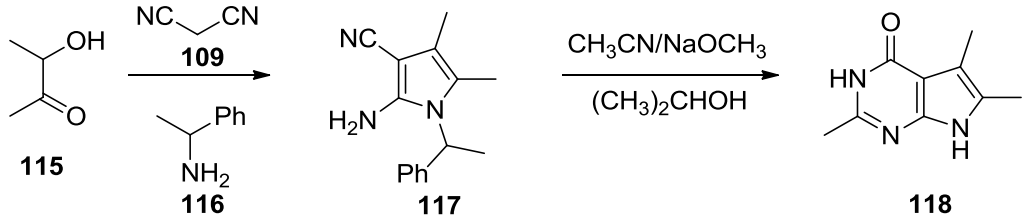

Scheme 23 Synthesis of 2,5,6-trimethyl pyrrolo[2,3-*d*]pyrimidine **118**.

Eger and coworkers[283, 284] reported in 1987 the synthesis of 2,5,6-trimethyl pyrrolo[2,3-*d*]pyrimidine **118** (Scheme 23) from 1-(1-phenylethyl)-2-amino-3-cyano-4,5-dimethylpyrrole **117** by heating with a mixture of acetonitrile and sodium methoxide. The pyrrole **117** was obtained by cyclocondensation of 3-hydroxy-2-butanone **115**, 1-phenyl-ethylamine **116** and malonodinitrile **109**.

Chen and coworkers[285] reported an efficient synthesis of pyrrolo[2,3-*d*]pyrimidine **125** (Scheme 24): Acetone **119** was condensed with malonodinitrile **109** to afford **120**. Bromination of **120** by NBS and benzoyl peroxide in chloroform afforded **121**; Cyclization of **121** with aryl amine **122** afforded the substituted pyrrole intermediate **123**. Compound **123** was then elaborated to the pyrrolo[2,3-*d*]pyrimidine **125**.

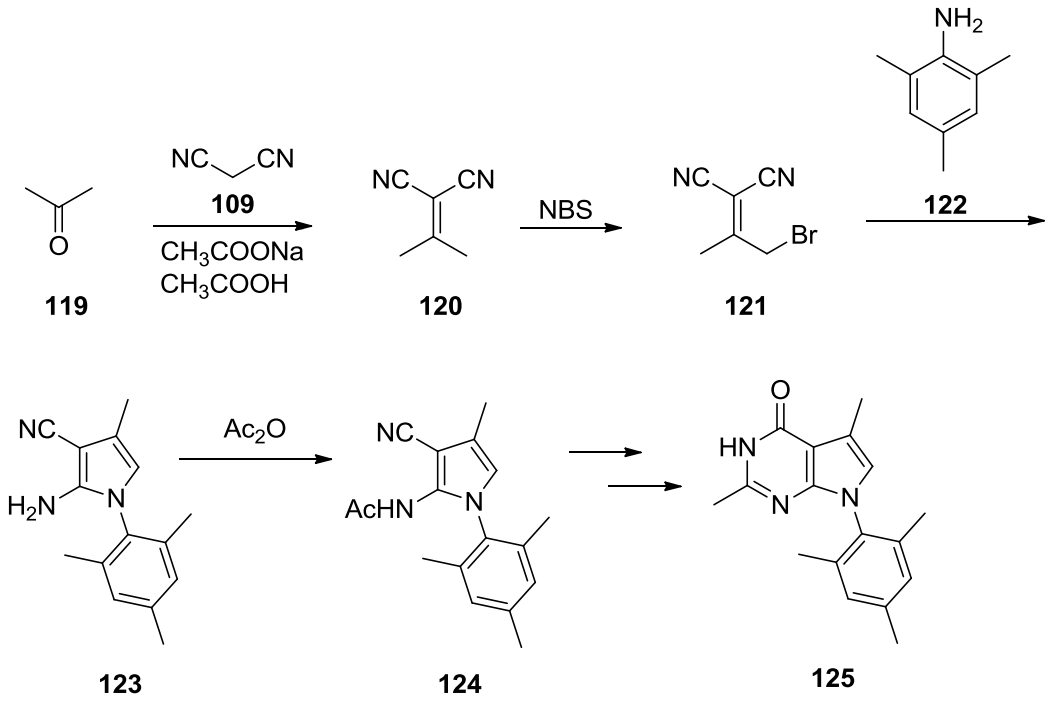

Scheme 24 Synthesis of 2,5,-dimethyl-N^7-substitutedpyrrolo[2,3-*d*]pyrimidine **125**.

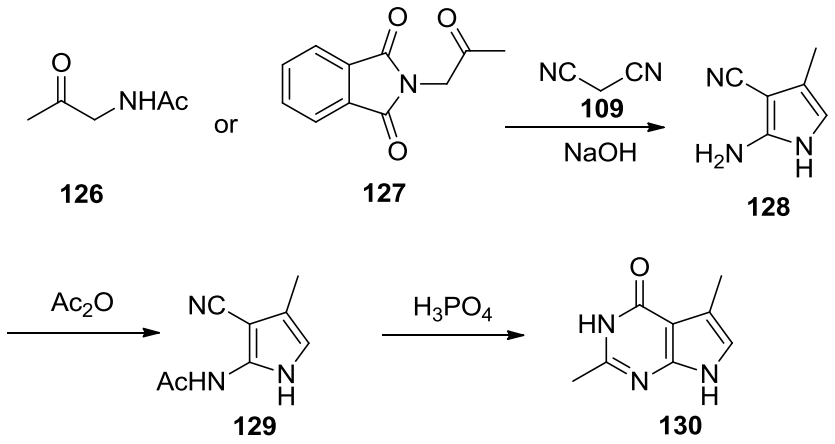

Scheme 25 Synthesis of 2,5-dimethyl pyrrolo[2,3-*d*]pyrimidine **130**.

Girgis and coworkers[286] reported in 1985 the synthesis of 2,5-dimethyl pyrrolo[2,3-*d*]pyrimidine **130** (Scheme 25) from 2-acetylamino-3-cyano-4-methylpyrrole **129** by heating with 85% phosphoric acid. The pyrrole **129** was obtained by acetylation

of 2-amino-3-cyano-4-methylpyrrole **128** with acetic anhydride. Cyclocondensation of **126** or **127** with malonodinitrile **109** by sodium hydroxide afforded the precursor pyrrole **128**.[287, 288]

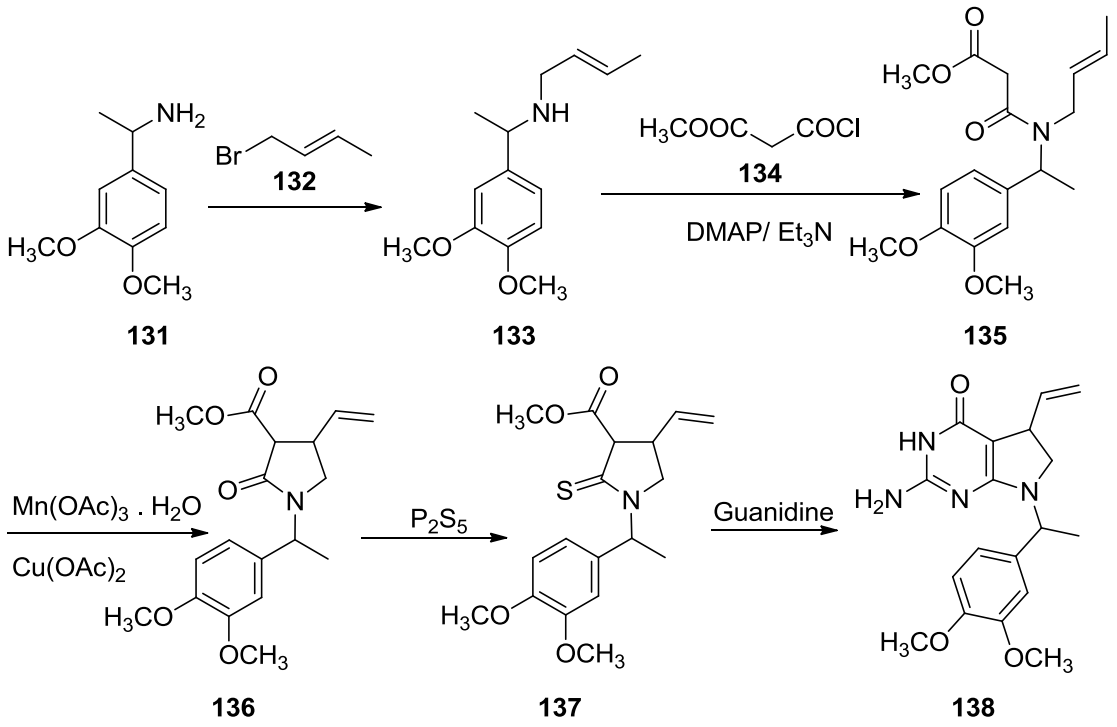

Scheme 26 Synthesis of N^7-substituted analogs of PMX **138**.

Taylor and coworkers[289] reported in 2001 the synthesis of a pyrrolo[2,3-*d*]pyrimidine analog of PMX **138** by a novel route (Scheme 26). A manganic triacetate dihydrate catalized radical cyclization of racemic methyl *N*-crotyl-*N*-[1-(3,4-phenyl)-eth-1-yl)malonamide **135**, afforded a diastereomeric mixture of the 3-carbomethoxy-2-pyrrolidinone **136**.[290] Compound **135** was afforded by alkylation of racemic 1-(3,4-dimethoxy-phenyl)-ethylamine **131** with crotyl bromide **132** followed by a DMAP catalyzed acylation with methyl malonyl chloride **134**. The pyrrolidinone **136** was converted to the thiolactam **137** with P_2S_5 followed by cyclocondensation with guanidine

to afford the N^7-protected 5,6-dihydro-5-allyl-pyrrolo[2,3-*d*]pyrimidine **138** successfully. This compound was then elaborated to afford analogs of PMX.

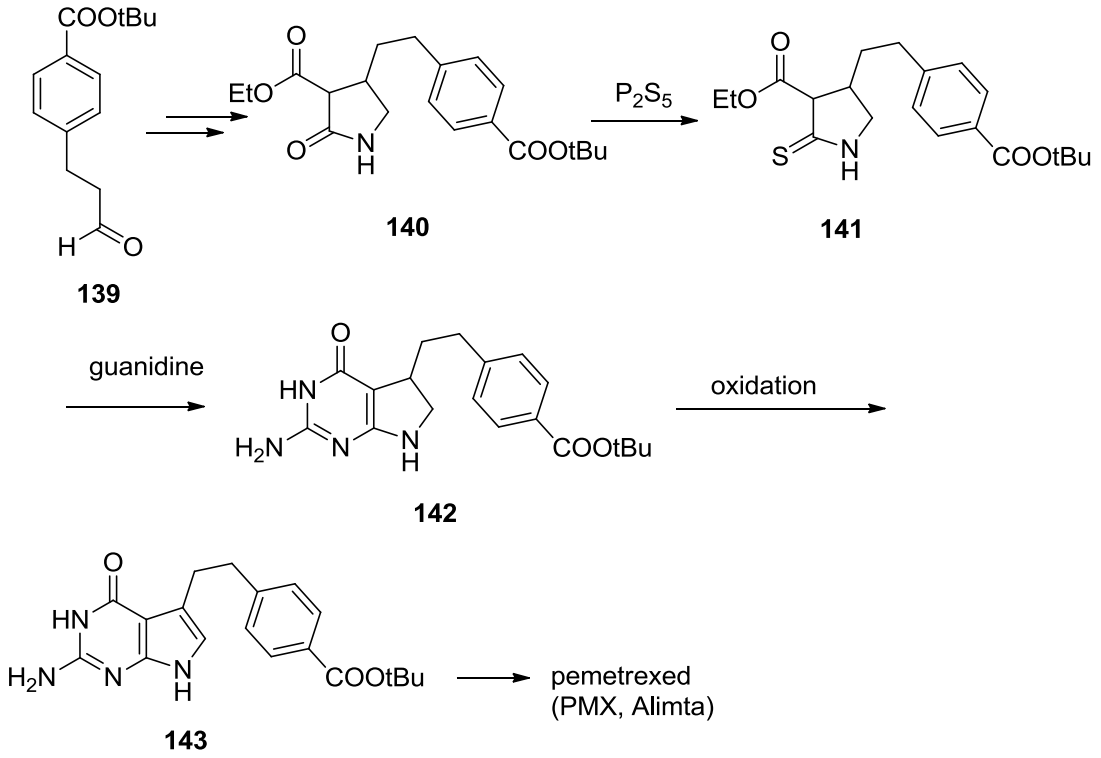

Scheme 27 Synthesis of PMX *via* a guanidine cyclization.

Barnett and coworkers[291] reported in 1993 the synthesis of a 2-amino-4-oxo-5,6-dihydropyrrolo[2,3-*d*]pyrimidine **142** *via* a guanidine cyclization of a preformed 3-carbethoxy-2-thiopyrrolidine intermediate **141** as the key step (Scheme 27). This intermediate **141** was prepared in several steps from 4-propionaldehyde benzoic acid *tert*-butyl ester **139**. Compound **142** was oxidized to the pyrrolo[2,3-*d*]pyrimidine intermediate **143**, which was then elaborated to PMX in several steps.

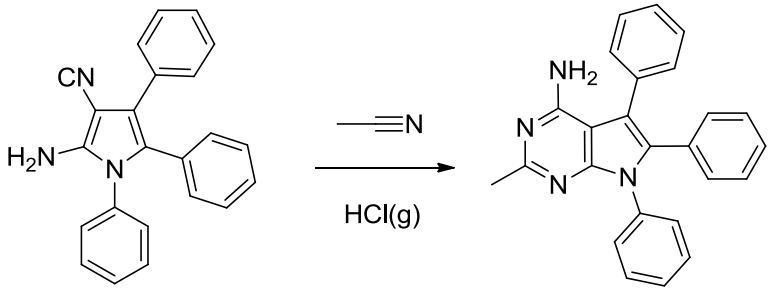

Scheme 28 Synthesis of 2-methyl-4-amino-pyrrolo[2,3-*d*]pyrimidine **145**.

Dave and coworkers[292] reported in 1980 a general procedure for the synthesis of condensed pyrimidines. The condensation between acetonitrile and substituted pyrrole **144** (scheme 28) under HCl (g) condition afforded 2-methyl pyrrolo[2,3-*d*]pyrimidine **145** in 60% yield.

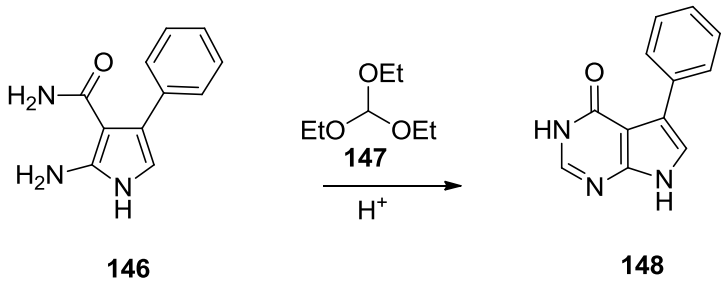

Scheme 29 Synthesis of 5-substituted 2-des-4-oxo-pyrrolo[2,3-*d*]pyrimidine **148**.

Bookser and coworkers[293] reported in 2005 the synthesis of pyrrolo[2,3-*d*]pyrimidine **148** (scheme 29) *via* the condensation between substituted pyrrole **146** and triethylorthoformate **147** under acidic conditions.

2. Sonogashira coupling in antifolate synthesis

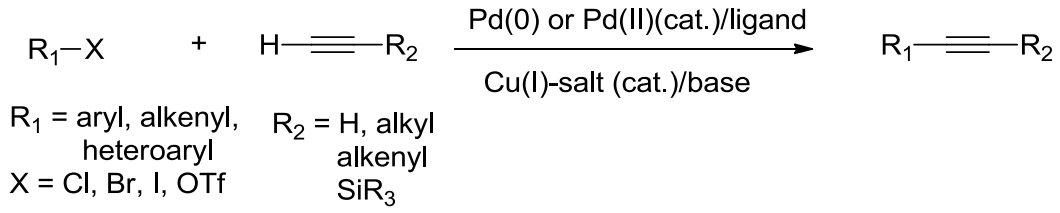

Scheme 30 A general transformation of Sonogashira coupling.[294, 295]

Sonogashira and coworkers[296] reported in 1975 the synthesis of symmetrically substituted alkynes *via* a coupling reaction between acetylene gas and aryl iodides or vinyl bromides in the presence of catalytic amounts of $Pd(PPh_3)Cl_2$ and CuI under mild conditions (Scheme 30). Thus, the copper-palladium catalyzed coupling of terminal alkynes with aryl and vinyl halides to give enynes is named the Sonogashira cross-coupling. Typically, two catalysts, a zerovalent palladium complex and a halide salt of copper (I), are necessary for the reaction. Copper (I) salts, such as copper (I) iodide, react with the terminal alkyne and produce a copper (I) acetylide, which acts as an activated species to increase the rate of the coupling reactions.[294] However, the copper-free Sonogashira coupling of aryl iodides with terminal acetylenes has been developed recently.[297-300] The Sonogashira coupling reaction also requires a base to neutralize the hydrogen halide produced as the byproduct of this coupling reaction. The reactivity order of the aryl and vinyl halides is as: I ≈ OTf > Br >> Cl.[294, 295]

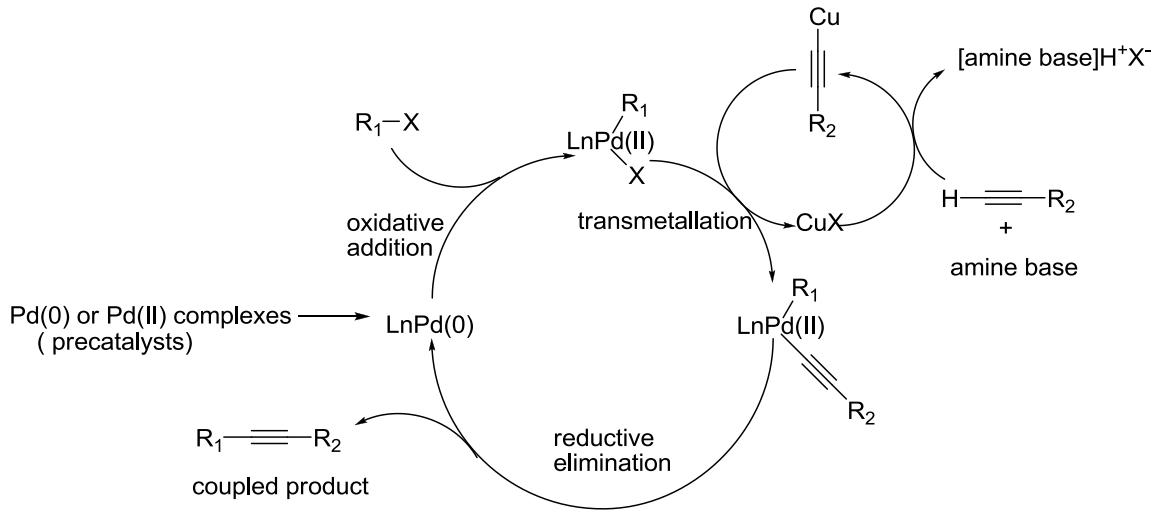

Scheme 31 Mechanism of Sonogashira cross-coupling.[301]

Sonogashira coupling is believed to involve oxidative addition-reductive elimination pathway (Scheme 31), although the mechanism is not clearly understood.

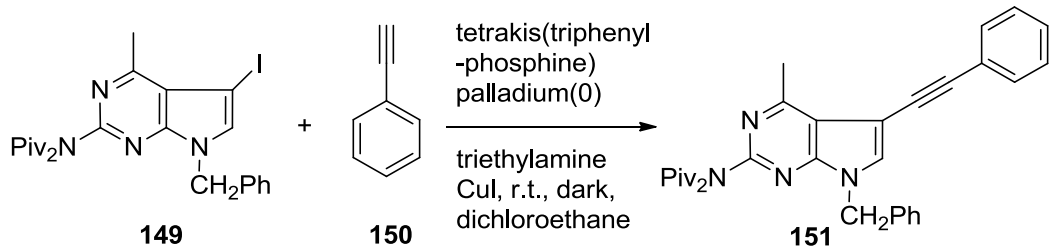

Scheme 32 Synthesis of *N*-(7-benzyl-4-methyl-5-(phenylethynyl)-7*H*-pyrrolo[2,3-*d*]pyrimidin-2-yl)-*N*-pivaloylpivalamide **151**.

Gangjee coworkers reported[302] in 2007 the synthesis of *N*-(7-benzyl-4-methyl-5-(phenylethynyl)-7*H*-pyrrolo[2,3-*d*]pyrimidin-2-yl)-*N*-pivaloylpivalamide **151** from *N*-(7-benzyl-5-iodo-4-methyl-7*H*-pyrrolo[2,3-*d*]pyrimidin-2-yl)-*N*-pivaloylpivalamide **149** and phenylacetylene **150** *via* a Sonogashira cross-coupling in the presence of

tetrakis(triphenylphosphine)palladium(0) and CuI as catalysts in dichloromethane (Scheme 32).

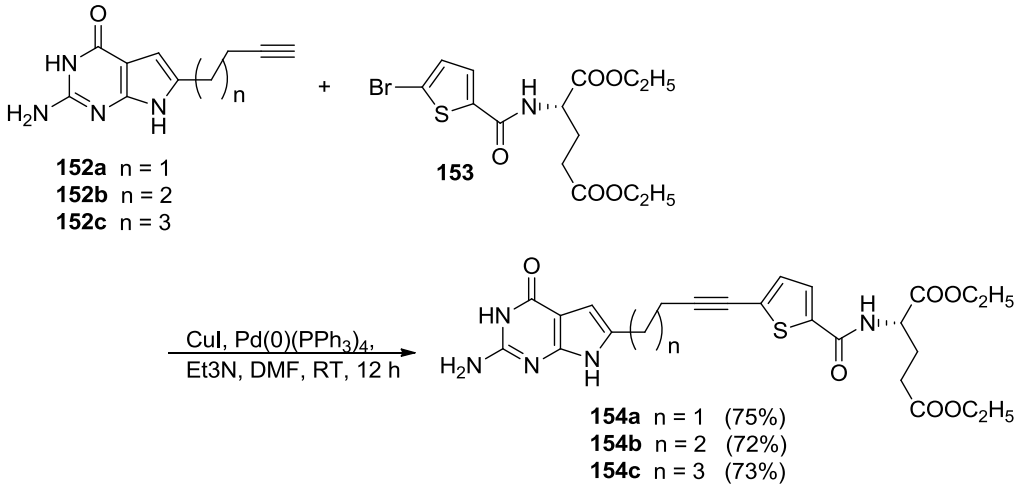

Scheme 33 Synthesis of classical 2-amino-4-oxo-6-substituted-pyrrolo[2,3-*d*]-pyrimidines by Sonogashira coupling.[113]

In 2010, Wang and Gangjee *et al.* [113] reported the synthesis of classical 2-amino-4-oxo-6-substituted-pyrrolo[2,3-*d*]-pyrimidines **154a-c** (Scheme 33) from terminal alkynes **152a-c** and thiophenyl bromide **153** *via* a Sonogashira cross-coupling in the presence of tetrakis(triphenylphosphine)palladium(0) and CuI as catalysts in DMF (Scheme 33).

3. Heck coupling reaction in one-step aldehyde synthesis

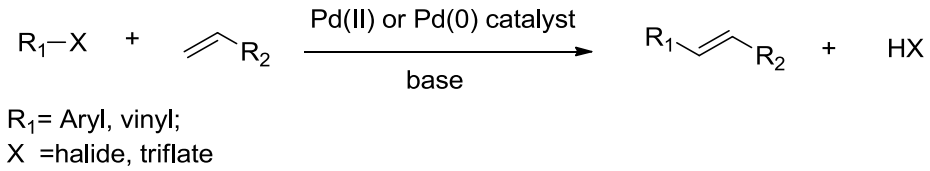

Scheme 34 General transformation of Heck coupling.

The Heck coupling reaction (also called the Mizoroki-Heck reaction) is the chemical reaction of an aryl or vinyl halide (or triflate) with an alkene and a base and palladium catalyst to form a substituted alkene.[303, 304] Together with the other palladium-catalyzed cross-coupling reactions, this reaction is of great importance in modern organic synthesis as reviewed.[305-307] Richard F. Heck was awarded the 2010 Nobel Prize in Chemistry for the discovery and development of this reaction. A General transformation of Heck coupling is shown in Scheme 34.

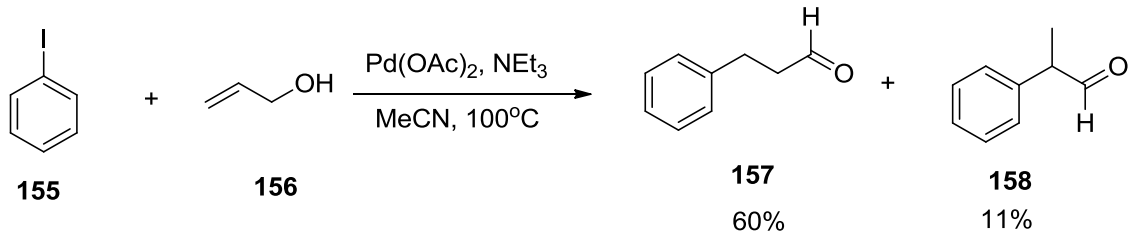

Scheme 35 Heck coupling to synthesis aldehyde **157**.

From the very beginning of Heck coupling, Heck disclosed in 1968 the formation of 3-aryl aldehydes and ketones by the reaction of primary and secondary allylic alcohols with aryl palladium complexes prepared in situ from arylmercuric chlorides or acetates and either an equimolecular amount of a palladium (II) salt, or a catalytic amount of this salt with an equimolecular amount of copper (II) chloride to regenerate the palladium after each reaction cycle.[308] The teams of Heck and Chalk reported in 1976 simultaneously, but independently, a strong improvement in these couplings by disclosing that such compounds are also obtained using aryl iodides or bromides and, furthermore, with a catalytic amount of a palladium catalyst (Scheme 35).[309, 310]

As shown in Scheme 35, this reaction was carried out with catalytic amount of palladium acetate at 100 °C in MeCN for 0.5 hour to afford aldehydes **157** with good yield (60%) from phenyl iodide **155** and allyl alcohol **156**.[309, 310] This kind of Heck coupling reactions with unsaturated alcohols has been widely used to synthesize aldehydes from aryl halides in one step reaction.[305-307]

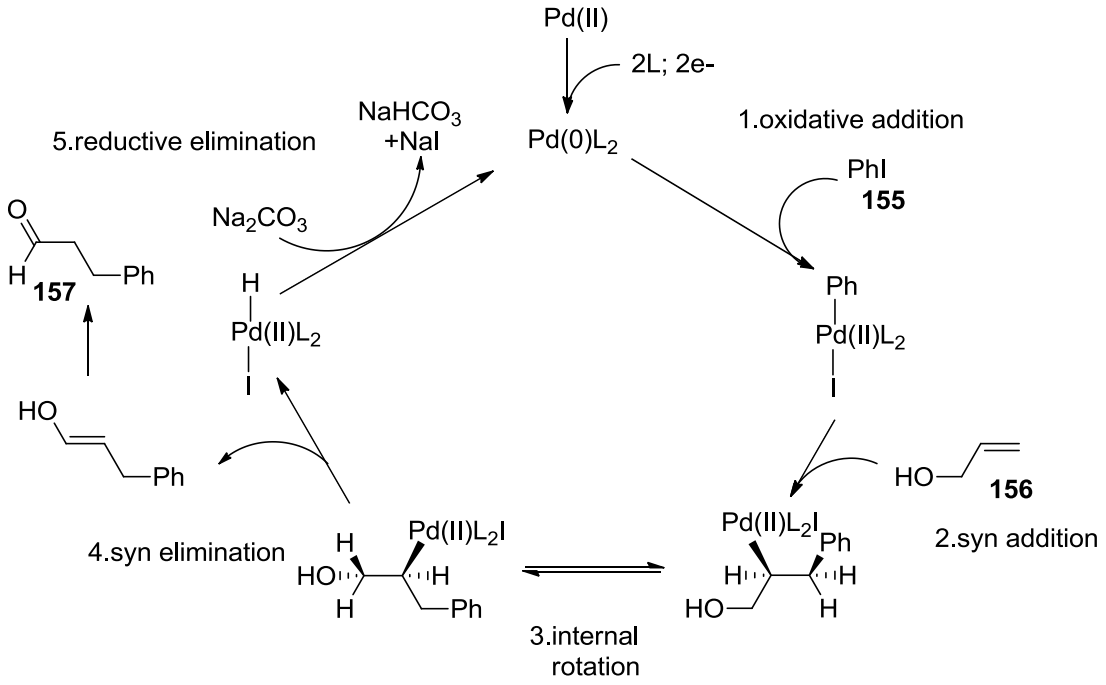

Scheme 36 A proposed mechanism of Heck coupling to synthesis aldehyde **157**.

A possible mechanism of this Heck coupling to synthesize aldehydes **157** from phenyl iodide and allyl alcohol was proposed in Scheme 36.

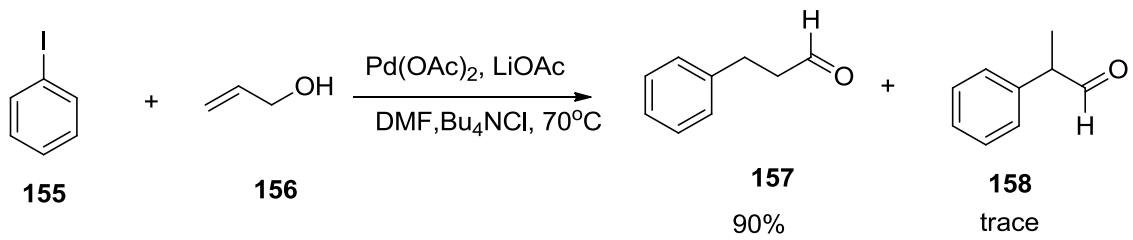

Scheme 37 Improved Heck coupling to synthesis aldehyde **157**.

Larock and coworkers reported[311] reported in 1989 an improved Heck coupling to synthesis aldehyde **157** with much better yield (90%) and lower temperature (70 °C). (Scheme 37) This reaction between phenyl iodide **155** and allyl alcohol **156** is carried out successfully with assistance of palladium acetate as the key catalyst, Bu_4NCl as the phase transfer catalyst and lithium acetate as the base. The easy availability of the reactants and catalysts plused the excellent yield and pretty mild condition made this reaction very attractive to synthesize aldehydes as versatile intermediates.[112, 312-314] However, the applications of this condition to heterocycle (such as thiophene and furan) halides other than phenyl halides were not reported, which highly limited the application of this reaction.[311]

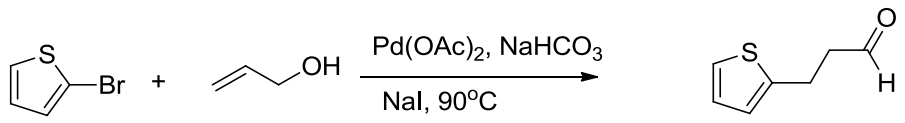

159 **156** **160**

yield: 76%

Scheme 38 Heck coupling with thiophenyl bromide **159**.

Yoshida and coworkers reported[315, 316] in 1977 an improved Heck coupling with thiophenyl bromides as shown in Scheme 38. 2-Bromothiophene **159** was alkylated in the 2 position by reaction with allylic alcohol **156** in the presence of $Pd(OAc)_2$, NaI, $NaHCO_3$ at 90 °C under Ar_2 for 4 h gave 76% 3-(thiophen-2-yl)propanal **160**. Although this is a successful example of Heck coupling with thiophenyl bromides, the drawbacks of this reaction are very obvious: Only thiophenyl bromide without any substitutions on the thiophenyl ring was demonstrated; the reaction tolerance of different functional

groups (e.g. –COOMe, -C=O) on the thiophene ring is not known; the reaction condition is pretty hash: high temperature (90 °C) and argon protection needed.

Due to its potential use in synthesis of classical antifolates and analogs such as RTX and PMX,[269, 317] the mild conditioned and wide functional group tolerant Heck coupling of thiophenyl halides with allyl alcohols to afford aldehydes in one step is highly attractive.

III. STATEMENT OF THE PROBLEM

1. Synthesis of classical 6-Substituted pyrrolo[2,3-*d*]pyrimidine 2, 161 and 162 (n=4-6) analogues as folate receptor specific GARFTase inhibitors and as targeted anticancer agents[109]

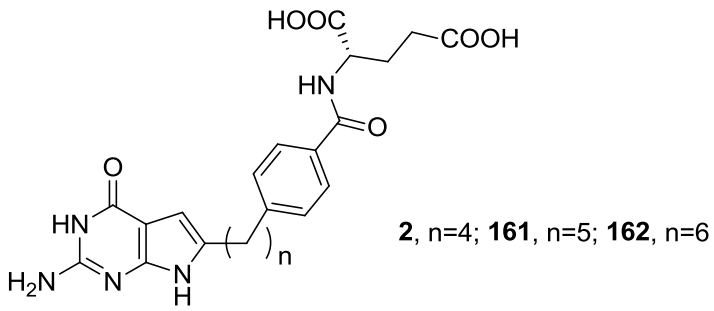

Figure 21 Structures of classical 6-Substituted Pyrrolo[2,3-*d*]pyrimidine **2**, **161**and **162** (n=4-6).[109]

The high affinity FRs offer a potential means of selective tumor targeting, given their restricted pattern of tissue expression and function.[73] For instance, FRα is expressed on the apical membrane surface of normal tissues such as kidney, placenta, and choroid plexus, whereas FRβ is expressed in placenta, spleen, and thymus. Importantly, FRα is overexpressed in a number of carcinomas including up to 90% of ovarian cancers.[81, 91]

Close associations were reported between FRα expression levels with grade and differentiation status of ovarian tumors. FRα in normal tissues (unlike tumors) is reported to be inaccessible to the circulation. [73] FRβ is expressed in a wide range of myeloid leukemia cells.[80] FRβ in normal hematopoetic cells differs from that in leukemia cells in its inability to bind folate ligand.[78]

The concept of targeting FRs in cancer is not new. Folate-conjugated cytotoxins, liposomes, radionuclides, or cytotoxic antifolates[73, 107, 318, 319] have all been used to target

FRs. Unfortunately, for most folate-based therapeutics such as classical antifolates [including RTX, PMX, and lometrexol (LMX)], tumor selectivity is lost, since substrates are shared between FRs and the ubiquitously expressed RFC. Indeed, this likely explains the severe myelosuppression encountered in phase 1 study with LMX.[150]

One strategy for selectively targeting tumor cells *via* FRs involves prodrug conjugates in which folate or pteroate is covalently linked to cytotoxins such as mitomycin ^{18}C that, upon internalization, are selectively cleaved to release the cytotoxic drug. While these folate drug conjugates are unlikely to be RFC substrates, the success of this tumor targeting approach could be significantly compromised by inefficient cleavage and lack of release of the cytotoxic moiety, resulting in decreased chemotherapeutic activity. Alternatively, premature cleavage of the conjugates (prior to tumor internalization) could decrease selectivity and increase toxicity to normal proliferative tissues. In addition, the use of folic acid conjugates could ultimately release free folic acid within the tumor which could function as a nutrient for the tumor. If, however, a FR-targeted ligand were itself cytotoxic without RFC activity, selective tumor targeting would ensue. Antifolates that selectively target FRs over RFC have been described[107] and, more recently, cyclopenta[*g*]quinazoline antifolates,[111, 320] all of which potently inhibit thymidylate synthase (TS) within cells. When tested in mice,[320] a cyclopenta[*g*]quinazoline antifolate had no toxicity to normal tissues, as reflected in lack of weight loss, nor were there any macroscopic signs of toxicity to major organs, consistent with the premise that FR targeting is highly selective.

On the basis of the clinical success of PMX,[321] Gangjee et al.[322, 323] designed and synthesized classical 6-substituted 2-amino- 4-oxopyrrolo[2,3-*d*]pyrimidine antifolates

with three- and four carbon bridges as inhibitors of dihydrofolate reductase (DHFR) and/or TS. Both **1** and **2**, (Figure 22) were poor inhibitors of purified human DHFR and TS and were only modest inhibitors of tumor CCRF-CEM leukemia cell growth in the presence of supraphysiologic folate. This inhibition was largely protected by hypoxanthine (but not thymidine), indicating the inhibition of the purine biosynthesis pathway rather than the pyrimidine by **1** and **2**.[322, 323]

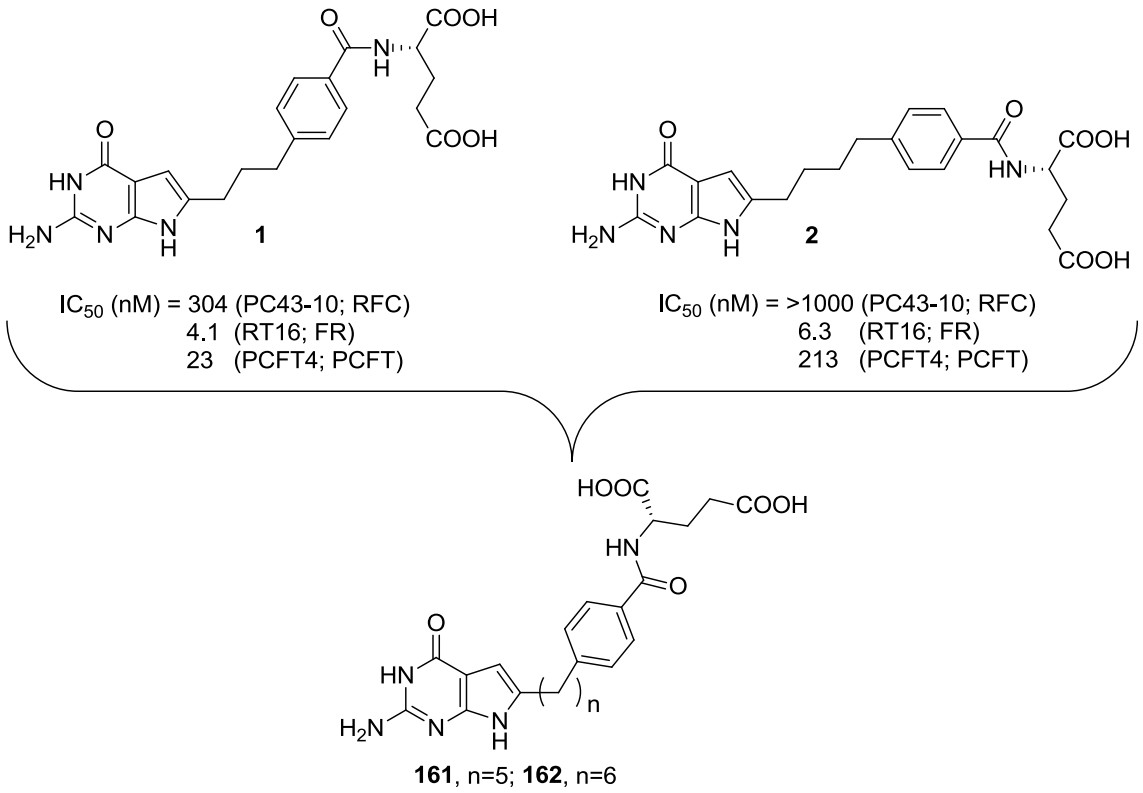

Figure 22 Design of Classical 6-Substituted Pyrrolo[2,3-*d*]pyrimidine **161** and **162.**[109]

It was proposed that compounds **1** and **2**, along with their five and six-carbon bridge homologues **161** and **162** (Figure 22), could be selective high affinity ligands for FRs with potent inhibitory activity against FR-expressing Chinese hamster ovary (CHO) cells and human tumor cells.[109] In addition, the folate-dependent purine biosynthetic enzyme,

glycinamide ribonucleotide formyltransferase (GARFTase), was proposed as the major intracellular target responsible for the cytotoxic activity of this class of agents. While antifolates that target GARFTase including LMX have been described[324] and are under continued development, to our knowledge, this is the first report[109] of GARFTase inhibitors that are selectively transported into tumor cells by FRs but not RFC and that exhibit potent inhibitory activities against FR-expressing tumor cells.[109]

2. Synthesis of classical 6-substituted pyrrolo[2,3-*d*]pyrimidine 163 (n=2) as folate receptor specific GARFTase inhibitors and as targeted anticancer agents[114]

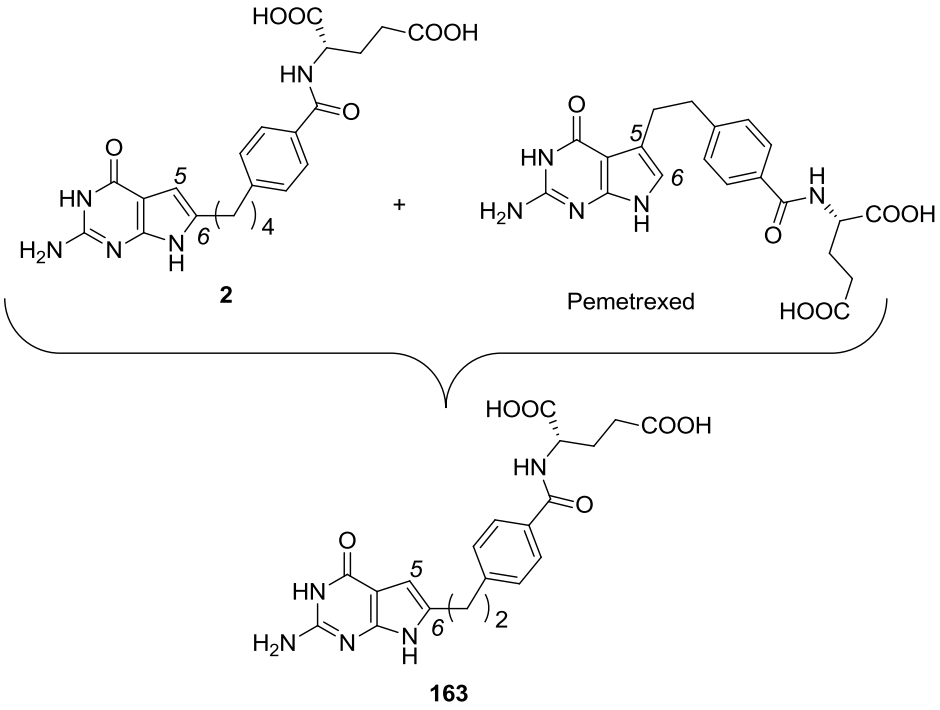

Figure 23 Design of **163** as a hybrid of **2** and Pemetrexed (PMX).[114]

We reported a series of 6-substituted pyrrolo[2,3-*d*]pyrimidine classical antifolates

2, **161** and **162** (Figure 22) described above that are specifically taken up by the folate receptor (FR) and inhibit FR expressing tumor cells (KB and IGROV1) at nanomolar IC_{50} values.[109] These compounds are the 6-regioisomers of the well known antifolate PMX, in that the bridge is substituted in the 6- rather than 5-position of the pyrrolo[2,3-*d*]pyrimidine ring.

In addition, these analogs are not transported *via* RFC into normal cells. GARFTase was confirmed as the target enzyme for these compounds. The 3- and 4-bridge carbon analogs were most inhibitory toward FR-expressing cells, primarily due to the potent inhibition of GARFTase. The 3- and 4-bridge carbon analogs did not inhibit human DHFR or TS.

Pemetrexed(PMX) is clinically used for the treatment of mesothelioma and non–small cell lung cancer(NSCLC) and is currently being evaluated for the treatment of a variety of other solid tumors in the US.[187] More recently, PMX has been approved in combination with cisplatin for the first-line treatment of patients with locally advanced or metastatic NSCLC other than squamous cell histology.[188] PMX is a reported to be multitargeted antifolate that inhibits several folate metabolizing enzymes: TS, DHFR, AICARFTase and GARFTase.[188] However, PMX suffers from dose-limiting toxicity due to its transport by RFC which is ubiquitously expressed in normal cells. To determine if transposing the side chain from the 5-position of PMX to the 6-position would maintain the multitarget attributes of PMX and perhaps provide selectivity for FR over RFC, the 6-regioisomer of PMX, **163** was synthesized and evaluated as a hybrid of **2** and pemetrexed (PMX) in Figure 23.

3. Synthesis of 6-substituted pyrrolo[2,3-*d*]pyrimidines with a straight chain for folate receptor transport and GARFTase enzyme inhibition SAR study

A highly active compound of the previous series (Figure 22) included a 4 carbon bridge analog **2** that was a targeted agent, selectively transported into tumor cells by folate receptors (FRs) and the proton-coupled folate transporter (PCFT) (but not RFC) whereupon it inhibited *de novo* purine biosynthesis at the level of GARFTase. Compound **2** was highly active toward both KB and IGROV1 tumor cells in culture.[109]

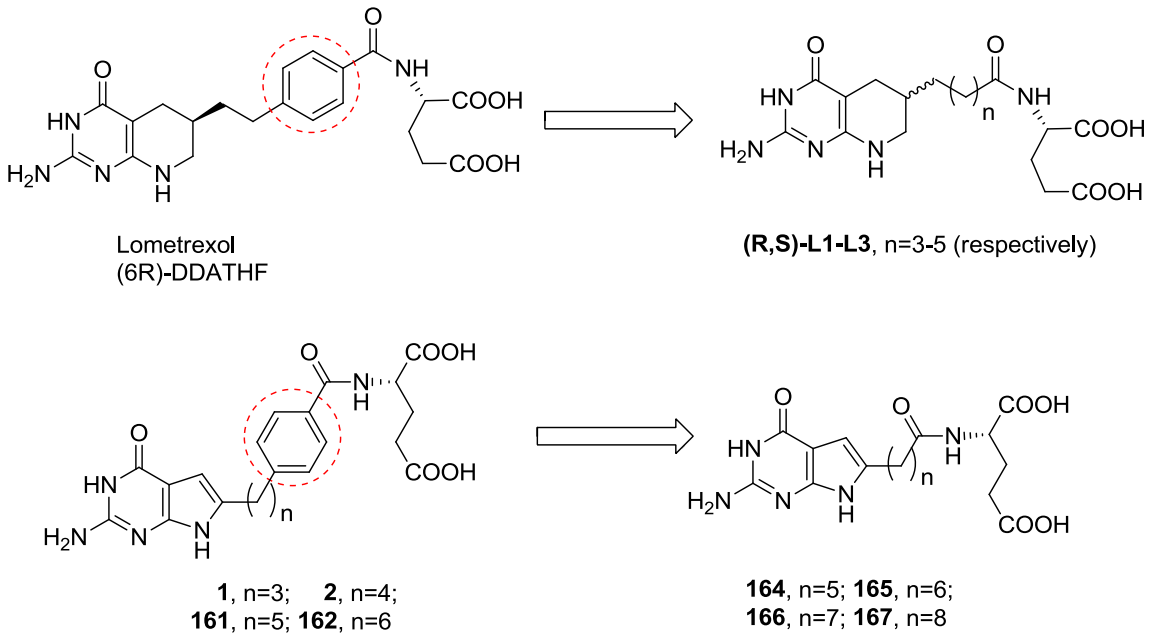

Figure 24 6-Substituted straight chain compounds design: replacement of the phenyl ring by methylene units.[325]

To further explore the SAR of the GARFTase inhibition and non-RFC targeted specificity of these compounds, several series of analogs were designed and synthesized as summaried above.

At the same time, it was of interest to inspect the disclosed SAR of the known GARFTase inhibitor in clinical trial, lometrexol (LMX), to facilitate our study. A series of lometrexol analogs were reported in which the phenyl ring in the bridge was replaced by a methylene bridge of variable length.[324, 326] (Figure 24)

Table 4 GARFTase inhibitory activities of Lometrexol and its straight chain analogs[324]

Compound	**Lometrexol** (n=2)	**L1** (n=4)	**L2** (n=5)	**L3** (n=6)
K*i* (μM)	0.10	0.049	0.028	0.018

Replacement of the phenyl ring of lometrexol by either two, three, or four more methylene units did not abrogate activity against GARFTase. In fact, there was an increase in binding affinity of analogs to GARFTase as the methylene chain was extended in the bridge region between the heterocycle and the glutamate (Table 4).[324] A similar design strategy was employed with our 6-substituted pyrrolo[2,3-*d*]pyrimidines (Figure 24). Straight chain compounds **164-167** (n=5-8) were designed with replacement of the phenyl ring of lead compound **2** by methylene bridges of variable length (Figure 24). [325] These analogs served as probes for the binding of the central portion of the molecule to FR and/or PCFT transport as well as to GARFTase.

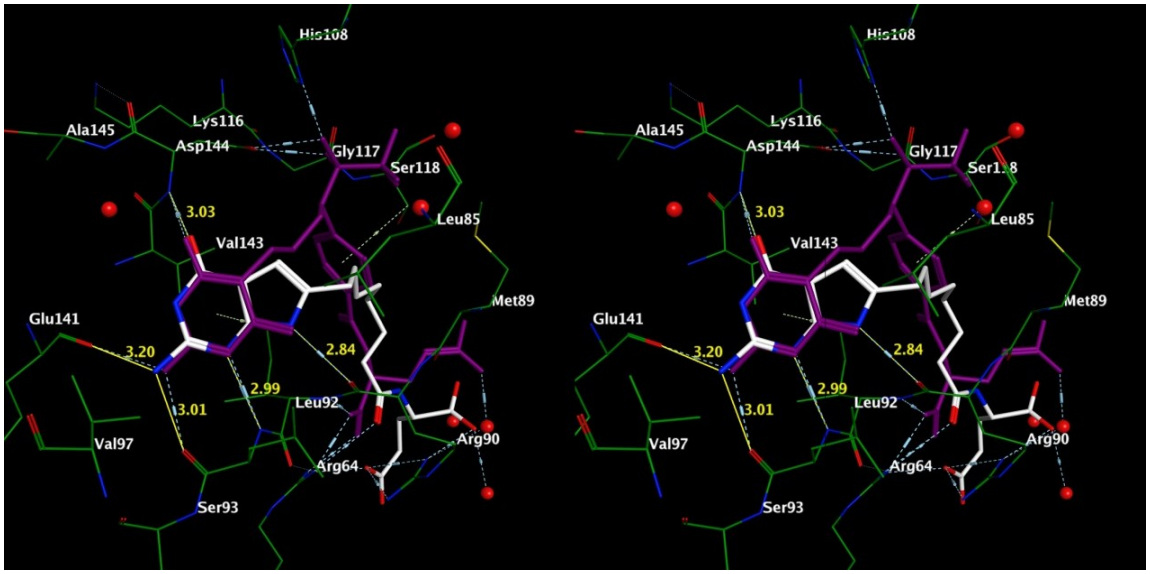

Figure 25 Stereoview. Overlay of the docked pose of **166** (white) with an analog of DDACTHF (purple) in hGARFTase (PDB ID: 1NJS)[325]

The docked pose of **166** (n=7) in the hGARFTase active site is shown in Figure 25.[325] The cofactor binding pocket of hGARFTase is located at the interface between the N-terminal mononucleotide binding domain and the C-terminal half of the structure. The binding site for the folate cofactor moiety consists of three parts: the pteridine binding cleft, the benzoylglutamate region, and the formyl transfer region.[139] The docked pose shows the pyrrolo[2,3-*d*]pyrimidine scaffold of **166** (n=7) to be buried deep in the active site and occupies the same location as the diaminopyrimidone ring in the native crystal structure ligand (10-CF_3CO-DDACTHF, purple). This orientation of the scaffold permits the 2-amino moiety to form hydrogen bonds to Glu141 and the backbone of Leu92. The N1 nitrogen interacts with the backbone of Leu92 to form a hydrogen bond. The 4-oxo moiety forms a hydrogen bond with Asp144 and forms water-mediated hydrogen bonds with Asp142 and Ala140. The molecule is oriented in a manner which aids the N7

nitrogen to form a hydrogen bond with Arg90. As is shown with an analog of DDACTHF (purple), several hydrophobic residues flank the pocket which holds the pyrrolo[2,3-*d*]pyrimidine scaffold. The hydrophobic pocket consists of Leu85, Ile91, Leu92, Val97 (not shown), and the folate binding loop residues 141-146. The amide NH of the glutamate side chain forms a hydrogen bond with Met89. The 7-carbon side chain of **166** (n=7) shifts the glutamate side chain away from the corresponding glutamate side chain of the analog of DDACTHF. The carbonyl group of the glutamate side chain interacts with Arg64, which is not seen with the corresponding carbonyl group of the side chain of the analog of DDACTHF. The γ-carboxylic acid interacts with Arg64. The α-carboxylic acid of the glutamate side chain interacts with Arg90. Thus, the interaction pattern of the α- and γ-carboxylic acid moieties of **166** (n=7) are reversed compared to the corresponding α- and γ-carboxylic acids of the analog of DDACTHF and could represent an alternate conformation for the side chain. These interactions could account, in part, for the potent activity observed for **166** (n=7) against hGARFTase.

4. Synthesis of isosteric isomers of compound 2 as folate receptor specific GARFTase inhibitors of selectively targeted anticancer agents

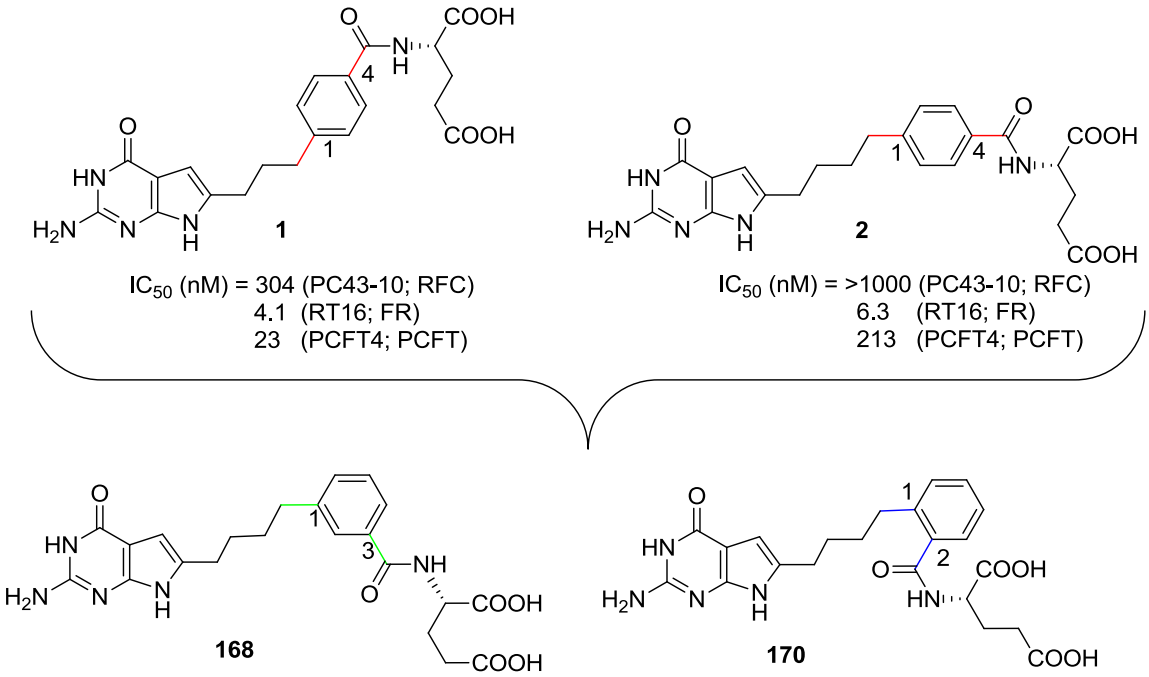

Figure 26 Design of **168** and **170**.

Gangjee and coworkers[109] described 6-substituted classical pyrrolo[2,3-*d*]pyrimidines, **1** and **2** as potent GARFTase inhibitors with selective transport by FR and PCFT over RFC, providing tumor targeting capability. Interestingly, the four carbon chian compound **2** was not a substrate of RFC, whereas the three carbon chain compound **1** showed significant growth inhibitory activity (IC_{50} of 304 nM) toward RFC-expressing PC43-10 cells. This result demonstrated the impact of the length of the bridge domain of 6-substituted classical pyrrolo[2,3-*d*]pyrimidines on selective transport by FRs and/or by PCFT versus RFC. Compound **1** with a 3-carbon bridge was the most potent compound toward cells expressing FRs and PCFT, but was also transported by RFC; whereas the 4-carbon bridge analog **2** was selectively transported by FRs and by PCFT but not by RFC,

but was less potent than **1** as an inhibitor of tumor cells in culture, suggesting that the chain length of the carbon bridge for optimum potency and transport selectivity is in between 3- and 4-atoms.

Thus, in an attempt to determine the optimum length of carbon bridge for GARFTase inhibitory activity and selective transport by FRs and/or PCFT over RFC, **168** and **170** with 1,3- and 1,2- substituted phenyl rings (Figure 26) were designed as analogs with chain lengths between three and four carbons. The bond angle of the 1,4-disubstituted compound **2** is 180^{o} , which is greater than that of the 1,2-disubstituted compound **170** as 60^{o} and the 1,3-disubstituted compound **168** as 120^{o}. Thus, the total lengths of the carbon bridge of **168** and **170** would be in between 3 and 4 atoms. These compounds are proposed to have similar or possible more potent activities than **1**without RFC transport providing targeted therapy for tumors that express FR and/or PCFT.

5. Synthesis of classical 5-substituted pyrrolo[2,3-*d*]pyrimidines (n=1-6) with a phenyl ring in the chain as folate receptor specific TS, DHFR, GARFTase and/or AICARFTase multiple enzyme inhibitors (MTI) against tumors[327]

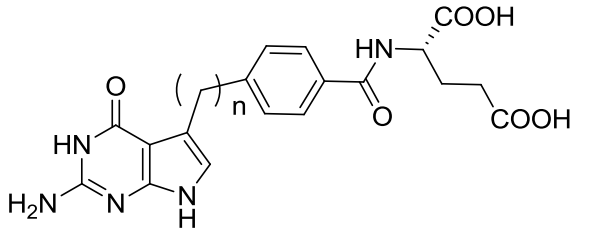

172, n=1; **173**, n=3;
175, n=4; **176**, n=5;
177, n=6

Figure 27 Structures of 5-substituted pyrrolo[2,3-*d*]pyrimidines **172-177** (n=1-6).[327]

Folate-dependent biosynthetic pathways serve as important therapeutic targets for cancer chemotherapy. Antifolate drugs for cancer include potent inhibitors of dihydrofolate reductase (DHFR) [methotrexate (MTX)], thymidylate synthase (TS) [raltitrexed (RTX), GW1843U, pemetrexed (PMX)], and both of the purine biosynthetic enzymes, β-glycinamide ribonucleotide formyl transferase (GARFTase) [lometrexol (LMX), PMX] and 5-aminoimidazole-4-carboxamide ribonucleotide formyl transferase (AICARFTase) [PMX]. While all these agents are transported by RFC, the expression of RFC in both normal and tumor cells presents a potential obstacle to antitumor selectivity. Further, loss of RFC is frequently associated with antifolate resistance. Thus, it is of interest to design targeted antifolates that are substrates for transporters other than RFC with limited expression and/or transport into normal tissues compared with tumors. If these drugs also inhibited targets other than or in addition to DHFR and TS, this would afford further benefit by circumventing MTX, 5-FU (5-fluorouracil), PMX and RTX tumor resistance due to increased DHFR or TS. This rationale provided the impetus to develop targeted agents that are selectively transported into tumors by FRs over RFC, with intracellular targets other than or in addition to DHFR and TS.

We recently reported[109] a series of 6-substituted pyrrolo[2,3-*d*]pyrimidine classical antifolates **1** and **2** that are specifically taken up by the folate receptor (FR) and inhibit FR expressing tumor cells (KB and IGROV1) at nanomolar IC_{50} values. These compounds are 6-regioisomers of the well known antifolate PMX in that the bridge is substituted in 6- rather than 5-position of the pyrrolo[2,3-*d*]pyrimidine ring.

In addition, these analogs are not transported via RFC into normal cells. GARFTase was confirmed as the target enzyme for these compounds. The 3- and 4-bridge carbon

analogs (compounds **1** and **2**, respectively) were most inhibitory toward FR-expressing cells, primarily due to the potent inhibition of GARFTase. Compounds **1** and **2** did not inhibit human DHFR or TS.

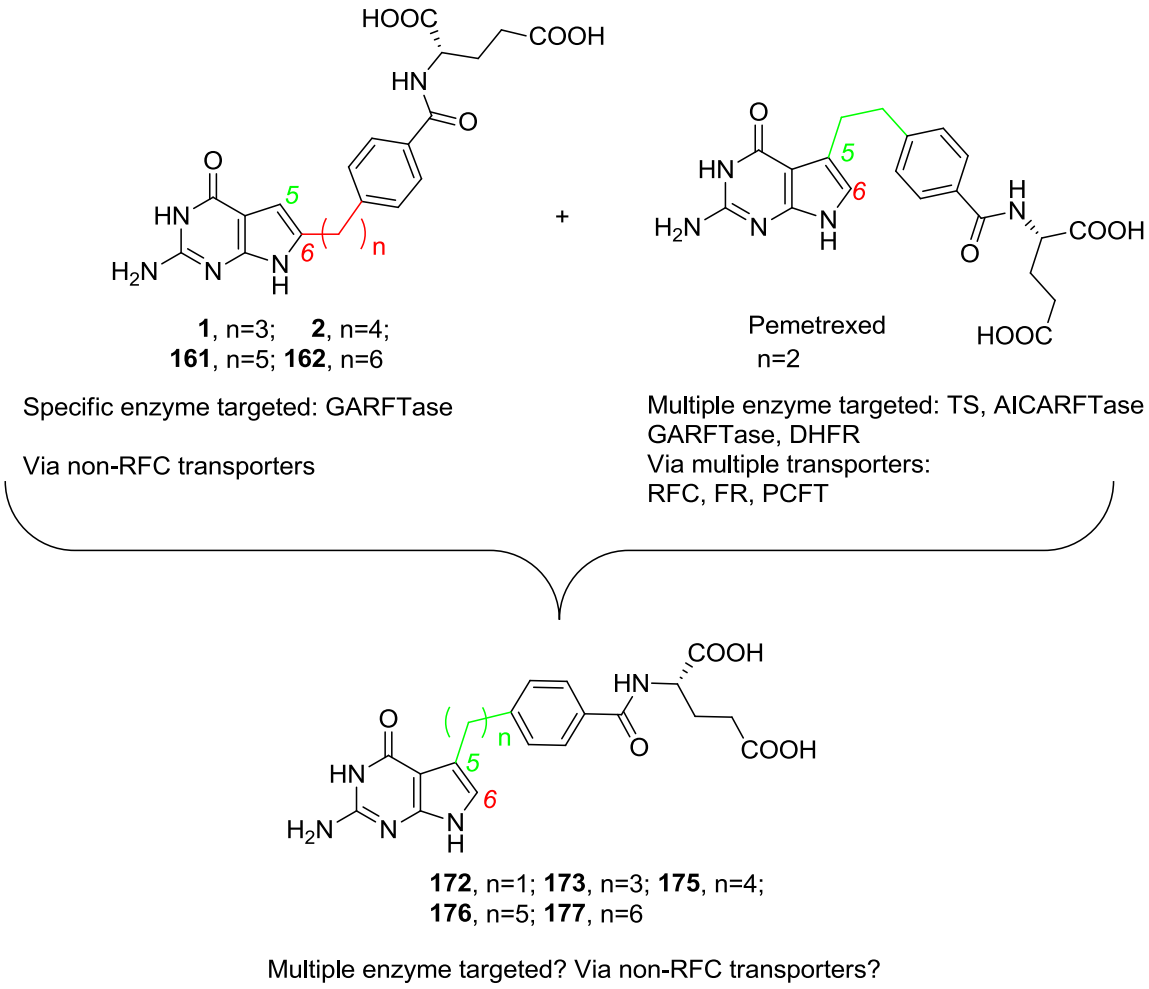

Figure 28 Design of 5-substituted pyrrolo[2,3-*d*]pyrimidines **172-177** (n=1-6).[327]

As mentioned above, pemetrexed(PMX) is clinically used for the treatment of mesothelioma and non–small cell lung cancer(NSCLC) and is currently being evaluated for the treatment of a variety of other solid tumors in the US.[187] More recently, PMX has been approved in combination with cisplatin for the first-line treatment of patients with

locally advanced or metastatic NSCLC other than squamous cell histology.[188] PMX is a multitargeted antifolate that inhibits several folate metabolism enzymes: TS, DHFR, AICARFTase and GARFTase. [188] However, PMX suffers from dose-limiting toxicity due to its transport by RFC which is ubiquitously expressed in normal cells.[328] To determine if altering the length of the side chain of PMX would maintain the multitarget attributes of PMX and perhaps provide selectivity for FR over RFC, we synthesized and evaluated the one to six carbon chain homologs of PMX (n=2) **172-177** (n=1-6, except n=2). (Figure 28)

Molecular Modeling Studies[327]:

Molecular modeling studies were performed using LeadIT 1.3.0 and visualized using MOE 2011.10.[327] Redocking the native crystal structure ligands (BW2315U89 for AICARFTase (PDB ID: 1PL0), 10-CF_3CO-DDACTHF for hGARFTase (PDB ID: 1NJS)[4], and PMX for FRb) into their respective crystal structures afforded docked poses with RMSD ~ 1Å.

Docking studies with AICARFTase (PDB ID: 1PL0) [327]

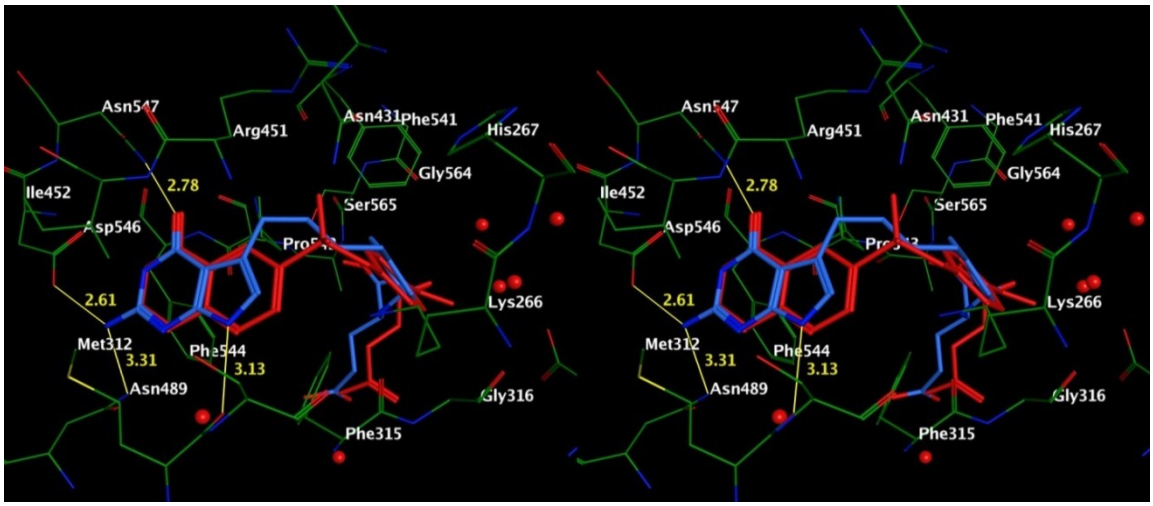

Figure 29 Stereoview. Overlay of the docked pose of **175** (blue) with BW2315U89 (red) in AICARFTase (PDB ID: 1PL0). [327]

Figure 29 shows the overlay of the docked poses of **175** (red) with the crystal structure ligand BW2315U89 (blue) (a potent inhibitor) in AICARFTase (PDB ID: 1PL0[39]). The pyrrolo[2,3-*d*]pyrimidine scaffold of **175** occupies the same location as the dihydroquinazoline scaffold of BW2315U89. Analogous to BW2315U89, the 2-NH_2 and N3 nitrogens of **175** interact with Asp546 while the 4-oxo moiety forms a hydrogen bond with the side chain of Asn547. The *N*7-nitrogen of **175** forms a hydrogen bond with the backbone of Met312. The pyrrolo[2,3-*d*]pyrimidine scaffold of **175** forms hydrophobic interactions with Met312, Phe315, Ile452, Pro543 and Phe544. The aryl glutamate section of **175** is oriented similar to the phenyl glutamate side chain of BW2315U89.

Docking studies with hGARFTase (PDB ID: 1NJS) [327]

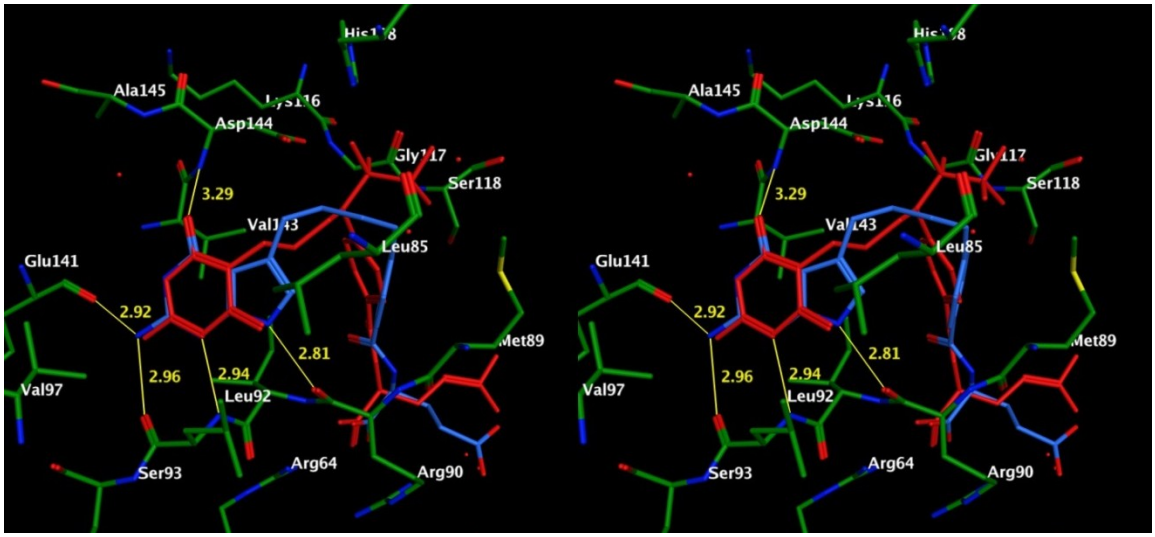

Figure 30 Stereoview. Overlay of the docked pose of **175** (blue) with 10-CF_3CO-DDACTHF (red) in hGARFTase (PDB ID: 1NJS). [327]

Figure 30 shows the docked pose of **175** in the hGARFTase active site. The cofactor binding pocket of hGARFTase is located at the interface between the N-terminal mononucleotide binding domain and the C-terminal half of the structure. The binding site for the folate cofactor moiety consists of three parts: the pteridine binding cleft, the benzoylglutamate region, and the formyl transfer region.[1] The docked pose shows the pyrrolo[2,3-*d*]pyrimidine scaffold of **175** to be buried deep in the active site and occupies the same location as the diaminopyrimidone ring in the native crystal structure ligand (10-CF_3CO-DDACTHF, not shown). This orientation of the scaffold permits the 2-amino moiety to form hydrogen bonds to the backbone of Glu141 and Ser93. The N1 nitrogen interacts with the backbone of Leu92 to form a hydrogen bond. The 4-oxo moiety forms a hydrogen bond with Asp144 and forms water-mediated hydrogen bonds with Asp142 and Ala140 (not shown).

The molecule is oriented in a manner which aids the *N*7 nitrogen to form a hydrogen bond with Arg90. The pyrrolo[2,3-*d*]pyrimidine scaffold resided in a hydrophobic pocket formed by Leu85, Ile91 (not shown), Leu92, Val97, and the folate binding loop residues 141-146. The flexible 4-atom side chain helps to orient the thiophene moiety into the benzoylglutamate region of the protein. The amide NH of the glutamate side chain forms a hydrogen bond with Met89. The α-carboxylic acid of the glutamate side chain interacts with Arg64 and additionally interacts with the backbone of Ile91. The γ-carboxylic acid can form a water-mediated hydrogen bond with Arg90. The interaction of the flexible glutamate side chain is very similar to the interaction network observed for the glutamate side chain of 10-CF_3CO-DDACTHF. These docking results suggest that **175** should bind and inhibit the two folate dependent puring biosynthetic enzymes (GARFTase and AICARFTase).

6. Synthesis of classical 5-substituted pyrrolo[2,3-*d*]pyrimidines (n=1-6) with a thiophenyl ring in the chain as folate receptor specific TS, DHFR, GARFTase and AICARFTase multiple enzyme inhibitors (MTI) against tumors

Gangjee and coworkers[113, 329] recently reported a series of 6-substituted pyrrolo[2,3-*d*]pyrimidine thienoyl antifolates. (Figure 31) The best characterized of this series compound **3** included a 4 carbon bridge and was selectively transported into cells by folate receptors (FRs) and the proton-coupled folate transporter (PCFT) (but not RFC) whereupon it inhibited *de novo* purine biosynthesis at the level of GARFTase. Compound **3** was highly active toward both KB and IGROV1 tumors. *In vivo* in SCID mice with KB tumor xenograft, Compound **3** was highly active against both early and advanced stage

tumors. Based on the 5-substituted pyrrolo[2,3-*d*]pyrimidine structure of PMX and our results with the 6-substituted compound **3**, it was of interest to synthesize 5-substituted

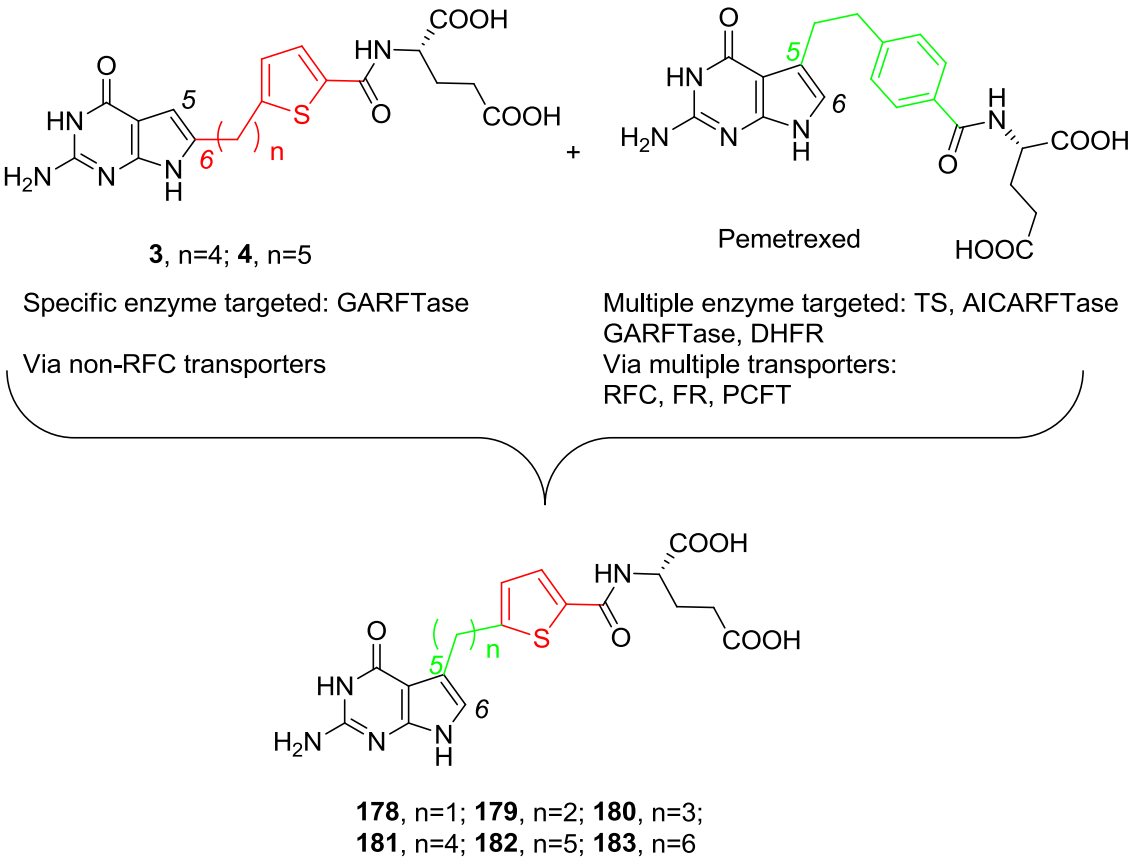

Figure 31 Design of 5-substituted pyrrolo[2,3-*d*]pyrimidines **178-183**. (n=1-6)

pyrrolo[2,3-*d*]pyrimidine thienoyl analogs with 1 to 6 carbon atoms in the bridge (**178-183**) as hybrid molecules of PMX and **3**. These analogs could be envisaged to afford multi-targeted attributes of PMX, while preserving FRα and/or PCFT specificity of 6-substituted analogs previously reported[62b] (Figure 31).

7. Synthesis of classical 5-substituted pyrrolo[2,3-*d*]pyrimidines with a straight side chain as folate receptor specific anticancer agents

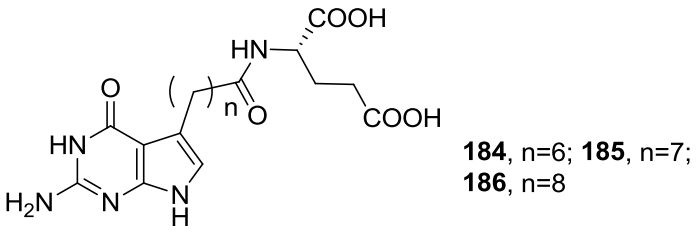

Figure 32 Structures of 5-substituted pyrrolo[2,3-*d*]pyrimidines **184-186** (n=6-8) with a straight side chain.

A similar design strategy was employed with the 5-substituted pyrrolo[2,3-*d*]pyrimidines **184-186** (n=6-8) (Figure 32) as with 6-substituted analogs described above.

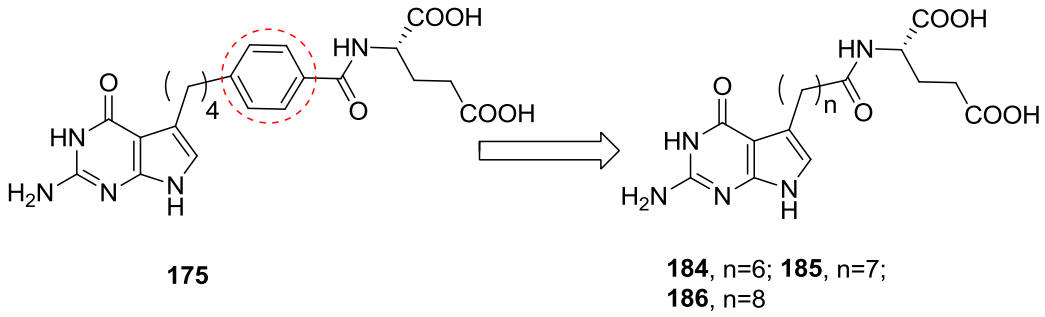

Figure 33 Design of 5-substituted pyrrolo[2,3-*d*]pyrimidines **184-186** (n=6-8) with a straight side chain.

Straight chain **184-186** (n=6-8) were designed with replacement of the phenyl ring of the lead compound **175** by methylene bridges of variable length (Figure 33).[325] These analogs served as probes for the binding of the central portion of the molecule to

GARFTase as well as to FR and/or PCFT transport and to other folate metabolizing enzmes: TS, DHFR and AICARFTase.

8. Synthesis of classical 7-Substituted pyrrolo[2,3-*d*]pyrimidines with a straight side chain as folate receptor specific anticancer agents

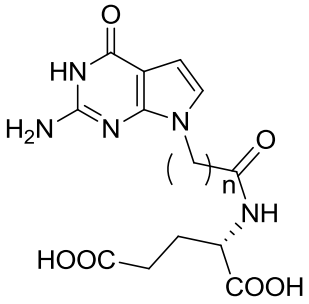

187, n=5; **188**, n=6;
189, n=7; **190**, n=8

Figure 34 Structures of 7-substituted pyrrolo[2,3-*d*]pyrimidines **187-190** (n=5-8) with a straight side chain.

As indicated above, both the 6-substituted and 5-substituted pyrrolo[2,3-*d*]pyrimidines with straight chains in place of the aryl group in the side chain were designed to achieve folate receptor specific anticancer agents. The biological activities of these straight chain analogs demonatrated that different regio positions (5-, or 6-) of the pyrrolo[2,3-*d*]pyrimidine is critical for both folate transport specificity as well as folate enzyme inhibition.

Thus, it was of interest to synthesize 7-substituted pyrrolo[2,3-*d*]pyrimidine analogs **187-190** (n=5-8) to explore the effects of side chain orientation for both the folate transport specificity and folate enzyme inhibition. (Figure 34) In addition, it could serve as an excellent comparision with both of our 6-substituted and 5-substituted pyrrolo[2,3-*d*]pyrimidines to make a more completed SAR. It was speculated that the flexibility of

the straight chain analogs would have the opportunity to orient an appropriate confirmation critical to binding to FR as well as folate metabolizing enzymes.

9. Synthesis of 6-substituted pyrrolo[2,3-*d*]pyrimidine glutmate derivatives as folate receptor specific anticancer agents

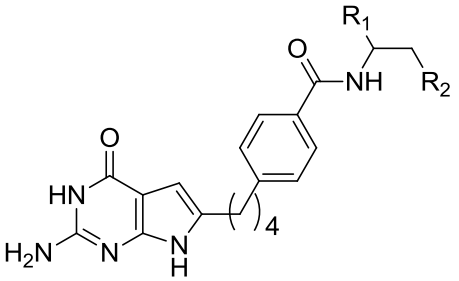

197, R_1=H, R_2=Me;
198, R_1=COOH, R_2=Me;
199, R_1=H, R_2=CH_2COOH;

Figure 35 Designed analogs with variations in the glutamate moiety.

As part of a continuing effort to develop novel classical antifolates as antitumor agents, Gangjee and coworkers[330] recently reported a series of classical 2,4-diamino-5-substituted-furo[2,3-*d*]pyrimidines with either an α- or γ-carboxylic acid in the glutamate moiety. The structure-activity relationship indicated that for these compounds the α-carboxylic acid is more important than the γ-carboxylic acid both for DHFR inhibitory activity and human RFC binding affinity. To investigate the structural requirements of the glutamate carboxlic acids of antifolates with respect to FR substrate activity, a series of analogs **197-199** (Figure 35) with and without carboxylic acids in the glutamate portion of **2** were designed and synthesized as the first series in a broader program to determine the structure –activity relationship for FR and the importance of the α- and the γ-

carboxylic acid groups to biological activity.

IV. CHEMICAL DISCUSSION

1: Synthesis of classical 6-substituted pyrrolo[2,3-*d*]pyrimidine 2, 161 and 162 (n=4-6)

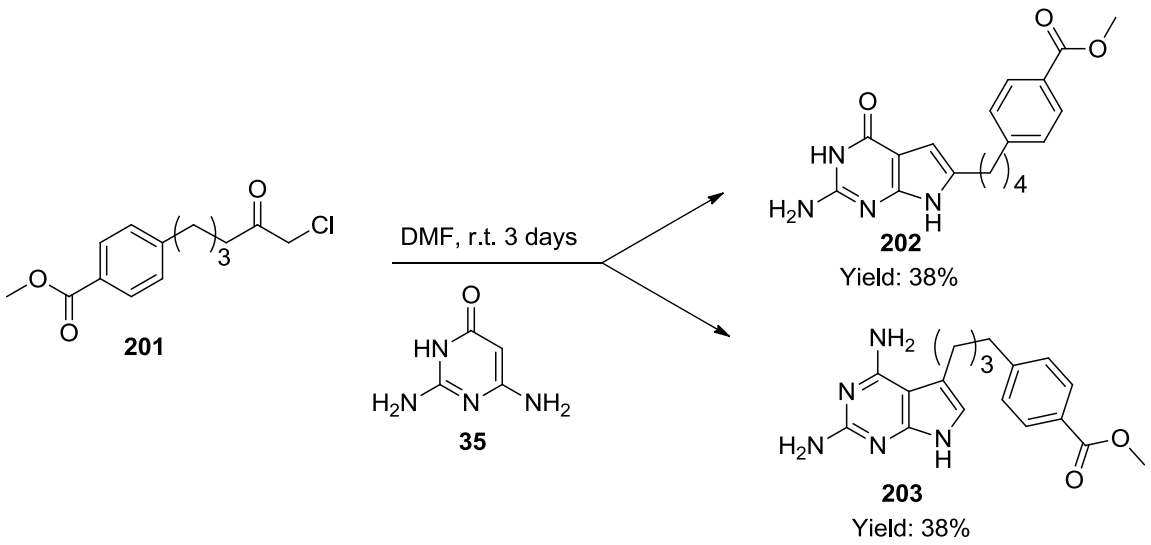

Scheme 39 Synthesis of intermediates **202** and **203**. [322, 323]

Compounds **2** , **161** and **162** (n=4-6) were obtained via a nine-step synthesis from the commercially available methyl 4-formylbenzoate **205** using an α-bromomethyl ketone condensation with pyrimidine as the key step as outlined in Scheme 1.[109] In the previously reported synthesis,[322, 323] the α-chloromethylketones were used to afford both the 6-substituted pyrrolo[2,3-*d*]pyrimidine, as well as the 5-substituted furo[2,3-*d*]pyrimidine and involved a separation of the two compounds. (Scheme 39)

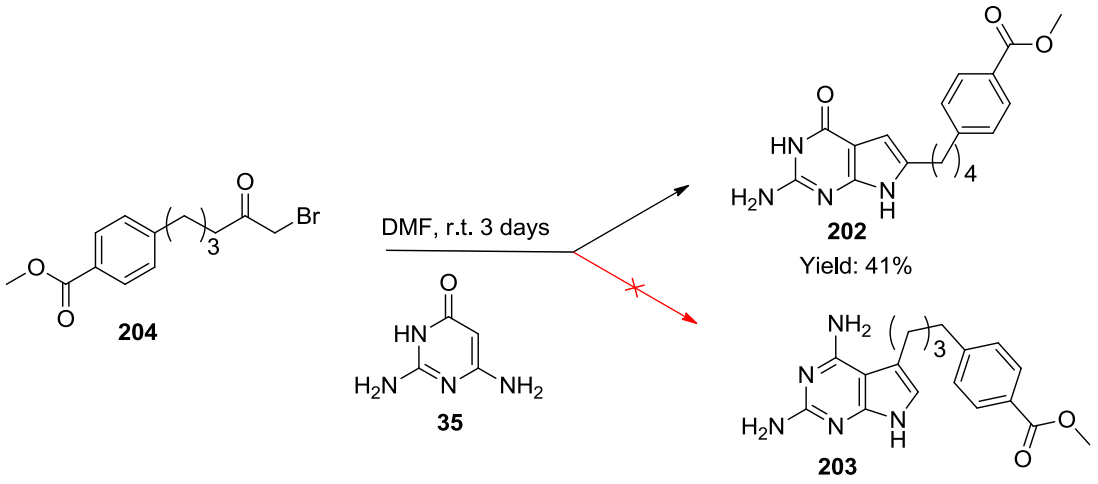

Scheme 40 Synthesis of 6-substituted pyrrolo[2,3-*d*]pyrimidines with the α-bromomethylketone.

In this study, the α-bromomethylketones were selected to afford regiospecifically the 6-substituted pyrrolo[2,3-*d*]pyrimidines without the furo[2,3-*d*]pyrimidines and circumvent the separation step.[109]

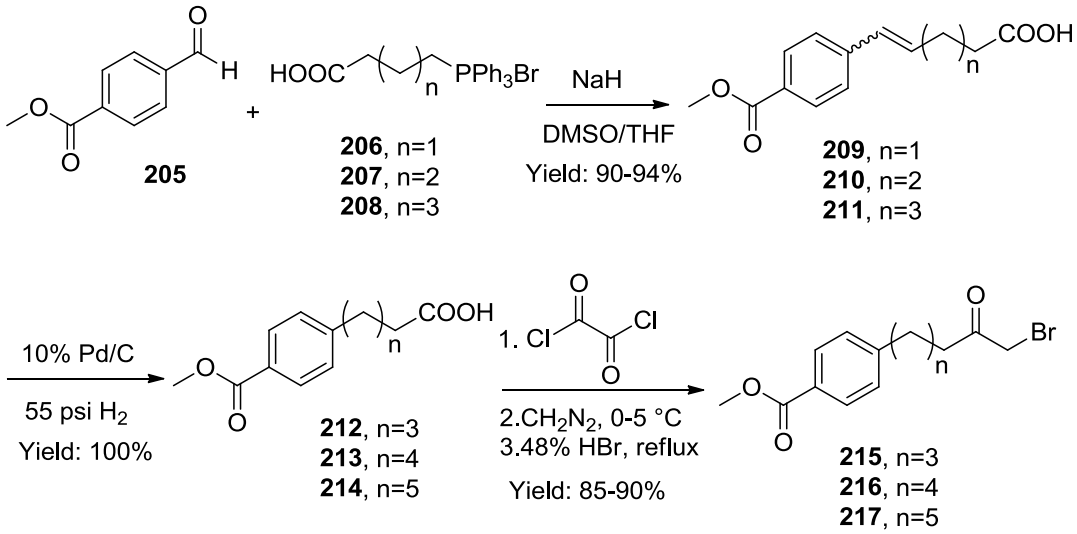

Scheme 41 Synthesis of intermediate α-bromomethylketones **215-217**.

Thus, a Wittig reaction[331] of **205** with triphenylphosphonium bromides **206-208** in 1:1 DMSO/THF with 2 equiv of NaH afforded the unsaturated acids **209-211** as a mixture

of *E*- and *Z*-isomers. (Scheme 41) Hydrogenation of **209-211** afforded the saturated acids **212-214**, which was converted to the acid chloride and immediately reacted with diazomethane followed by 48% HBr to give the desired *α*-bromomethylketones **215-217**.[332]

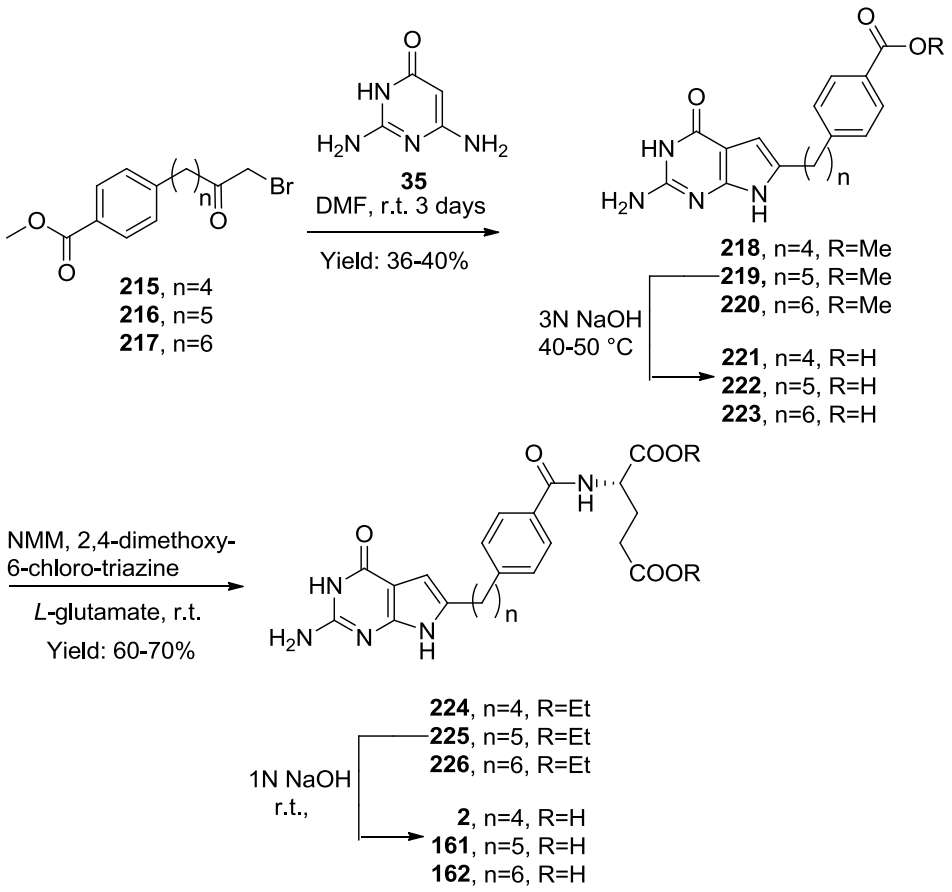

Scheme 42 Synthesis of 6-substituted pyrrolo[2,3-*d*]pyrimidine **2**, **161** and **162**.

With the desired α-bromomethylketones **215-217** in hand, the next step was the condensation of 2,4-diamino-6-hydroxypyrimidine with **215-217** (Scheme 42). Optimal reaction yields were obtained at room temperature for 3 days and only the pyrrolo[2,3-*d*]pyrimidines **218-220** were obtained. No side product furo[2,3-*d*]pyrimidines were found in this reaction compared with condensation with α-chloromethylketones that

afford both pyrrolo[2,3-*d*]pyrimidines and furo[2,3-*d*]pyrimidines. Hydrolysis of **218-220** afforded the corresponding free acids **221-223**. Subsequent coupling with L-glutamate diethyl ester using *N*-methyl morpholine and 2,4-dimethoxy-6-chloro-triazine as the activating agents afforded the diesters **224-226**. Final saponification of the diesters gave the target compounds **2**, **161** and **162**.[109]

Synthetic improvements compared with the known methods[322 323]:

1. *α*-Bromomethyl ketones **215-217** was reacted with 2,4-diamino-6-hydroxypyrimidine **35** to afford only pyrrolo[2,3-*d*]pyrimidines **218-220**. No side product furo[2,3-*d*]pyrimidines were found in this reaction compared with condensation with α-chloromethylketones to afford both pyrrolo[2,3-*d*]pyrimidines and furo[2,3-*d*]pyrimidines, which facilitate a much easier separation of the product.

2. Methanol instead of methanol and DMSO (1:1) mixture was used as the solvent for the hydrolysis of **218-220** to afford **221-223**. DMSO is difficult to remove.

3. Better peptide coupling reagents: *N*-methyl morphorine and 2,4-dimethoxy-6-chloro-triazine instead of the triethylamine and isobutyl chloroformate were used as peptide coupling reagents for the synthesis of **224-226**. Isobutyl chloroformate is flammable and very toxic. *N*-methyl morphorine and 2,4-dimethoxy-6-chloro-triazine are safer and more convenient as the activating agents for the synthesis of diesters **224-226** in this study.

2. Synthesis of classical 6-substituted pyrrolo[2,3-*d*]pyrimidine 163 (n=2)

Compound **163** was obtained via a Sonogashira coupling reaction between the intermediates **230** (Scheme 43) and **234** (Scheme 44) as the key step.[114, 333] The intermediate **230** was obtained by a four-step synthesis from the commercially available

2,4-diamino-6-hydroxy primidine **35** (Scheme 43). Compound **28** was condensed with α-chloro acetaldehyde **227** to afford the pyrrolo[2,3-*d*]pyrimidine **228**.[334] Protection of **228** with a pivaloy group provided compound **229**, which was converted to the 6-substituted mercury salt and immediately reacted with iodine to give the desired 6-iodo pyrrolo[2,3-*d*]pyrimidine **230**.

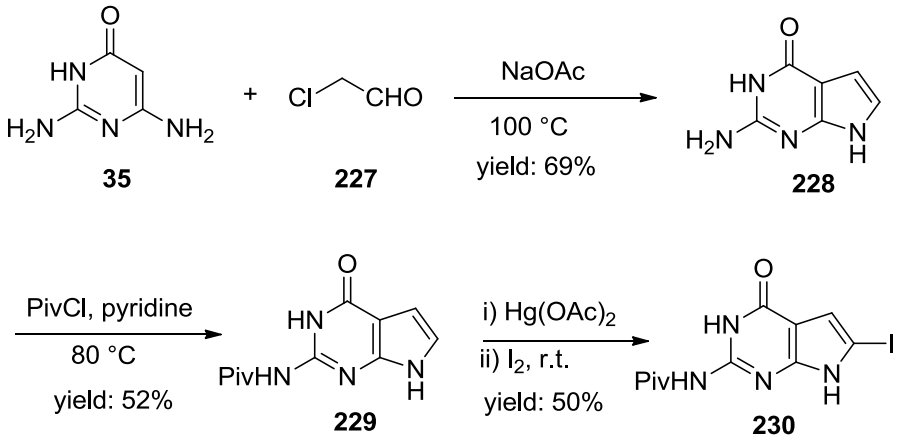

35 **227** **228** **229** **230**

Scheme 43 Synthesis of intermediate 6-iodo-pyrrolo[2,3-*d*]pyrimidine **230**.

The synthesis of intermediate **234** began with the coupling of commercially available 4-iodobenzoic acid **231**(Scheme 44) and diethyl-*L*-glutamate hydrochloride to afford diethyl 4-iodobenzoyl-*L*-glutamate **232**. The yield of **232** was 95 %, which was better than that reported by Taylor and co-workers (75%).[114, 333]

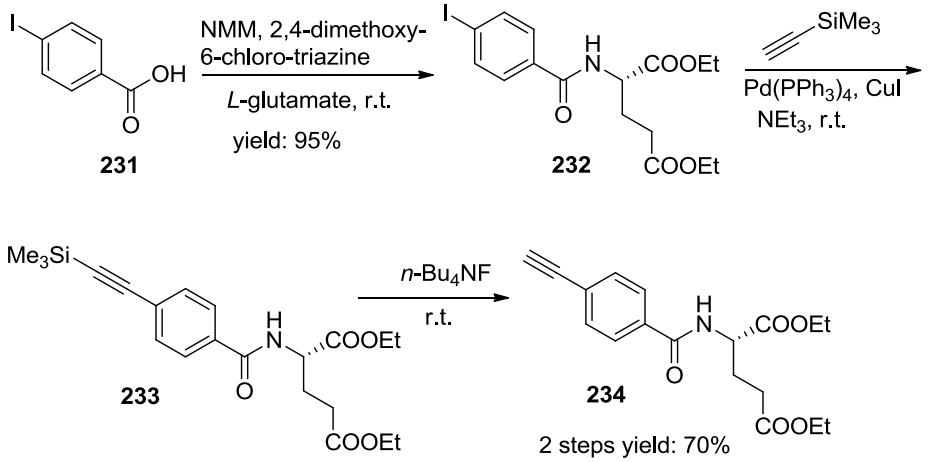

231 **232** **233** **234**

Scheme 44 Synthesis of intermediate acetylene **234** by Sonogashira coupling.

Palladium catalyzed coupling of **232** with trimethylsilyl acetylene, in the presence of tetrakis-(triphenylphosphine) palladium (0) ($Pd(PPh_4)_3$), copper (I) iodide (CuI) and triethylamine, gave **233** as a reddish oil, which was immediately desilyated using n-Bu_4NF to afford the acetylene **234** (74% over two steps).

With the 6-iodo pyrrolo[2,3-*d*]pyrimidine **230** in hand, a palladium catalyzed carbon-carbon coupling reaction with the aryl iodide **230** and the acetylene **234** (Scheme 45) led to the 6-substituted compound **235**. Instead of using the reaction condition of 5% Pd/C, 48 h described by Taylor and co-workers[114, 333] to get 72% yield of the hydrogenation of **235**, a 10% Pd/C, 5 hour-condition was employed to get a complete transformation (100% yield of **236**) without any partial reduction. No separation is needed for **236** because of the complete transformation of this reduction. Compound **236** was then converted to the target compound **163** by a convenient deprotection with 1N sodium hydroxide solution.

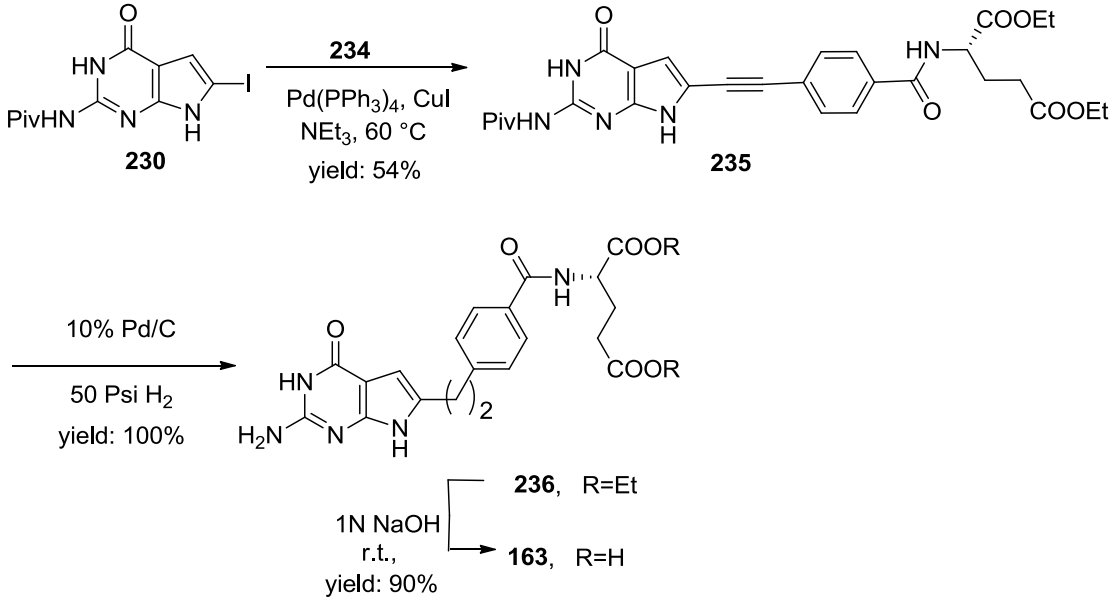

Scheme 45 Synthesis of 6-substituted pyrrolo[2,3-*d*]pyrimidine **163** (n=2).

3. Synthesis of 6-substituted pyrrolo[2,3-*d*]pyrimidine 164-167 (n=5-8) with a straight side chain

Compounds **164-167** (n=5-8) were obtained via a seven-step synthesis from the commercially available alkyl carboxylic acid esters**237-240** using an α-bromomethyl ketone condensation with pyrimidine as the key step as outlined in Scheme 47.

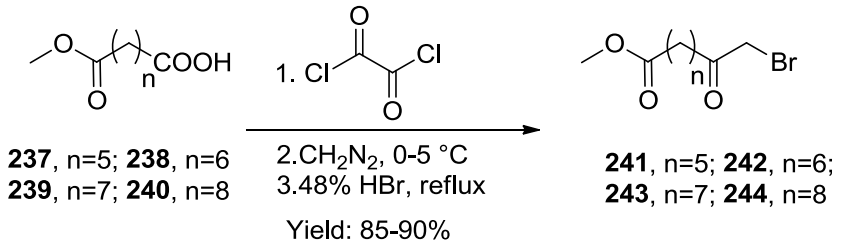

237, n=5; **238**, n=6
239, n=7; **240**, n=8

241, n=5; **242**, n=6;
243, n=7; **244**, n=8

Scheme 46 Synthesis of intermediate straight chain α-bromomethyl ketones **241-244**.

Commercially available carboxylic acids **237-240** were converted to the acid chlorides and immediately reacted with diazomethane followed by 48% HBr to give the desired α-bromomethylketones **241-244**. (Scheme 46)

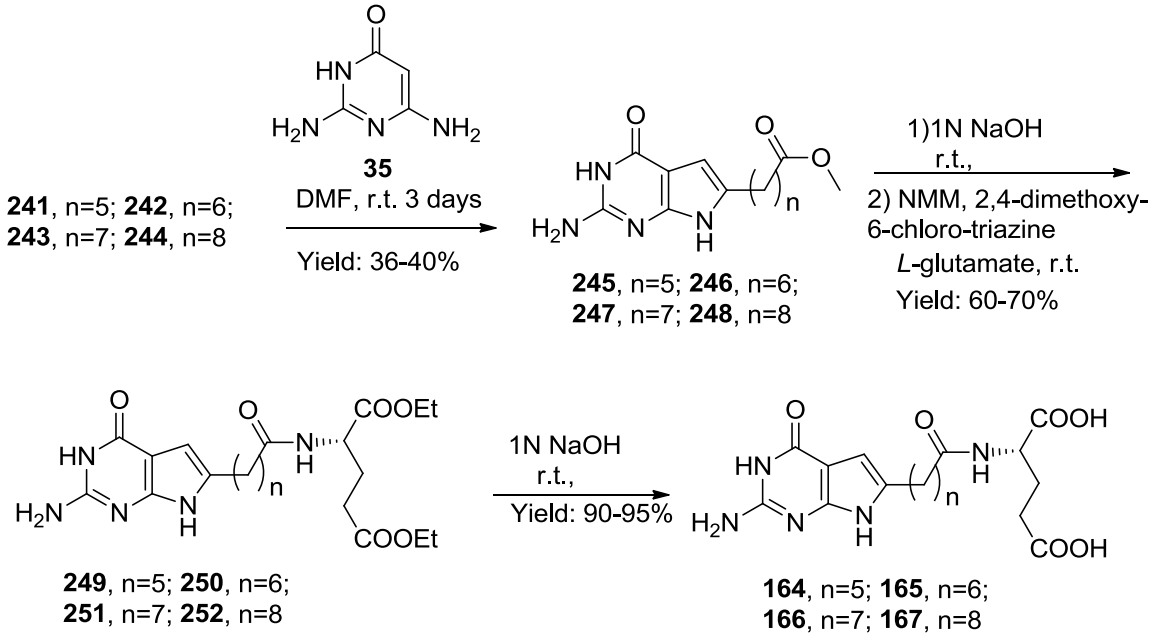

241, n=5; **242**, n=6;
243, n=7; **244**, n=8

245, n=5; **246**, n=6;
247, n=7; **248**, n=8

249, n=5; **250**, n=6;
251, n=7; **252**, n=8

164, n=5; **165**, n=6;
166, n=7; **167**, n=8

Scheme 47 Synthesis of 6-substituted pyrrolo[2,3-*d*]pyrimidine **164-167** (n=5-8).

With the desired α- bromomethylketones **241-244** in hand, the next step was the condensation of 2,4-diamino-6-hydroxypyrimidine **35** with **241-244** (Scheme 47). Optimal yields were obtained at room temperature for 3 days and only pyrrolo[2,3-*d*]pyrimidines **245-248** were obtained. No side product furo[2,3-*d*]pyrimidines were found in this reaction compared with condensation with α-chloromethylketones to afford both pyrrolo[2,3-*d*]pyrimidines and furo[2, 3-*d*]pyrimidines. Hydrolysis of **245-248** afforded the corresponding free acids. Subsequent coupling with L-glutamate diethyl ester using *N*-methyl morpholine and 2,4-dimethoxy-6-chloro-triazine as the activating agents afforded the diesters **249-252**. Final saponification of the diesters gave the target compounds **164-167**.

4.Synthesis of 6-substituted pyrrolo[2,3-*d*]pyrimidine 168 and 170 as isosteric isomers of compound 2

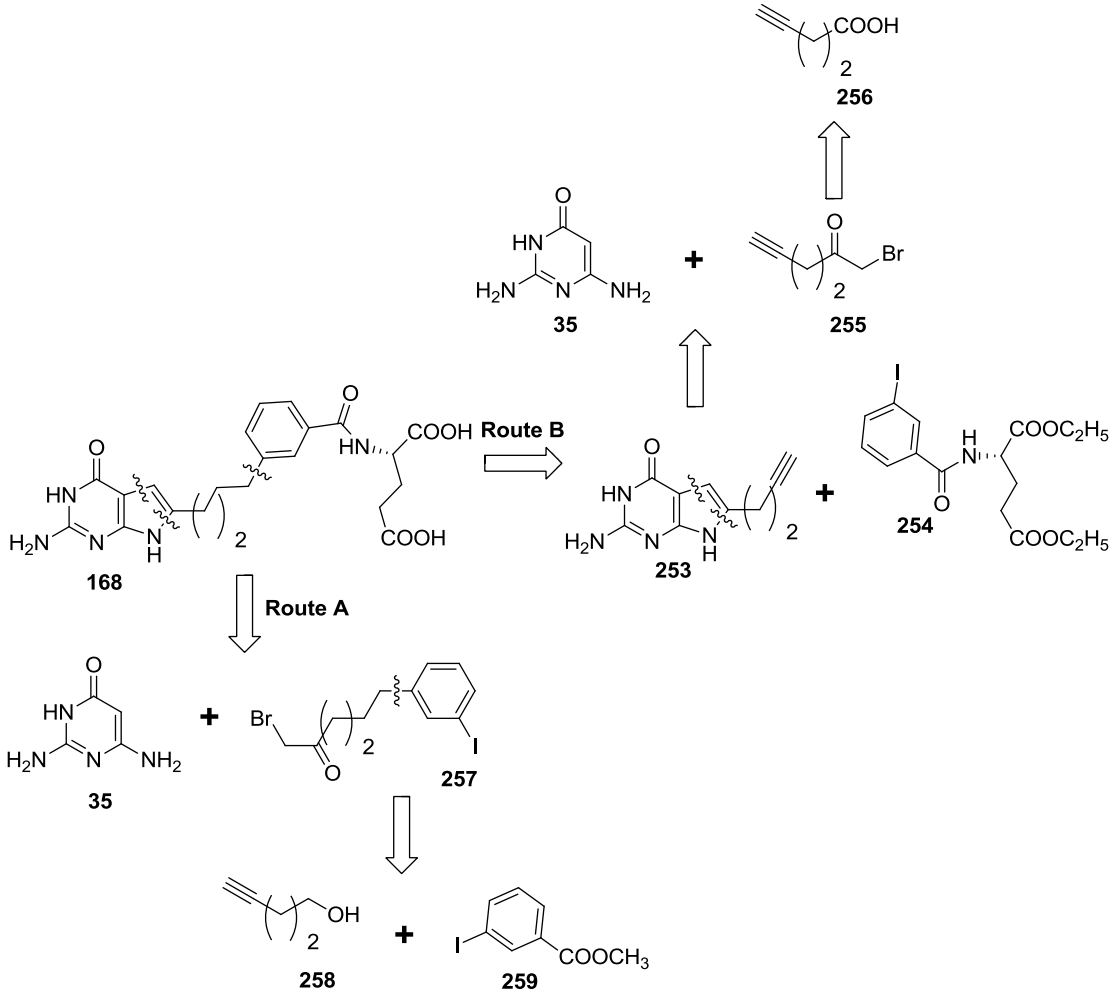

Scheme 48 Retro synthetic analysis of 6-substituted pyrrolo[2,3-*d*]pyrimidine **168**.

Two retro synthetic routes were proposed as shown in Scheme 48.[115] From route A, it was anticipated that a Sonogashira coupling of the iodide **259** with commercially available terminal acetylene alcohols, **258**, followed by hydrogenation, Jones oxidation and homologation would afford the α-bromomethylketone **257**. Sequential coupling with 2,6-diamino-3*H*-pyrimidin-4-one **35**, hydrolysis, *L*-glutamate peptide coupling and saponification would afford the target compound **168**. The target compound could also be

synthesized from route B. The commercially available terminal acetylene carboxylic acid **256** would first be converted to the α-bromomethylketone **255**, which could undergo coupling reaction with **35** to give the key intermediate 2-amino-4-oxo-6-alkynl-pyrrolo[2,3-*d*]pyrimidine, **253**. Sequential Sonogashira coupling with iodide, **254**, hydrogenation and sponification would afford the target compounds.

From a retro-synthetic stand point of view, route B would be better than route A for compounds with the isosteric replacement of 1,4-disubstituted phenyl ring on the side chain , since the common intermediate **253** generated from route B could be used to synthsize several other analogs for SAR studies.

Thus, compound **168** was obtained via a Sonogashira coupling reaction between the intermediates **253** and **263** as the key step.

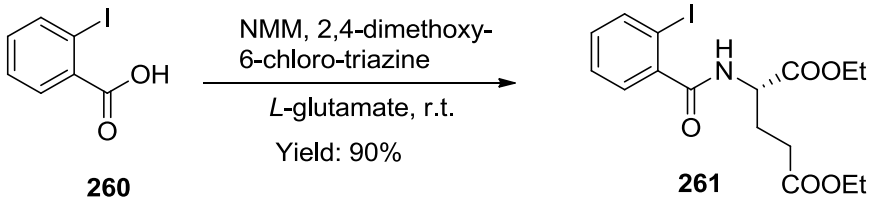

260 **261**

Scheme 49 Synthesis of intermediate **261**.

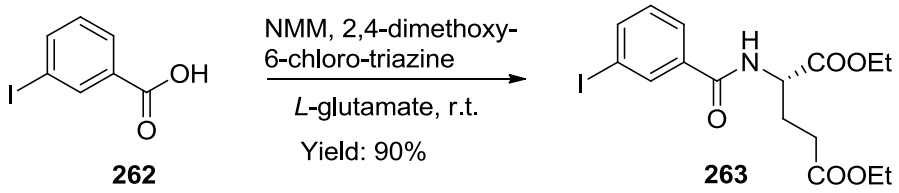

262 **263**

Scheme 50 Synthesis of intermediate **263**.

The synthesis of intermediate **261** (Scheme 49) began with the coupling of

commercially available 2-iodobenzoic acid **260** and diethyl-*L*-glutamate hydrochloride to afford diethyl 2-iodobenzoyl-L-glutamate **261**. The diethyl 3-iodobenzoyl-*L*-glutamate **263** was synthesized by the same procedure as shown (**Scheme 50)**.

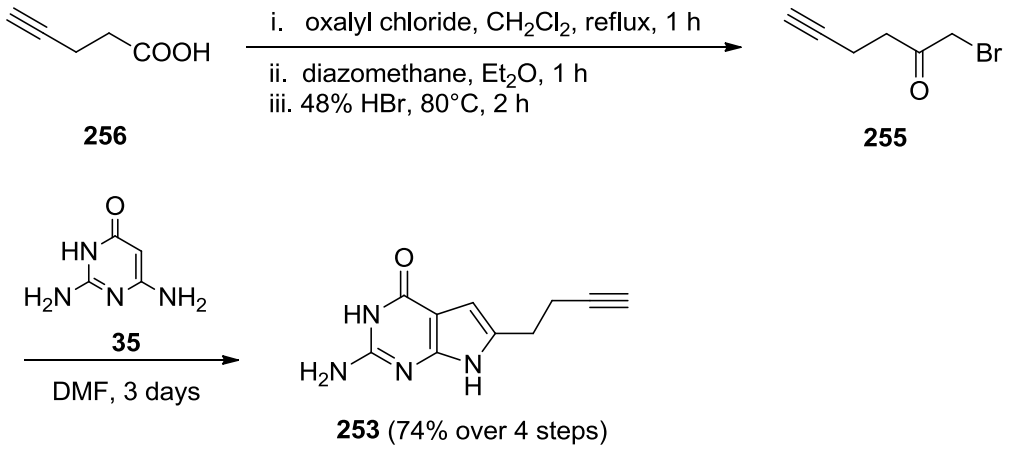

Scheme 51 Synthesis of intermediate **253.**

The other key intermediate **253** was obtained by a five-step synthesis from the commercially available pent-4-ynoic acid **256**. (Scheme 51) Carboxylic acid **256** was converted to the acid chloride and immediately reacted with diazomethane followed by 48% HBr to give the desired α-bromomethylketone **255**. Condensation of 2,6-diamino-3*H*-pyrimidin-4-one, **35** with α-bromomethylketone **255** at room temperature for 3 days afforded the desired terminal alkyne **253**.

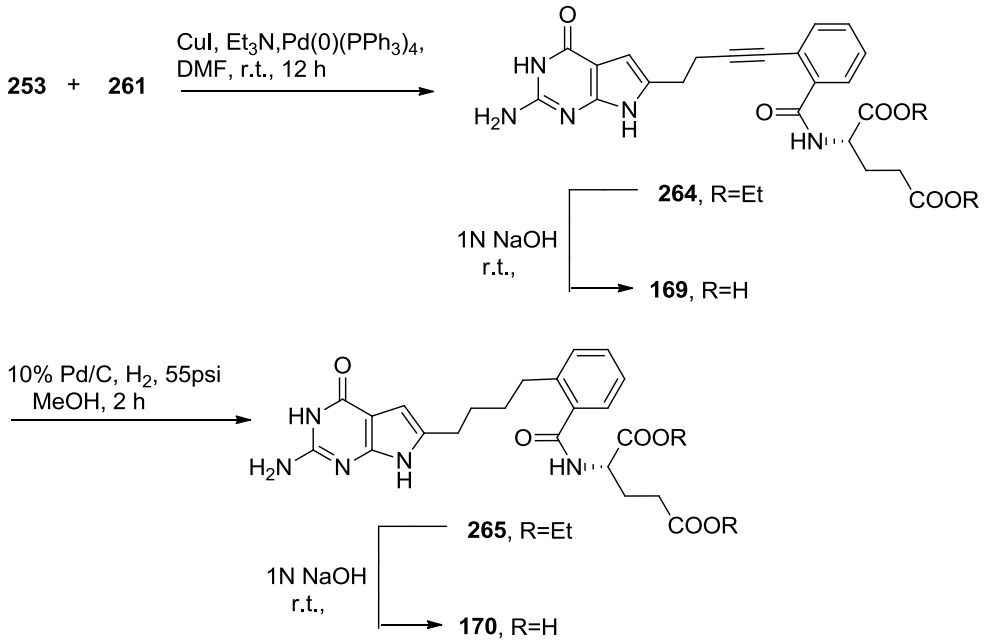

Scheme 52 Synthesis of **169** and **170**.

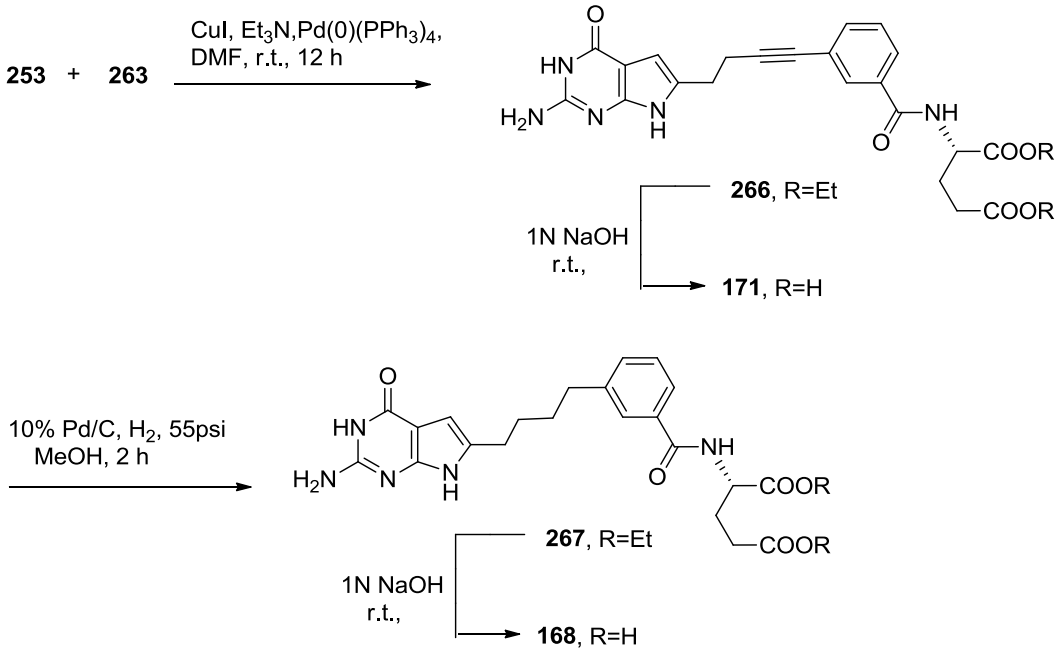

Scheme 53 Synthesis of **168** and **171**.

Compounds **264** and **266** were obtained by a Sonogashira coupling of **253** with

iodide **261** and **263** in the presence of tetrakis-(triphenylphosphine) palladium (0) ($Pd(PPh_4)_3$), copper(I) iodide (CuI) and triethylamine. Hydrogenation and saponification of **264** and **266** afforded **170** and **168**, respectively. (Scheme 52, Scheme 53)

5. Synthesis of classical 5-substituted pyrrolo[2,3-*d*]pyrimidines with a phenyl side chain 172-177 (n=1-6)

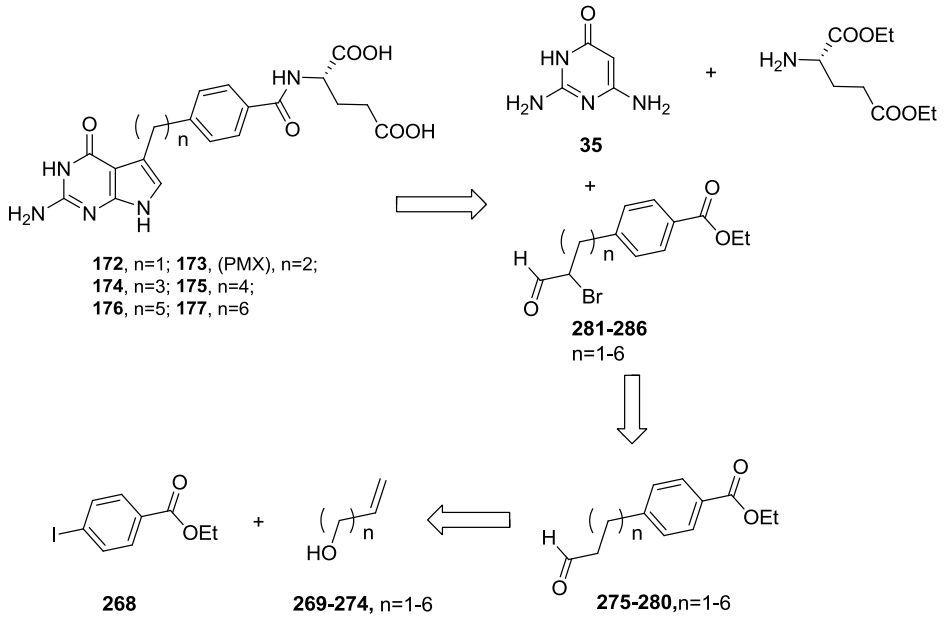

Scheme 54 Retro synthesis analysis of 5-substituted pyrrolo[2,3-*d*]pyrimidines with phenyl side chain analogues **172-177** (n=1-6).

A retro synthesis analysis of 5-substituted pyrrolo[2,3-*d*]pyrimidines with phenyl side chain analogues **172-177** (n=1-6) was shown. (Scheme 54) The 5-substituted pyrrolo[2,3-*d*]pyrimidine ring could be synthesized from the cyclolization between 2,4-diamino-4-oxo-pyrimidine **35** and α-bromo aldehydes **281-286**, which could be obtained by α-bromonation of the corresponding aldehydes **275-280**. The aldehydes **275-280** could

be easily obtained by a one step Heck coupling from benzyl iodide **268** and allyl alcohols **269-274**.

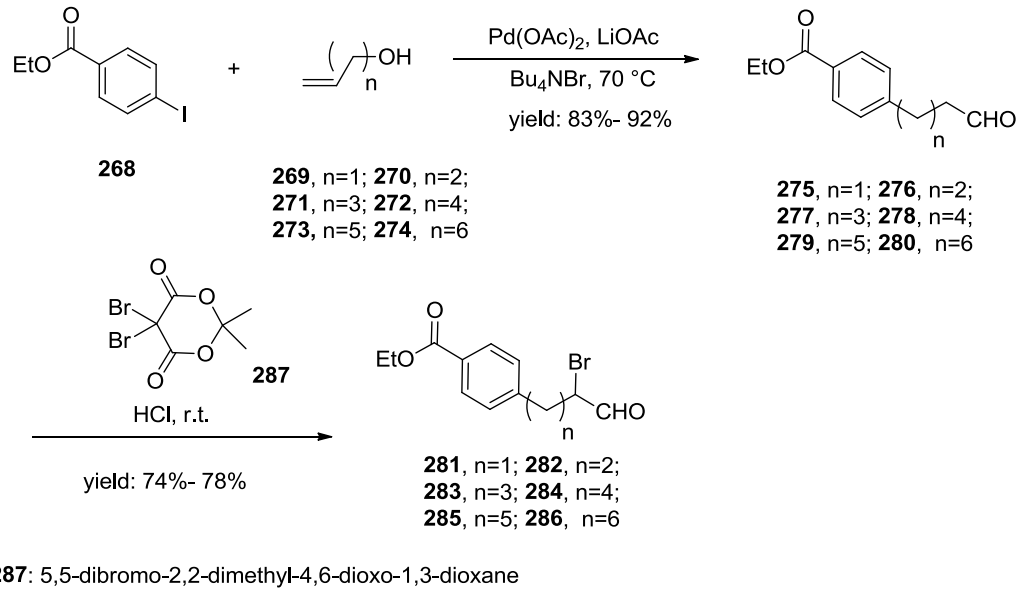

Scheme 55 Synthesis of intermediate **281-286.**

Thus, a Heck coupling reaction[335] of **268** with alcohols **269-274** in DMF at 70 ^{o}C afforded the aldehydes **275-280** (yields: 83-92%). α-Bromonation of **275-280** with 5,5-dibromo-2,2-dimethyl-4,6-dioxo-1,3-dioxane **287**[336] at room temperature afforded the corresponding α-bromo aldehydes **281-286** (yields: 74-78%). (Scheme 55)

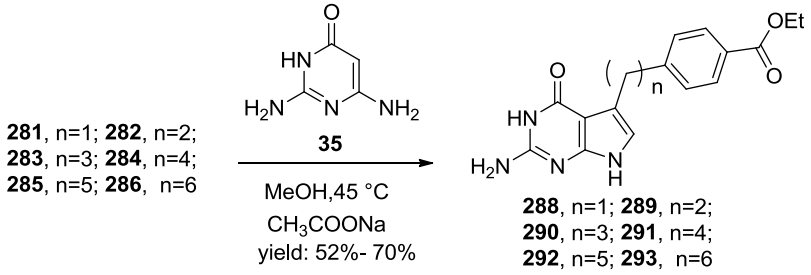

Scheme 56 Synthesis of intermediate **288-293**.

The 5-substituted pyrrolo[2,3-*d*]pyrimidines **288-293**were synthesized by condensation of **281-286** with 2,4-diamino-6-hydroxypyrimidine **35** at 45 ^{o}C in the presence of sodium acetate (yields: 45-50%). (Scheme 56)

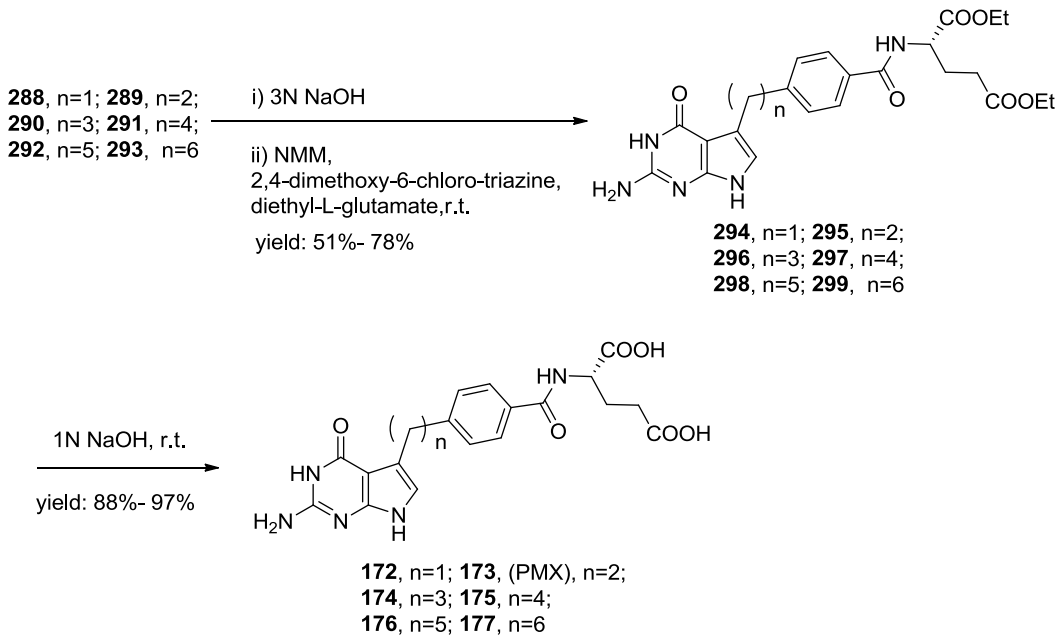

Scheme 57 Synthesis of 5-substituted pyrrolo[2,3-*d*]pyrimidine with phenyl side chain analogues **172-177** (n=1-6).

Subsequent hydrolysis with 3N NaOH followed by coupling with diethyl *L*-glutamate using *N*-methyl morpholine and 2,4-dimethoxy-6-chlorotriazine as the activating agents afforded the diesters **294-299** (yields: 51-78% over two steps). Final saponification of the diesters with 1N NaOH gave the target compounds 5-substituted pyrrolo[2,3-*d*]pyrimidines **172-177** (yields: 88-97%). (Scheme 57)

6. Synthesis of 5-substituted pyrrolo[2,3-*d*]pyrimidines with a thiophenyl side chain analogues 178-183 (n=1-6)

The thiophenyl side chain analogues **178-183** (n=1-6) were proposed to be synthesized by the similar procedure as their phenyl analogs. The only synthetic challenge of this series is synthesis of the intermediate aldehyde with a thiophenyl side chain **300**.

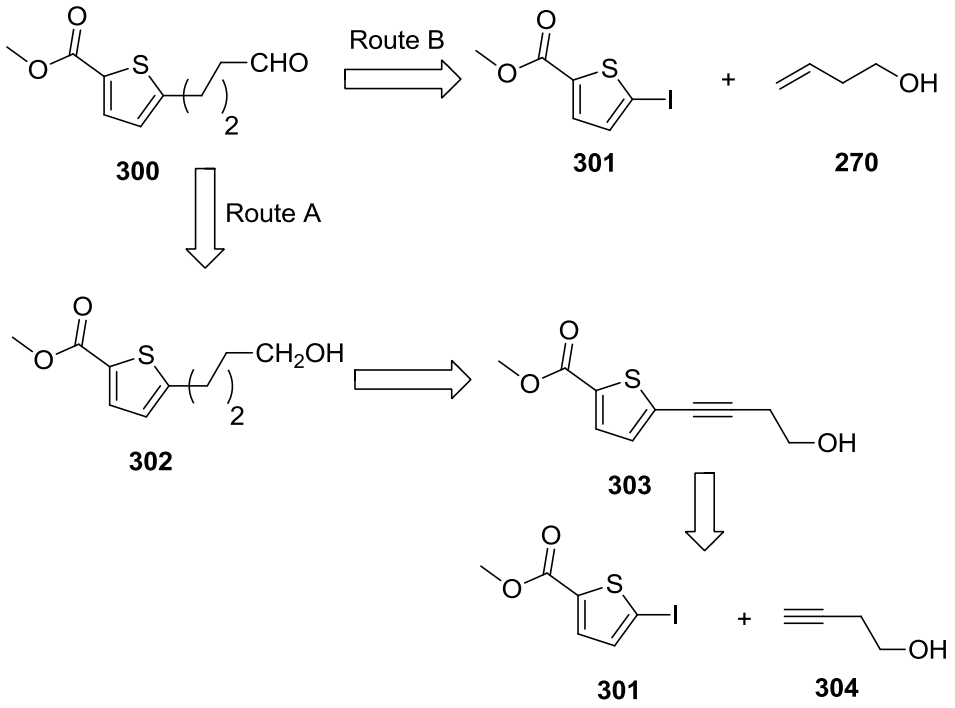

Scheme 58 Retro synthesis analysis of intermediate **300**.

A retro synthesis analysis of intermediate **300** was shown. (Scheme 58) By route A, the aldehyde **300** could be obtained in a three step reaction from a Sonogashira coupling of iodide **301** and alkyne **304** followed by the reduction of the triple bond and oxidization of the alcohol **302** to aldehyde **300**. By route B, the aldehyde **300** could be obtained by a one step Heck coupling of thiophenyl iodide **301** with allyl alcohol **270** as the synthesis

of its phenyl analogs described above.

It is obvious that the better way to synthesize it is by a one step Heck coupling. However, this Heck coupling of the thiophene iodide (with an ester group) and the allyl alcohol has not been reported in the literature.

To investigate the heterocycle Heck coupling, the key intermediate thiophene bromide **306** was proposed first because of the ease of its synthesis from commercially available carboxylic acid **305** by esterification.

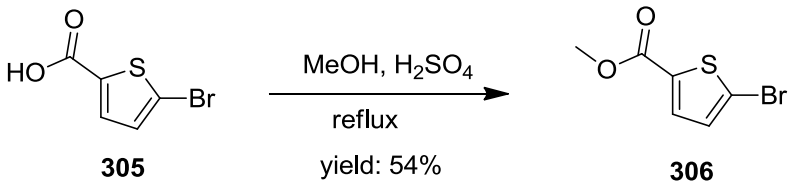

305 **306**

Scheme 59 Synthesis of intermediate **306**.

The intermediate **306** was successfully obtained by reflux of the carboxylic acid **305** with H_2SO_4 and methanol in 54% yield as shown. (Scheme 59)

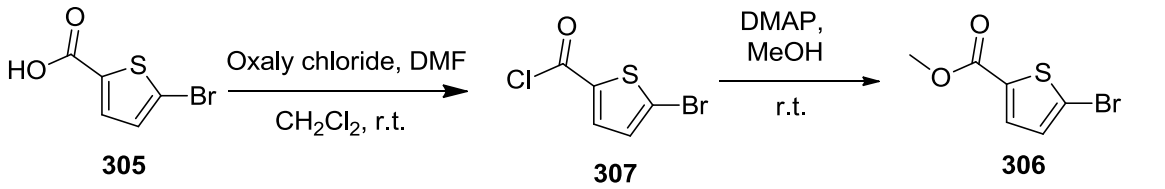

305 **307** **306**

two steps yield: 93%

Scheme 60 Improved synthesis of intermediate **306**.

A significantly improved yield of 93% was achieved by reaction of **305** with oxaly chloride with the assistance of DMF followed by esterification with methanol and DMAP. (Scheme 60)

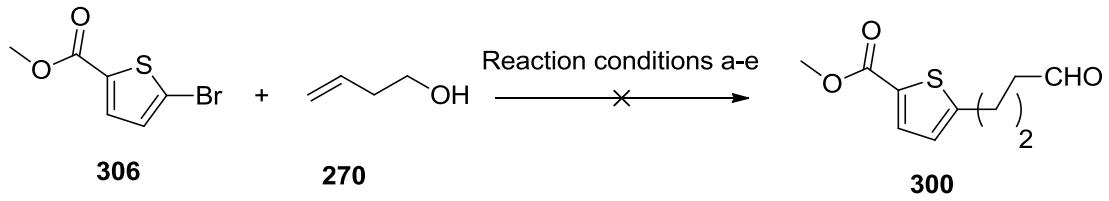

306 270 300

Scheme 61 Heck coupling of the thiophene bromide **306**.

Unfortunately, the Heck coupling of the thiophene bromide **306** and allyl alcohol **270** under the previous condition[335] was unsuccessful. (Scheme 61)

Several different reaction conditions were further explored to precede this Heck coupling. The different conditions attempted are listed in Table 5.

Table 5 Attempted conditions for Heck coupling of the thiophene bromide **306**.

Entry	$Pd(OAc)_2$	Temperature (^oC)	Time (h)	Yield
a	0.05 eq	70	12	Decomposed[a]
b	0.05 eq	70	1	Decomposed[a]
c	0.05 eq	r.t.	12	No reaction[b]
d	0.05 eq	45	12	No reaction[b]
e	0.5 eq	45	12	No reaction[b]

a. No starting material or product found on TLC
b. No convertion from starting material found on TLC

The most probable reason for the unsuccess of this reaction is the low reactivity of the bromide in the Heck coupling. The more reactive thiophene iodide **301** was proposed

to provide a better Heck coupling reactant.

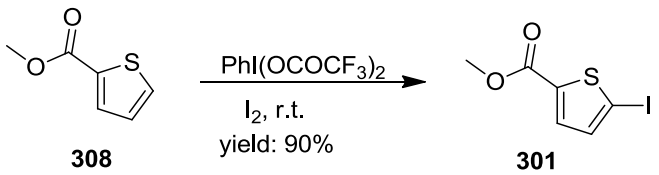

Scheme 62 Synthesis of the thiophene iodide **301**.

The thiophene iodide **301** was successfully synthesized by iodination of **308** with $PhI(OCOCF_3)_2$ and iodine at room temperature with 90% yield. (Scheme 62)

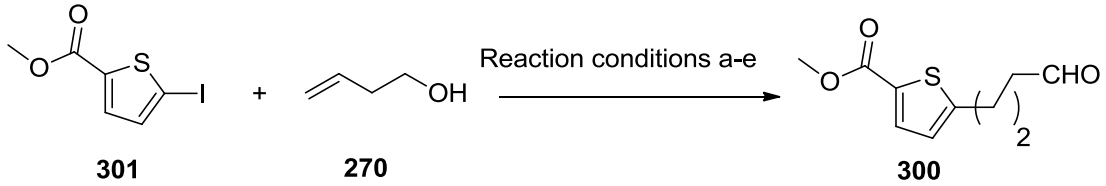

Scheme 63 Improved Heck coupling of **300**

Further exploration of Heck coupling of this thiophene iodide **301** with ally alcohol **270** is shown in Scheme 63.

Unfortunately, the Heck coupling of the thiophene iodide **301** and allyl alcohol **270** under the previous condition[335] was unsuccessful as the thiophene bromide **306**.

Table 6 Attempted conditions for the Heck coupling of the thiophene iodide.

Entry	$Pd(OAc)_2$	Temperature (^oC)	Time (h)	Yield
a	0.05 eq	70	12	Decomposed[a]
b	0.05 eq	70	1	Decomposed[a]

c	0.05 eq	r.t.	12	No reaction[b]
d	0.5 eq	r.t.	12	No reaction[b]
e	0.5 eq	45	2h	65%

a. No starting material or product found on TLC
b. No convertion from starting material found on TLC

Several different reaction conditions were further explored to precede this Heck coupling. The different conditions attempted are listed in **Table 6**. The condition tried first (Entry a) is 0.05eq $Pd(OAc)_2$ at 70 ^oC for 12h as reported with the phenyl iodide before.[335] The reactant **301** was found to be decomposed due to the high temperature. The same result was found when the reaction time was reduced to 1h (Entry b). The reaction was tried at room temperature with different equivalents of $Pd(OAc)_2$ (0.05eq, Entry c; 0.5eq, Entry d) for 12h. No reaction was found under these conditions. A sucessful reaction condition was found with a good yield of 65% when the reaction temperature increased to 45 ^oC for 2h and the equivalent of $Pd(OAc)_2$ increased to 0.5eq (Entry e). Thus, a successful Heck coupling of the thiophene iodide **301** and allyl alcohol **270** to synthesize the aldehyde **300** in one step was discovered. The reaction condition is mild (45 ^oC) and the yield is good (65%). In addition, the reaction is fast (2h) and easy to handle (no argon protection needed).

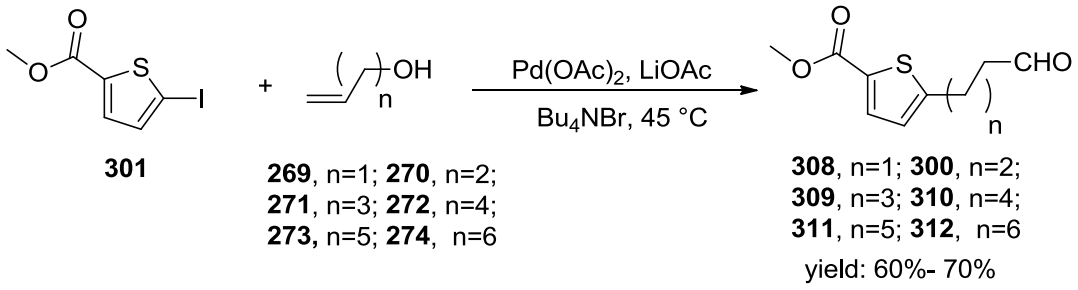

Scheme 64 Synthesis of intermediate **308-312.**

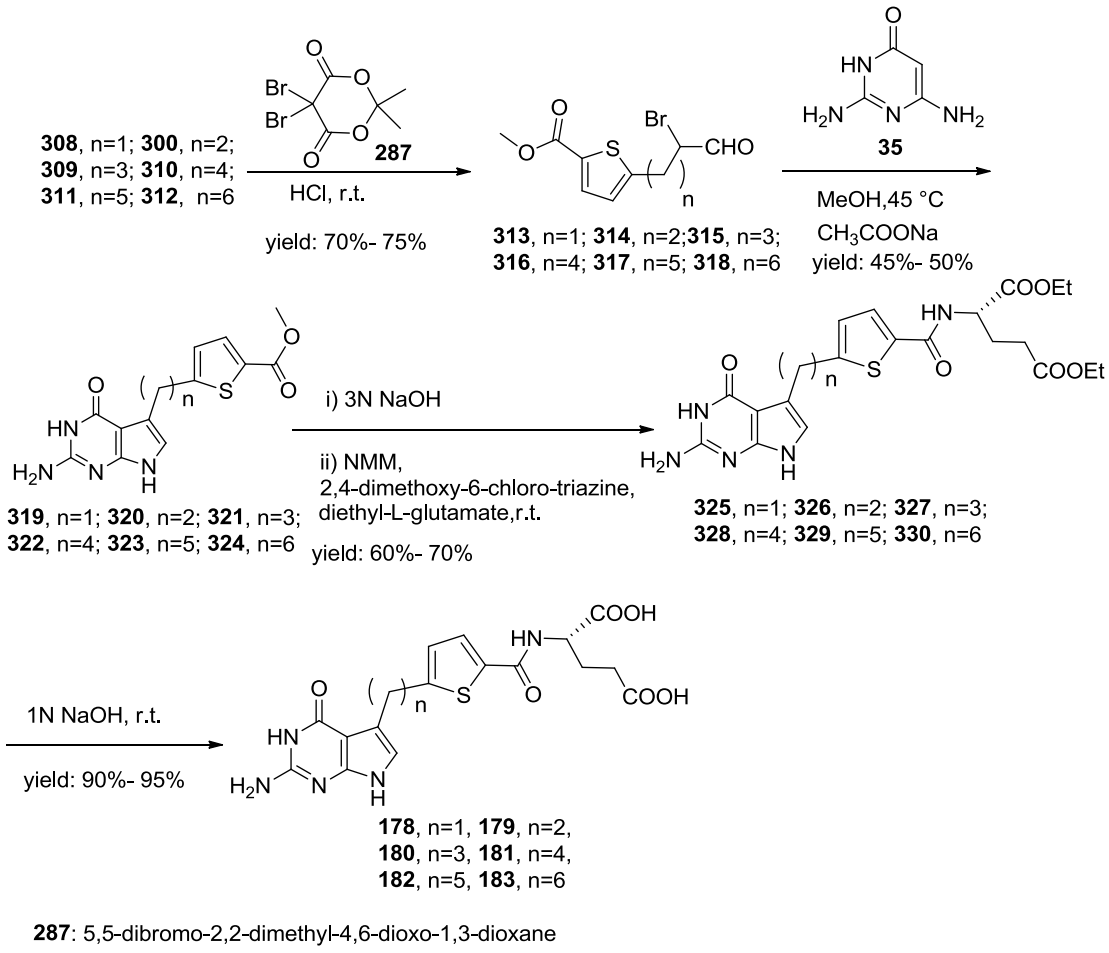

Scheme 65 Synthesis of **178-183**.

With the desired of Heck coupling of thiophene iodide **300**, other aldehydes of the series (n=1-6) were successfully synthesized at the same reaction condition in 60-70% yields as shown in Scheme 64.

Compounds **178-183** were obtained starting from the methyl 5-iodothiophene-2-carboxylate **301** using an α-bromo aldehyde condensation with 2,4-diamino-4-oxo-pyrimidine **35** as the key step as outlined in Scheme 65. Thus, a Heck coupling reaction of **301** with alcohols **269-274** in DMF at 45 ^{o}C afforded the aldehydes **308-312** (yields: 60-70%). (Scheme 64)

α-Bromonation of **308-312** with 5,5-dibromo-2,2-dimethyl-4,6-dioxo-1,3-dioxane **287** at room temperature afforded the corresponding α-bromo aldehydes **313-318** (yields: 70-75%)**.** (Scheme 65) The 5-substituted pyrrolo[2,3-*d*]pyrimidines **319-324** were synthesized by condensation of **313-318** with 2,4-diamino-6-hydroxypyrimidine **35** at 45 ^{o}C in the presence of sodium acetate. Subsequent hydrolysis with 3N NaOH and then coupling with diethyl *L*-glutamate using *N*-methyl morpholine and 2,4-dimethoxy-6-chlorotriazine as the activating agents afforded the diesters **325-330** (yields: 60-70% over two steps). Final saponification of the diesters with 1N NaOH gave the target compounds 5-substituted pyrrolo[2,3-*d*]pyrimidines **178-183** (yields: 88-97%).

7. Synthesis of classical 5-substituted pyrrolo[2,3-*d*]pyrimidine with straight side chain analogues 184-186 (n=6-8)

Compounds **184-186** (n=6-8) were obtained using an *α*-bromo aldehyde condensation with 2,4-diamino-4-oxo- pyrimidine **35** as the key step as outlined in Scheme 68. These analogs were proposed to be synthesized by the same procedure as their phenyl and thiophenyl analogs. The only synthetic challenge of this series is the intermediate aldehyde with a straight side chain which is not commercially available.

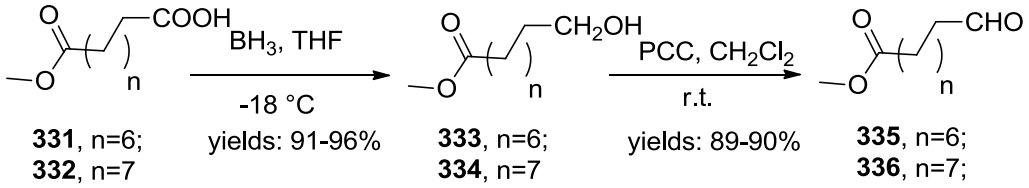

Scheme 66 Synthesis of intermediate aldehydes **335-336**.

The intermediate aldehydes **335-336** were obtained successfully by reduction of the commercially available carboxylic acid **331-332** to the corresponding alcohols **333-334** by BH_3 in THF at -18 ^oC followed by PCC oxidation. (Scheme 66)

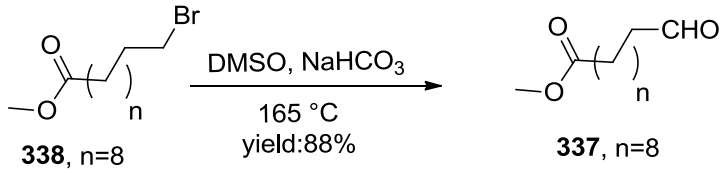

Scheme 67 Synthesis of intermediate aldehyde **337**.

The intermediate aldehyde **337** was afforded successfully in 88% yield by reaction of the commercially available bromide **338** with DMSO and $NaHCO_3$ at 165 ^oC. (Scheme 67)

With the desired intermediate straight chain aldehydes **335-337** in hand, the synthesis of compounds **184-186** (n=6-8) is pretty straight forward as shown in Scheme 68:

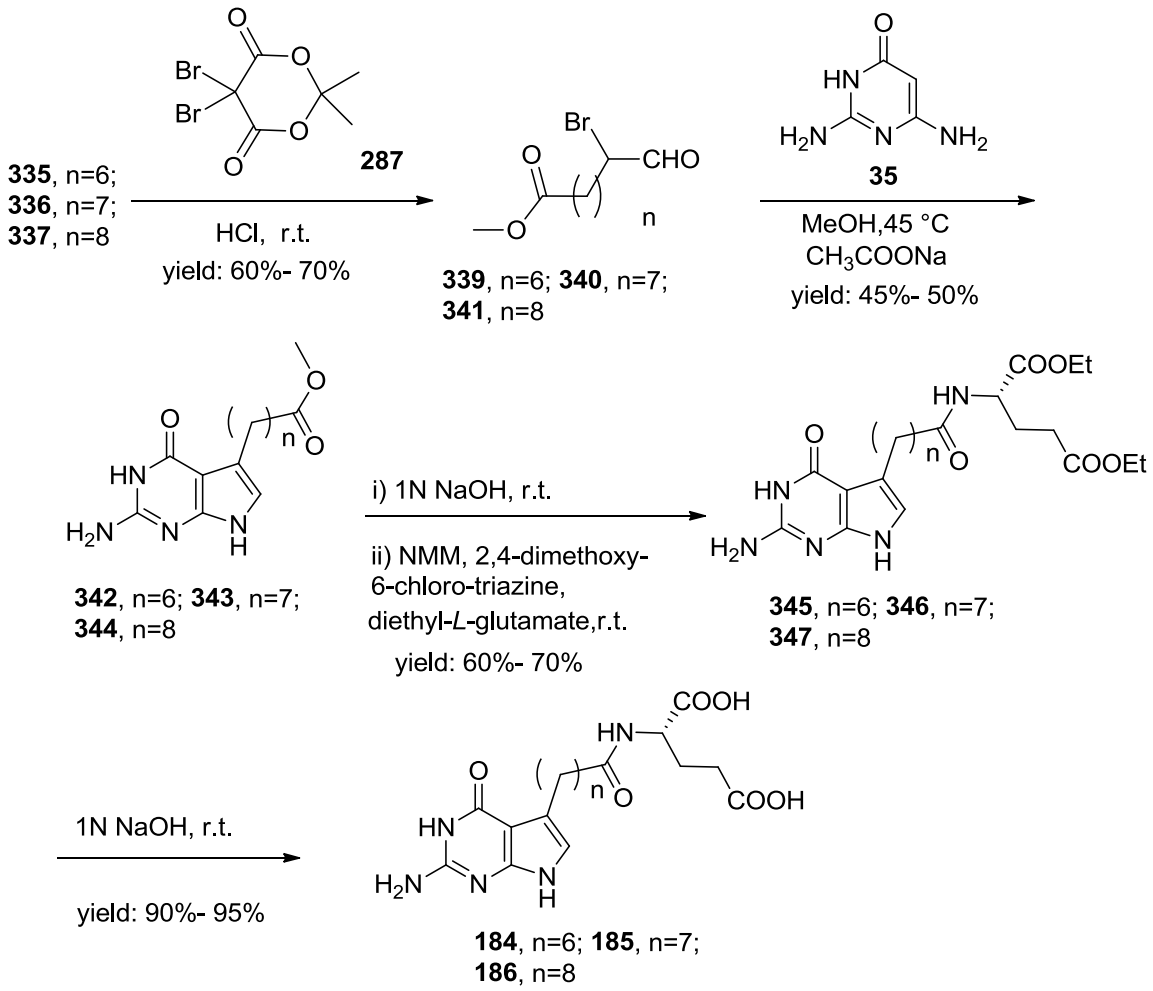

Scheme 68 Synthesis of **184-186** (n=6-8).

α-Bromonation of **335-337** with 5,5-dibromo-2,2-dimethyl-4,6-dioxo-1,3-dioxane **287** at room temperature afforded the corresponding α-bromo aldehydes **339-341** (yields: 60-70%)**.** The 5-substituted pyrrolo[2,3-*d*]pyrimidines **342-344** were synthesized by condensation of **339-341** with 2,4-diamino-6-hydroxypyrimidine **35** at 45 ^{o}C in the presence of sodium acetate (yields: 45-50%). Subsequent hydrolysis with 1N NaOH and then coupling with diethyl *L*-glutamate using *N*-methyl morpholine and 2,4-dimethoxy-6-chlorotriazine as the activating agents afforded the diesters **345-347** (yields: 60-70% over

two steps). Final saponification of the diesters with 1N NaOH gave the target compounds 5-substituted pyrrolo[2,3-*d*]pyrimidines **184-186** (n=6-8) (yields: 90-95%).

8. Synthesis of classical 7-substituted pyrrolo[2,3-*d*]pyrimidines with a straight side chain 187-190 (n=5-8)

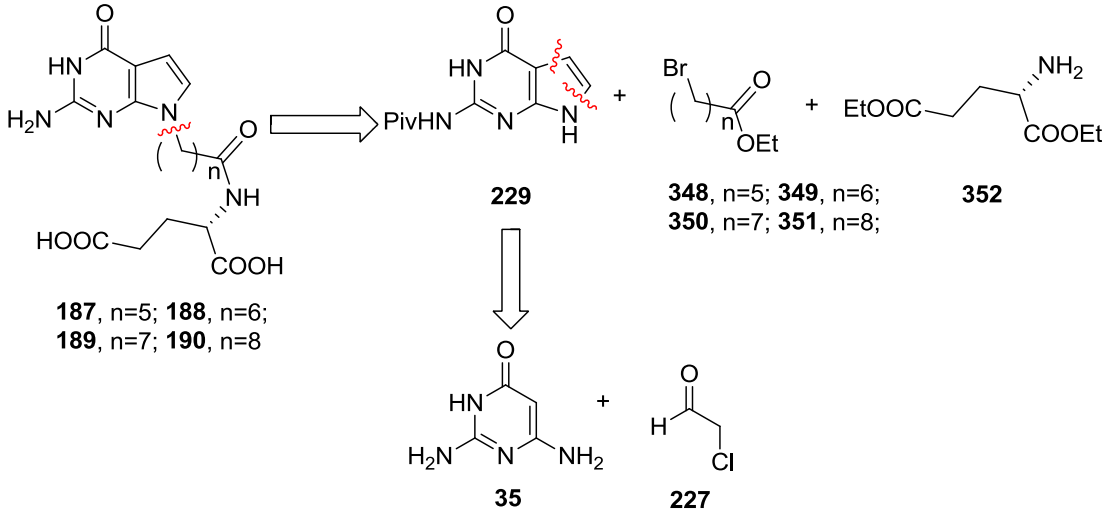

Scheme 69 Retro synthesis analysis of 7-substituted pyrrolo[2,3-*d*]pyrimidine **187-190** (n=5-8).

The retro synthesis analysis of 7-substituted pyrrolo[2,3-*d*]pyrimidine **187-190** (n=5-8) is shown in Scheme 69. These analogs could be obtained by the reaction of the bromide **348-351** with the known intermediate **229**, which could be obtained from the cyclolization of 2,4-diamino-6-hydroxypyrimidine **28** with α-chloro aldehyde **227**. The alkylation of the 7-*N* of **229** is the key step in this synthesis.

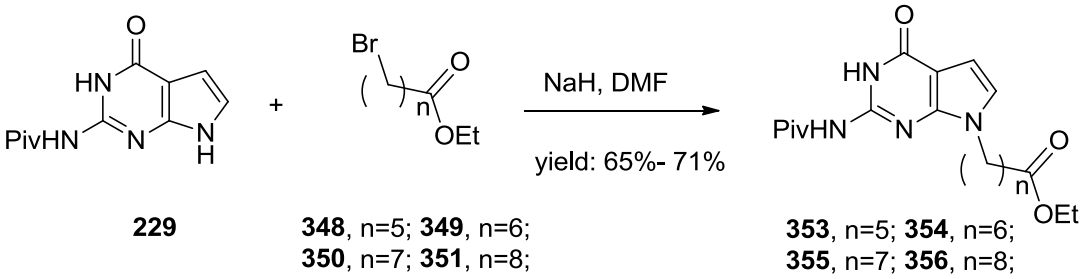

Scheme 70 Synthesis of intermediates **353-356**.

The 7-substituted pyrrolo[2,3-*d*]pyrimidines **353-356** were obtained by N7-alkylation of the common intermediate **229** by bromides **348-351** with NaH in DMF. The intermediate **229** has a pivaloyl group protected at the N2- position to ensure the exclusive alkylation at the N7- position. (Scheme 70)

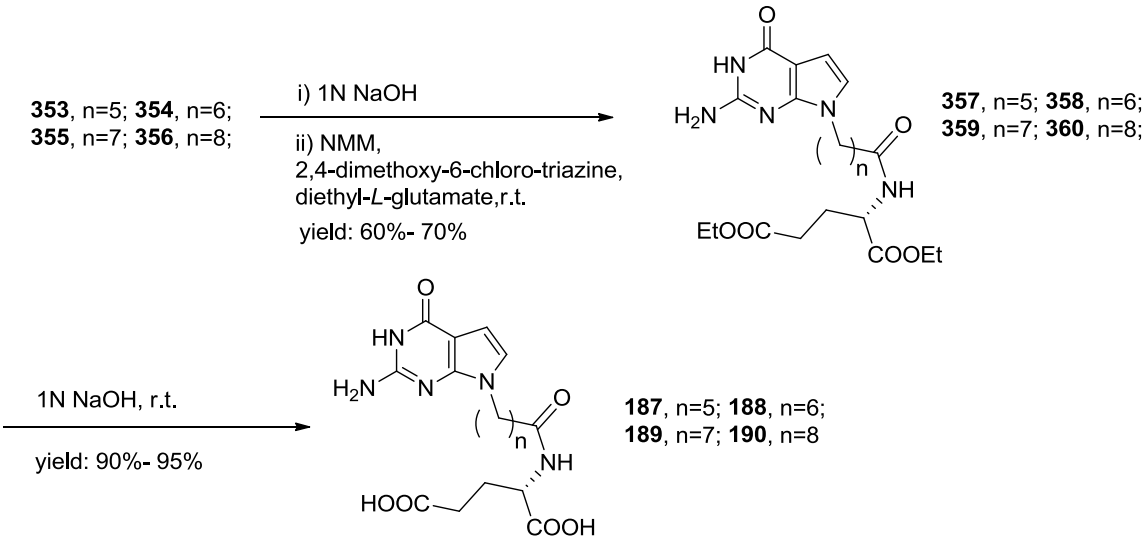

Scheme 71 Synthesis of 7-substituted pyrrolo[2,3-*d*]pyrimidine **187-190** (n=5-8).

With the desired intermediate 7-substituted pyrrolo[2,3-*d*]pyrimidines **353-356** in hand, the synthesis of compounds **187-190** (n=5-8) was carried out as shown in Scheme 71. Subsequent hydrolysis **353-356** with 1N NaOH and then coupling with diethyl *L*-

glutamate using *N*-methyl morpholine and 2,4-dimethoxy-6-chlorotriazine as the activating agents afforded the diesters **357-360** (yields: 60-70% over two steps). Final saponification of the diesters with 1N NaOH gave the target compounds 7-substituted pyrrolo[2,3-*d*]pyrimidines **187-190** (n=5-8) (yields: 90-95%)**.**

9. Synthesis of 175 glutmate derivatives

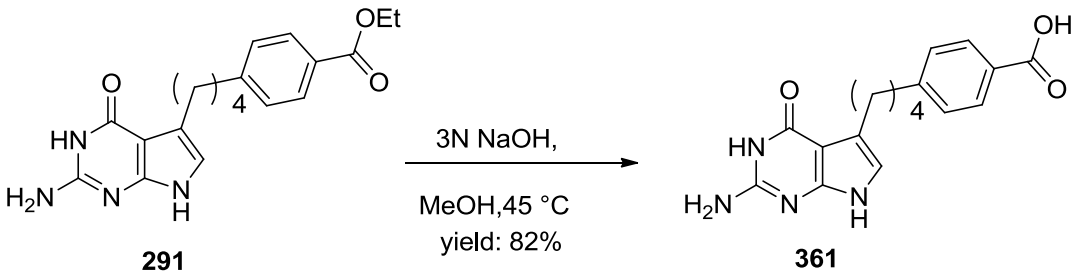

Scheme 72 Synthesis of pteroic acid **361**.

The **175** glutmate derivatives were synthesized by coupling with its pteroic acid **361** and the corresponding glutamate derivatives. As shown in Scheme 72, the pteroic acid **361** was synthesized from the previously described intermediate **291** by hydrolysis with 3N NaOH at 45 ^{o}C (yield: 82%).

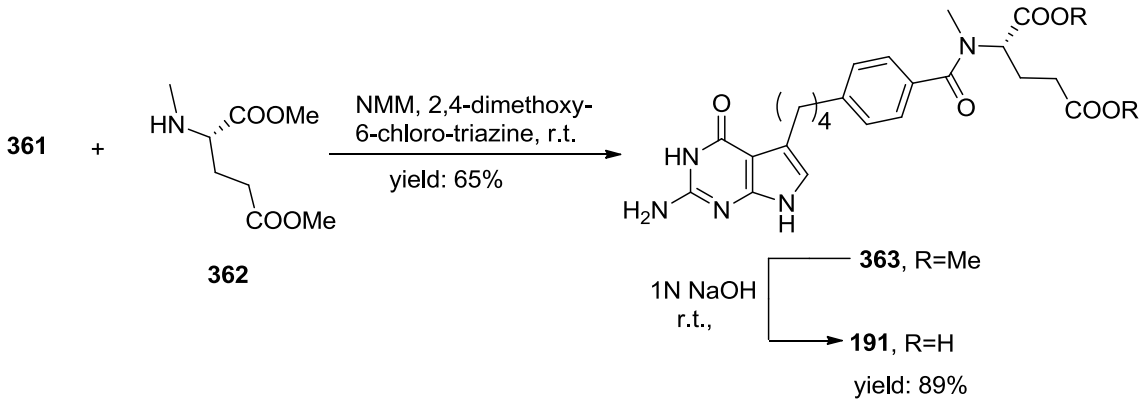

Scheme 73 Synthesis of *N*-methyl compound **191**.

With the desired intermediate pteroic acid **361** in hand, **191** was obtained by peptide coupling of **361** with the *N*-methyl *L*-glutamate **362** using *N*-methyl morpholine and 2,4-dimethoxy-6-chlorotriazine as the activating agents (yields: 65%). Final saponification of the diesters with 1N NaOH gave the target compound 5-substituted pyrrolo[2,3-*d*]pyrimidine with a *N*-methylated *L*-glutamate **191** (yield: 89%). (Scheme 73)

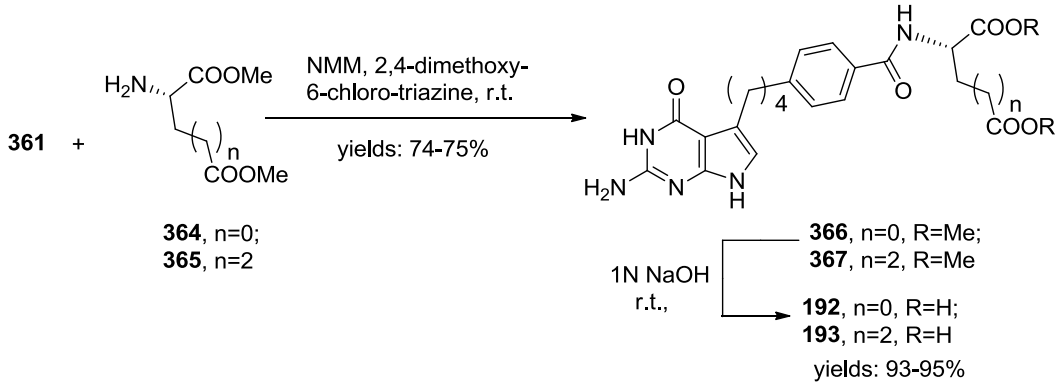

Scheme 74 Synthesis of glutmate derivatives **192** and **193**.

The other two derivatives with a aspartic acid **192** and a homoglutamic acid **193** were synthesized similiarly by coupling reactions of the pteroic acid **361** with the glutamate derivatives **364-365** using N-methyl morpholine and 2,4-dimethoxy-6-chlorotriazine as the activating agents (yields: 74-75%). Final saponification of the diesters with 1N NaOH gave the target compounds 5-substituted pyrrolo[2,3-*d*]pyrimidines with aspartic acid **192** and homoglutamate **193** as shown in Scheme 74 (yields: 93-95%).

10. Synthesis of compound 166 glutmate derivatives

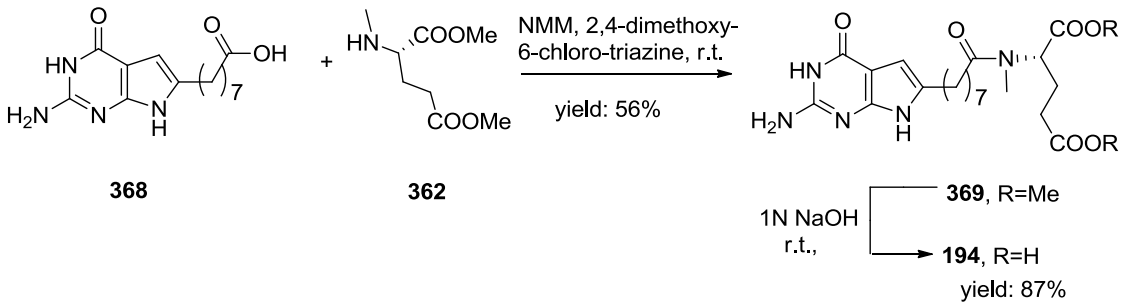

368 **362** **369**, R=Me **194**, R=H

Scheme 75 Synthesis of *N*-methy compound **194**.

The **166** glutmate derivatives were synthesized by coupling with its pteroic acid **368** and the corresponding glutamate derivatives. As shown in Scheme 75, **194** was obtained by peptide coupling of **368** with the *N*-methyl *L*-glutamate **362** using *N*-methyl morpholine and 2,4-dimethoxy-6-chlorotriazine as the activating agents (yields: 56%). Final saponification of the diesters with 1N NaOH gave the target compounds 6-substituted straight side chain pyrrolo[2,3-*d*]pyrimidines with a *N*-methylated *L*-glutamate **194** (yield: 82%). (Scheme 75)

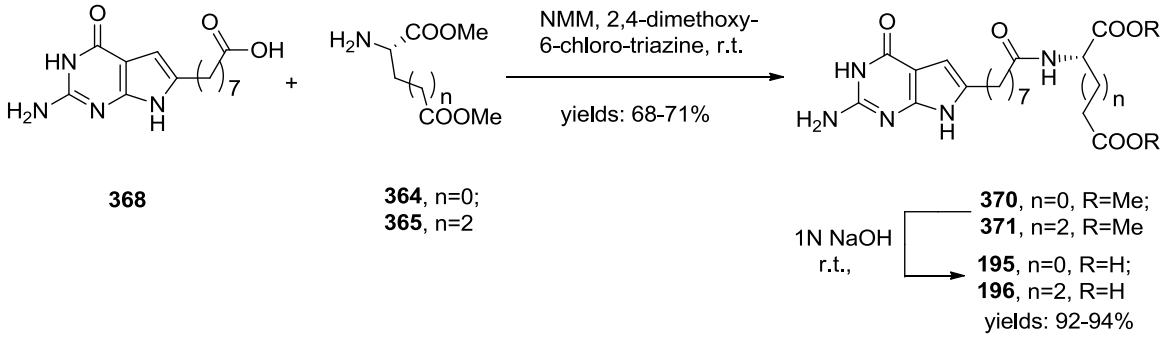

368 **364**, n=0; **365**, n=2 **370**, n=0, R=Me; **371**, n=2, R=Me **195**, n=0, R=H; **196**, n=2, R=H

Scheme 76 Synthesis of glutmate derivatives **195** and **196**.

The other two derivatives with a aspartic acid **195** and a homoglutamic acid **196** were synthesized similiarly by coupling reactions of the pteroic acid **368** with the

glutamate derivatives **364-365** using *N*-methyl morpholine and 2,4-dimethoxy-6-chlorotriazine as the activating agents (yields: 68-71%). Final saponification of the diesters with 1N NaOH gave the target compounds 6-substituted straighy side chain pyrrolo[2,3-*d*]pyrimidines with aspartic acid **195** and homoglutamate **196** as shown in Scheme 76 (yields: 92-94%).

11. Synthesis of 6-substituted pyrrolo[2,3-*d*]pyrimidines as compound 2 glutmate derivatives

The compound **2** glutmate derivative **197** was synthesized by coupling with glutamate derivative **372** using *N*-methyl morpholine and 2,4-dimethoxy-6-chlorotriazine as the activating agents in Scheme 77 (yields: 64%).

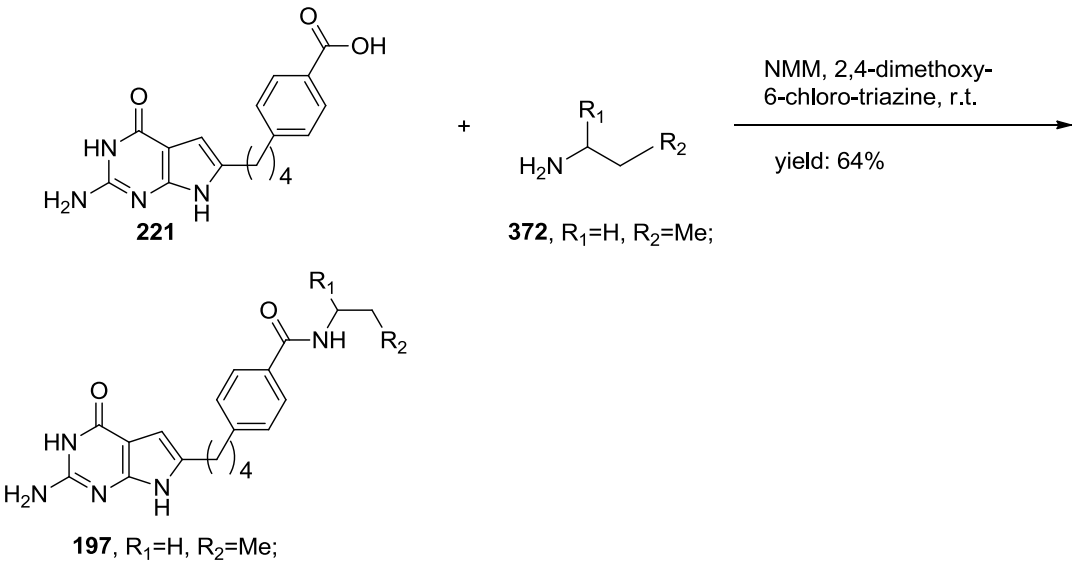

Scheme 77 Synthesis of glutmate derivative **197**.

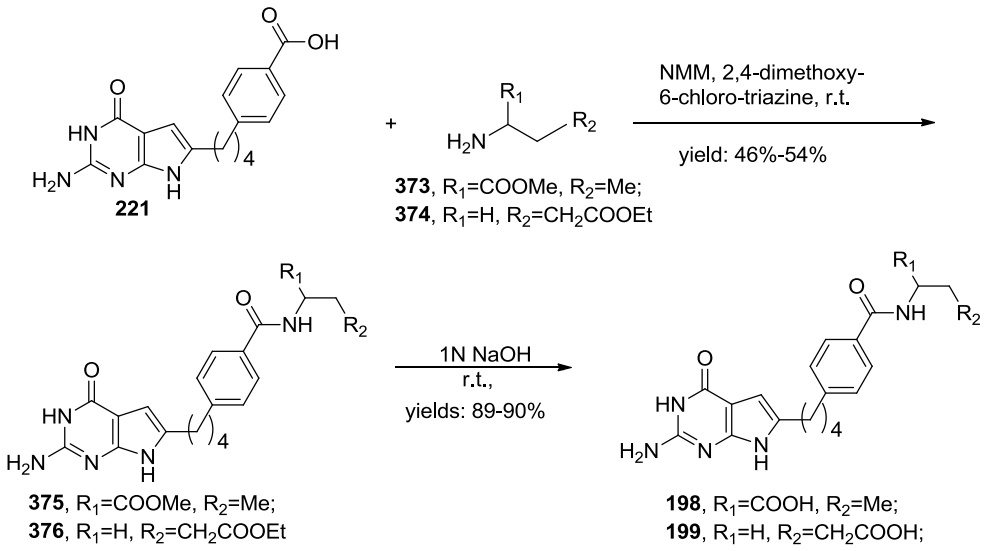

Scheme 78 Synthesis of glutmate derivatives **198** and **199**.

The compound **2** glutmate derivatives were synthesized by coupling with glutamate derivative using *N*-methyl morpholine and 2,4-dimethoxy-6-chlorotriazine as the activating agents (yields: 46-54%). Final saponification of the diesters with 1N NaOH gave the target compounds gave the target compounds 6-substituted pyrrolo[2,3-*d*]pyrimidines with glutmate derivatives **198** and **199** as shown in Scheme 78 (yields: 89-90%).

12. Synthesis of 6-substituted pyrrolo[2,3-*d*]pyrimidines as compound 161 glutmate derivatives

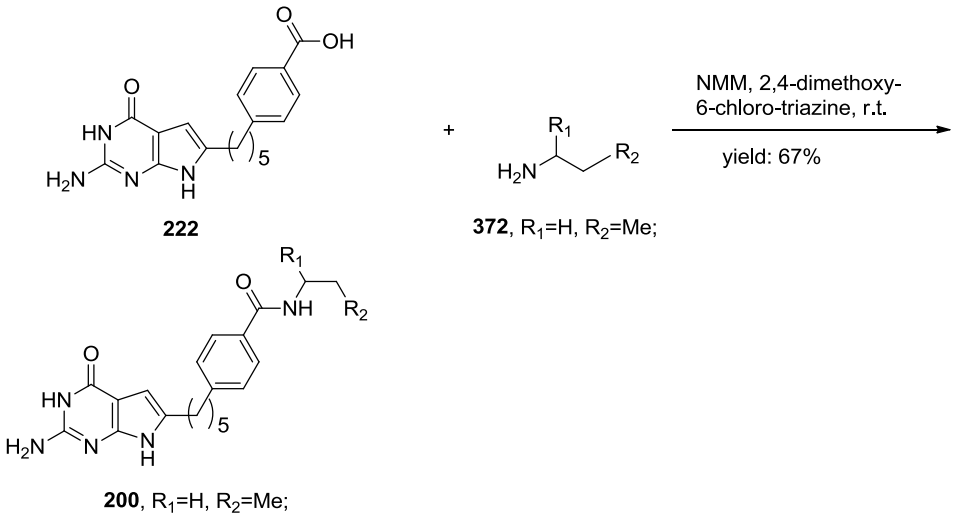

Scheme 79 Synthesis of glutmate derivative **200**.

Similarly, the 5 carbon chain **161** glutmate derivative **200** was synthesized by the peptide coupling of pteroic acid **222** with the corresponding glutamate derivative **372** in 67% yield as shown in Scheme 79.

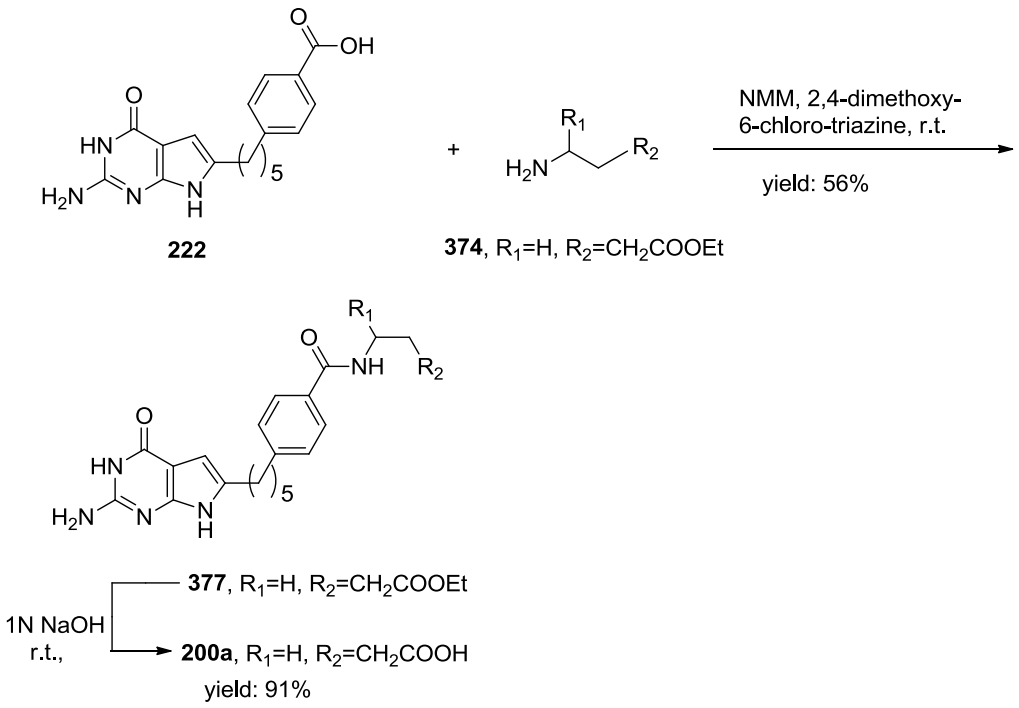

Scheme 80 Synthesis of glutmate derivative **200a**.

Similarly, the 5 carbon chain **161** glutmate derivative **200a** was synthesized by the peptide coupling of pteroic acid **222** with the corresponding glutamate derivative **374** followed by hydrolysis with 1N NaOH as shown in Scheme 80.

V. SUMMARY

Twelve series of classical 5-, 6- and 7-substituted pyrrolo[2,3-*d*]pyrimidines were designed and synthesized. Extensive structure modifications of the pyrrolo[2,3-*d*] pyrimidine scaffold were investigated to determine selective transport *via* FR or/and PCFT and tumor targeted antifolates with GARFTase or multiple folate metabolizing enzyme inhibition.

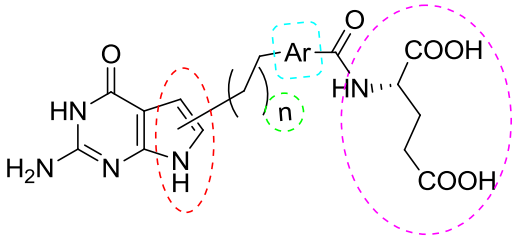

Figure 36 Extensive structure modifications on the pyrrolo[2,3-*d*]pyrimidine scaffold to find FR and PCFT specific tumor targeted antifolates.

The design strategies employed included (Figure 36):

1. Variation of the side chain substitution position (5-,6- and 7-substituted)
2. Variation of the side chain length (n=1-6)
3. Isosteric replacement of the 1,4-disubstituted phenyl ring with 1,2- and 1,3-disubstituted phenyl ring and 2,5- disubstituted thiophenyl ring
4. Replacement the *L*-glutamate with variation at the α and γ carboxylic acids

As a part of this study, a total of one hundred and fifty six new compounds (including new intermediates) were synthesized and separated. Of these, twelve series consisting of forty two classical antifolate final compounds were submitted for biological evaluation. In addition, bulk synthesis of some potent final compounds (**2**, 2.0g; **161**, 500mg; **175**, 1.0g; **166**, 500mg; **194**, 500mg) was carried out to facilitate *in vivo*

evaluation.

During the synthesis of the target compounds, several synthetic improvements were achieved successfully including:

1. α-Bromo ketones instead of α-chloro ketones were synthesized to react with 2,4-diamino-6-hydroxypyrimidine to selectively afford pyrrolo[2,3-*d*]pyrimidines without side product furo[2,3-*d*]pyrimidines.

2. Instead of using the reported reaction condition to get 72% yield in the hydrogenation of **235**, a 10% Pd/C, 5 h condition was employed to get a complete transformation (100% yield of **236**) without any partial reduction. The troublesome separation of **236** was avoided.

More importantly, a new Heck coupling of the thiophene iodide **301** and allyl alcohols to synthesize aldehydes in one step was discovered. The reaction condition is mild (45 ^{o}C) with a good yield (65%) and the labile ester group of **301** is tolerated at this condition. In addition, the reaction is fast (2h) and easy to handle (no argon protection needed). Due to its potential use in analog synthesis of clinically used antifolates such as RTX and PMX, this mild conditioned and easy to handle Heck coupling reaction is highly attractive.

During this study, the SAR of folate transporters (RFC, FR and PCFT) and GARFTase inhibitors were extensively explored. The 6-substituted straight chain compound **166** (n=7) was extremely potent against KB tumor cells (IC_{50}=1.3 nM, about 80-fold more potent than clinically used PMX) without any RFC activity. The intracellular enzyme target of **166** was subsequently identified as GARFTase. The 5-substituted phenyl compound **175** (n=4) showed AICARFTase as the primary target with

potent KB tumor cell inhibition (IC_{50}=7.9 nM, about 8-fold more potent than PMX) and also indirectly activated AMPK cell signaling pathway *via* ZMP accumulation which transmits an inhibitory signal to the mTOR complex leading to tumor cell apoptosis. Both of these compounds were selected for animal study to determine the antitumor activity against human tumor xenograft in mice. Due to their potent antitumor activities, these two compounds serve as leads for future structural optimization.

The target compounds synthesized as part of this study are all classical antifolates and listed below:

1. **(*S*)-2-(4-(4-(2-amino-4-oxo-4,7-dihydro-3*H*-pyrrolo[2,3-*d*]pyrimidin-6-yl)butyl)benzamido)pentanedioic acid (2)**
2. **(*S*)-2-(4-(5-(2-amino-4-oxo-4,7-dihydro-3*H*-pyrrolo[2,3-*d*]pyrimidin-6-yl)pentyl)benzamido)pentanedioic acid (161)**
3. **(*S*)-2-(4-(6-(2-amino-4-oxo-4,7-dihydro-3*H*-pyrrolo[2,3-*d*]pyrimidin-6-yl)hexyl)benzamido)pentanedioic acid (162)**
4. **(*S*)-2-(4-(2-(2-amino-4-oxo-4,7-dihydro-3*H*-pyrrolo[2,3-*d*]pyrimidin-6-yl)ethyl)benzamido)pentanedioic acid (163)**
5. **(*S*)-2-(6-(2-amino-4-oxo-4,7-dihydro-3*H*-pyrrolo[2,3-*d*]pyrimidin-6-yl)hexanamido)pentanedioic acid (164)**
6. **(*S*)-2-(7-(2-amino-4-oxo-4,7-dihydro-3*H*-pyrrolo[2,3-*d*]pyrimidin-6-yl)heptanamido)pentanedioic acid (165)**
7. **(*S*)-2-(8-(2-amino-4-oxo-4,7-dihydro-3*H*-pyrrolo[2,3-*d*]pyrimidin-6-yl)octanamido)pentanedioic acid (166)**

8. **(*S*)-2-(9-(2-amino-4-oxo-4,7-dihydro-3*H*-pyrrolo[2,3-*d*]pyrimidin-6-yl)nonanamido)pentanedioic acid (167)**

9. **(S)-2-(3-(4-(2-amino-4-oxo-4,7-dihydro-3H-pyrrolo[2,3-*d*]pyrimidin-6-yl)butyl)benzamido)pentanedioic acid (168)**

10. **(*S*)-2-(2-(4-(2-amino-4-oxo-4,7-dihydro-3*H*-pyrrolo[2,3-*d*]pyrimidin-6-yl)but-1-yn-1-yl)benzamido)pentanedioic acid (169)**

11. **(*S*)-2-(2-(4-(2-amino-4-oxo-4,7-dihydro-3*H*-pyrrolo[2,3-*d*]pyrimidin-6-yl)butyl)benzamido)pentanedioic acid (170)**

12. **(S)-2-(3-(4-(2-amino-4-oxo-4,7-dihydro-3H-pyrrolo[2,3-*d*]pyrimidin-6-yl)but-1-yn-1-yl)benzamido)pentanedioic acid (171)**

13. **(*S*)-2-(4-((2-amino-4-oxo-4,7-dihydro-3*H*-pyrrolo[2,3-*d*]pyrimidin-5-yl)methyl)benzamido)pentanedioic acid (172)**

14. **(*S*)-2-(4-(2-(2-amino-4-oxo-4,7-dihydro-3*H*-pyrrolo[2,3-*d*]pyrimidin-5-yl)ethyl)benzamido)pentanedioic acid (173)**

15. **(*S*)-2-(4-(3-(2-amino-4-oxo-4,7-dihydro-3*H*-pyrrolo[2,3-*d*]pyrimidin-5-yl)propyl)benzamido)pentanedioic acid (174)**

16. **(*S*)-2-(4-(4-(2-amino-4-oxo-4,7-dihydro-3*H*-pyrrolo[2,3-*d*]pyrimidin-5-yl)butyl)benzamido)pentanedioic acid (175)**

17. **(*S*)-2-(4-(5-(2-amino-4-oxo-4,7-dihydro-3*H*-pyrrolo[2,3-*d*]pyrimidin-5-yl)pentyl)benzamido)pentanedioic acid (176)**

18. **(*S*)-2-(4-(6-(2-amino-4-oxo-4,7-dihydro-3*H*-pyrrolo[2,3-*d*]pyrimidin-5-yl)hexyl)benzamido)pentanedioic acid (177)**

19. **(*S*)-2-(5-((2-amino-4-oxo-4,7-dihydro-3*H*-pyrrolo[2,3-*d*]pyrimidin-5-yl)methyl)thiophene-2-carboxamido)pentanedioic acid (178)**

20. **(*S*)-2-(5-(2-(2-amino-4-oxo-4,7-dihydro-3*H*-pyrrolo[2,3-*d*]pyrimidin-5-yl)ethyl)thiophene-2-carboxamido)pentanedioic acid (179)**

21. **(*S*)-2-(5-(3-(2-amino-4-oxo-4,7-dihydro-3*H*-pyrrolo[2,3-*d*]pyrimidin-5-yl)propyl)thiophene-2-carboxamido)pentanedioic acid (180)**

22. **(*S*)-2-(5-(4-(2-amino-4-oxo-4,7-dihydro-3*H*-pyrrolo[2,3-*d*]pyrimidin-5-yl)butyl)thiophene-2-carboxamido)pentanedioic acid (181)**

23. **(*S*)-2-(5-(5-(2-amino-4-oxo-4,7-dihydro-3*H*-pyrrolo[2,3-*d*]pyrimidin-5-yl)pentyl)thiophene-2-carboxamido)pentanedioic acid (182)**

24. **(*S*)-2-(5-(6-(2-amino-4-oxo-4,7-dihydro-3*H*-pyrrolo[2,3-*d*]pyrimidin-5-yl)hexyl)thiophene-2-carboxamido)pentanedioic acid (183)**

25. **(*S*)-2-(7-(2-amino-4-oxo-4,7-dihydro-3*H*-pyrrolo[2,3-*d*]pyrimidin-5-yl)heptanamido)pentanedioic acid (184)**

26. **(*S*)-2-(8-(2-amino-4-oxo-4,7-dihydro-3*H*-pyrrolo[2,3-*d*]pyrimidin-5-yl)octanamido)pentanedioic acid (185)**

27. **(*S*)-2-(9-(2-amino-4-oxo-4,7-dihydro-3*H*-pyrrolo[2,3-*d*]pyrimidin-5-yl)nonanamido)pentanedioic acid (186)**

28. **(*S*)-2-(6-(2-amino-4-oxo-3*H*-pyrrolo[2,3-*d*]pyrimidin-7(4*H*)-yl)hexanamido)pentanedioic acid (187)**

29. **(*S*)-2-(7-(2-amino-4-oxo-3*H*-pyrrolo[2,3-*d*]pyrimidin-7(4H)-yl)heptanamido)pentanedioic acid (188)**

30. **(*S*)-2-(8-(2-amino-4-oxo-3*H*-pyrrolo[2,3-*d*]pyrimidin-7(4*H*)-yl)octanamido)pentanedioic acid (189)**

31. **(*S*)-2-(9-(2-amino-4-oxo-3*H*-pyrrolo[2,3-*d*]pyrimidin-7(4*H*)-yl)nonanamido)pentanedioic acid (190)**

32. **(*S*)-2-(4-(4-(2-amino-4-oxo-4,7-dihydro-3*H*-pyrrolo[2,3-*d*]pyrimidin-5-yl)butyl)-*N*-methylbenzamido)pentanedioic acid (191)**

33. **(*S*)-2-(4-(4-(2-amino-4-oxo-4,7-dihydro-3*H*-pyrrolo[2,3-*d*]pyrimidin-5-yl)butyl)benzamido)succinic acid (192)**

34. **(*S*)-2-(4-(4-(2-amino-4-oxo-4,7-dihydro-3*H*-pyrrolo[2,3-*d*]pyrimidin-5-yl)butyl)benzamido)hexanedioic acid (193)**

35. **(*S*)-2-(8-(2-amino-4-oxo-4,7-dihydro-3*H*-pyrrolo[2,3-*d*]pyrimidin-6-yl)-*N*-methyloctanamido)pentanedioic acid (194)**

36. **(*S*)-2-(8-(2-amino-4-oxo-4,7-dihydro-3*H*-pyrrolo[2,3-*d*]pyrimidin-6-yl)octanamido)succinic acid (195)**

37. **(*S*)-2-(8-(2-amino-4-oxo-4,7-dihydro-3*H*-pyrrolo[2,3-*d*]pyrimidin-6-yl)octanamido)hexanedioic acid (196)**

38. **4-(4-(2-amino-4-oxo-4,7-dihydro-3*H*-pyrrolo[2,3-*d*]pyrimidin-6-yl)butyl)-*N*-propylbenzamide (197)**

39. **2-(4-(4-(2-amino-4-oxo-4,7-dihydro-3*H*-pyrrolo[2,3-*d*]pyrimidin-6-yl)butyl)benzamido)butanoic acid (198)**

40. **4-(4-(4-(2-amino-4-oxo-4,7-dihydro-3*H*-pyrrolo[2,3-*d*]pyrimidin-6-yl)butyl)benzamido)butanoic acid (199)**

41. **4-(5-(2-amino-4-oxo-4,7-dihydro-3*H*-pyrrolo[2,3-*d*]pyrimidin-6-yl)pentyl)-*N*-propylbenzamide (200)**

42. **4-(4-(5-(2-amino-4-oxo-4,7-dihydro-3*H*-pyrrolo[2,3-*d*]pyrimidin-6-yl)pentyl)benzamido)butanoic acid (200a)**

VI. EXPERIMENTAL SECTION

All evaporations were carried out *in vacuo* with a rotary evaporator. Analytical samples were dried *in vacuo* (0.2 mmHg) in a CHEM-DRY drying apparatus over P_2O_5 at 80 ^oC. Melting points were determined on a MEL-TEMP II melting point apparatus with a FLUKE 51 K/J electronic thermometer and are uncorrected. Nuclear magnetic resonance spectra for proton (^1H NMR) were recorded on either a Bruker WH-400 (400 MHz) spectrometer or a Bruker WH-500 (500 MHz) spectrometer. The chemical shift values are expressed in ppm (parts per million) relative to tetramethylsilane as an internal standard: *s*, singlet; *d*, doublet; *t*, triplet; *q*, quartet; *m*, multiplet; *br*, broad singlet. Mass spectra were recorded on a VG-7070 double-focusingmass spectrometer or in a LKB-9000 instrument in the electron ionization (EI) mode. Chemical names follow IUPAC nomenclature. Thin-layer chromatography (TLC) was performed on Whatman Sil G/UV254 silica gel plates with a fluorescent indicator, and the spots were visualized under 254 and 365 nm illumination. All analytical samples were homogeneous on TLC in three different solvent systems. Proportions of solvents used for TLC are by volume. Column chromatography was performed on a 230-400 mesh silica gel (Fisher, Somerville, NJ) column. Elemental analyses were performed by Atlantic Microlab, Inc., Norcross, GA. Element compositions are within 0.4% of the calculated values. Fractional moles of water frequently found in the analytical sample of antifolates could not be prevented in spite of 24-48 h of drying *in vacuo* and was confirmed where possible by the presence in the ^1H NMR spectra. All solvents and chemicals were purchased from Aldrich Chemical Co. or Fisher Scientific and were used as received. For all the compounds submitted for biological evaluation, a single spot in three different solvent

systems with three different R_f values confirmed >95% purity.

(4*E*/*Z*)-5-[4-(Methoxycarbonyl)phenyl]pent-4-enoic acid (209): Compound **209** was synthesized as reported previously:[22] To a suspension of methyl 4-formylbenzoate (**205**) (3.2 g, 20mmol) and (3-carboxypropyl)triphenylphosphonium bromide **206** (8.6 g, 20 mmol) in 80 mL DMSO/THF (1:1) was added 2 equiv of NaH (92%) (1.0 g, 40 mmol) in one portion in an ice bath and N_2 atmosphere. The resulting suspension was stirred in an ice bath for an additional 30 min and slowly warmed to room temperature for another 6 h. TLC indicated the disappearance of the aldehyde spot and formation of two spots centered at Rf) 0.19 (hexane/EtOAc, 3:1). To the reaction mixture cooled in an ice bath was added ice/water (100 g) followed by concentrated HCl (10 mL). The resulting solution was extracted with ether (100 mL X 3) and dried over Na_2SO_4. After evaporation of solvent, the residue was loaded on a silica gel column (4 X 20 cm) and flash-chromatographed with hexane/EtOAc (2:1) and the desired fractions were pooled. After evaporation of solvent the residue was recrystallized from ethyl ether to afford 4.4 g, yield 94% as white crystals, mp 121-123 °C (lit.[22] mp 118-121 °C), R_f = 0.20 (Hexane/EtOAc, 3:1). ^{1}H NMR (DMSO-d_6) δ 2.40-2.46 (m, 4 H, 2 CH_2), 3.84(s, 3H, OCH_3), 6.47-6.52 (m, 2 H, CH=CH), 7.52 (d, 2 H, C_6H_4, J = 4.1 Hz), 7.89 (d, 2 H, C_6H_4, J = 4.2 Hz), 12.18 (br, 1H, COOH).

(5*E*/*Z*)-6-[4-(Methoxycarbonyl)phenyl]hex-5-enoic acid (210): Compound **210** was synthesized as described for **209:** yield 90% as white crystals, mp 77-81 °C, R_f = 0.22 (Hexane/EtOAc, 3:1). ^{1}H NMR (DMSO-d_6) δ 1.60-1.76 (m, 2 H, CH_2), 2.20-2.35 (m, 4 H, 2 CH_2), 3.84(s, 3H, OCH_3), 6.45-6.55 (m, 2 H, CH=CH), 7.53 (d, 2 H, C_6H_4, J = 4.0 Hz), 7.89 (d, 2 H, C_6H_4, J = 4.0 Hz), 12.06 (br, 1H, COOH). Anal. calcd. for ($C_{14}H_{16}O_4$):

C, 67.74; H, 6.45; found: C, 67.94; H, 6.66.

(6*E*/*Z*)-7-[4-(Methoxycarbonyl)phenyl]hept-6-enoic acid (211): Compound **211** was synthesized as described for **209:** yield 92% as white crystals, mp 72-73 °C, R_f = 0.26 (Hexane/EtOAc, 3:1). ^{1}H NMR ($CDCl_3$) δ 1.48-1.76 (m, 4 H, 2 CH_2), 2.23-2.44 (m, 4 H, 2 CH_2), 3.91(s, 3H, OCH_3), 6.30-6.50 (m, 2 H, CH=CH), 7.32 (d, 2 H, C_6H_4, J = 4.0 Hz), 7.97 (d, 2 H, C_6H_4, J = 4.0 Hz). Anal. calcd. for ($C_{15}H_{18}O_4$): C, 68.70; H, 6.87; found: C, 68.43; H, 7.10.

5-[4-(Methoxycarbonyl)phenyl]pentanoic acid (212): Compound **212** was synthesized as reported previously:[22] To a solution of **209** (3.0 g, 15 mmol) in EtOAc/CHCl3 (2:1, 50 mL) was added 10% Pd/C (500 mg). The resulting suspension was hydrogenated in a Parr apparatus overnight at 45-50 psi hydrogen pressure. TLC indicated the disappearance of the starting material and the formation of one major spot at Rf) 0.29 (hexane/EtOAc, 3:1). The reaction mixture was filtered through Celite and washed with methanol (30 mL). After evaporation of the solvent, the residue was loaded on to a silica gel column (4 x 20 cm) and flash-chromatographed with hexane/EtOAc (3:1) and the desired fractions were pooled. After evaporation of the solvent and recrystallization from Et_2O/EtOAc (2:1), 3.0 g (100%) of **212** was obtained as white crystals, mp 85-86 °C (lit.[22] mp 86.9-88.5 °C), R_f = 0.25 (Hexane/EtOAc, 3:1). ^{1}H NMR (DMSO-d_6) δ 1.40-1.70 (m, 4 H, 2 CH_2), 2.23 (t, 2 H, CH_2), 2.66 (t, 2 H, CH_2), 3.83 (s, 3 H, OCH_3), 7.34 (d, 2 H, C_6H_4, J = 3.9 Hz), 7.88 (d, 2 H, C_6H_4, J = 3.9 Hz), 12.04 (s, 1H, COOH).

6-[4-(Methoxycarbonyl)phenyl]hexanoic acid (213): Compound **213** was synthesized as described for **212:** yield 99% as white crystals, mp 49-51 °C, R_f = 0.26

(Hexane/EtOAc, 3:1). ^{1}H NMR ($CDCl_3$) δ 1.34-1.43 (m, 2 H, CH_2), 1.58-1.72 (m, 4 H, 2 CH_2), 2.35 (t, 2 H, CH_2), 2.66 (t, 2 H, CH_2), 3.89(s, 3H, OCH_3), 7.23 (d, 2 H, C_6H_4, J = 4.0 Hz), 7.94 (d, 2 H, C_6H_4, J = 4.0 Hz). Anal. calcd. for ($C_{14}H_{18}O_4$): C, 67.20; H, 7.20; found: C, 67.45; H, 7.30.

7-[4-(Methoxycarbonyl)phenyl]heptanoic acid (214): Compound **214** was synthesized as described for **212:** yield 94% as white crystals, mp 66-67 °C, R_f = 0.26 (Hexane/EtOAc, 3:1). ^{1}H NMR ($CDCl_3$) δ 1.27-1.42 (m, 4 H, 2 CH_2), 1.50-1.71 (m, 4 H, 2 CH_2), 2.33 (t, 2 H, CH_2), 2.64 (t, 2 H, CH_2), 3.89(s, 3H, OCH_3), 7.20 (d, 2 H, C_6H_4, J = 4.0 Hz), 7.94 (d, 2 H, C_6H_4, J = 4.0 Hz). Anal. calcd. for ($C_{15}H_{20}O_4 \cdot 0.1CH_3COOC_2H_5$): C, 67.72; H, 7.68; found: C, 67.69; H, 7.60.

Methyl 4-(6-bromo-5-oxohexyl)benzoate (215): To a solution of 5-[4-(methoxycarbonyl)phenyl]pentanoic acid **(212)** (0.36 g, 1.5 mmol) in a 50 mL flask was added oxalyl chloride (1.5 mL) and anhydrous CH_2Cl_2 (10 mL). The resulting solution was refluxed for 1 h and then cooled to room temperature. After evaporation of solvent under reduced pressure, the residue was dissolved in ethyl ether (20 mL). The resulting solution was added dropwise to an ice-cooled ether solution of diazomethane (generated in situ from 1.4 g *N*-nitroso-*N*-methylurea) over 10 min. To this solution was added 48% HBr (1.5 mL). The resulting mixture was refluxed for 1.5 h. After the mixture was cooled to room temperature, the organic layer was separated and the aqueous layer was extracted with ether (20 mL x 3). The combined organic layers were washed with two portions of 10% Na_2CO_3 solution and dried over Na_2SO_4. The solvent was evaporated to afford 0.44 g (90%) of **215** as yellow needles: mp 65-66 °C, R_f = 0.45 (Hexane/EtOAc, 3:1). ^{1}H NMR (DMSO-d_6) δ 1.43-1.65 (m, 4 H, 2 CH_2), 2.54-2.74 (m, 4 H, 2 CH_2), 3.83 (s, 3 H,

OCH_3), 4.32(s, 2H, CH_2Br), 7.34 (d, 2 H, C_6H_4, J = 4.0 Hz), 7.87 (d, 2 H, C_6H_4, J = 4.0 Hz).

Methyl 4-(7-bromo-6-oxoheptyl)benzoate (216): Compound **216** was synthesized as described for **215:** yield 80% as white crystals, mp 55-56 °C, R_f = 0.52 (Hexane/EtOAc, 3:1). ^{1}H NMR ($CDCl_3$) δ 1.30-1.42 (m, 2 H, CH_2), 1.59-1.72 (m, 4 H, 2 CH_2), 2.61-2.70 (m, 4 H, 2 CH_2), 3.87 (s, 2H, CH_2Br), 3.90 (s, 3 H, OCH_3), 7.23 (d, 2 H, C_6H_4, J = 4.0 Hz), 7.95 (d, 2 H, C_6H_4, J = 4.0 Hz). HRMS calcd. for $C_{15}H_{19}BrO_3$ 326.0518, found 326.0524.

Methyl 4-(8-bromo-7-oxooctyl)benzoate (217): Compound **217** was synthesized as described for **215:** yield 85% as yellow crystals, mp 47-48 °C, R_f = 0.53 (Hexane/EtOAc, 3:1). ^{1}H NMR ($CDCl_3$) δ 1.30-1.39 (m, 4 H, 2 CH_2), 1.60-1.71 (m, 4 H, 2 CH_2), 2.58-2.69 (m, 4 H, 2 CH_2), 3.87 (s, 2H, CH_2Br), 3.90 (s, 3 H, OCH_3), 7.23 (d, 2 H, C_6H_4, J = 4.0 Hz), 7.95 (d, 2 H, C_6H_4, J = 4.0 Hz). HRMS calcd. for $C_{16}H_{21}BrO_3$ 340.0674, found 340.0683.

Methyl 4-[4-(2-amino-4-oxo-4,7-dihydro-3*H*-pyrrolo[2,3-*d*]pyrimidin-6-yl)butyl]benzoate (218): To a suspension of 2,4-diamino-6-hydroxypyrimidine **35** (1.53 g, 12.2 mmol) in anhydrous DMF (40 mL) was added **215** (3.82 g, 12.2 mmol). The resulting mixture was stirred under N_2 at room temperature for 3 days. TLC showed the disappearance of starting materials and the formation of one major spot at R_f = 0.28 ($CHCl_3$/MeOH, 6:1). After evaporation of solvent, CH_3OH (20 mL) was added followed by silica gel (5 g). Evaporation of the solvent afforded a plug, which was loaded onto a silica gel column (3.5 cm x 15 cm) and eluted initially with $CHCl_3$ followed by 10% MeOH in $CHCl_3$ and then 15% MeOH in $CHCl_3$. Fractions showing R_f = 0.28 were

pooled and evaporated, and the resulting solid was recrystallized from MeOH to afford 1.53 g (37%) of **218** as yellow crystals: mp 240-241 °C (lit.[22] mp 241.9-243.7 °C). This compound was identical in all respects to that reported in the literature.[22] ^{1}H NMR (DMSO-d_6) δ 1.52-1.62 (m, 4 H, 2 CH_2), 2.49-2.71 (m, 4 H, 2 CH_2), 3.83 (s, 3 H, OCH_3), 5.84 (s, 1 H, CH), 5.95 (s, 2 H, 2-NH_2), 7.34 (d, 2 H, C_6H_4, J = 4.0 Hz), 7.87 (d, 2 H, C_6H_4, J = 4.0 Hz) 10.12 (s, 1 H, 3-NH), 10.80 (s, 1H, 7-NH).

Methyl 4-[5-(2-amino-4-oxo-4,7-dihydro-3*H*-pyrrolo[2,3-*d*]pyrimidin-6-yl)pentyl]benzoate (219): Compound **219** was synthesized as described for **218:** yield 35% as yellow crystals, mp 229-230 °C, R_f = 0.31 ($CHCl_3$/MeOH, 6:1). ^{1}H NMR (DMSO-d_6) δ 1.26-1.36 (m, 2 H, CH_2), 1.52-1.66 (m, 4 H, 2 CH_2), 2.48-2.68 (m, 4 H, 2 CH_2), 3.82 (s, 3 H, OCH_3), 5.84 (s, 1 H, CH), 5.95 (s, 2 H, 2-NH_2), 7.33 (d, 2 H, C_6H_4, J = 4.0 Hz), 7.86 (d, 2 H, C_6H_4, J = 4.0 Hz) 10.12 (s, 1 H, 3-NH), 10.79 (s, 1H, 7-NH). Anal. calcd. for ($C_{19}H_{22}N_4O_3 \cdot 0.2\ H_2O$): C, 63.74; H, 6.31; N, 15.65; found: C, 63.78; H, 6.26; N, 15.44.

Methyl 4-[6-(2-amino-4-oxo-4,7-dihydro-3*H*-pyrrolo[2,3-*d*]pyrimidin-6-yl)hexyl]benzoate (220): Compound **220** was synthesized as described for **218:** yield 35% as yellow crystals, mp 219-221 °C, R_f = 0.35 ($CHCl_3$/MeOH, 6:1). ^{1}H NMR (DMSO-d_6) δ 1.25-1.35 (m, 4 H, 2 CH_2), 1.47-1.65 (m, 4 H, 2 CH_2), 2.49-2.67 (m, 4 H, 2 CH_2), 3.82 (s, 3 H, OCH_3), 5.83 (s, 1 H, CH), 5.95 (s, 2 H, 2-NH_2), 7.33 (d, 2 H, C_6H_4, J = 4.0 Hz), 7.86 (d, 2 H, C_6H_4, J = 4.0 Hz) 10.11 (s, 1 H, 3-NH), 10.76 (s, 1H, 7-NH). Anal. calcd. for ($C_{20}H_{24}N_4O_3 \cdot 0.67\ H_2O$): C, 63.13; H, 6.71; N, 14.72; found: C, 63.16; H, 6.65; N, 14.58.

4-[4-(2-Amino-4-oxo-4,7-dihydro-3*H*-pyrrolo[2,3-*d*]pyrimidin-6-yl)butyl]benzoic

acid (221): To a suspension of **218** (178 mg, 0.5 mmol) in 10 mL CH_3OH was added 3 N NaOH (10 mL). The resulting mixture was stirred under N_2 at 40-50 °C for 24 h. TLC indicated the disappearance of starting material and the formation of one major spot at the origin. The resulting solution was passed through Celite and washed with a minimum amount of CH_3OH. The combined filtrate was evaporated under reduced pressure to dryness. To this residue was added distilled water (10 mL). The solution was cooled in an ice bath, and the pH was adjusted 3 to 4 using 3 N HCl. The resulting suspension was chilled in a dry ice/acetone bath and thawed to 4 °C overnight in a refrigerator. The precipitate was filtered, washed with cold water, and dried in a desiccator under reduced pressure using P_2O_5 to afford 120 mg (74%) of **221** as a brown powder: mp >262 °C (dec) (lit.[22] mp >266 °C), R_f = 0.20 ($CHCl_3$/MeOH, 5:1). This compound was identical in all respects to that reported in the literature.[22]

4-[5-(2-Amino-4-oxo-4,7-dihydro-3*H*-pyrrolo[2,3-*d*]pyrimidin-6-yl)pentyl]benzoic acid (222): Compound **222** was synthesized as described for **221:** yield 90% as a brown powder, mp >271 °C (dec), R_f = 0.18 ($CHCl_3$/MeOH, 5:1). ^{1}H NMR (DMSO-d_6) δ 1.26-1.36 (m, 2 H, CH_2), 1.55-1.67 (m, 4 H, 2 CH_2), 2.48-2.69 (m, 4 H, 2 CH_2), 5.85 (s, 1 H, CH), 5.96 (s, 2 H, 2-NH_2), 7.31 (d, 2 H, C_6H_4, J = 4.0 Hz), 7.84 (d, 2 H, C_6H_4, J = 4.0 Hz) , 10.12 (s, 1 H, 3-NH), 10.80 (s, 1H, 7-NH). Anal. calcd. for ($C_{18}H_{20}N_4O_3 \cdot 0.75$ CH_3OH): C, 61.80; H, 6.36; N, 15.37; found: C, 62.05; H, 6.05; N, 15.08.

4-[6-(2-Amino-4-oxo-4,7-dihydro-3*H*-pyrrolo[2,3-*d*]pyrimidin-6-yl)hexyl]benzoic acid (223): Compound **223** was synthesized as described for **221:** yield 98% as a brown powder, mp >276 °C (dec), R_f = 0.18 ($CHCl_3$/MeOH, 5:1). ^{1}H NMR (DMSO-d_6) δ 1.24-1.35 (m, 4 H, 2 CH_2), 1.48-1.64 (m, 4 H, 2 CH_2), 2.49-2.66 (m, 4 H, 2 CH_2), 5.84

(s, 1 H, CH), 5.97 (s, 2 H, 2-NH_2), 7.29 (d, 2 H, C_6H_4, J = 4.0 Hz), 7.84 (d, 2 H, C_6H_4, J = 4.0 Hz), 10.13 (s, 1 H, 3-NH), 10.77 (s, 1H, 7-NH). Anal. calcd. for ($C_{19}H_{22}N_4O_3 \cdot 1.4 H_2O$): C, 60.11; H, 6.58; N, 14.76; found: C, 60.13; H, 6.38; N, 14.38.

(*S*)-diethyl 2-(4-(4-(2-amino-4-oxo-4,7-dihydro-3*H*-pyrrolo[2,3-*d*]pyrimidin-6-yl)butyl)benzamido)pentanedioate (224): To a solution of **221** (290 mg, 0.89 mmol) in anhydrous DMF (40 mL) was added 6-chloro-2,4-dimethoxy-1,3,5-triazine (180 mg, 1.07 mmol) and *N*-methylmorpholine (105 mg, 1.07 mmol). After the mixture was stirred at r.t. for 2 h, *N*-methylmorpholine (105 mg, 1.07 mmol) and dimethyl *L*-glutamate hydrochloride (423 mg, 1.78 mmol) were added all at once. The mixture was stirred at r.t. for 4 h. TLC showed the formation of one major spot at R_f = 0.55 ($CHCl_3$/MeOH, 5:1). The reaction mixture was evaporated to dryness under reduced pressure. The residue was dissolved in a minimum amount of $CHCl_3$/MeOH, 5:1, and chromatographed on a silica gel column (2 cm x 15 cm) with 4% MeOH in $CHCl_3$ as the eluent. Fractions that showed the desired single spot at R_f = 0.55 were pooled and evaporated to dryness to afford **224** 307mg, yield 68% as a yellow syrup, which was used directly for the next step. ^{1}H NMR (DMSO-d_6) δ 1.08-1.28 (m, 6 H, 2 CH_3), 1.52-1.68 (m, 4 H, 2 CH_2), 1.88-2.15 (m, 2 H, CH_2), 2.40-2.68 (m, 6 H, 3 CH_2), 3.98-4.12 (m, 4 H, 2 CH_2), 4.36-4.46 (m, 1 H, CH), 5.84 (s, 1 H, CH), 5.94 (s, 2 H, 2-NH_2), 7.28 (d, 2 H, C_6H_4, J = 4.0 Hz), 7.78 (d, 2 H, C_6H_4, J = 4.0 Hz), 8.63 (d, 1 H, CONH, , J = 4.4 Hz), 10.11 (s, 1 H, 3-NH), 10.78 (s, 1H, 7-NH).

(*S*)-diethyl 2-(4-(5-(2-amino-4-oxo-4,7-dihydro-3*H*-pyrrolo[2,3-*d*]pyrimidin-6-yl)pentyl)benzamido)pentanedioate (225): Compound **225** was synthesized as described for **224:** yield 88% as a yellow syrup, R_f = 0.57 ($CHCl_3$/MeOH, 5:1). ^{1}H NMR

(DMSO-d_6) δ 1.14-1.23 (m, 6 H, 2 CH_3), 1.28-1.38 (m, 2 H, CH_2), 1.55-1.67 (m, 4 H, 2 CH_2), 1.90-2.20 (m, 2 H, CH_2), 2.40-2.68 (m, 6 H, 3 CH_2), 4.02-4.12 (m, 4 H, 2 CH_2), 4.38-4.46 (m, 1 H, CH), 5.85 (s, 1 H, CH), 5.96 (s, 2 H, 2-NH_2), 7.30 (d, 2 H, C_6H_4, J = 4.0 Hz), 7.79 (d, 2 H, C_6H_4, J = 4.0 Hz), 8.64 (d, 1 H, CONH, , J = 4.4 Hz), 10.12 (s, 1 H, 3-NH), 10.80 (s, 1H, 7-NH). Anal. calcd. for ($C_{27}H_{35}N_5O_6 \cdot 0.75\ H_2O$): C, 60.15; H, 6.82; N, 12.99; found: C, 60.30; H, 6.86; N, 12.66.

(*S*)-diethyl 2-(4-(6-(2-amino-4-oxo-4,7-dihydro-3*H*-pyrrolo[2,3-*d*]pyrimidin-6-yl)hexyl)benzamido)pentanedioate (226): Compound **226** was synthesized as described for **224:** yield 77% as a yellow syrup, R_f = 0.60 ($CHCl_3$/MeOH, 5:1). ^{1}H NMR (DMSO-d_6) δ 1.11-1.21 (m, 6 H, 2 CH_3), 1.25-1.34 (m, 4 H, 2 CH_2), 1.48-1.64 (m, 4 H, 2 CH_2), 1.92-2.16 (m, 2 H, CH_2), 2.39-2.46 (m, 2 H, CH_2), 2.49-2.66 (m, 4 H, 2 CH_2), 4.01-4.14 (m, 4 H, 2 CH_2), 4.37-4.47 (m, 1 H, CH), 5.82 (s, 1 H, CH), 5.94 (s, 2 H, 2-NH_2), 7.28 (d, 2 H, C_6H_4, J = 4.0 Hz), 7.78 (d, 2 H, C_6H_4, J = 4.0 Hz), 8.63 (d, 1 H, CONH, , J = 3.8 Hz), 10.10 (s, 1 H, 3-NH), 10.77 (s, 1H, 7-NH). Anal. calcd. for ($C_{28}H_{37}N_5O_6 \cdot 1.0\ H_2O$): C, 60.31; H, 7.05; N, 12.56; found: C, 60.18; H, 7.02; N, 12.48.

(*S*)-2-(4-(4-(2-amino-4-oxo-4,7-dihydro-3*H*-pyrrolo[2,3-*d*]pyrimidin-6-yl)butyl)benzamido)pentanedioic acid (2): To a solution of the diester **224** (580 mg, 1.14 mmol) was added 1 N NaOH (15 mL), and the mixture was stirred under N_2 at room temperature for 1 h. Add one or two drops of methanol to help the dissolution of the reactant if necessary. The TLC showed the disappearance of the starting material (R_f = 0.55) and formation of one major spot at the origin ($CHCl_3$/MeOH, 5:1). The reaction mixture was evaporated to dryness under reduced pressure. The residue was dissolved in water (10 mL), the resulting solution was cooled in an ice bath, and the pH was adjusted

to 3-4 with dropwise addition of 1 N HCl. The resulting suspension was frozen in a dry ice/acetone bath, thawed in a refrigerator to 4-5 °C, and filtered. The residue was washed with a small amount of cold water and ethyl acetate and dried in vacuo using P_2O_5 to afford 380 mg (73%) **2** as a yellow powder: mp 172-173 °C (lit.[22] mp 171-173 °C), R_f = 0.05 ($CHCl_3$/MeOH, 5:1). ^{1}H NMR (DMSO-d_6) δ 1.58 (br, 4 H, 2 CH_2), 1.88-2.10 (m, 2 H, CH_2), 2.29-2.37 (t, 2 H, CH_2), 2.52-2.70 (m, 4 H, 2 CH_2), 4.32-4.42 (m, 1 H, CH), 5.83 (s, 1 H, CH), 5.97 (s, 2 H, 2-NH_2), 7.26 (d, 2 H, C_6H_4, J = 4.0 Hz), 7.78 (d, 2 H, C_6H_4, J = 4.0 Hz), 8.50 (d, 1 H, CONH, , J = 3.0 Hz), 10.14 (s, 1 H, 3-NH), 10.78 (s, 1H, 7-NH), 12.21 (br, 2 H, 2 COOH). Anal. calcd. for ($C_{22}H_{25}N_5O_6 \cdot 1.5\ H_2O$): C, 54.76; H, 5.85; N, 14.52; found: C, 54.88; H, 5.73; N, 14.29.

(*S*)-2-(4-(5-(2-amino-4-oxo-4,7-dihydro-3*H*-pyrrolo[2,3-*d*]pyrimidin-6-yl)pentyl)benzamido)pentanedioic acid (161): Compound **161** was synthesized as described for **2**, yield 60% as a yellow powder, mp 208-209 °C, R_f = 0.05 ($CHCl_3$/MeOH, 5:1). ^{1}H NMR (DMSO-d_6) δ 1.26-1.36 (m, 2 H, CH_2), 1.54-1.66 (m, 4 H, 2 CH_2), 1.88-2.20 (m, 2 H, CH_2), 2.31-2.39 (t, 2 H, CH_2), 2.52-2.68 (m, 4 H, 2 CH_2), 4.32-4.42 (m, 1 H, CH), 5.85 (s, 1 H, CH), 5.99 (s, 2 H, 2-NH_2), 7.29 (d, 2 H, C_6H_4, J = 4.0 Hz), 7.79 (d, 2 H, C_6H_4, J = 4.0 Hz), 8.52 (d, 1 H, CONH, , J = 3.9 Hz), 10.14 (s, 1 H, 3-NH), 10.80 (s, 1H, 7-NH), 12.24 (br, 2 H, 2 COOH). Anal. calcd. for ($C_{23}H_{27}N_5O_6 \cdot 1.0\ H_2O$): C, 56.66; H, 6.00; N, 14.36; found: C, 56.69; H, 5.90; N, 14.11.

(*S*)-2-(4-(6-(2-amino-4-oxo-4,7-dihydro-3*H*-pyrrolo[2,3-*d*]pyrimidin-6-yl)hexyl)benzamido)pentanedioic acid (162): Compound **162** was synthesized as described for **2**, yield 83% as a yellow powder, mp 220-221 °C, R_f = 0.05 ($CHCl_3$/MeOH, 5:1). ^{1}H NMR (DMSO-d_6) δ 1.25-1.35 (m, 4 H, 2 CH_2), 1.48-1.65 (m, 4

H, 2 CH_2), 1.88-2.15 (m, 2 H, CH_2), 2.30-2.38 (t, 2 H, CH_2), 2.49-2.68 (m, 4 H, 2 CH_2), 4.33-4.43 (m, 1 H, CH), 5.83 (s, 1 H, CH), 5.96 (s, 2 H, 2-NH_2), 7.28 (d, 2 H, C_6H_4, J = 4.0 Hz), 7.90 (d, 2 H, C_6H_4, J = 4.0 Hz), 8.52 (d, 1 H, CONH, , J = 3.8 Hz), 10.12 (s, 1 H, 3-NH), 10.78 (s, 1H, 7-NH), 12.21 (br, 2 H, 2 COOH). Anal. calcd. for ($C_{24}H_{29}N_5O_6 \cdot 2.5$ H_2O): C, 54.54; H, 6.48; N, 13.25; found: C, 54.74; H, 6.12; N, 13.12.

(*S*)-diethyl 2-(4-iodobenzamido)pentanedioate(232): To a solution 4-iodobenzoic acid **231** (1.24 g, 5 mmol) in anhydrous DMF (40 mL) was added 6-chloro-2,4-dimethoxy-1,3,5-triazine (1.05 g, 6 mmol) and *N*-methylmorpholine (0.65 mL, 6 mmol). After the mixture was stirred at r.t. for 2 h, *N*-methylmorpholine (0.65 mL, 6 mmol) and dimethyl *L*-glutamate hydrochloride (1.44 g, 6 mmol) were added all at once. The mixture was stirred at r.t. for 4 h. TLC showed the formation of one major spot at R_f = 0.42 (Hexane/EtOAc, 2:1). The reaction mixture was evaporated to dryness under reduced pressure. The residue was chromatographed on a silica gel column (2 cm x 15 cm) with Hexane/EtOAc, 3:1 as the eluent. Fractions were pooled and evaporated to dryness to afford **232** 2.05 g, yield 95% as white crystals, mp 105-106 °C (lit.[2] mp 105-106 °C), R_f = 0.42 (Hexane/EtOAc, 2:1). ^{1}H NMR ($CDCl_3$) δ 1.18-1.26(t, 3 H, J = 7.2 Hz, γ-$COOCH_2CH_3$), 1.27-1.33 (t, 3 H, J = 7.2 Hz, α-$COOCH_2CH_3$), 2.10-2.35 (m, 2 H, β-CH_2), 2.38-2.56 (m, 2 H, γ-CH_2), 4.06-4.16 (m, 2 H, γ-$COOCH_2CH_3$), 4.20-4.28 (m, 2 H, α-$COOCH_2CH_3$), 4.72-4.77 (m, 1 H, α-CH), 7.10 (d, 1 H, J = 6.7 Hz, CONH, exch), 7.55 (d, 2 H, J = 8.6 Hz, C_6H_4), 7.80 (d, 2 H, J = 8.6 Hz, C_6H_4).

(*S*)-diethyl 2-(4-((trimethylsilyl)ethynyl)benzamido)pentanedioate (233): A mixture of **232** (1.30 g, 3 mmol), trimethylsilyl acetylene (0.87 g, 9 mmol), tetrakis(triphenylphosphine)palladium (0.35 g, 0.3 mmol), copper iodide (0.114 g, 0.6

mmol), and triethylamine (0.6 mL) in 1,2-dichloroethane (15 mL) was stirred at room temperature under nitrogen in the dark overnight. Methylene chloride (20 mL) was added to the reaction mixture, and the mixture was washed with brine (20 mL x 2). The organic layer was separated and the solvent evaporated. The residue obtained was loaded onto a silica gel column and eluted with 4:1 hexanes/ethyl acetate. Fractions containing the product (TLC, R_f = 0.44, Hexane/EtOAc, 2:1) were pooled and the solvent evaporated to afford 1.22 g (100%) of **233** as a red oil. ^{1}H NMR ($CDCl_3$) δ 0.26 (s, 9H, -Si(CH_3)$_3$), 1.20-1.24 (t, 3 H, J = 7.2 Hz, γ-COOCH$_2$C*H*$_3$), 1.28-1.32 (t, 3 H, J = 7.2 Hz, α-COOCH$_2$C*H*$_3$), 2.10-2.36 (m, 2 H, β-C*H*$_2$), 2.38-2.56 (m, 2 H, γ-C*H*$_2$), 4.06-4.15 (m, 2 H, γ-COOC*H*$_2$CH$_3$), 4.20-4.28 (m, 2 H, α-COOC*H*$_2$CH$_3$), 4.74-4.81 (m, 1 H, α-CH), 7.06 (d, 1 H, J = 7.4 Hz, CON*H*, exch), 7.52 (d, 2 H, J = 8.5 Hz, C_6H_4), 7.76 (d, 2 H, J = 8.5 Hz, C_6H_4).

(*S*)-diethyl 2-(4-ethynylbenzamido)pentanedioate (234): Compound **233** (1.21 g, 3mmol) was dissolved in THF (15 mL), to which tetrabutylammonium fluoride (3 mL of a 1 M solution in THF) was added, and the solution stirred at room temperature for 2 h. Methylene chloride (20 mL) was added to the reaction mixture and washed with brine (20 mL x 2), then the organic layer separated and dried over Na_2SO_4 and the solvent was evaporated. The crude residue was flash chromatographed on silica gel and eluted with 2:1 hexanes/ethyl acetate. Fractions containing the desired product (TLC) were pooled and evaporated to afford 0.72 g (72%) of **234** as a red oil : TLC R_f 0.25 (hexanes/ethyl acetate, 2:1); ^{1}H NMR ($CDCl_3$) δ 1.20-1.24 (t, 3 H, J = 7.2 Hz, γ-COOCH$_2$C*H*$_3$), 1.28-1.32 (t, 3 H, J = 7.2 Hz, α-COOCH$_2$C*H*$_3$), 2.09-2.37 (m, 2 H, β-C*H*$_2$), 2.38-2.56 (m, 2 H, γ-C*H*$_2$), 3.20 (s, 1H, -CH), 4.06-4.15 (m, 2 H, γ-COOC*H*$_2$CH$_3$), 4.20-4.28 (m, 2 H, α-

COOC*H*$_2$CH$_3$), 4.74-4.81 (m, 1 H, α-CH), 7.13 (d, 1 H, *J* = 7.4 Hz, CON*H*, exch), 7.55 (d, 2 H, *J* = 8.5 Hz, C_6H_4), 7.78 (d, 2 H, *J* = 8.5 Hz, C_6H_4).

2-amino-3*H*-pyrrolo[2,3-*d*]pyrimidin-4(7*H*)-one (228): To a solution of 2,4-diamino-6-hydroxypyrimidine **28** (5.0 g, 40 mmol) and sodium acetate (4.88 g, 60 mmol) in water (200 mL) at 100 °C was added a 50% solution of chloroacetaldehyde in water **227** (5.0 mL, 40 mmol), dropwise, over a period of 15 min. The reaction mixture was stirred under reflux for a further 5 h. The resulting suspension was refrigerated overnight, and the precipitate obtained was filtered, washed with cold water (25 mL x 2), then with cold acetone (20 mL x 2) and dried to afford 4.15 g (69%) of **228** as a grey solid: TLC R_f 0.45 ($CHCl_3$/MeOH, 3:1); mp 322 °C (lit[2] mp 323-324 °C); ^{1}H NMR (DMSO-d_6) δ 6.04 (bs, 2 H, 2-NH_2, exch), 6.18 (q, 1 H, 5-H), 6.60 (q, 1 H, 6-H), 10.22 (bs, 1 H, 3-NH, exch), 10.96 (bs, 1 H, 7-NH, exch).

***N*-(4-oxo-4,7-dihydro-3*H*-pyrrolo[2,3-*d*]pyrimidin-2-yl)pivalamide (229):** A mixture of **228** (3.67 g, 24.5 mmol), pyridine (40 mL) and pivaloyl chloride (10.5 mL) was heated at 80-90 °C for 2 h. Volatiles were stripped under vacuum, and the residue was dissolved in methanol (20 mL), silica gel (5 g) was added, and the solvent was evaporated to form a plug which was dried, loaded on top of a silica gel column and eluted with 2:1 ethyl acetate/hexanes. Fractions containing the product (TLC) were pooled and the solvent evaporated to afford 2.07 g (36%) of **229** as an yellow solid: TLC R_f 0.50 (acetate/hexanes, 5:1); mp 293 °C (lit[300] 295 °C); ^{1}H NMR (DMSO-d_6) δ 1.24 (s, 9 H, -C(CH_3)$_3$), 6.40 (q, 1 H, 5-H), 6.95 (q, 1 H, 6-H), 10.80 (bs, 1 H, 2-N*H*Piv or 3-NH, exch), 11.58 (bs, 1 H, 2-N*H*Piv or 3-NH, exch), 11.84 (bs, 1 H, 7-NH, exch).

***N*-(6-iodo-4-oxo-4,7-dihydro-3*H*-pyrrolo[2,3-*d*]pyrimidin-2-yl)pivalamide (230):**

To a solution of **229** (150 mg, 0.64 mmol) in glacial acetic acid (5 mL) was added mercuric acetate (239 mg, 0.75 mmol) that was completely dissolved in glacial acetic acid (15 mL). The mixture was stirred at room temperature for 10 min, poured into saturated NaCl (10 mL), and stirred for 30 min. The precipitate was filtered, washed with water (3 mL), followed by MeOH (3 mL), and dried. The precipitate was combined with MeOH (5 mL) and stirred at room temperature for 1 h to remove starting material and filtrated to afford the crude. A mixture of this crude, iodine (0.19 g, 0.75 mmol) and CH_2Cl_2 (5 mL) was stirred at room temperature overnight. The solvent was removed under reduced pressure. The residue was washed with 3 M $Na_2S_2O_3$ (5 mL x 2), followed by water (5 mL x 2), and dried *in vacuo*. The crude product was purified by column chromatography on silica gel and eluted with 1:1 ethyl acetate/hexanes. The fractions containing the desired product (TLC) were pooled and evaporated to afford 175 mg (78%) of **230** as a white solid: TLC R_f 0.60 (ethyl acetate/hexanes, 2:1); mp 210 °C dec (lit.[2] mp 211 °C dec); ^{1}H NMR (DMSO-d_6) δ 1.23 (s, 9 H, -C(CH_3)$_3$), 6.61 (s, 1 H, 5-H), 10.88 (s, 1 H, 2-N*H*Piv or 3-NH, exch), 11.88 (s, 1 H, 2-N*H*Piv or 3-NH, exch), 12.10 (s, 1 H, 7-NH, exch).

(*S*)-diethyl 2-(4-((4-oxo-2-pivalamido-4,7-dihydro-3*H*-pyrrolo[2,3-*d*]pyrimidin-6-yl)ethynyl)benzamido)pentanedioate (235): To a 50-mL round-bottom flask covered with aluminum foil were added **230** (180 mg, 0.5 mmol) and acetylene **234** (248 mg, 0.75 mmol), copper(I) iodide (25 mg, 0.1 mmol) and tetrakis(triphenyl phosphine)palladium (0) (30 mg, 0.025 mmol)dissolved in anhydrous DMF (10 mL), followed by the addition of triethylamine (0.25 mL). The dark brown solution was stirred at 60 °C under nitrogen for 4h. The volatiles were removed *in vacuo* and the crude residue was flash

chromatographed on silica gel and eluted with 3% MeOH in CH_2Cl_2 to afford the compound **235** 135 mg (48%) as a yellow solid: TLC R_f 0.65 (MeOH/CH_2Cl_2, 1:9); mp 260 °C dec; ^{1}H NMR (DMSO-d_6) δ 1.15-1.22 (m, 6H, -2CH_3), 1.25 (s, 9 H, -C(CH_3)$_3$), 1.99-2.15 (m, 2 H, β-CH_2), 2.43-2.45 (m, 2 H, γ-CH_2), 4.02-4.15 (m, 4 H, α, γ-COOC$H_2$$CH_3$), 4.42-4.48 (m, 1 H, α-CH), 6.85 (s, 1 H, 5-H), 7.65 (d, 2 H, C_6H_4, J = 8.5 Hz), 7.94 (d, 2 H, C_6H_4, J = 8.5 Hz), 8.85 (d, 1 H, CONH, , J = 7.5 Hz), 10.98 (s, 1 H, 2-N*H*Piv or 3-NH, exch), 11.97 (s, 1 H, 2-N*H*Piv or 3-NH, exch), 12.27 (s, 1 H, 7-NH, exch).

(*S*)-diethyl 2-(4-(2-(4-oxo-2-pivalamido-4,7-dihydro-3*H*-pyrrolo[2,3-*d*]pyrimidin-6-yl)ethyl)benzamido)pentanedioate (236): To a solution of **235** (50 mg) in MeOH/CH_2Cl_2 (1:1, 30 mL) was added 10% Pd/C (50 mg). The resulting suspension was hydrogenated in a Parr apparatus for 5h at 50 psi hydrogen pressure. The reaction mixture was filtered through Celite and washed with methanol (30 mL). After evaporation of the solvent, 50 mg (100%) of **236** was obtained as a grey solid: mp 142 °C, R_f 0.65 (MeOH/CH_2Cl_2, 1:9). ^{1}H NMR (DMSO-d_6) δ 1.13-1.21 (m, 6H, -2CH_3), 1.24 (s, 9 H, -C(CH_3)$_3$), 1.96-2.13 (m, 2 H, β-CH_2), 2.41-2.45 (t, 2 H, γ-CH_2, J = 7.6 Hz), 2.91-3.04 (m, 4H, -CH_2CH_2-), 4.00-4.14 (m, 4 H, α, γ-COOC$H_2$$CH_3$), 4.38-4.45 (m, 1 H, α-CH), 6.10 (s, 1 H, 5-H), 7.33 (d, 2 H, C_6H_4, J = 8.2 Hz), 7.79 (d, 2 H, C_6H_4, J = 8.2 Hz), 8.65 (d, 1 H, CONH, , J = 7.5 Hz), 10.76 (s, 1 H, 2-N*H*Piv or 3-NH, exch), 11.40 (s, 1 H, 2-N*H*Piv or 3-NH, exch), 11.82 (s, 1 H, 7-NH, exch).

(*S*)-2-(4-(2-(2-amino-4-oxo-4,7-dihydro-3*H*-pyrrolo[2,3-*d*]pyrimidin-6-yl)ethyl)benzamido)pentanedioic acid (163): To a solution of the diester **236** (50 mg) was added 1 N NaOH (4 mL), and the mixture was stirred under N_2 at room temperature

for 3 days. TLC (CH_2Cl_2/MeOH, 9:1) showed the disappearance of the starting material (R_f = 0.65) and formation of one major spot at the origin. The reaction mixture was evaporated to dryness under reduced pressure. The residue was dissolved in water (3 mL), the resulting solution was cooled in an ice bath, and the pH was adjusted to 3-4 with dropwise addition of 1 N HCl. The resulting suspension was frozen in a dry ice/acetone bath, thawed in a refrigerator to 4-5 °C, and filtered. The residue was washed with a small amount of cold water and ethyl acetate and dried in vacuo using P_2O_5 to afford 30 mg (80%) of **163** as a pale white powder: mp 209 °C (lit.[2] mp 210-213 °C), R_f = 0.05 ($CHCl_3$/MeOH, 5:1). ^{1}H NMR (DMSO-d_6) δ 1.90-2.11 (m, 2 H, CH_2), 2.31-2.37 (t, 2 H, CH_2), 2.77-2.84 (t, 2 H, CH_2), 2.92-2.98 (t, 2 H, CH_2), 4.34-4.41 (m, 1 H, CH), 5.86 (s, 1 H, CH), 5.97 (s, 2 H, 2-NH_2), 7.31 (d, 2 H, C_6H_4, J = 8.0 Hz), 7.79 (d, 2 H, C_6H_4, J = 8.0 Hz), 8.51 (d, 1 H, CONH, , J = 8.0 Hz), 10.12 (s, 1 H, 3-NH), 10.89 (s, 1H, 7-NH), 12.60 (br, 2 H, 2 COOH). Anal. ($C_{20}H_{21}N_5O_6 \cdot 0.75\ H_2O$) Cal. C: 54.48, H: 5.14, N: 15.88. Found C: 54.49, H: 5.04, N: 15.53.

Ethyl 8-bromo-7-oxooctanoate (241): To a solution of 7-methoxy-7-oxoheptanoic acid **(237)** (0.32 g, 1.5 mmol) in a 50 mL flask was added oxalyl chloride (1.5 mL) and anhydrous CH_2Cl_2 (10 mL). The resulting solution was refluxed for 1 h and then cooled to room temperature. After evaporation of solvent under reduced pressure, the residue was dissolved in ethyl ether (20 mL). The resulting solution was added dropwise to an ice-cooled ether solution of diazomethane (generated in situ from 1.4 g *N*-nitroso-*N*-methylurea) over 10 min. To this solution was added 48% HBr (1.5 mL). The resulting mixture was refluxed for 1.5 h. After the mixture was cooled to room temperature, the organic layer was separated and the aqueous layer was extracted with ethyl ether (20 mL

x 3). The combined organic layers were washed with two portions of 10% Na_2CO_3 solution and dried over Na_2SO_4. The solvent was evaporated to afford 0.38 g **241**: yield 79% as white crystals, mp 68-69 °C, R_f = 0.50 (Hexane/EtOAc, 5:1). ^{1}H NMR ($CDCl_3$) δ 1.24-1,27 (t, 3 H, CH_3, J = 7.5 Hz), 1.32-1.37 (m, 2 H, CH_2), 1.62-1.65 (m, 4 H, 2 CH_2), 2.28-2.31 (t, 2 H, CH_2, J = 7.5 Hz), 2.65-2.69 (m, 2 H, CH_2), 3.87 (s, 2H, CH_2Br), 4.10-4.14 (q, 2 H, CH_2, J = 7.5 Hz).

Methyl 9-bromo-8-oxononanoate (242): Compound **242** was synthesized as described for **241:** yield 83% as light yellow crystals, mp 70-71 °C, R_f = 0.51 (Hexane/EtOAc, 5:1). ^{1}H NMR ($CDCl_3$) δ 1.32-1.33 (m, 4 H, 2 CH_2), 1.60-1.63 (m, 4 H, 2 CH_2), 2.28-2.31 (t, 2 H, CH_2, J = 7.5 Hz), 2.63-2.66 (t, 2 H, CH_2, J = 7.5 Hz), 3.66 (s, 3H, CH_3), 3.87 (s, 2H, CH_2Br).

Methyl 10-bromo-9-oxodecanoate (243): Compound **243** was synthesized as described for **241**: yield 78% as yellow crystals, mp 123-124 °C, R_f = 0.51 (Hexane/EtOAc, 5:1). ^{1}H NMR ($CDCl_3$) δ 1.31-1.33 (m, 6 H, 3 CH_2), 1.60-1.62 (m, 4 H, 2 CH_2), 2.28-2.31 (t, 2 H, CH_2, J = 7.5 Hz), 2.63-2.66 (t, 2 H, CH_2, J = 7.5 Hz), 3.66 (s, 3H, CH_3), 3.87 (s, 2H, CH_2Br).

Methyl 11-bromo-10-oxoundecanoate (244): Compound **244** was synthesized as described for **241**: yield 72% as yellow crystals, mp 92-93 °C, R_f = 0.52 (Hexane/EtOAc, 3:1). ^{1}H NMR ($CDCl_3$) δ 1.31-1.33 (m, 8 H, 4 CH_2), 1.59-1.62 (m, 4 H, 2 CH_2), 2.28-2.31 (t, 2 H, CH_2, J = 7.5 Hz), 2.62-2.65 (t, 2 H, CH_2, J = 7.5 Hz), 3.66 (s, 3H, CH_3), 3.87 (s, 2H, CH_2Br).

Ethyl 6-(2-amino-4-oxo-4,7-dihydro-3*H*-pyrrolo[2,3-*d*]pyrimidin-6-yl)hexanoate (245): To a suspension of 2,4-diamino-6-hydroxypyrimidine **35** (1.26 g, 10.0 mmol) in

anhydrous DMF (40 mL) was added **241** (2.64 g, 10.0 mmol). The resulting mixture was stirred under N_2 at room temperature for 3 days. TLC showed the disappearance of starting materials and the formation of one major spot. After evaporation of solvent, CH_3OH (20 mL) was added followed by silica gel (5 g). Evaporation of the solvent afforded a plug, which was loaded onto a silica gel column (3.5 cm x 15 cm) and eluted initially with $CHCl_3$ followed by 10% MeOH in $CHCl_3$ and then 15% MeOH in $CHCl_3$. Fractions showing R_f = 0.39 were pooled and evaporated to afford 1.20 g **245**: yield 41% as a yellow solid, mp 189-190 °C, R_f = 0.39 ($CHCl_3$/MeOH, 5:1). ^{1}H NMR (DMSO-d_6) δ 1.15-1.17 (t, 3 H, CH_3, J = 7.5 Hz), 1.26-1.31 (m, 2 H, CH_2), 1.52-1.57 (m, 4 H, 2 CH_2), 2.25-2.28 (t, 2 H, CH_2, J = 7.5 Hz), 2.44-2.47 (t, 2 H, CH_2, J = 7.5 Hz), 4.01-4.06 (m, 2 H, OCH_2), 5.84 (s, 1 H, CH), 5.94 (s, 2 H, 2-NH_2), 10.10 (s, 1 H, 3-NH), 10.77 (s, 1H, 7-NH).

Methyl 7-(2-amino-4-oxo-4,7-dihydro-3*H*-pyrrolo[2,3-*d*]pyrimidin-6-yl)heptanoate (246): Compound **246** was synthesized as described for **245**: yield 39% as a yellow solid, mp 178-179 °C, R_f = 0.39 ($CHCl_3$/MeOH, 5:1). ^{1}H NMR (DMSO-d_6) δ 1.24-1.29 (m, 4 H, 2 CH_2), 1.49-1.56 (m, 4 H, 2 CH_2), 2.27-2.30 (t, 2 H, CH_2, J = 7.5 Hz), 2.44-2.47 (m, 2 H, CH_2), 3.57 (s, 3 H, OCH_3), 5.83 (s, 1 H, CH), 5.94 (s, 2 H, 2-NH_2), 10.11 (s, 1 H, 3-NH), 10.77 (s, 1H, 7-NH).

Methyl 8-(2-amino-4-oxo-4,7-dihydro-3*H*-pyrrolo[2,3-*d*]pyrimidin-6-yl)octanoate (247): Compound **247** was synthesized as described for **245**: yield 43% as a yellow solid, mp 162-163 °C, R_f = 0.41 ($CHCl_3$/MeOH, 5:1). ^{1}H NMR (DMSO-d_6) δ 1.21-1.30 (m, 6 H, 3 CH_2), 1.49-1.56 (m, 4 H, 2 CH_2), 2.27-2.29 (t, 2 H, CH_2, J = 7.5 Hz), 2.43-2.47 (t, 2 H, CH_2, J = 7.5 Hz), 3.57 (s, 3 H, OCH_3), 5.84 (s, 1 H, CH), 6.00 (s, 2 H, 2-NH_2), 10.16

(s, 1 H, 3-NH), 10.79 (s, 1H, 7-NH).

Methyl 9-(2-amino-4-oxo-4,7-dihydro-3*H*-pyrrolo[2,3-*d*]pyrimidin-6-yl)nonanoate (248): Compound **248** was synthesized as described for **245**: yield 42% as a yellow solid, mp 165-166 °C, R_f = 0.41 ($CHCl_3$/MeOH, 5:1). ^{1}H NMR (DMSO-d_6) δ 1.21-1.30 (m, 8 H, 4 CH_2), 1.49-1.56 (m, 4 H, 2 CH_2), 2.26-2.29 (t, 2 H, CH_2, J = 7.5 Hz), 2.44-2.47 (t, 2 H, CH_2, J = 7.5 Hz), 3.57 (s, 3 H, OCH_3), 5.85 (s, 1 H, CH), 6.03 (s, 2 H, 2-NH_2), 10.20 (s, 1 H, 3-NH), 10.81 (s, 1H, 7-NH).

(*S*)-diethyl 2-(6-(2-amino-4-oxo-4,7-dihydro-3*H*-pyrrolo[2,3-*d*]pyrimidin-6-yl)hexanamido)pentanedioate (249): To a suspension of **245** (100 mg, 0.34 mmol) in 10 mL CH_3OH was added 1 N NaOH (10 mL). The resulting mixture was stirred under N_2 at r.t. for 24 h. TLC indicated the disappearance of starting material and the formation of one major spot at the origin. The resulting solution was cooled in an ice bath, and the pH was adjusted 3 to 4 using 3 N HCl. The resulting suspension was chilled in a dry ice/acetone bath and thawed to 4 °C overnight in a refrigerator. The precipitate was filtered, washed with cold water, and dried in a desiccator under reduced pressure using P_2O_5 to a brown powder, which was used directly for the next step.

To a solution of this brown powder in anhydrous DMF (5 mL) was added 6-chloro-2,4-dimethoxy-1,3,5-triazine (72 mg, 0.42 mmol) and *N*-methylmorpholine (43 mg, 0.42 mmol). After the mixture was stirred at r.t. for 2 h, *N*-methylmorpholine (43 mg, 0.42 mmol) and dimethyl *L*-glutamate hydrochloride (120 mg, 0.51 mmol) were added all at once. The mixture was stirred at r.t. for 4 h. TLC showed the formation of one major spot at R_f = 0.62 ($CHCl_3$/MeOH, 5:1). The reaction mixture was evaporated to dryness under reduced pressure. The residue was dissolved in a minimum amount of $CHCl_3$/MeOH, 5:1,

and chromatographed on a silica gel column (2 cm x 15 cm) with 4% MeOH in $CHCl_3$ as the eluent. Fractions that showed the desired single spot at R_f = 0.62 were pooled and evaporated to dryness to afford **249** 102 mg: yield 67% as a yellow syrup, R_f = 0.62 ($CHCl_3$/MeOH, 5:1). ^{1}H NMR (DMSO-d_6) δ 1.15-1.18 (t, 6 H, 2 CH_3, J = 7.0 Hz), 1.23-1.29 (m, 2 H, CH_2), 1.48-1.58 (m, 4 H, 2 CH_2), 1.76-1.82 (m, 1 H, CH), 1.92-1.98 (m, 1 H, CH), 2.09-2.12 (t, 2 H, CH_2, J = 7.0 Hz), 2.33-2.37 (m, 2 H, CH_2), 2.44-2.47 (m, 2 H, CH_2), 4.02-4.07 (m, 4 H, 2 CH_2), 4.19-4.24 (m, 1 H, CH), 5.84 (s, 1 H, CH), 5.94 (s, 2 H, 2-NH_2), 8.16 (d, 1 H, CONH, , J = 3.8 Hz), 10.10 (s, 1 H, 3-NH), 10.76 (s, 1H, 7-NH).

(*S*)-diethyl 2-(7-(2-amino-4-oxo-4,7-dihydro-3*H*-pyrrolo[2,3-*d*]pyrimidin-6-yl)heptanamido)pentanedioate (250): Compound **250** was synthesized as described for **249**: yield 70% as a yellow syrup, R_f = 0.62 ($CHCl_3$/MeOH, 5:1). ^{1}H NMR (DMSO-d_6) δ 1.15-1.18 (m, 6 H, 2 CH_3), 1.23-1.30 (m, 4 H, 2 CH_2), 1.48-1.58 (m, 4 H, 2 CH_2), 1.76-1.82 (m, 1 H, CH), 1.92-1.99 (m, 1 H, CH), 2.09-2.12 (t, 2 H, CH_2, J = 7.0 Hz), 2.33-2.37 (m, 2 H, CH_2), 2.44-2.47 (m, 2 H, CH_2), 4.02-4.08 (m, 4 H, 2 CH_2), 4.20-4.24 (m, 1 H, CH), 5.83 (s, 1 H, CH), 5.93 (s, 2 H, 2-NH_2), 8.15 (d, 1 H, CONH, , J = 3.8 Hz), 10.10 (s, 1 H, 3-NH), 10.77 (s, 1H, 7-NH).

(*S*)-diethyl 2-(8-(2-amino-4-oxo-4,7-dihydro-3*H*-pyrrolo[2,3-*d*]pyrimidin-6-yl)octanamido)pentanedioate (251): Compound **251** was synthesized as described for **249**: yield 68% as a yellow syrup, R_f = 0.64 ($CHCl_3$/MeOH, 5:1). ^{1}H NMR (DMSO-d_6) δ 1.16-1.19 (t, 6 H, 2 CH_3, J = 7.0 Hz), 1.22-1.32 (m, 6 H, 3 CH_2), 1.47-1.57 (m, 4 H, 2 CH_2), 1.76-1.82 (m, 1 H, CH), 1.92-1.99 (m, 1 H, CH), 2.09-2.12 (t, 2 H, CH_2, J = 7.0 Hz), 2.34-2.37 (m, 2 H, CH_2), 2.45-2.48 (m, 2 H, CH_2), 4.02-4.08 (m, 4 H, 2 CH_2),

4.20-4.24 (m, 1 H, CH), 5.84 (s, 1 H, CH), 5.94 (s, 2 H, 2-NH_2), 8.15 (d, 1 H, CONH, , *J* = 3.8 Hz), 10.10 (s, 1 H, 3-NH), 10.76 (s, 1H, 7-NH).

(*S*)-diethyl 2-(9-(2-amino-4-oxo-4,7-dihydro-3*H*-pyrrolo[2,3-*d*]pyrimidin-6-yl)nonanamido)pentanedioate (252): Compound **252** was synthesized as described for **249**: yield 66% as a yellow syrup, R_f = 0.64 ($CHCl_3$/MeOH, 5:1). ^{1}H NMR (DMSO-d_6) δ 1.15-1.18 (t, 6 H, 2 CH_3, *J* = 7.0 Hz), 1.22-1.32 (m, 8 H, 4 CH_2), 1.47-1.57 (m, 4 H, 2 CH_2), 1.76-1.82 (m, 1 H, CH), 1.92-1.99 (m, 1 H, CH), 2.09-2.12 (t, 2 H, CH_2, *J* = 7.0 Hz), 2.34-2.37 (m, 2 H, CH_2), 2.45-2.48 (m, 2 H, CH_2), 4.02-4.08 (m, 4 H, 2 CH_2), 4.20-4.24 (m, 1 H, CH), 5.83 (s, 1 H, CH), 5.94 (s, 2 H, 2-NH_2), 8.15 (d, 1 H, CONH, , *J* = 3.8 Hz), 10.10 (s, 1 H, 3-NH), 10.77 (s, 1H, 7-NH).

(*S*)-2-(6-(2-amino-4-oxo-4,7-dihydro-3*H*-pyrrolo[2,3-*d*]pyrimidin-6-yl)hexanamido)pentanedioic acid (164): To a solution of the diester **249** (100 mg, 0.22 mmol) was added 1 N NaOH (5 mL), and the mixture was stirred under N_2 at room temperature for 1 h. TLC showed the disappearance of the starting material and formation of one major spot at the origin ($CHCl_3$/MeOH, 5:1). The resulting solution was cooled in an ice bath, and the pH was adjusted to 3-4 with dropwise addition of 1 N HCl. The resulting suspension was frozen in a dry ice/acetone bath, thawed in a refrigerator to 4-5 °C, and filtered. The residue was washed with a small amount of cold water and ethyl acetate and dried in vacuo using P_2O_5 to afford 78 mg **164**: yield 90% as a white powder, mp 145-146 °C decomposed, R_f = 0.08 ($CHCl_3$/MeOH, 5:1). ^{1}H NMR (DMSO-d_6) δ 1.24-1.30 (m, 2 H, CH_2), 1.48-1.58 (m, 4 H, 2 CH_2), 1.71-1.79 (m, 1 H, CH), 1.88-1.95 (m, 1 H, CH), 2.09-2.12 (t, 2 H, CH_2, *J* = 7.5 Hz), 2.24-2.27 (m, 2 H, CH_2, *J* = 7.5 Hz), 2.44-2.47 (m, 2 H, CH_2), 4.16-4.21 (m, 1 H, CH), 5.84 (s, 1 H, CH), 5.95 (s, 2 H, 2-

NH_2), 7.99 (d, 1 H, CONH, , J = 4.0 Hz), 10.10 (s, 1 H, 3-NH), 10.76 (s, 1H, 7-NH), 12.50 (br, 2 H, 2 COOH). Anal. ($C_{17}H_{23}N_5O_6 \cdot 2.0\ H_2O$) Cal. C: 47.55, H: 6.34, N: 16.31. Found C: 47.88, H: 6.01, N: 15.98.

(*S*)-2-(7-(2-amino-4-oxo-4,7-dihydro-3*H*-pyrrolo[2,3-*d*]pyrimidin-6-yl)heptanamido)pentanedioic acid (165): Compound **165** was synthesized as described for **164**: yield 91% as a pale yellow powder, mp 116-117 °C decomposed, R_f = 0.08 ($CHCl_3$/MeOH, 5:1). ^{1}H NMR (DMSO-d_6) δ 1.22-1.32 (m, 4 H, 2 CH_2), 1.45-1.58 (m, 4 H, 2 CH_2), 1.71-1.79 (m, 1 H, CH), 1.91-1.98 (m, 1 H, CH), 2.09-2.12 (t, 2 H, CH_2, J = 7.5 Hz), 2.24-2.28 (m, 2 H, CH_2, J = 7.5 Hz), 2.44-2.47 (m, 2 H, CH_2), 4.16-4.21 (m, 1 H, CH), 5.84 (s, 1 H, CH), 5.94 (s, 2 H, 2-NH_2), 8.02 (d, 1 H, CONH, , J = 4.0 Hz), 10.10 (s, 1 H, 3-NH), 10.76 (s, 1H, 7-NH), 12.12 (br, 1 H, 1 COOH), 12.52 (br, 1 H, 1 COOH). Anal. ($C_{18}H_{25}N_5O_6 \cdot 0.5\ H_2O$) Cal. C: 51.92, H: 6.29, N: 16.82. Found C: 51.92, H: 6.43, N: 16.59.

(*S*)-2-(8-(2-amino-4-oxo-4,7-dihydro-3*H*-pyrrolo[2,3-*d*]pyrimidin-6-yl)octanamido)pentanedioic acid (166): Compound **166** was synthesized as described for **164**: yield 95% as a yellow powder, mp 135-136 °C decomposed, R_f = 0.08 ($CHCl_3$/MeOH, 5:1). ^{1}H NMR (DMSO-d_6) δ 1.20-1.32 (m, 6 H, 3 CH_2), 1.45-1.58 (m, 4 H, 2 CH_2), 1.71-1.79 (m, 1 H, CH), 1.90-1.98 (m, 1 H, CH), 2.08-2.12 (t, 2 H, CH_2, J = 7.5 Hz), 2.24-2.28 (m, 2 H, CH_2, J = 7.5 Hz), 2.44-2.47 (t, 2 H, CH_2, J = 7.5 Hz), 4.16-4.21 (m, 1 H, CH), 5.84 (s, 1 H, CH), 5.94 (s, 2 H, 2-NH_2), 8.02 (d, 1 H, CONH, J = 3.8 Hz), 10.11 (s, 1 H, 3-NH), 10.76 (s, 1H, 7-NH). Anal. ($C_{19}H_{27}N_5O_6 \cdot 0.5\ H_2O$) Cal. C: 53.01, H: 6.56, N: 16.27. Found C: 53.29, H: 6.76, N: 16.19.

(*S*)-2-(9-(2-amino-4-oxo-4,7-dihydro-3*H*-pyrrolo[2,3-*d*]pyrimidin-6-

yl)nonanamido)pentanedioic acid (167): Compound **167** was synthesized as described for **164**: yield 90% as a pale yellow powder, mp 123-124 °C decomposed, R_f = 0.08 ($CHCl_3$/MeOH, 5:1). ^{1}H NMR (DMSO-d_6) δ 1.20-1.32 (m, 8 H, 4 CH_2), 1.42-1.58 (m, 4 H, 2 CH_2), 1.71-1.79 (m, 1 H, CH), 1.90-1.98 (m, 1 H, CH), 2.08-2.11 (t, 2 H, CH_2, J = 7.5 Hz), 2.24-2.28 (m, 2 H, CH_2, J = 7.5 Hz), 2.44-2.47 (t, 2 H, CH_2, J = 7.5 Hz), 4.16-4.21 (m, 1 H, CH), 5.84 (s, 1 H, CH), 5.94 (s, 2 H, 2-NH_2), 8.01 (d, 1 H, CONH, J = 3.8 Hz), 10.11 (s, 1 H, 3-NH), 10.76 (s, 1H, 7-NH). Anal. ($C_{20}H_{29}N_5O_6 \cdot 0.5\ H_2O$) Cal. C: 54.04, H: 6.80, N: 15.76. Found C: 54.17, H: 6.85, N: 15.67.

(*S*)-diethyl 2-(2-iodobenzamido)pentanedioate (261): To a solution 2-iodobenzoic acid **260** (2.48 g, 10 mmol) in anhydrous DMF (40 mL) was added 6-chloro-2,4-dimethoxy-1,3,5-triazine (2.10 g, 12 mmol) and *N*-methylmorpholine (1.30 mL, 12 mmol). After the mixture was stirred at r.t. for 2 h, *N*-methylmorpholine (1.30 mL, 12 mmol) and dimethyl *L*-glutamate hydrochloride (2.88 g, 12 mmol) were added all at once. The mixture was stirred at r.t. for 4 h. TLC showed the formation of one major spot at R_f = 0.38 (Hexane/EtOAc, 2:1). The reaction mixture was evaporated to dryness under reduced pressure. The residue was chromatographed on a silica gel column (2 cm x 15 cm) with Hexane/EtOAc, 3:1 as the eluent. Fractions were pooled and evaporated to dryness to afford **261** 4.32 g, yield 99% as white crystals, mp 111 °C, R_f = 0.38 (Hexane/EtOAc, 2:1). ^{1}H NMR ($CDCl_3$) δ 1.23-1.26(t, 3 H, J = 7.2 Hz, γ-$COOCH_2CH_3$), 1.30-1.33 (t, 3 H, J = 7.0 Hz, α-$COOCH_2CH_3$), 2.09-2.16 (m, 1 H, β-CH_2), 2.31-2.39 (m, 1 H, β-CH_2), 2.46-2.60 (m, 2 H, γ-CH_2), 4.11-4.15 (m, 2 H, γ-$COOCH_2CH_3$), 4.22-4.27 (m, 2 H, α-$COOCH_2CH_3$), 4.79-4.83 (m, 1 H, α-CH), 6.53-6.54 (d, 1 H, J = 4.0 Hz, CONH, exch),

7.09-7.13 (t, 1 H, C_6H_4 , J = 8.6 Hz), 7.37-7.42 (m, 2 H, C_6H_4), 7.86-7.88 (d, 1 H, C_6H_4, J = 4.0 Hz,).

(*S*)-diethyl 2-(3-iodobenzamido)pentanedioate (263): Compound **263** was synthesized as described for **261:** yield 98% as white crystals: mp 103 °C, R_f = 0.40 (Hexane/EtOAc, 2:1). ^{1}H NMR ($CDCl_3$) δ 1.23-1.25(t, 3 H, J = 7.2 Hz, γ-$COOCH_2CH_3$), 1.30-1.32 (t, 3 H, J = 7.0 Hz, α-$COOCH_2CH_3$), 2.11-2.18 (m, 1 H, β-CH_2), 2.28-2.34 (m, 1 H, β-CH_2), 2.40-2.53 (m, 2 H, γ-CH_2), 4.12-4.16 (m, 2 H, γ-$COOCH_2CH_3$), 4.24-4.26 (m, 2 H, α-$COOCH_2CH_3$), 4.74-4.77 (m, 1 H, α-CH), 7.02-7.04 (d, 1 H, J = 4.0 Hz, CONH, exch), 7.17-7.20 (t, 1 H, J = 4.0 Hz, C_6H_4), 7.76-7.78 (d, 1 H, J = 1.0 Hz, C_6H_4), 7.84-7.85 (d, 1 H, J = 1.0 Hz, C_6H_4), 8.16-8.17 (t, 1 H, J = 1.0 Hz, C_6H_4).

1-bromohex-5-yn-2-one (255): To a solution of pent-4-ynoic acid **256** (1.96 g, 20 mmol) in a 50 mL flask was added oxalyl chloride (8.0 mL) and anhydrous CH_2Cl_2 (10 mL). The resulting solution was refluxed for 1 h and then cooled to room temperature. After evaporation of solvent under reduced pressure, the residue was dissolved in ethyl ether (20 mL). The resulting solution was added dropwise to an ice-cooled ether solution of diazomethane (generated in situ from 14 g *N*-nitroso-*N*-methylurea) over 10 min. To this solution was added 48% HBr (15 mL). The resulting mixture was refluxed for 1.5 h. After the mixture was cooled to room temperature, the organic layer was separated and the aqueous layer was extracted with ether (20 mL x 3). The combined organic layers were washed with two portions of 10% Na_2CO_3 solution and dried over Na_2SO_4. The solvent was evaporated to afford 3.25 g (93%) of **255** as a yellow oil, R_f = 0.52 (Hexane/EtOAc, 3:1). ^{1}H NMR ($CDCl_3$) δ 1.97-1.98 (t, 1 H, CH, J = 2.0 Hz), 2.48-2.51 (t, 2 H, CH_2, J = 7.0 Hz), 2.90-2.93 (t, 2 H, CH_2, J = 7.0 Hz), 3.83 (s, 3 H, OCH_3), 3.91

(s, 2H, CH_2Br).

2-amino-6-(but-3-yn-1-yl)-3*H*-pyrrolo[2,3-*d*]pyrimidin-4(7*H*)-one (253): To a suspension of 2,4-diamino-6-hydroxypyrimidine **35** (2.20 g, 17.4 mmol) in anhydrous DMF (40 mL) was added **255** (3.05 g, 17.4 mmol). The resulting mixture was stirred under N_2 at room temperature for 3 days. TLC showed the disappearance of starting materials and the formation of one major spot at R_f = 0.32 ($CHCl_3$/MeOH, 4:1). After evaporation of solvent, CH_3OH (20 mL) was added followed by silica gel (5 g). Evaporation of the solvent afforded a plug, which was loaded onto a silica gel column (3.5 cm x 15 cm) and eluted initially with $CHCl_3$ followed by 10% MeOH in $CHCl_3$ and then 15% MeOH in $CHCl_3$. Fractions showing R_f = 0.32 were pooled and evaporated to afford 2.67 g (76%) of **253** as a yellow powder: mp 230-231 °C (lit.[22] mp 230-231 °C). ^{1}H NMR (DMSO-d_6) δ 2.43-2.47 (m, 2 H, CH_2), 2.66-2.69 (t, 2 H, CH_2, J = 7.0 Hz), 2.78-2.79 (t, 1 H, CH, J = 2.5 Hz), 5.97 (s, 1 H, CH), 6.14 (s, 2 H, 2-NH_2), 10.30 (s, 1 H, 3-NH), 10.90 (s, 1H, 7-NH).

(*S*)-diethyl 2-(2-(4-(2-amino-4-oxo-4,7-dihydro-3*H*-pyrrolo[2,3-*d*]pyrimidin-6-yl)but-1-yn-1-yl)benzamido)pentanedioate (264): To a 25-mL round-bottomed flask, equipped with a magnetic stirrer and gas inlet, was added a mixture of tetrakis(triphenylphosphine)palladium(0) (23.2 mg, 0.02 mmol), triethylamine (10 mL), **253** (87 mg, 0.2 mmol) and anhydrous DMF (10 mL). To the stirred mixture, under N_2, was added copper(I) iodide (7.6 mg, 0.04 mmol) and **261** (40 mg, 0.2 mmol), and the reaction mixture was stirred at room temperature overnight (17-18 h). Silica gel (0.5 g) was then added, and the solvent was evaporated under reduced pressure. The resulting plug was loaded on to a silica gel column (3.5 × 12 cm) and eluted with $CHCl_3$ followed

by 3% MeOH in $CHCl_3$ and then 5% MeOH in $CHCl_3$. Fractions with desired R_f(TLC) were pooled and evaporated to afford **264** as a yellow syrup 50 mg, yield: 50%, R_f = 0.32 ($CHCl_3$/MeOH, 10:1). ^{1}H NMR (DMSO-d_6) δ 1.12-1.14 (t, 3H, -CH_3, J = 7.0 Hz), 1.19-1.22 (t, 3H, -CH_3, J = 7.0 Hz), 1.90-2.11 (m, 2 H, β-CH_2), 2.46-2.48 (m, 2 H, γ-CH_2), 2.67-2.70 (t, 2 H, CH_2, J = 7.0 Hz), 2.76-2.79 (t, 2 H, CH_2, J = 7.0 Hz), 4.01-4.15 (m, 4 H, α, γ-COOC$H_2$$CH_3$), 4.44-4.48 (m, 1 H, α-CH), 5.99 (s, 1 H, 5-H),), 6.06 (s, 2 H, 2-NH_2), 7.40-7.50 (m, 4 H, C_6H_4), 8.69-8.71 (d, 1 H, CONH, , J = 4.0 Hz), 10.21 (s, 1 H, 3-NH, exch), 10.85 (s, 1 H, 7-NH, exch).

(*S*)-diethyl 2-(2-(4-(2-amino-4-oxo-4,7-dihydro-3*H*-pyrrolo[2,3-*d*]pyrimidin-6-yl)butyl)benzamido)pentanedioate (265): To a solution of **264** (120 mg) in MeOH/CH_2Cl_2 (1:1, 30 mL) was added 10% Pd/C (240 mg). The resulting suspension was hydrogenated in a Parr apparatus for 5h at 55 psi hydrogen pressure. The reaction mixture was filtered through Celite and washed with methanol (30 mL). After evaporation of the solvent, 120 mg (100%) of **265** was obtained as a white syrup, R_f = 0.32 ($CHCl_3$/MeOH, 10:1). ^{1}H NMR (DMSO-d_6) δ 1.12-1.14 (t, 3H, -CH_3, J = 7.0 Hz), 1.19-1.22 (t, 3H, -CH_3, J = 7.0 Hz), 1.53-1.58 (m, 4 H, 2 CH_2), 1.90-2.11 (m, 2 H, β-CH_2), 2.46-2.48 (m, 2 H, γ-CH_2), 2.73 (s, 2 H, CH_2), 2.89 (s, 2 H, CH_2), 4.03-4.14 (m, 4 H, α, γ-COOC$H_2$$CH_3$), 4.39-4.43 (m, 1 H, α-CH), 5.83 (s, 1 H, 5-H), 5.93 (s, 2 H, 2-NH_2), 7.24-7.26 (m, 1 H, C_6H_4), 7.30-7.31 (m, 1 H, C_6H_4), 7.34-7.37 (m, 1 H, C_6H_4), 8.65-8.67 (d, 1 H, CONH, , J = 4.0 Hz), 10.09 (s, 1 H, 3-NH, exch), 10.75 (s, 1 H, 7-NH, exch).

(*S*)-2-(2-(4-(2-amino-4-oxo-4,7-dihydro-3*H*-pyrrolo[2,3-*d*]pyrimidin-6-yl)but-1-yn-1-yl)benzamido)pentanedioic acid (169): Compound **169** was synthesized as described

for **2:** yield 98% as a pale powder: mp 167 °C decomposed, R_f = 0.05 ($CHCl_3$/MeOH, 5:1). ^{1}H NMR (DMSO-d_6) δ 1.81-2.11 (m, 2 H, β-CH_2), 2.38-2.41 (t, 2 H, γ-CH_2, J = 7.0 Hz), 2.68-2.70 (t, 2 H, CH_2, J = 7.0 Hz), 2.76-2.79 (t, 2 H, CH_2, J = 7.0 Hz), 4.43-4.47 (m, 1 H, α-CH), 5.98 (s, 2 H, 2-NH_2), 6.00 (s, 1 H, 5-H), 7.39-7.45 (m, 1 H, C_6H_4), 7.48-7.50 (m, 1 H, C_6H_4), 8.69-8.71 (d, 1 H, CONH, J = 4.0 Hz), 10.14 (s, 1 H, 3-NH, exch), 10.84 (s, 1 H, 7-NH, exch).

(*S*)-2-(2-(4-(2-amino-4-oxo-4,7-dihydro-3*H*-pyrrolo[2,3-*d*]pyrimidin-6-yl)butyl)benzamido)pentanedioic acid (170): Compound **170** was synthesized as described for **2:** yield 90% as a pink powder: mp 177-178 °C decomposed, R_f = 0.05 ($CHCl_3$/MeOH, 5:1). ^{1}H NMR (DMSO-d_6) δ 1.50-1.62 (m, 4 H, 2 CH_2), 1.90-2.11 (m, 2 H, β-CH_2), 2.36-2.38 (m, 2 H, γ-CH_2), 2.73 (s, 2 H, CH_2), 2.89 (s, 2 H, CH_2), 4.34-4.39 (m, 1 H, α-CH), 5.85 (s, 1 H, 5-H),), 6.05 (s, 2 H, 2-NH_2), 7.23-7.25 (m, 2 H, C_6H_4), 7.30-7.34 (m, 2 H, C_6H_4), 8.54-8.56 (d, 1 H, CONH, J = 5.0 Hz), 10.21 (s, 1 H, 3-NH, exch), 10.79 (s, 1 H, 7-NH, exch). Anal. ($C_{22}H_{25}N_5O_6 \cdot 1.1\ H_2O$) Cal. C: 55.60, H: 5.77, N: 14.74. Found C: 55.32, H: 5.58, N: 14.40.

(*S*)-diethyl 2-(3-(4-(2-amino-4-oxo-4,7-dihydro-3*H*-pyrrolo[2,3-*d*]pyrimidin-6-yl)but-1-yn-1-yl)benzamido)pentanedioate (266): Compound **266** was synthesized as described for **264:** yield 73% as a yellow powder: mp 178-179 °C decomposed, R_f = 0.32 ($CHCl_3$/MeOH, 10:1). ^{1}H NMR (DMSO-d_6) δ 1.15-1.16 (t, 3H, -CH_3, J = 7.0 Hz), 1.19-1.20 (t, 3H, -CH_3, J = 7.0 Hz), 1.98-2.14 (m, 2 H, β-CH_2), 2.42-2.45 (m, 2 H, γ-CH_2), 2.73-2.76 (t, 2 H, CH_2, J = 7.0 Hz), 2.78-2.81 (t, 2 H, CH_2, J = 7.0 Hz), 4.03-4.13 (m, 4 H, α, γ-COOC$H_2$$CH_3$), 4.41-4.45 (m, 1 H, α-CH), 5.99 (s, 2 H, 2-NH_2), 6.01 (s, 1 H, 5-H), 7.44-7.47 (t, 1 H, C_6H_4, J = 4.0 Hz), 7.53-7.54 (d, 1 H, C_6H_4, J = 4.0 Hz), 7.80-7.82

(d, 1 H, C_6H_4, J = 4.0 Hz), 7.90 (s, 1 H, C_6H_4), 8.79-8.80 (d, 1 H, CONH, , J = 4.0 Hz), 10.14 (s, 1 H, 3-NH, exch), 10.88 (s, 1 H, 7-NH, exch).

(*S*)-diethyl 2-(3-(4-(2-amino-4-oxo-4,7-dihydro-3*H*-pyrrolo[2,3-*d*]pyrimidin-6-yl)butyl)benzamido)pentanedioate (267): Compound **267** was synthesized as described for **265:** yield 100% as a white syrup, R_f = 0.32 ($CHCl_3$/MeOH, 10:1). ^{1}H NMR (DMSO-d_6) δ 1.15-1.16 (t, 3H, -CH_3, J = 7.0 Hz), 1.19-1.20 (t, 3H, -CH_3, J = 7.0 Hz), 1.58-1.64 (m, 4 H, 2 CH_2), 1.98-2.14 (m, 2 H, β-CH_2), 2.63-2.65 (m, 2 H, γ-CH_2), 2.73-2.76 (t, 2 H, CH_2, J = 7.0 Hz), 2.78-2.81 (t, 2 H, CH_2, J = 7.0 Hz), 4.03-4.13 (m, 4 H, α, γ-COOC$H_2$$CH_3$), 4.41-4.45 (m, 1 H, α-CH), 5.85 (s, 1 H, 5-H), 5.93 (s, 2 H, 2-NH_2), 7.36-7.37 (m, 2 H, C_6H_4), 7.70 (s, 1 H, C_6H_4), 7.95 (s, 1 H, C_6H_4), 8.65-8.67 (d, 1 H, CONH, , J = 4.0 Hz), 10.10 (s, 1 H, 3-NH, exch), 10.78 (s, 1 H, 7-NH, exch).

(*S*)-2-(3-(4-(2-amino-4-oxo-4,7-dihydro-3*H*-pyrrolo[2,3-*d*]pyrimidin-6-yl)but-1-yn-1-yl)benzamido)pentanedioic acid (171): Compound **171** was synthesized as described for **2**: yield 60% as a blue powder: mp 140-141 °C decomposed,R_f = 0.05 ($CHCl_3$/MeOH, 5:1). ^{1}H NMR (DMSO-d_6) δ 1.81-2.11 (m, 2 H, β-CH_2), 2.33-2.36 (t, 2 H, γ-CH_2, J = 7.0 Hz), 2.73-2.76 (t, 2 H, CH_2, J = 7.0 Hz), 2.79-2.81 (t, 2 H, CH_2, J = 7.0 Hz), 4.43-4.47 (m, 1 H, α-CH), 5.99 (s, 2 H, 2-NH_2), 6.01 (s, 1 H, 5-H), 7.36-7.37 (m, 2 H, C_6H_4), 7.70 (s, 1 H, C_6H_4), 7.95 (s, 1 H, C_6H_4), 8.65-8.66 (d, 1 H, CONH, J = 4.0 Hz), 10.15 (s, 1 H, 3-NH, exch), 10.88 (s, 1 H, 7-NH, exch).

(*S*)-2-(3-(4-(2-amino-4-oxo-4,7-dihydro-3*H*-pyrrolo[2,3-*d*]pyrimidin-6-yl)butyl)benzamido)pentanedioic acid (168): Compound **168** was synthesized as described for **2**: yield 90% as a pale powder: mp 190-191 °C decomposed, R_f = 0.05 ($CHCl_3$/MeOH, 5:1). ^{1}H NMR (DMSO-d_6) δ 1.55-1.65 (m, 4 H, 2 CH_2), 1.81-2.11 (m, 2

H, β-CH_2), 2.34-2.37 (t, 2 H, γ-CH_2, J = 7.0 Hz), 2.53-2.56 (m, 2 H, CH_2), 2.64-2.65 (m, 2 H, CH_2), 4.38-4.42 (m, 1 H, α-CH), 5.85 (s, 1 H, 5-H), 5.96 (s, 2 H, 2-NH_2), 7.36-7.37 (m, 2 H, C_6H_4), 7.68-7.69 (m, 1 H, C_6H_4), 7.71 (s, 1 H, C_6H_4), 8.53-8.54 (d, 1 H, CONH, J = 4.0 Hz), 10.13 (s, 1 H, 3-NH, exch), 10.78 (s, 1 H, 7-NH, exch). Anal. ($C_{22}H_{25}N_5O_6 \cdot 1.0\ H_2O$) Cal. C: 55.81, H: 5.75, N: 14.79. Found C: 55.47, H: 5.43, N: 14.40.

Ethyl 4-(3-oxopropyl)benzoate (275): To a solution of ethyl 4-iodobenzoate **(268)** (5 mmol, 1.38 g) in 20 mL anhydrous DMF was added prop-2-en-1-ol **269** (6 mmol, 348 mg), LiCl (5 mmol, 210 mg), LiOAc (12.5 mmol, 850 mg), Bu_4NCl (2.5 mmol, 840 mg), $Pd(OAc)_2$ (0.3 mmol, 60 mg) and the mixture was stirred at 70 °C for 3 hours. TLC (hexane/EtOAc, 3:1) showed the disappearance of the starting material (R_f = 0.70) and formation of one major spot at R_f = 0.60. To the reaction mixture cooled to room temperature was added ethyl acetate (30 mL). The resulting solution was extracted with H_2O (10 mL X 3) and dried over Na_2SO_4. After evaporation of solvent, the residue was loaded on a silica gel column (4 X 20 cm) and flash-chromatographed with hexane/EtOAc (2:1) and the desired fractions were pooled. After evaporation of solvent the residue was dried in vacuo using P_2O_5 to afford **275** 0.83 g, yield 83% as colorless liquid, R_f = 0.60 (hexane/EtOAc, 3:1). ^{1}H NMR ($CDCl_3$) δ 1.37-1.40 (t, 3 H, CH_3, J = 7.0 Hz), 2.80-2.83 (t, 2 H, CH_2, J = 7.5 Hz), 3.00-3.03 (t, 2 H, CH_2, J = 7.5 Hz), 4.34-4.39 (q, 2 H, CH_2, J = 7.0 Hz), 7.25-7.27 (d, 2 H, 2 CH, J = 4.0 Hz), 7.96-7.98 (d, 2 H, 2 CH, J = 4.3 Hz), 9.82-9.83 (t, 1 H, CHO, J = 1.5 Hz).

Ethyl 4-(4-oxobutyl)benzoate (276): Compound **276** was synthesized as described for **275:** yield 88% as colorless liquid, R_f = 0.62 (hexane/EtOAc, 3:1). ^{1}H NMR ($CDCl_3$) δ 1.38-1.40 (t, 3 H, CH_3, J = 7.0 Hz), 1.95-2.01 (m, 2 H, CH_2), 2.45-2.48 (t, 2 H, CH_2, J =

7.5 Hz), 2.70-2.73 (t, 2 H, CH_2, J = 7.5 Hz), 4.35-4.39 (q, 2 H, CH_2, J = 7.0 Hz), 7.23-7.25 (d, 2 H, 2 CH, J = 4.3 Hz), 7.96-7.98 (d, 2 H, 2 CH, J = 4.3 Hz), 9.76-9.77 (t, 1 H, CHO, J = 1.5 Hz).

Ethyl 4-(5-oxopentyl)benzoate (277): Compound **277** was synthesized as described for **275:** yield 84% as colorless liquid, R_f = 0.62 (hexane/EtOAc, 3:1). ^{1}H NMR ($CDCl_3$) δ 1.37-1.40 (t, 3 H, CH_3, J = 7.0 Hz), 1.66-1.70 (m, 4 H, 2 CH_2), 2.45-2.47 (t, 2 H, CH_2, J = 7.0 Hz), 2.68-2.70 (t, 2 H, CH_2, J = 7.0 Hz), 4.34-4.38 (q, 2 H, CH_2, J = 7.0 Hz), 7.22-7.24 (d, 2 H, 2 CH, J = 4.0 Hz), 7.95-7.97 (d, 2 H, 2 CH, J = 4.0 Hz), 9.75-9.76 (t, 1 H, CHO, J = 1.5 Hz).

Ethyl 4-(6-oxohexyl)benzoate (278): Compound **278** was synthesized as described for **275**: yield 86% as colorless liquid, R_f = 0.62 (hexane/EtOAc, 3:1). ^{1}H NMR ($CDCl_3$) δ 1.25-1.27 (m, 2 H, CH_2), 1.37-1.40 (t, 3 H, CH_3, J = 7.0 Hz), 1.64-1.68 (m, 4 H, 2 CH_2), 2.41-2.44 (t, 2 H, CH_2, J = 7.5 Hz), 2.65-2.68 (t, 2 H, CH_2, J = 7.5 Hz), 4.34-4.38 (q, 2 H, CH_2, J = 7.0 Hz), 7.22-7.24 (d, 2 H, 2 CH, J = 4.3 Hz), 7.95-7.96 (d, 2 H, 2 CH, J = 4.3 Hz), 9.75-9.76 (t, 1 H, CHO, J = 2.0 Hz).

Ethyl 4-(7-oxoheptyl)benzoate (279): Compound **279** was synthesized as described for **275:** yield 92% as colorless liquid, R_f = 0.63 (hexane/EtOAc, 3:1). ^{1}H NMR ($CDCl_3$) δ 1.34-1.36 (m, 4 H, 2 CH_2), 1.37-1.40 (t, 3 H, CH_3, J = 7.0 Hz), 1.58-1.65 (m, 4 H, 2 CH_2), 2.40-2.43 (t, 2 H, CH_2, J = 7.5 Hz), 2.64-2.67 (t, 2 H, CH_2, J = 7.5 Hz), 4.34-4.38 (q, 2 H, CH_2, J = 7.0 Hz), 7.22-7.24 (d, 2 H, 2 CH, J = 4.3 Hz), 7.94-7.96 (d, 2 H, 2 CH, J = 4.3 Hz), 9.75-9.76 (t, 1 H, CHO, J = 2.0 Hz).

Ethyl 4-(8-oxooctyl)benzoate (280): Compound **280** was synthesized as described for **275:** yield 87% as colorless liquid, R_f = 0.63 (hexane/EtOAc, 3:1). ^{1}H NMR ($CDCl_3$) δ

1.28-1.34 (m, 6 H, 3 CH_2), 1.37-1.40 (t, 3 H, CH_3, J = 7.0 Hz), 1.60-1.63 (m, 4 H, 2 CH_2), 2.40-2.43 (t, 2 H, CH_2, J = 7.5 Hz), 2.63-2.66 (t, 2 H, CH_2, J = 7.5 Hz), 4.34-4.38 (q, 2 H, CH_2, J = 7.0 Hz), 7.22-7.24 (d, 2 H, 2 CH, J = 4.3 Hz), 7.94-7.96 (d, 2 H, 2 CH, J = 4.3 Hz), 9.75-9.76 (t, 1 H, CHO, J = 2.0 Hz).

Ethyl 4-(3-bromo-4-oxobutyl)benzoate (282): To a solution of aldehyde **276** (1 mmol, 220 mg) in 5 mL anhydrous Et_2O was added **287** (0.5 mmol, 150 mg), 2N HCl in Et_2O solution (0.1 mmol, 50 µL) and the mixture was stirred at room temperature for 24 hours. TLC (hexane/EtOAc, 3:1) showed the disappearance of the starting material (R_f = 0.62) and formation of one major spot at R_f = 0.50. The reaction solution was washed with 5% $NaHCO_3$ solution and extracted with H_2O (10 mL X 3) and dried over Na_2SO_4. After evaporation of solvent, the residue was loaded on a silica gel column (4 X 20 cm) and flash-chromatographed with hexane/EtOAc (2:1) and the desired fractions were pooled. After evaporation of solvent the residue was dried in vacuo using P_2O_5 to afford **282** 235 mg **:** yield 78% as colorless oil, R_f = 0.50 (hexane/EtOAc, 3:1). ^{1}H NMR ($CDCl_3$) δ 1.38-1.41 (t, 3 H, CH_3, J = 7.0 Hz), 2.19-2.27 (m, 1 H, CH_2), 2.34-2.42 (m, 1 H, CH_2), 2.79-2.85 (m, 1 H, CH_2), 2.91-2.97 (m, 1 H, CH_2), 4.16-4.18 (m, 1 H, CHBr), 4.35-4.39 (q, 2 H, CH_2, J = 7.0 Hz), 7.27-7.29 (d, 2 H, 2 CH, J = 4.3 Hz), 7.98-8.00 (d, 2 H, 2 CH, J = 4.3 Hz), 9.46-9.47 (d, 1 H, CHO, J = 1.0 Hz).

Ethyl 4-(2-bromo-3-oxopropyl)benzoate (281): Compound **281** was synthesized as described for **282. 281** is not stable. Use directly to next step without purification.

Ethyl 4-(4-bromo-5-oxopentyl)benzoate (283): Compound **283** was synthesized as described for **282:** yield 77% as colorless oil, R_f = 0.52 (hexane/EtOAc, 3:1). ^{1}H NMR ($CDCl_3$) δ 1.38-1.41 (t, 3 H, CH_3, J = 7.0 Hz), 1.73-1.82 (m, 2 H, CH_2), 1.86-1.96 (m, 1

H, CH_2), 2.03-2.10 (m, 1 H, CH_2), 2.71-2.75 (m, 2 H, CH_2), 4.21-4.25 (m, 1 H, CHBr), 4.35-4.39 (q, 2 H, CH_2, J = 7.0 Hz), 7.23-7.25 (d, 2 H, 2 CH, J = 4.3 Hz), 7.96-7.98 (d, 2 H, 2 CH, J = 4.3 Hz), 9.42-9.43 (d, 1 H, CHO, J = 1.3 Hz).

Ethyl 4-(5-bromo-6-oxohexyl)benzoate (284): Compound **284** was synthesized as described for **282:** yield 75% as colorless oil, R_f = 0.52 (hexane/EtOAc, 3:1). ^{1}H NMR ($CDCl_3$) δ 1.37-1.41 (t, 3 H, CH_3, J = 7.0 Hz), 1.63-1.75 (m, 4 H, 2 CH_2), 1.87-1.99 (m, 1 H, CH_2), 2.03-2.12 (m, 1 H, CH_2), 2.67-2.71 (t, 2 H, CH_2, J = 7.0 Hz), 4.19-4.22 (m, 1 H, CHBr), 4.34-4.39 (q, 2 H, CH_2, J = 7.0 Hz), 7.22-7.24 (d, 2 H, 2 CH, J = 4.0 Hz), 7.95-7.97 (d, 2 H, 2 CH, J = 4.0 Hz), 9.42-9.43 (d, 1 H, CHO, J = 1.2 Hz).

Ethyl 4-(6-bromo-7-oxoheptyl)benzoate (285): Compound **285** was synthesized as described for **282:** yield 77% as colorless oil, R_f = 0.54 (hexane/EtOAc, 3:1). ^{1}H NMR ($CDCl_3$) δ 1.30-1.40 (m, 2 H, CH_2), 1.37-1.40 (t, 3 H, CH_3, J = 7.0 Hz), 1.62-1.70 (m, 4 H, 2 CH_2), 1.86-1.94 (m, 1 H, CH_2), 2.00-2.07 (m, 1 H, CH_2), 2.65-2.68 (t, 2 H, CH_2, J = 7.5 Hz), 4.18-4.22 (m, 1 H, CHBr), 4.34-4.38 (q, 2 H, CH_2, J = 7.0 Hz), 7.22-7.24 (d, 2 H, 2 CH, J = 4.3 Hz), 7.95-7.96 (d, 2 H, 2 CH, J = 4.0 Hz), 9.42-9.43 (d, 1 H, CHO, J = 1.5 Hz).

Ethyl 4-(7-bromo-8-oxooctyl)benzoate (286): Compound **286** was synthesized as described for **282:** yield 74% as colorless oil, R_f = 0.56 (hexane/EtOAc, 3:1). ^{1}H NMR ($CDCl_3$) δ 1.30-1.40 (m, 4 H, 2 CH_2), 1.37-1.40 (t, 3 H, CH_3, J = 7.0 Hz), 1.62-1.64 (m, 4 H, 2 CH_2), 1.86-1.94 (m, 1 H, CH_2), 2.00-2.07 (m, 1 H, CH_2), 2.64-2.67 (t, 2 H, CH_2, J = 7.5 Hz), 4.19-4.22 (m, 1 H, CHBr), 4.34-4.38 (q, 2 H, CH_2, J = 7.0 Hz), 7.22-7.24 (d, 2 H, 2 CH, J = 4.0 Hz), 7.95-7.96 (d, 2 H, 2 CH, J = 4.0 Hz), 9.42-9.43 (d, 1 H, CHO, J = 1.5 Hz).

Ethyl 4-(2-(2-amino-4-oxo-4,7-dihydro-3*H*-pyrrolo[2,3-*d*]pyrimidin-5-yl)ethyl)benzoate (289): To a solution of 2,4-diamino-6-hydroxypyrimidine **35** (151 mg, 1.2 mmol) and sodium acetate (180 mg, 2.2 mmol) in water (3 mL) and methanol (3 mL) was added α-bromo aldehyde **282** (330 mg, 1.1 mmol) The reaction mixture was stirred at 45 °C for 3 hours. TLC showed the disappearance of starting materials and the formation of one major spot at R_f = 0.38 ($CHCl_3$/MeOH, 5:1). After evaporation of solvent, CH_3OH (10 mL) was added followed by silica gel (3 g). Evaporation of the solvent afforded a plug, which was loaded onto a silica gel column (3.5 cm x 15 cm) and eluted initially with $CHCl_3$ followed by 10% MeOH in $CHCl_3$ and then 15% MeOH in $CHCl_3$. Fractions showing R_f = 0.38 were pooled and evaporated to afford **289** 230 mg, yield 70% as a pink solid: mp > 250 °C decomposed. ^{1}H NMR (DMSO-d_6) δ 1.29-1.32 (t, 3 H, CH_3, J = 7.5 Hz), 2.83-2.86 (t, 2 H, CH_2, J = 7.0 Hz), 2.98-3.01 (t, 2 H, CH_2, J = 7.0 Hz), 4.27-4.31 (q, 2 H, CH_2, J = 7.5 Hz), 6.03 (s, 2 H, 2-NH_2), 6.29-6.30 (d, 1 H, CH, J = 1.0 Hz), 7.33-7.34 (d, 2 H, CH, J = 4.0 Hz), 7.85-7.86 (d, 2 H, CH, J = 4.0 Hz), 10.21 (s, 1 H, 3-NH), 10.60 (s, 1H, 7-NH).

Ethyl 4-((2-amino-4-oxo-4,7-dihydro-3*H*-pyrrolo[2,3-*d*]pyrimidin-5-yl)methyl)benzoate (288): Compound **288** was synthesized as described for **289:** yield 35% over two steps as a yellow solid: mp > 232 °C decomposed, R_f = 0.42 ($CHCl_3$/MeOH, 5:1). ^{1}H NMR (DMSO-d_6) δ 1.28-1.31 (t, 3 H, CH_3, J = 7.5 Hz), 4.00 (s, 2 H, CH_2), 4.26-4.30 (q, 2 H, CH_2, J = 7.5 Hz), 6.00 (s, 2 H, 2-NH_2), 6.34-6.35 (d, 1 H, CH, J = 1.0 Hz), 7.40-7.42 (d, 2 H, CH, J = 4.0 Hz), 7.82-7.84 (d, 2 H, CH, J = 4.0 Hz), 10.12 (s, 1 H, 3-NH), 10.74 (s, 1H, 7-NH).

Ethyl 4-(3-(2-amino-4-oxo-4,7-dihydro-3*H*-pyrrolo[2,3-*d*]pyrimidin-5-

yl)propyl)benzoate (290): Compound **290** was synthesized as described for **289:** yield 68% as a purple solid: mp > 264 °C decomposed, R_f = 0.42 ($CHCl_3$/MeOH, 5:1). ^{1}H NMR (DMSO-d_6) δ 1.29-1.32 (t, 3 H, CH_3, J = 7.5 Hz), 1.89-1.95 (m, 2 H, CH_2), 2.56-2.59 (t, 2 H, CH_2, J = 7.5 Hz), 2.65-2.68 (t, 2 H, CH_2, J = 7.5 Hz), 4.27-4.31 (q, 2 H, CH_2, J = 7.5 Hz), 5.96 (s, 2 H, 2-NH_2), 6.35-6.36 (d, 1 H, CH, J = 1.0 Hz), 7.33-7.35 (d, 2 H, CH, J = 4.0 Hz), 7.85-7.87 (d, 2 H, CH, J = 4.0 Hz), 10.08 (s, 1 H, 3-NH), 10.63 (s, 1H, 7-NH).

Ethyl 4-(4-(2-amino-4-oxo-4,7-dihydro-3*H*-pyrrolo[2,3-*d*]pyrimidin-5-yl)butyl)benzoate (291): Compound **291** was synthesized as described for **289:** yield 53% as a blue solid: mp > 256 °C decomposed, R_f = 0.44 ($CHCl_3$/MeOH, 5:1). ^{1}H NMR (DMSO-d_6) δ 1.29-1.32 (t, 3 H, CH_3, J = 7.5 Hz), 1.56-1.62 (m, 4 H, 2 CH_2), 2.57-2.59 (t, 2 H, CH_2, J = 7.5 Hz), 2.64-2.67 (t, 2 H, CH_2, J = 7.5 Hz), 4.27-4.31 (q, 2 H, CH_2, J = 7.5 Hz), 5.94 (s, 2 H, 2-NH_2), 6.31-6.32 (d, 1 H, CH, J = 1.0 Hz), 7.32-7.34 (d, 2 H, CH, J = 4.0 Hz), 7.84-7.86 (d, 2 H, CH, J = 4.0 Hz), 10.08 (s, 1 H, 3-NH), 10.59 (s, 1H, 7-NH).

Ethyl 4-(5-(2-amino-4-oxo-4,7-dihydro-3*H*-pyrrolo[2,3-*d*]pyrimidin-5-yl)pentyl)benzoate (292): Compound **292** was synthesized as described for **289:** yield 60% as a pink solid: mp > 212 °C decomposed, R_f = 0.45 ($CHCl_3$/MeOH, 5:1). ^{1}H NMR (DMSO-d_6) δ 1.29-1.32 (m, 5 H, CH_3, CH_2), 1.58-1.62 (m, 4 H, 2 CH_2), 2.52-2.55 (t, 2 H, CH_2, J = 7.5 Hz), 2.62-2.65 (t, 2 H, CH_2, J = 7.5 Hz), 4.27-4.31 (q, 2 H, CH_2, J = 7.5 Hz), 5.94 (s, 2 H, 2-NH_2), 6.30-6.31 (d, 1 H, CH, J = 1.0 Hz), 7.32-7.34 (d, 2 H, CH, J = 4.0 Hz), 7.85-7.86 (d, 2 H, CH, J = 4.0 Hz), 10.08 (s, 1 H, 3-NH), 10.58 (s, 1H, 7-NH).

Ethyl 4-(6-(2-amino-4-oxo-4,7-dihydro-3*H*-pyrrolo[2,3-*d*]pyrimidin-5-

yl)hexyl)benzoate (293): Compound **293** was synthesized as described for **289:** yield 52% as a pink solid: mp > 208 °C decomposed, R_f = 0.45 ($CHCl_3$/MeOH, 5:1). ^{1}H NMR (DMSO-d_6) δ 1.27-1.33 (m, 7 H, CH_3, 2 CH_2), 1.53-1.60 (m, 4 H, 2 CH_2), 2.52-2.55 (t, 2 H, CH_2, J = 7.5 Hz), 2.61-2.64 (t, 2 H, CH_2, J = 7.5 Hz), 4.27-4.31 (q, 2 H, CH_2, J = 7.5 Hz), 5.94 (s, 2 H, 2-NH_2), 6.30-6.31 (d, 1 H, CH, J = 1.0 Hz), 7.32-7.34 (d, 2 H, CH, J = 4.0 Hz), 7.85-7.87 (d, 2 H, CH, J = 4.0 Hz), 10.06 (s, 1 H, 3-NH), 10.57 (s, 1H, 7-NH).

(*S*)-diethyl 2-(4-((2-amino-4-oxo-4,7-dihydro-3*H*-pyrrolo[2,3-*d*]pyrimidin-5-yl)methyl)benzamido)pentanedioate (294): To a suspension of **288** (100 mg, 0.35 mmol) in 10 mL CH_3OH was added 3 N NaOH (10 mL). The resulting mixture was stirred under N_2 at 40-50 °C for 24 h. TLC indicated the disappearance of starting material and the formation of one major spot at the origin. The resulting solution was passed through Celite and washed with a minimum amount of CH_3OH. The combined filtrate was evaporated under reduced pressure to dryness. To this residue was added distilled water (10 mL). The solution was cooled in an ice bath, and the pH was adjusted 3 to 4 using 3 N HCl. The resulting suspension was chilled in a dry ice/acetone bath and thawed to 4 °C overnight in a refrigerator. The precipitate was filtered, washed with cold water, and dried in a desiccator under reduced pressure using P_2O_5 to a brown powder, which was used directly for the next step.

To a solution of this brown powder in anhydrous DMF (10 mL) was added 6-chloro-2,4-dimethoxy-1,3,5-triazine (72 mg, 0.42 mmol) and *N*-methylmorpholine (43 mg, 0.42 mmol). After the mixture was stirred at r.t. for 2 h, *N*-methylmorpholine (43 mg, 0.42 mmol) and dimethyl *L*-glutamate hydrochloride (126 mg, 0.53 mmol) were added all at once. The mixture was stirred at r.t. for 4 h. TLC showed the formation of one major spot

at R_f = 0.38 ($CHCl_3$/MeOH, 5:1). The reaction mixture was evaporated to dryness under reduced pressure. The residue was dissolved in a minimum amount of $CHCl_3$/MeOH, 5:1, and chromatographed on a silica gel column (2 cm x 15 cm) with 4% MeOH in $CHCl_3$ as the eluent. Fractions that showed the desired single spot at R_f = 0.38 were pooled and evaporated to dryness to afford **294** 100 mg, yield 61% as a yellow syrup. ^{1}H NMR (DMSO-d_6) δ 1.14-1.19 (m, 6 H, 2 CH_3), 1.88-2.15 (m, 2 H, CH_2), 2.42-2.45 (m, 2 H, CH_2), 3.98 (s, 2 H, CH_2), 4.03-4.12 (m, 4 H, 2 CH_2), 4.36-4.46 (m, 1 H, CH), 6.00 (s, 2 H, 2-NH_2), 6.32-6.33 (d, 1 H, CH, J = 1.0 Hz), 7.36-7.38 (d, 2 H, C_6H_4, J = 4.0 Hz), 7.73-7.75 (d, 2 H, C_6H_4, J = 4.0 Hz), 8.59-8.61 (d, 1 H, CONH, , J = 4.0 Hz), 10.13 (s, 1 H, 3-NH), 10.74 (s, 1H, 7-NH).

(*S*)-diethyl 2-(4-(2-(2-amino-4-oxo-4,7-dihydro-3*H*-pyrrolo[2,3-*d*]pyrimidin-5-yl)ethyl)benzamido)pentanedioate (295): Compound **295** was synthesized as described for **294**: yield 51% as a colorless syrup, R_f = 0.40 ($CHCl_3$/MeOH, 5:1). ^{1}H NMR (DMSO-d_6) δ 1.15-1.20 (m, 6 H, 2 CH_3), 1.97-2.03 (m, 1 H, CH_2), 2.06-2.13 (m, 1 H, CH_2), 2.42-2.45 (m, 2 H, CH_2), 2.84-2.87 (t, 2 H, CH_2, J = 7.0 Hz), 2.96-2.99 (t, 2 H, CH_2, J = 7.0 Hz), 4.02-4.13 (m, 4 H, 2 CH_2), 4.40-4.44 (m, 1 H, CH), 5.99 (s, 2 H, 2-NH_2), 6.30-6.31 (d, 1 H, CH, J = 1.0 Hz), 7.28-7.30 (d, 2 H, C_6H_4, J = 4.0 Hz), 7.77-7.78 (d, 2 H, C_6H_4, J = 4.0 Hz), 8.61-8.62 (d, 1 H, CONH, , J = 4.0 Hz), 10.13 (s, 1 H, 3-NH), 10.60 (s, 1H, 7-NH).

(*S*)-diethyl 2-(4-(3-(2-amino-4-oxo-4,7-dihydro-3*H*-pyrrolo[2,3-*d*]pyrimidin-5-yl)propyl)benzamido)pentanedioate (296): Compound **296** was synthesized as described for **294**: yield 65% as a colorless syrup, R_f = 0.40 ($CHCl_3$/MeOH, 5:1). ^{1}H NMR (DMSO-d_6) δ 1.15-1.20 (m, 6 H, 2 CH_3), 1.91-1.94 (m, 2 H, CH_2), 1.97-2.03 (m, 1

H, CH_2), 2.06-2.13 (m, 1 H, CH_2), 2.42-2.45 (m, 2 H, CH_2), 2.57-2.60 (t, 2 H, CH_2, J = 7.0 Hz), 2.63-2.66 (t, 2 H, CH_2, J = 7.0 Hz), 4.02-4.13 (m, 4 H, 2 CH_2), 4.42-4.45 (m, 1 H, CH), 5.95 (s, 2 H, 2-NH_2), 6.35-6.36 (d, 1 H, CH, J = 1.0 Hz), 7.29-7.30 (d, 2 H, C_6H_4, J = 4.0 Hz), 7.78-7.80 (d, 2 H, C_6H_4, J = 4.0 Hz), 8.62-8.64 (d, 1 H, CONH, , J = 4.0 Hz), 10.08 (s, 1 H, 3-NH), 10.62 (s, 1H, 7-NH).

(*S*)-diethyl 2-(4-(4-(2-amino-4-oxo-4,7-dihydro-3*H*-pyrrolo[2,3-*d*]pyrimidin-5-yl)butyl)benzamido)pentanedioate (297): Compound **297** was synthesized as described for **294**: yield 70% as a light blue syrup, R_f = 0.40 ($CHCl_3$/MeOH, 5:1). ^{1}H NMR (DMSO-d_6) δ 1.15-1.20 (m, 6 H, 2 CH_3), 1.55-1.64 (m, 4 H, 2 CH_2), 1.97-2.03 (m, 1 H, CH_2), 2.06-2.13 (m, 1 H, CH_2), 2.42-2.45 (m, 2 H, CH_2), 2.57-2.59 (t, 2 H, CH_2, J = 7.5 Hz), 2.64-2.67 (t, 2 H, CH_2, J = 7.5 Hz), 4.02-4.13 (m, 4 H, 2 CH_2), 4.42-4.45 (m, 1 H, CH), 5.94 (s, 2 H, 2-NH_2), 6.31-6.32 (d, 1 H, CH, J = 1.0 Hz), 7.28-7.29 (d, 2 H, C_6H_4, J = 4.0 Hz), 7.76-7.78 (d, 2 H, C_6H_4, J = 4.0 Hz), 8.61-8.62 (d, 1 H, CONH, , J = 4.0 Hz), 10.08 (s, 1 H, 3-NH), 10.59 (s, 1H, 7-NH).

(*S*)-diethyl 2-(4-(5-(2-amino-4-oxo-4,7-dihydro-3*H*-pyrrolo[2,3-*d*]pyrimidin-5-yl)pentyl)benzamido)pentanedioate (298): Compound **298** was synthesized as described for **294**: yield 67% as a light blue syrup, R_f = 0.40 ($CHCl_3$/MeOH, 5:1). ^{1}H NMR (DMSO-d_6) δ 1.15-1.20 (m, 6 H, 2 CH_3), 1.29-1.33 (m, 2 H, CH_2), 1.55-1.62 (m, 4 H, 2 CH_2), 1.97-2.03 (m, 1 H, CH_2), 2.06-2.13 (m, 1 H, CH_2), 2.42-2.45 (m, 2 H, CH_2), 2.51-2.53 (m, 2 H, CH_2), 2.61-2.64 (t, 2 H, CH_2, J = 7.5 Hz), 4.02-4.12 (m, 4 H, 2 CH_2), 4.41-4.45 (m, 1 H, CH), 5.94 (s, 2 H, 2-NH_2), 6.31-6.32 (d, 1 H, CH, J = 1.0 Hz), 7.28-7.29 (d, 2 H, C_6H_4, J = 4.0 Hz), 7.77-7.79 (d, 2 H, C_6H_4, J = 4.0 Hz), 8.62-8.63 (d, 1 H, CONH, , J = 4.0 Hz), 10.07 (s, 1 H, 3-NH), 10.58 (s, 1H, 7-NH).

(*S*)-diethyl 2-(4-(6-(2-amino-4-oxo-4,7-dihydro-3*H*-pyrrolo[2,3-*d*]pyrimidin-5-yl)hexyl)benzamido)pentanedioate (299): Compound **299** was synthesized as described for **294**: yield 78% as a colorless syrup, R_f = 0.42 ($CHCl_3$/MeOH, 5:1). ^{1}H NMR (DMSO-d_6) δ 1.15-1.20 (m, 6 H, 2 CH_3), 1.27-1.34 (m, 4 H, 2 CH_2), 1.53-1.62 (m, 4 H, 2 CH_2), 1.97-2.03 (m, 1 H, CH_2), 2.06-2.13 (m, 1 H, CH_2), 2.42-2.45 (m, 2 H, CH_2), 2.51-2.53 (m, 2 H, CH_2), 2.60-2.63 (t, 2 H, CH_2, J = 7.5 Hz), 4.02-4.12 (m, 4 H, 2 CH_2), 4.41-4.44 (m, 1 H, CH), 5.93 (s, 2 H, 2-NH_2), 6.30-6.31 (d, 1 H, CH, J = 1.0 Hz), 7.28-7.29 (d, 2 H, C_6H_4, J = 4.0 Hz), 7.77-7.79 (d, 2 H, C_6H_4, J = 4.0 Hz), 8.62-8.63 (d, 1 H, CONH, , J = 4.0 Hz), 10.06 (s, 1 H, 3-NH), 10.57 (s, 1H, 7-NH).

(*S*)-2-(4-((2-amino-4-oxo-4,7-dihydro-3*H*-pyrrolo[2,3-*d*]pyrimidin-5-yl)methyl)benzamido)pentanedioic acid (172): Compound **172** was synthesized as described for **2**: yield 94% as a yellow powder: mp > 264 °C decomposed, R_f = 0.05 ($CHCl_3$/MeOH, 5:1). ^{1}H NMR 400M (DMSO-d_6) δ 1.88-2.15 (m, 2 H, CH_2), 2.42-2.45 (m, 2 H, CH_2), 3.98 (s, 2 H, CH_2), 4.37-4.39 (m, 1 H, CH), 6.00 (s, 2 H, 2-NH_2), 6.32 (s, 1 H, CH), 7.36-7.38 (d, 2 H, C_6H_4, J = 4.0 Hz), 7.74-7.76 (d, 2 H, C_6H_4, J = 4.0 Hz), 8.46-8.48 (d, 1 H, CONH, , J = 4.0 Hz), 10.13 (s, 1 H, 3-NH), 10.73 (s, 1H, 7-NH). Anal. ($C_{19}H_{19}N_5O_6 \cdot 1.5\ H_2O$) Cal. C: 51.82, H: 5.04, N: 15.90. Found C: 51.93, H: 5.14, N: 15.56.

(*S*)-2-(4-(2-(2-amino-4-oxo-4,7-dihydro-3*H*-pyrrolo[2,3-*d*]pyrimidin-5-yl)ethyl)benzamido)pentanedioic acid (173): Compound **173** was synthesized as described for **2**: yield 96% as a pink powder: mp > 250 °C decomposed, identical in all respects (NMR, mp) reported ed by the method of Taylor et al.,[189] R_f = 0.07 ($CHCl_3$/MeOH, 5:1). ^{1}H NMR 400M (DMSO-d_6) δ 1.97-2.03 (m, 1 H, CH_2), 2.06-2.13

(m, 1 H, CH_2), 2.42-2.45 (m, 2 H, CH_2), 2.84-2.87 (t, 2 H, CH_2, J = 7.0 Hz), 2.96-2.99 (t, 2 H, CH_2, J = 7.0 Hz), 4.36-4.40 (m, 1 H, CH), 6.00 (s, 2 H, 2-NH_2), 6.30 (s, 1 H, CH), 7.27-7.29 (d, 2 H, C_6H_4, J = 4.0 Hz), 7.77-7.79 (d, 2 H, C_6H_4, J = 4.0 Hz), 8.50-8.52 (d, 1 H, CONH, , J = 4.0 Hz), 10.15 (s, 1 H, 3-NH), 10.61 (s, 1H, 7-NH).Anal. ($C_{20}H_{21}N_5O_6 \cdot 1.2\ H_2O$) Cal. C: 53.45, H: 5.26, N: 15.58. Found C: 53.49, H: 5.38, N: 15.48.

(*S*)-2-(4-(3-(2-amino-4-oxo-4,7-dihydro-3*H*-pyrrolo[2,3-*d*]pyrimidin-5-yl)propyl)benzamido)pentanedioic acid (174): Compound **174** was synthesized as described for **2**: yield 97% as a pale blue powder: mp > 189 °C decomposed,R_f = 0.07 ($CHCl_3$/MeOH, 5:1). ^{1}H NMR (DMSO-d_6) δ 1.90-1.94 (m, 2 H, CH_2), 1.94-2.00 (m, 1 H, CH_2), 2.06-2.13 (m, 1 H, CH_2), 2.33-2.36 (m, 2 H, CH_2), 2.57-2.60 (t, 2 H, CH_2, J = 7.0 Hz), 2.63-2.66 (t, 2 H, CH_2, J = 7.0 Hz), 4.36-4.40 (m, 1 H, CH), 5.96 (s, 2 H, 2-NH_2), 6.35-6.36 (d, 1 H, CH, J = 1.0 Hz), 7.28-7.30 (d, 2 H, C_6H_4, J = 4.0 Hz), 7.78-7.80 (d, 2 H, C_6H_4, J = 4.0 Hz), 8.50-8.52 (d, 1 H, CONH, , J = 4.0 Hz), 10.08 (s, 1 H, 3-NH), 10.62 (s, 1H, 7-NH). Anal. ($C_{21}H_{23}N_5O_6 \cdot 0.70\ H_2O$) Cal. C: 55.52, H: 5.42, N: 15.42. Found C: 55.62, H: 5.41, N: 15.03.

(*S*)-2-(4-(4-(2-amino-4-oxo-4,7-dihydro-3*H*-pyrrolo[2,3-*d*]pyrimidin-5-yl)butyl)benzamido)pentanedioic acid (175): Compound **175** was synthesized as described for **2**: yield 88% as a blue powder: mp > 153 °C decomposed, R_f = 0.07 ($CHCl_3$/MeOH, 5:1). ^{1}H NMR (DMSO-d_6) δ 1.55-1.63 (m, 4 H, 2 CH_2), 1.92-2.00 (m, 1 H, CH_2), 2.03-2.13 (m, 1 H, CH_2), 2.33-2.36 (t, 2 H, CH_2, J = 7.5 Hz), 2.57-2.60 (t, 2 H, CH_2, J = 7.5 Hz), 2.62-2.65 (t, 2 H, CH_2, J = 7.5 Hz), 4.37-4.39 (m, 1 H, CH), 5.95 (s, 2 H, 2-NH_2), 6.31-6.32 (d, 1 H, CH, J = 1.0 Hz), 7.27-7.29 (d, 2 H, C_6H_4, J = 4.0 Hz), 7.77-7.79 (d, 2 H, C_6H_4, J = 4.0 Hz), 8.49-8.50 (d, 1 H, CONH, , J = 4.0 Hz), 10.09 (s, 1 H, 3-

NH), 10.58 (s, 1H, 7-NH). Anal. ($C_{22}H_{25}N_5O_6 \cdot 1.2\ H_2O$) Cal. C: 55.38, H: 5.79, N: 14.68. Found C: 55.08, H: 5.57, N: 14.37.

(*S*)-2-(4-(5-(2-amino-4-oxo-4,7-dihydro-3*H*-pyrrolo[2,3-*d*]pyrimidin-5-yl)pentyl)benzamido)pentanedioic acid (176): Compound **176** was synthesized as described for **2**: yield 93% as a blue powder: mp > 167 °C decomposed, R_f = 0.08 ($CHCl_3$/MeOH, 5:1). ^{1}H NMR (DMSO-d_6) δ 1.29-1.32 (m, 2 H, CH_2), 1.58-1.62 (m, 4 H, 2 CH_2), 1.92-2.00 (m, 1 H, CH_2), 2.03-2.13 (m, 1 H, CH_2), 2.33-2.36 (t, 2 H, CH_2, J = 7.5 Hz), 2.53-2.55 (m, 2 H, CH_2), 2.61-2.64 (t, 2 H, CH_2, J = 7.5 Hz), 4.37-4.40 (m, 1 H, CH), 5.94 (s, 2 H, 2-NH_2), 6.31-6.32 (d, 1 H, CH, J = 1.0 Hz), 7.27-7.29 (d, 2 H, C_6H_4, J = 4.0 Hz), 7.77-7.79 (d, 2 H, C_6H_4, J = 4.0 Hz), 8.50-8.51 (d, 1 H, CONH, , J = 4.0 Hz), 10.08 (s, 1 H, 3-NH), 10.58 (s, 1H, 7-NH). Anal. ($C_{23}H_{27}N_5O_6 \cdot 1.0\ H_2O$) Cal. C: 56.66, H: 6.00, N: 14.36. Found C: 56.73, H: 6.09, N: 14.13.

(*S*)-2-(4-(6-(2-amino-4-oxo-4,7-dihydro-3*H*-pyrrolo[2,3-*d*]pyrimidin-5-yl)hexyl)benzamido)pentanedioic acid (177): Compound **177** was synthesized as described for **2**: yield 93% as a blue powder: mp > 178 °C decomposed, R_f = 0.10 ($CHCl_3$/MeOH, 5:1). ^{1}H NMR (DMSO-d_6) δ 1.27-1.32 (m, 4 H, 2 CH_2), 1.53-1.62 (m, 4 H, 2 CH_2), 1.92-2.00 (m, 1 H, CH_2), 2.03-2.13 (m, 1 H, CH_2), 2.33-2.36 (t, 2 H, CH_2, J = 7.5 Hz), 2.52-2.54 (m, 2 H, CH_2), 2.59-2.62 (t, 2 H, CH_2, J = 7.5 Hz), 4.36-4.41 (m, 1 H, CH), 5.94 (s, 2 H, 2-NH_2), 6.31-6.32 (d, 1 H, CH, J = 1.0 Hz), 7.27-7.29 (d, 2 H, C_6H_4, J = 4.0 Hz), 7.77-7.79 (d, 2 H, C_6H_4, J = 4.0 Hz), 8.49-8.51 (d, 1 H, CONH, , J = 4.0 Hz), 10.07 (s, 1 H, 3-NH), 10.57 (s, 1H, 7-NH). Anal. ($C_{24}H_{29}N_5O_6 \cdot 1.77CH_3OH \cdot 0.1HCl$) Cal. C: 56.91, Cl: 0.65, H: 6.70, N: 12.88. Found C: 56.58, Cl: 0.62, H: 6.19, N: 12.85.

Methyl 5-(3-oxopropyl)thiophene-2-carboxylate (308): To a solution of 5-

iodothiophene-2-carboxylate **301** (5 mmol, 1.34 g) in 20 mL anhydrous DMF was added prop-2-en-1-ol **269** (15 mmol, 900 mg), LiCl (5 mmol, 210 mg), LiOAc (12.5 mmol, 850 mg), Bu_4NCl (5 mmol, 2.78 g), $Pd(OAc)_2$ (2.5 mmol, 500 mg) and the mixture was stirred at 45 °C for 2 hours. TLC (hexane/EtOAc, 3:1) showed the disappearance of the starting material and formation of one major spot at R_f = 0.50. To the reaction mixture cooled to room temperature was added ethyl acetate (30 mL). The resulting solution was extracted with H_2O (10 mL X 3) and dried over Na_2SO_4. After evaporation of solvent, the residue was loaded on a silica gel column (4 X 20 cm) and flash-chromatographed with hexane/EtOAc (5:1) and the desired fractions were pooled. After evaporation of solvent the residue was dried in vacuo using P_2O_5 to afford **308** 0.48 g, yield 52% as yellow liquid, R_f = 0.50 (hexane/EtOAc, 3:1). ^{1}H NMR ($CDCl_3$) δ 2.86-2.89 (t, 2 H, CH_2, J = 7.5 Hz), 3.16-3.19 (t, 2 H, CH_2, J = 7.5 Hz), 3.86 (s, 3 H, CH_3), 6.82-6.83 (d, 1 H, 1 CH, J = 2.0 Hz), 7.62-7.63 (d, 1 H, CH, J = 2.0 Hz), 9.83 (s, 1 H, CHO).

Methyl 5-(4-oxobutyl)thiophene-2-carboxylate (300): Compound **300** was synthesized as described for **308:** yield 65% as yellow liquid, R_f = 0.53 (hexane/EtOAc, 3:1). ^{1}H NMR ($CDCl_3$) δ 2.00-2.05 (m, 2 H, CH_2), 2.51-2.54 (t, 2 H, CH_2, J = 7.5 Hz), 2.88-2.91 (t, 2 H, CH_2, J = 7.5 Hz), 3.86 (s, 3 H, CH_3), 6.80-6.81 (d, 1 H, 1 CH, J = 2.0 Hz), 7.63-7.64 (d, 1 H, CH, J = 2.0 Hz), 9.78 (s, 1 H, CHO).

Methyl 5-(5-oxopentyl)thiophene-2-carboxylate (309): Compound **309** was synthesized as described for **308:** yield 54% as yellow liquid, R_f = 0.54 (hexane/EtOAc, 3:1). ^{1}H NMR ($CDCl_3$) δ 1.70-1.75 (m, 4 H, 2 CH_2), 2.46-2.49 (t, 2 H, CH_2, J = 7.5 Hz), 2.85-2.88 (t, 2 H, CH_2, J = 7.5 Hz), 3.86 (s, 3 H, CH_3), 6.79-6.80 (d, 1 H, 1 CH, J = 2.0 Hz), 7.62-7.63 (d, 1 H, CH, J = 2.0 Hz), 9.76-9.77 (t, 1 H, CHO, J = 1.5 Hz).

Methyl 5-(6-oxohexyl)thiophene-2-carboxylate (310): Compound **310** was synthesized as described for **308:** yield 65% as yellow liquid, R_f = 0.54 (hexane/EtOAc, 3:1). ^{1}H NMR ($CDCl_3$) δ 1.38-1.44 (m, 2 H, CH_2), 1.64-1.75 (m, 4 H, 2 CH_2), 2.42-2.46 (t, 2 H, CH_2, J = 7.5 Hz), 2.83-2.86 (t, 2 H, CH_2, J = 7.5 Hz), 3.86 (s, 3 H, CH_3), 6.77-6.78 (d, 1 H, 1 CH, J = 2.0 Hz), 7.62-7.63 (d, 1 H, CH, J = 2.0 Hz), 9.76-9.77 (t, 1 H, CHO, J = 1.5 Hz).

Methyl 5-(7-oxoheptyl)thiophene-2-carboxylate (311): Compound **311** was synthesized as described for **308:** yield 70% as yellow liquid, R_f = 0.55 (hexane/EtOAc, 3:1). ^{1}H NMR ($CDCl_3$) δ 1.35-1.40 (m, 4 H, 2 CH_2), 1.60-1.73 (m, 4 H, 2 CH_2), 2.41-2.44 (t, 2 H, CH_2, J = 7.5 Hz), 2.81-2.84 (t, 2 H, CH_2, J = 7.5 Hz), 3.86 (s, 3 H, CH_3), 6.77-6.78 (d, 1 H, 1 CH, J = 2.0 Hz), 7.62-7.63 (d, 1 H, CH, J = 2.0 Hz), 9.76-9.77 (t, 1 H, CHO, J = 1.5 Hz).

Methyl 5-(8-oxooctyl)thiophene-2-carboxylate (312): Compound **312** was synthesized as described for **308:** yield 61% as brown liquid, R_f = 0.57 (hexane/EtOAc, 3:1). ^{1}H NMR ($CDCl_3$) δ 1.30-1.40 (m, 6 H, 3 CH_2), 1.54-1.60 (m, 4 H, 2 CH_2), 2.40-2.44 (t, 2 H, CH_2, J = 7.5 Hz), 2.81-2.84 (t, 2 H, CH_2, J = 7.5 Hz), 3.86 (s, 3 H, CH_3), 6.77-6.78 (d, 1 H, 1 CH, J = 2.0 Hz), 7.62-7.63 (d, 1 H, CH, J = 2.0 Hz), 9.76-9.77 (t, 1 H, CHO, J = 1.5 Hz).

Methyl 5-(2-bromo-3-oxopropyl)thiophene-2-carboxylate (313): To a solution of aldehyde **308** (2.9 mmol, 540 mg) in 5 mL anhydrous Et_2O was added **287** (1.45 mmol, 435 mg), 2N HCl in Et_2O solution (0.29 mmol, 150 µL) and the mixture was stirred at room temperature for 24 hours. TLC (hexane/EtOAc, 3:1) showed the disappearance of the starting material and formation of one major spot at R_f = 0.43. The reaction solution

was washed with 5% $NaHCO_3$ solution and extracted with H_2O (10 mL X 3) and dried over Na_2SO_4. After evaporation of solvent, the residue was loaded on a silica gel column (4 X 20 cm) and flash-chromatographed with hexane/EtOAc (5:1) and the desired fractions were pooled. After evaporation of solvent the residue was dried in vacuo using P_2O_5 to afford **313** 440 mg **:** yield 57% as yellow oil, R_f = 0.43 (hexane/EtOAc, 3:1). ^{1}H NMR ($CDCl_3$) δ 3.16-3.19 (m, 2 H, CH_2), 3.92 (s, 3 H, CH_3), 4.35-4.40 (m, 1 H, CHBr), 6.92-6.93 (d, 1 H, 1 CH, J = 2.0 Hz), 7.75-7.76 (d, 1 H, CH, J = 2.0 Hz), 9.51-9.52 (d, 1 H, CHO, J = 1.0 Hz).

Methyl 5-(3-bromo-4-oxobutyl)thiophene-2-carboxylate (314): Compound **314** was synthesized as described for **313:** yield 65% as yellow oil, R_f = 0.45 (hexane/EtOAc, 3:1). ^{1}H NMR ($CDCl_3$) δ 2.88-2.89 (m, 2 H, CH_2), 2.95-2.96 (m, 2 H, CH_2), 3.87 (s, 3 H, CH_3), 4.23-4.26 (m, 1 H, CHBr), 6.86-6.87 (d, 1 H, 1 CH, J = 2.0 Hz), 7.64-7.65 (d, 1 H, CH, J = 2.0 Hz), 9.48-9.49 (d, 1 H, CHO, J = 1.0 Hz).

Methyl 5-(4-bromo-5-oxopentyl)thiophene-2-carboxylate (315): Compound **315** was synthesized as described for **313:** yield 68% as yellow oil, R_f = 0.45 (hexane/EtOAc, 3:1). ^{1}H NMR ($CDCl_3$) δ 1.71-1.72 (m, 2 H, CH_2), 1.93-2.00 (m, 1 H, CH_2), 2.08-2.13 (m, 1 H, CH_2), 2.85-2.90 (m, 2 H, CH_2), 3.86 (s, 3 H, CH_3), 4.23-4.25 (m, 1 H, CHBr), 6.79-6.80 (d, 1 H, 1 CH, J = 2.0 Hz), 7.62-7.63 (d, 1 H, CH, J = 2.0 Hz), 9.44-9.45 (d, 1 H, CHO, J = 1.0 Hz).

Methyl 5-(5-bromo-6-oxohexyl)thiophene-2-carboxylate (316): Compound **316** was synthesized as described for **313. 316** is not stable. Use directly to next step without purification.

Methyl 5-(6-bromo-7-oxoheptyl)thiophene-2-carboxylate (317): Compound **317** was

synthesized as described for **313:** yield 60% as yellow oil, R_f = 0.47 (hexane/EtOAc, 3:1). ^{1}H NMR ($CDCl_3$) δ 1.37-1.42 (m, 2 H, CH_2), 1.56-1.59 (m, 4 H, 2 CH_2), 2.04-2.08 (m, 2 H, CH_2), 2.82-2.85 (t, 2 H, CH_2, J = 7.5 Hz), 3.85 (s, 3 H, CH_3), 4.19-4.22 (m, 1 H, CHBr), 6.77-6.78 (d, 1 H, 1 CH, J = 2.0 Hz), 7.62-7.63 (d, 1 H, CH, J = 2.0 Hz), 9.42-9.43 (d, 1 H, CHO, J = 1.0 Hz).

Methyl 5-(7-bromo-8-oxooctyl)thiophene-2-carboxylate (318): Compound **318** was synthesized as described for **313:** yield 65% as yellow oil, R_f = 0.50 (hexane/EtOAc, 3:1). ^{1}H NMR ($CDCl_3$) δ 1.34-1.39 (m, 4 H, 2 CH_2), 1.57-1.61 (m, 4 H, 2 CH_2), 2.00-2.06 (m, 2 H, CH_2), 2.81-2.84 (t, 2 H, CH_2, J = 7.5 Hz), 3.86 (s, 3 H, CH_3), 4.19-4.26 (m, 1 H, CHBr), 6.77-6.78 (d, 1 H, 1 CH, J = 2.0 Hz), 7.62-7.63 (d, 1 H, CH, J = 2.0 Hz), 9.42-9.43 (d, 1 H, CHO, J = 1.0 Hz).

Methyl 5-((2-amino-4-oxo-4,7-dihydro-3*H*-pyrrolo[2,3-*d*]pyrimidin-5-yl)methyl)thiophene-2-carboxylate (319): To a solution of 2,4-diamino-6-hydroxypyrimidine **35** (171 mg, 1.36 mmol) and sodium acetate (223 mg, 2.72 mmol) in water (3 mL) and methanol (3 mL) was added α-bromo aldehyde **313** (360 mg, 1.36 mmol) The reaction mixture was stirred at 45 °C for 3 hours. TLC showed the disappearance of starting materials and the formation of one major spot at R_f = 0.40 ($CHCl_3$/MeOH, 5:1). After evaporation of solvent, CH_3OH (10 mL) was added followed by silica gel (3 g). Evaporation of the solvent afforded a plug, which was loaded onto a silica gel column (3.5 cm x 15 cm) and eluted initially with $CHCl_3$ followed by 10% MeOH in $CHCl_3$ and then 15% MeOH in $CHCl_3$. Fractions showing R_f = 0.40 were pooled and evaporated to afford **319** 245 mg, yield 59% as a white solid: mp 220-221 °C decomposed. ^{1}H NMR (DMSO-d_6) δ 3.76 (s, 3 H, CH_3), 4.16 (s, 2 H, CH_2), 6.02 (s, 2 H,

2-NH_2), 6.47-6.48 (d, 1 H, CH, J = 1.3 Hz), 6.97-6.98 (d, 1 H, CH, J = 1.8 Hz), 7.59-7.60 (d, 1 H, CH, J = 1.8 Hz), 10.15 (s, 1 H, 3-NH), 10.80 (s, 1H, 7-NH).

Methyl 5-(2-(2-amino-4-oxo-4,7-dihydro-3*H*-pyrrolo[2,3-*d*]pyrimidin-5-yl)ethyl)thiophene-2-carboxylate (320): Compound **320** was synthesized as described for **319:** yield 50% as a yellow solid: mp 185-186 °C decomposed, R_f = 0.40 ($CHCl_3$/MeOH, 5:1). ^{1}H NMR (DMSO-d_6) δ 2.88-2.91 (t, 2 H, CH_2, J = 7.5 Hz), 3.20-3.23 (t, 2 H, CH_2, J = 7.5 Hz), 3.77 (s, 3 H, CH_3), 5.99 (s, 2 H, 2-NH_2), 6.35-6.36 (d, 1 H, CH, J = 1.0 Hz), 6.90-6.91 (d, 1 H, CH, J = 1.8 Hz), 7.60-7.61 (d, 1 H, CH, J = 1.8 Hz), 10.15 (s, 1 H, 3-NH), 10.64 (s, 1H, 7-NH).

Methyl 5-(3-(2-amino-4-oxo-4,7-dihydro-3*H*-pyrrolo[2,3-*d*]pyrimidin-5-yl)propyl)thiophene-2-carboxylate (321): Compound **321** was synthesized as described for **319:** yield 64% as a clear syrup, R_f = 0.42 ($CHCl_3$/MeOH, 5:1). ^{1}H NMR (DMSO-d_6) δ 1.94-2.00 (m, 2 H, CH_2), 2.59-2.62 (t, 2 H, CH_2, J = 7.5 Hz), 2.81-2.84 (t, 2 H, CH_2, J = 7.5 Hz), 3.79 (s, 3 H, CH_3), 5.97 (s, 2 H, 2-NH_2), 6.36-6.37 (d, 1 H, CH, J = 1.0 Hz), 6.97-6.98 (d, 1 H, CH, J = 2.0 Hz), 7.63-7.64 (d, 1 H, CH, J = 2.0 Hz), 10.10 (s, 1 H, 3-NH), 10.65 (s, 1H, 7-NH).

Methyl 5-(4-(2-amino-4-oxo-4,7-dihydro-3*H*-pyrrolo[2,3-*d*]pyrimidin-5-yl)butyl)thiophene-2-carboxylate 37d (322): Compound **322** was synthesized as described for **319:** yield 46% as a light yellow solid: mp 150-151 °C decomposed, R_f = 0.44 ($CHCl_3$/MeOH, 5:1). ^{1}H NMR (DMSO-d_6) δ 1.62-1.64 (m, 4 H, 2 CH_2), 2.57-2.60 (t, 2 H, CH_2, J = 7.5 Hz), 2.83-2.86 (t, 2 H, CH_2, J = 7.5 Hz), 3.78 (s, 3 H, CH_3), 5.95 (s, 2 H, 2-NH_2), 6.33-6.34 (d, 1 H, CH, J = 1.0 Hz), 6.94-6.95 (d, 1 H, CH, J = 1.8 Hz), 7.62-7.63 (d, 1 H, CH, J = 1.8 Hz), 10.09 (s, 1 H, 3-NH), 10.60 (s, 1H, 7-NH).

Methyl 5-(5-(2-amino-4-oxo-4,7-dihydro-3*H*-pyrrolo[2,3-*d*]pyrimidin-5-yl)pentyl)thiophene-2-carboxylate (323): Compound **323** was synthesized as described for **319:** yield 47% as a pink solid: mp 139-140 °C decomposed,R_f = 0.46 ($CHCl_3$/MeOH, 5:1). ^{1}H NMR (DMSO-d_6) δ 1.32-1.34 (m, 2 H, CH_2), 1.58-1.66 (m, 4 H, 2 CH_2), 2.51-2.54 (m, 2 H, CH_2), 2.82-2.85 (t, 2 H, CH_2, J = 7.5 Hz), 3.78 (s, 3 H, CH_3), 5.94 (s, 2 H, 2-NH_2), 6.31-6.32 (d, 1 H, CH, J = 1.0 Hz), 6.94-6.95 (d, 1 H, CH, J = 1.8 Hz), 7.62-7.63 (d, 1 H, CH, J = 1.8 Hz), 10.08 (s, 1 H, 3-NH), 10.59 (s, 1H, 7-NH).

Methyl 5-(6-(2-amino-4-oxo-4,7-dihydro-3*H*-pyrrolo[2,3-*d*]pyrimidin-5-yl)hexyl)thiophene-2-carboxylate (324): Compound **324** was synthesized as described for **319:** yield 50% as a pink solid: mp 168-169 °C decomposed, R_f = 0.45 ($CHCl_3$/MeOH, 5:1). ^{1}H NMR (DMSO-d_6) δ 1.30-1.33 (m, 4 H, 2 CH_2), 1.55-1.64 (m, 4 H, 2 CH_2), 2.51-2.54 (m, 2 H, CH_2), 2.80-2.83 (t, 2 H, CH_2, J = 7.5 Hz), 3.78 (s, 3 H, CH_3), 5.94 (s, 2 H, 2-NH_2), 6.31-6.32 (d, 1 H, CH, J = 1.0 Hz), 6.94-6.95 (d, 1 H, CH, J = 1.8 Hz), 7.60-7.61 (d, 1 H, CH, J = 1.8 Hz), 10.07 (s, 1 H, 3-NH), 10.58 (s, 1H, 7-NH).

(*S*)-diethyl 2-(5-((2-amino-4-oxo-4,7-dihydro-3*H*-pyrrolo[2,3-*d*]pyrimidin-5-yl)methyl)thiophene-2-carboxamido)pentanedioate (325): To a suspension of **319** (75 mg, 0.26 mmol) in 3 mL CH_3OH was added 3 N NaOH (3 mL). The resulting mixture was stirred under N_2 at 40-50 °C for 24 h. TLC indicated the disappearance of starting material and the formation of one major spot at the origin. The resulting solution was passed through Celite and washed with a minimum amount of CH_3OH. The combined filtrate was evaporated under reduced pressure to dryness. To this residue was added distilled water (10 mL). The solution was cooled in an ice bath, and the pH was adjusted 3 to 4 using 3 N HCl. The resulting suspension was chilled in a dry ice/acetone bath and

thawed to 4 °C overnight in a refrigerator. The precipitate was filtered, washed with cold water, and dried in a desiccator under reduced pressure using P_2O_5 to a brown powder, which was used directly for the next step.

To a solution of this brown powder in anhydrous DMF (5 mL) was added 6-chloro-2,4-dimethoxy-1,3,5-triazine (55 mg, 0.31 mmol) and *N*-methylmorpholine (32 mg, 0.31 mmol). After the mixture was stirred at r.t. for 2 h, *N*-methylmorpholine (32 mg, 0.31 mmol) and dimethyl *L*-glutamate hydrochloride (75 mg, 0.31 mmol) were added all at once. The mixture was stirred at r.t. for 4 h. TLC showed the formation of one major spot at R_f = 0.42 ($CHCl_3$/MeOH, 5:1). The reaction mixture was evaporated to dryness under reduced pressure. The residue was dissolved in a minimum amount of $CHCl_3$/MeOH, 5:1, and chromatographed on a silica gel column (2 cm x 15 cm) with 4% MeOH in $CHCl_3$ as the eluent. Fractions that showed the desired single spot at R_f = 0.42 were pooled and evaporated to dryness to afford **325** 85 mg, yield 70% as a yellow syrup.

^{1}H NMR (DMSO-d_6) δ 1.14-1.19 (m, 6 H, 2 CH_3), 1.92-1.97 (m, 1 H, CH_2), 2.04-2.11 (m, 1 H, CH_2), 2.38-2.41 (m, 2 H, CH_2), 4.03-4.10 (m, 4 H, 2 CH_2), 4.13 (s, 2 H, CH_2), 4.34-4.38 (m, 1 H, CH), 6.01 (s, 2 H, 2-NH_2), 6.44-6.45 (d, 1 H, CH, J = 1.0 Hz), 6.90-6.91 (d, 1 H, CH, J = 1.8 Hz), 7.62-7.63 (d, 1 H, CH, J = 1.8 Hz), 8.52-8.53 (d, 1 H, CONH, , J = 4.0 Hz), 10.13 (s, 1 H, 3-NH), 10.78 (s, 1H, 7-NH).

(S)-diethyl 2-(5-(2-(2-amino-4-oxo-4,7-dihydro-3*H*-pyrrolo[2,3-*d*]pyrimidin-5-yl)ethyl)thiophene-2-carboxamido)pentanedioate (326): Compound **326** was synthesized as described for **325:** yield 72% as a yellow syrup, R_f = 0.42 ($CHCl_3$/MeOH, 5:1). ^{1}H NMR (DMSO-d_6) δ 1.15-1.20 (m, 6 H, 2 CH_3), 1.92-1.99 (m, 1 H, CH_2), 2.05-2.12 (m, 1 H, CH_2), 2.40-2.43 (t, 2 H, CH_2, J = 7.5 Hz), 2.87-2.90 (t, 2 H, CH_2, J = 7.5

Hz), 3.15-3.18 (t, 2 H, CH_2, J = 7.5 Hz), 4.02-4.13 (m, 4 H, 2 CH_2), 4.35-4.39 (m, 1 H, CH), 5.98 (s, 2 H, 2-NH_2), 6.35-6.36 (d, 1 H, CH, J = 1.0 Hz), 6.84-6.85 (d, 1 H, CH, J = 2.0 Hz), 7.64-7.65 (d, 1 H, CH, J = 2.0 Hz), 8.55-8.56 (d, 1 H, CONH, , J = 4.0 Hz), 10.14 (s, 1 H, 3-NH), 10.63 (s, 1H, 7-NH).

(*S*)-diethyl 2-(5-(3-(2-amino-4-oxo-4,7-dihydro-3*H*-pyrrolo[2,3-*d*]pyrimidin-5-yl)propyl)thiophene-2-carboxamido)pentanedioate (327): Compound **327** was synthesized as described for **325:** yield 60% as a colorless syrup, R_f = 0.44 ($CHCl_3$/MeOH, 5:1). ^{1}H NMR (DMSO-d_6) δ 1.15-1.20 (m, 6 H, 2 CH_3), 1.92-1.99 (m, 3 H, CH_2), 2.05-2.12 (m, 1 H, CH_2), 2.40-2.43 (t, 2 H, CH_2, J = 7.5 Hz), 2.59-2.62 (t, 2 H, CH_2, J = 7.5 Hz), 2.77-2.80 (t, 2 H, CH_2, J = 7.5 Hz), 4.02-4.13 (m, 4 H, 2 CH_2), 4.35-4.39 (m, 1 H, CH), 5.97 (s, 2 H, 2-NH_2), 6.36-6.37 (d, 1 H, CH, J = 1.0 Hz), 6.89-6.90 (d, 1 H, CH, J = 2.0 Hz), 7.67-7.68 (d, 1 H, CH, J = 2.0 Hz), 8.60-8.61 (d, 1 H, CONH, , J = 4.0 Hz), 10.10 (s, 1 H, 3-NH), 10.65 (s, 1H, 7-NH).

(*S*)-diethyl 2-(5-(4-(2-amino-4-oxo-4,7-dihydro-3*H*-pyrrolo[2,3-*d*]pyrimidin-5-yl)butyl)thiophene-2-carboxamido)pentanedioate (328): Compound **328** was synthesized as described for **325:** yield 52% as a colorless syrup, R_f = 0.45 ($CHCl_3$/MeOH, 5:1). ^{1}H NMR (DMSO-d_6) δ 1.15-1.20 (m, 6 H, 2 CH_3), 1.58-1.66 (m, 4 H, 2 CH_2), 1.92-1.99 (m, 3 H, CH_2), 2.05-2.12 (m, 1 H, CH_2), 2.40-2.43 (t, 2 H, CH_2, J = 7.5 Hz), 2.57-2.60 (t, 2 H, CH_2, J = 7.5 Hz), 2.79-2.81 (t, 2 H, CH_2, J = 7.5 Hz), 4.02-4.12 (m, 4 H, 2 CH_2), 4.35-4.39 (m, 1 H, CH), 5.94 (s, 2 H, 2-NH_2), 6.33-6.34 (d, 1 H, CH, J = 1.0 Hz), 6.87-6.88 (d, 1 H, CH, J = 2.0 Hz), 7.66-7.67 (d, 1 H, CH, J = 2.0 Hz), 8.58-8.60 (d, 1 H, CONH, , J = 4.0 Hz), 10.09 (s, 1 H, 3-NH), 10.60 (s, 1H, 7-NH).

(*S*)-diethyl 2-(5-(5-(2-amino-4-oxo-4,7-dihydro-3*H*-pyrrolo[2,3-*d*]pyrimidin-5-

yl)pentyl)thiophene-2-carboxamido)pentanedioate (329): Compound **329** was synthesized as described for **325:** yield 65% as a colorless syrup, R_f = 0.44 ($CHCl_3$/MeOH, 5:1). ^{1}H NMR (DMSO-d_6) δ 1.15-1.20 (m, 6 H, 2 CH_3), 1.30-1.36 (m, 2 H, CH_2), 1.58-1.66 (m, 4 H, 2 CH_2), 1.92-1.99 (m, 3 H, CH_2), 2.05-2.12 (m, 1 H, CH_2), 2.40-2.43 (t, 2 H, CH_2, J = 7.5 Hz), 2.52-2.55 (t, 2 H, CH_2, J = 7.5 Hz), 2.78-2.81 (t, 2 H, CH_2, J = 7.5 Hz), 4.02-4.12 (m, 4 H, 2 CH_2), 4.35-4.39 (m, 1 H, CH), 5.94 (s, 2 H, 2-NH_2), 6.32-6.33 (d, 1 H, CH, J = 1.0 Hz), 6.87-6.88 (d, 1 H, CH, J = 2.0 Hz), 7.66-7.67 (d, 1 H, CH, J = 2.0 Hz), 8.59-8.61 (d, 1 H, CONH, , J = 4.0 Hz), 10.08 (s, 1 H, 3-NH), 10.59 (s, 1H, 7-NH).

(*S*)-diethyl 2-(5-(6-(2-amino-4-oxo-4,7-dihydro-3*H*-pyrrolo[2,3-*d*]pyrimidin-5-yl)hexyl)thiophene-2-carboxamido)pentanedioate (330): Compound **330** was synthesized as described for **325:** yield 61% as a colorless syrup, R_f = 0.42 ($CHCl_3$/MeOH, 5:1). ^{1}H NMR (DMSO-d_6) δ 1.15-1.20 (m, 6 H, 2 CH_3), 1.29-1.35 (m, 4 H, 2 CH_2), 1.54-1.63 (m, 4 H, 2 CH_2), 1.92-1.99 (m, 3 H, CH_2), 2.05-2.12 (m, 1 H, CH_2), 2.40-2.43 (t, 2 H, CH_2, J = 7.5 Hz), 2.52-2.54 (t, 2 H, CH_2, J = 7.5 Hz), 2.76-2.79 (t, 2 H, CH_2, J = 7.5 Hz), 4.02-4.12 (m, 4 H, 2 CH_2), 4.35-4.40 (m, 1 H, CH), 5.94 (s, 2 H, 2-NH_2), 6.31-6.32 (d, 1 H, CH, J = 1.0 Hz), 6.87-6.88 (d, 1 H, CH, J = 2.0 Hz), 7.67-7.68 (d, 1 H, CH, J = 2.0 Hz), 8.59-8.61 (d, 1 H, CONH, , J = 4.0 Hz), 10.07 (s, 1 H, 3-NH), 10.58 (s, 1H, 7-NH).

(*S*)-2-(5-((2-amino-4-oxo-4,7-dihydro-3*H*-pyrrolo[2,3-*d*]pyrimidin-5-yl)methyl)thiophene-2-carboxamido)pentanedioic acid (178): Compound **178** was synthesized as described for **2**: yield 93% as a yellow powder: mp 188 °C decomposed, R_f = 0.05 ($CHCl_3$/MeOH, 5:1). ^{1}H NMR (DMSO-d_6) δ 1.87-1.92 (m, 1 H, CH_2), 2.00-

2.07 (m, 1 H, CH_2), 2.30-2.33 (t, 2 H, CH_2, J = 7.5 Hz), 4.12 (s, 2 H, CH_2), 4.29-4.33 (m, 1 H, CH), 6.02 (s, 2 H, 2-NH_2), 6.43-6.44 (d, 1 H, CH, J = 1.0 Hz), 6.90-6.91 (d, 1 H, CH, J = 1.8 Hz), 7.63-7.64 (d, 1 H, CH, J = 1.8 Hz), 8.42-8.44 (d, 1 H, CONH, , J = 4.0 Hz), 10.15 (s, 1 H, 3-NH), 10.79 (s, 1H, 7-NH). Anal. ($C_{17}H_{17}N_5O_6S \cdot 0.83CH_3OH$) Cal. C: 48.01, H: 4.59, N: 15.70, S: 7.19. Found C: 47.90, H: 4.26, N: 15.58, S: 7.22.

(*S*)-2-(5-(2-(2-amino-4-oxo-4,7-dihydro-3*H*-pyrrolo[2,3-*d*]pyrimidin-5-yl)ethyl)thiophene-2-carboxamido)pentanedioic acid (179): Compound **179** was synthesized as described for **2**: yield 90% as a pink powder: mp 181 °C decomposed, R_f = 0.05 ($CHCl_3$/MeOH, 5:1). ^{1}H NMR (DMSO-d_6) δ 1.88-1.93 (m, 1 H, CH_2), 2.02-2.08 (m, 1 H, CH_2), 2.31-2.34 (t, 2 H, CH_2, J = 7.5 Hz), 2.86-2.89 (t, 2 H, CH_2, J = 7.5 Hz), 3.14-3.17 (t, 2 H, CH_2, J = 7.5 Hz), 4.30-4.35 (m, 1 H, CH), 6.00 (s, 2 H, 2-NH_2), 6.35-6.36 (d, 1 H, CH, J = 1.0 Hz), 6.83-6.84 (d, 1 H, CH, J = 2.0 Hz), 7.64-7.65 (d, 1 H, CH, J = 2.0 Hz), 8.45-8.47 (d, 1 H, CONH, , J = 4.0 Hz), 10.16 (s, 1 H, 3-NH), 10.64 (s, 1H, 7-NH). Anal. ($C_{18}H_{19}N_5O_6S \cdot 1.1H_2O$) Cal. C: 47.70, H: 4.71, N: 15.45, S: 7.07. Found C: 47.95, H: 4.71, N: 15.09, S: 6.95.

(*S*)-2-(5-(3-(2-amino-4-oxo-4,7-dihydro-3*H*-pyrrolo[2,3-*d*]pyrimidin-5-yl)propyl)thiophene-2-carboxamido)pentanedioic acid (180): Compound **180** was synthesized as described for **2**: yield 90% as a pale blue powder: mp 159 °C decomposed, R_f = 0.06 ($CHCl_3$/MeOH, 5:1). ^{1}H NMR (DMSO-d_6) δ 1.88-1.97 (m, 3 H, CH_2), 2.01-2.08 (m, 1 H, CH_2), 2.31-2.34 (t, 2 H, CH_2, J = 7.5 Hz), 2.59-2.62 (t, 2 H, CH_2, J = 7.5 Hz), 2.77-2.80 (t, 2 H, CH_2, J = 7.5 Hz), 4.30-4.35 (m, 1 H, CH), 5.97 (s, 2 H, 2-NH_2), 6.36-6.37 (d, 1 H, CH, J = 1.0 Hz), 6.88-6.89 (d, 1 H, CH, J = 2.0 Hz), 7.67-7.68 (d, 1 H, CH, J = 2.0 Hz), 8.46-8.48 (d, 1 H, CONH, , J = 4.0 Hz), 10.11 (s, 1 H, 3-NH), 10.64

(s, 1H, 7-NH). Anal. ($C_{19}H_{21}N_5O_6S \cdot 0.95\ CH_3OH$) Cal. C: 50.14, H: 5.23, N: 14.65, S: 6.71. Found C: 50.52, H: 5.07, N: 14.29, S: 6.90.

(*S*)-2-(5-(4-(2-amino-4-oxo-4,7-dihydro-3*H*-pyrrolo[2,3-*d*]pyrimidin-5-yl)butyl)thiophene-2-carboxamido)pentanedioic acid (181): Compound **181** was synthesized as described for **2**: yield 96% as a blue powder: mp 141 °C decomposed, R_f = 0.06 ($CHCl_3$/MeOH, 5:1). ^{1}H NMR (DMSO-d_6) δ 1.59-1.66 (m, 4 H, 2 CH_2), 1.88-1.94 (m, 3 H, CH_2), 2.03-2.10 (m, 1 H, CH_2), 2.32-2.35 (t, 2 H, CH_2, J = 7.5 Hz), 2.57-2.60 (t, 2 H, CH_2, J = 7.5 Hz), 2.79-2.81 (t, 2 H, CH_2, J = 7.5 Hz), 4.31-4.35 (m, 1 H, CH), 5.95 (s, 2 H, 2-NH_2), 6.33-6.34 (d, 1 H, CH, J = 1.0 Hz), 6.87-6.88 (d, 1 H, CH, J = 2.0 Hz), 7.66-7.67 (d, 1 H, CH, J = 2.0 Hz), 8.47-8.49 (d, 1 H, CONH, , J = 4.0 Hz), 10.09 (s, 1 H, 3-NH), 10.60 (s, 1H, 7-NH). Anal. ($C_{20}H_{23}N_5O_6S \cdot 0.55\ CH_3OH$) Cal. C: 51.52, H: 5.30, N: 14.62, S: 6.69. Found C: 51.57, H: 5.25, N: 14.54, S: 6.70.

(*S*)-2-(5-(5-(2-amino-4-oxo-4,7-dihydro-3*H*-pyrrolo[2,3-*d*]pyrimidin-5-yl)pentyl)thiophene-2-carboxamido)pentanedioic acid (182): Compound **182** was synthesized as described for **2**: yield 95% as a pale yellow powder: mp 158 °C decomposed,R_f = 0.07 ($CHCl_3$/MeOH, 5:1). ^{1}H NMR (DMSO-d_6) δ 1.31-1.36 (m, 2 H, CH_2), 1.59-1.66 (m, 4 H, 2 CH_2), 1.88-1.94 (m, 3 H, CH_2), 2.03-2.10 (m, 1 H, CH_2), 2.32-2.35 (t, 2 H, CH_2, J = 7.5 Hz), 2.52-2.55 (t, 2 H, CH_2, J = 7.5 Hz), 2.77-2.80 (t, 2 H, CH_2, J = 7.5 Hz), 4.31-4.35 (m, 1 H, CH), 5.94 (s, 2 H, 2-NH_2), 6.32-6.33 (d, 1 H, CH, J = 1.0 Hz), 6.87-6.88 (d, 1 H, CH, J = 2.0 Hz), 7.66-7.67 (d, 1 H, CH, J = 2.0 Hz), 8.48-8.50 (d, 1 H, CONH, , J = 4.0 Hz), 10.08 (s, 1 H, 3-NH), 10.59 (s, 1H, 7-NH). Anal. ($C_{21}H_{25}N_5O_6S \cdot 0.70\ H_2O$) Cal. C: 51.70, H: 5.45, N: 14.36, S: 6.57. Found C: 51.82, H: 5.39, N: 14.05, S: 6.25.

(*S*)-2-(5-(6-(2-amino-4-oxo-4,7-dihydro-3*H*-pyrrolo[2,3-*d*]pyrimidin-5-yl)hexyl)thiophene-2-carboxamido)pentanedioic acid (183): Compound **183** was synthesized as described for **2**: yield 89% as a blue powder: mp 126 °C decomposed, R_f = 0.07 ($CHCl_3$/MeOH, 5:1). ^{1}H NMR (DMSO-d_6) δ 1.29-1.35 (m, 4 H, 2 CH_2), 1.53-1.64 (m, 4 H, 2 CH_2), 1.88-1.94 (m, 3 H, CH_2), 2.03-2.10 (m, 1 H, CH_2), 2.32-2.35 (t, 2 H, CH_2, J = 7.5 Hz), 2.52-2.55 (t, 2 H, CH_2, J = 7.5 Hz), 2.76-2.79 (t, 2 H, CH_2, J = 7.5 Hz), 4.31-4.35 (m, 1 H, CH), 5.94 (s, 2 H, 2-NH_2), 6.31-6.32 (d, 1 H, CH, J = 1.0 Hz), 6.87-6.88 (d, 1 H, CH, J = 2.0 Hz), 7.66-7.67 (d, 1 H, CH, J = 2.0 Hz), 8.48-8.50 (d, 1 H, CONH, , J = 4.0 Hz), 10.07 (s, 1 H, 3-NH), 10.58 (s, 1H, 7-NH). Anal. ($C_{22}H_{27}N_5O_6S \cdot 0.25\ H_2O$) Cal. C: 53.46, H: 5.61, N: 14.17, S: 6.49. Found C: 53.55, H: 5.79, N: 13.92, S: 6.38.

Methyl 9-hydroxynonanoate (333): To a solution of monomethyl azelate **331** (1.0 g, 5 mmol) in anhydrous THF 5 mL, $BH_3 \cdot$THF complex (1M in THF, 5 mL, 5 mmol) was added dropwise at -18 °C over 20 minutes. The resulting mixture was stirred at room temperature for 4 hours to get a colorless solution. TCL indicated there is no fluorescence for both starting material and the product. The reaction was quenched with water and K_2CO_3 (1.15 g, 8.4 mmol) at 0 °C. The organic layer was separated and the aqueous layer was extracted with ethyl ether (20 mL x 3). The combined organic layer was dried over Na_2SO_4 and evaporated to dryness under reduced pressure and chromatographed on a silica gel column (2 cm x 15 cm) with Hexane/EtOAc (3:1) as the eluent. The solvent was evaporated to afford **333** 0.90 g (yield : 96%) as a colorless oil. ^{1}H NMR ($CDCl_3$) δ 1.29-1.34 (m, 8 H, 4 CH_2), 1.55-1.57 (m, 2 H, CH_2), 1.60-1.63 (m, 2 H, CH_2), 2.29-2.32 (t, 2 H, CH_2, J = 7.5 Hz), 3.63-3.65 (t, 2 H, CH_2, J = 6.0 Hz), 3.67 (s, 3 H, CH_3).

Methyl 10-hydroxydecanoate (334): Compound **334** was synthesized as described for **333:** yield 91% as a colorless oil. ^{1}H NMR ($CDCl_3$) δ 1.26-1.34 (m, 10 H, 5 CH_2), 1.54-1.57 (m, 2 H, CH_2), 1.60-1.63 (m, 2 H, CH_2), 2.28-2.31 (t, 2 H, CH_2, J = 7.5 Hz), 3.62-3.64 (t, 2 H, CH_2, J = 6.0 Hz), 3.66 (s, 3 H, CH_3).

Methyl 9-oxononanoate (335): To a stirring suspension of PCC (1.62 g, 7.5 mmol) and silica gel (2 g) in anhydrous CH_2Cl_2 20 mL, a solution of **333** (0.94g, 5 mmol) in anhydrous CH_2Cl_2 10 mL was added dropwise at 0 °C over 20 minutes. The resulting mixture was stirred at room temperature for 4 hours. TCL indicated there is no fluorescence for both starting material and the product. The reaction was evaporated to dryness under reduced pressure and chromatographed on a silica gel column (2 cm x 15 cm) with Hexane/EtOAc (2:1) as the eluent. The solvent was evaporated to afford **335** 0.85 g (yield: 90%) as a yellow liquid. ^{1}H NMR ($CDCl_3$) δ 1.30-1.34 (m, 6 H, 3 CH_2), 1.59-1.64 (m, 4 H, 2 CH_2), 2.28-2.31 (t, 2 H, CH_2, J = 7.5 Hz), 2.40-2.43 (t, 2 H, CH_2, J = 7.5 Hz), 3.66 (s, 3 H, CH_3), 9.75-9.76 (t, 1 H, CHO, J = 1.0 Hz)

Methyl 10-oxodecanoate (336): Compound **336** was synthesized as described for **335:** yield 89% as a yellow liquid. ^{1}H NMR ($CDCl_3$) δ 1.27-1.33 (m, 8 H, 4 CH_2), 1.59-1.64 (m, 4 H, 2 CH_2), 2.28-2.31 (t, 2 H, CH_2, J = 7.5 Hz), 2.40-2.43 (t, 2 H, CH_2, J = 7.5 Hz), 3.66 (s, 3 H, CH_3), 9.75-9.76 (t, 1 H, CHO, J = 1.0 Hz).

Methyl 11-oxoundecanoate (337): A mixture of **338** (2.79 g, 10 mmol) and $NaHCO_3$ (2.0 g, 23 mmol) in DMSO 20 mL was stirred at 165 °C for 15 minutes until evolution of white fumes was noticed. The resulting mixture was cooled to room temperature. TCL indicated there is no fluorescence for both starting material and the product. The reaction was quenched with water and extracted with ethyl ether (20 mL x 3). The combined

organic layer was dried over Na_2SO_4 and evaporated to dryness under reduced pressure and chromatographed on a silica gel column (2 cm x 15 cm) with Hexane/EtOAc (3:1) as the eluent. The solvent was evaporated to afford **337** 1.88 g (yield : 88%) as a colorless oil. ^{1}H NMR ($CDCl_3$) δ 1.26-1.33 (m, 10 H, 5 CH_2), 1.59-1.62 (m, 4 H, 2 CH_2), 2.28-2.31 (t, 2 H, CH_2, J = 7.5 Hz), 2.40-2.43 (t, 2 H, CH_2, J = 7.5 Hz), 3.66 (s, 3 H, CH_3), 9.75-9.76 (t, 1 H, CHO, J = 1.0 Hz).

Methyl 8-bromo-9-oxononanoate (339): To a solution of aldehyde **335** (2.9 mmol, 536 mg) in 10 mL anhydrous Et_2O was added **287** (1.5mmol, 450mg), 2N HCl in Et_2O solution (0.3mmol, 150µL) and the mixture was stirred at room temperature for 24 hours. TCL indicated there is no fluorescence for both starting material and the product. The reaction solution was washed with 5% $NaHCO_3$ solution and extracted with H_2O (10 mL X 3) and dried over Na_2SO_4. After evaporation of solvent, the residue was loaded on a silica gel column (4 X 20 cm) and flash-chromatographed with hexane/EtOAc (4:1) and the desired fractions were pooled. After evaporation of solvent the residue was dried in vacuo using P_2O_5 to afford **339** 590 mg **:** yield 77% as a yellow liquid. ^{1}H NMR ($CDCl_3$) δ 1.31-1.36 (m, 4 H, 2 CH_2), 1.58-1.66 (m, 4 H, 2 CH_2), 1.89-1.94 (m, 1 H, CH_2), 2.00-2.07 (m, 1 H, CH_2), 2.29-2.32 (t, 2 H, CH_2, J = 7.5 Hz), 3.67 (s, 3 H, CH_3), 4.19-4.23 (m, 1 H, CHBr), 9.42-9.43 (d, 1 H, CHO, J = 1.5 Hz)**.**

Methyl 9-bromo-10-oxodecanoate (340): Compound **340** was synthesized as described for **339:** yield 75% as a yellow liquid. ^{1}H NMR ($CDCl_3$) δ 1.27-1.34 (m, 6 H, 3 CH_2), 1.58-1.64 (m, 4 H, 2 CH_2), 1.88-1.94 (m, 1 H, CH_2), 1.98-2.03 (m, 1 H, CH_2), 2.28-2.32 (t, 2 H, CH_2, J = 7.5 Hz), 3.66 (s, 3 H, CH_3), 4.19-4.23 (m, 1 H, CHBr), 9.42-9.43 (d, 1 H, CHO, J = 1.5 Hz)**.**

Methyl 10-bromo-11-oxoundecanoate (341): Compound **341** was synthesized as described for **339:** yield 75% as a yellow liquid. ^{1}H NMR ($CDCl_3$) δ 1.25-1.32 (m, 8 H, 4 CH_2), 1.58-1.63 (m, 4 H, 2 CH_2), 1.88-1.93 (m, 1 H, CH_2), 2.00-2.05 (m, 1 H, CH_2), 2.28-2.31 (t, 2 H, CH_2, J = 7.5 Hz), 3.66 (s, 3 H, CH_3), 4.19-4.22 (m, 1 H, CHBr), 9.42-9.43 (d, 1 H, CHO, J = 1.5 Hz)

Methyl 7-(2-amino-4-oxo-4,7-dihydro-3*H*-pyrrolo[2,3-*d*]pyrimidin-5-yl)heptanoate (342): To a solution of 2,4-diamino-6-hydroxypyrimidine **35** (360 mg, 2.8 mmol) and sodium acetate (451 mg, 5.5 mmol) in water (3 mL) and methanol (3 mL) was added α-bromo aldehyde **339** (730 mg, 2.8 mmol) The reaction mixture was stirred at 45 °C for 5 hours. TLC showed the disappearance of starting materials and the formation of one major spot at R_f = 0.50 ($CHCl_3$/MeOH, 5:1). After evaporation of solvent, CH_3OH (10 mL) was added followed by silica gel (3 g). Evaporation of the solvent afforded a plug, which was loaded onto a silica gel column (3.5 cm x 15 cm) and eluted initially with $CHCl_3$ followed by 10% MeOH in $CHCl_3$ and then 15% MeOH in $CHCl_3$. Fractions showing R_f = 0.50 were pooled and evaporated to afford **342** 460 mg, yield 56% as a red syrup, R_f = 0.50 ($CHCl_3$/MeOH, 5:1). ^{1}H NMR (DMSO-d_6) δ 1.25-1.28 (m, 4 H, 2 CH_2), 1.49-1.57 (m, 4 H, 2 CH_2), 2.26-2.29 (t, 2 H, CH_2, J = 7.5 Hz), 2.52-2.54 (m, 2 H, CH_2), 3.57 (s, 3 H, CH_3), 5.94 (s, 2 H, 2-NH_2), 6.31-6.32 (d, 1 H, CH, J = 1.0 Hz), 10.06 (s, 1 H, 3-NH), 10.58 (s, 1H, 7-NH).

Methyl 8-(2-amino-4-oxo-4,7-dihydro-3*H*-pyrrolo[2,3-*d*]pyrimidin-5-yl)octanoate (343): Compound **343** was synthesized as described for **342:** yield 58% as a red syrup, R_f = 0.48 ($CHCl_3$/MeOH, 5:1). ^{1}H NMR (DMSO-d_6) δ 1.23-1.27 (m, 6 H, 3 CH_2), 1.49-1.57 (m, 4 H, 2 CH_2), 2.26-2.29 (t, 2 H, CH_2, J = 7.5 Hz), 2.52-2.54 (m, 2 H, CH_2), 3.57

(s, 3 H, CH_3), 5.94 (s, 2 H, 2-NH_2), 6.30-6.31 (d, 1 H, CH, J = 1.0 Hz), 10.06 (s, 1 H, 3-NH), 10.58 (s, 1H, 7-NH).

Methyl 9-(2-amino-4-oxo-4,7-dihydro-3*H*-pyrrolo[2,3-*d*]pyrimidin-5-yl)nonanoate (344): Compound **344** was synthesized as described for **342**: yield 53% as a pink syrup, R_f = 0.50 ($CHCl_3$/MeOH, 5:1).^{1}H NMR (DMSO-d_6) δ 1.20-1.27 (m, 8 H, 4 CH_2), 1.48-1.57 (m, 4 H, 2 CH_2), 2.26-2.29 (t, 2 H, CH_2, J = 7.5 Hz), 2.52-2.54 (m, 2 H, CH_2), 3.57 (s, 3 H, CH_3), 5.95 (s, 2 H, 2-NH_2), 6.30-6.31 (d, 1 H, CH, J = 1.0 Hz), 10.08 (s, 1 H, 3-NH), 10.57 (s, 1H, 7-NH).

(*S*)-diethyl 2-(7-(2-amino-4-oxo-4,7-dihydro-3*H*-pyrrolo[2,3-*d*]pyrimidin-5-yl)heptanamido)pentanedioate (345): To a suspension of **342** (56 mg, 0.20 mmol) in 3 mL CH_3OH was added 1 N NaOH (3 mL). The resulting mixture was stirred under N_2 at room temperature for 2 h. TLC indicated the disappearance of starting material and the formation of one major spot at the origin. The resulting solution was passed through Celite and washed with a minimum amount of CH_3OH. The combined filtrate was evaporated under reduced pressure to dryness. To this residue was added distilled water (10 mL). The solution was cooled in an ice bath, and the pH was adjusted 3 to 4 using 1 N HCl. The resulting suspension was chilled in a dry ice/acetone bath and thawed to 4 °C overnight in a refrigerator. The precipitate was filtered, washed with cold water, and dried in a desiccator under reduced pressure using P_2O_5 to a brown powder, which was used directly for the next step.

To a solution of this brown powder in anhydrous DMF (5 mL) was added 6-chloro-2,4-dimethoxy-1,3,5-triazine (50 mg, 0.24 mmol) and *N*-methylmorpholine (25 mg, 0.24 mmol). After the mixture was stirred at r.t. for 2 h, *N*-methylmorpholine (25 mg, 0.24

mmol) and dimethyl *L*-glutamate hydrochloride (72 mg, 0.30 mmol) were added all at once. The mixture was stirred at r.t. for 4 h. TLC showed the formation of one major spot at R_f = 0.52 ($CHCl_3$/MeOH, 5:1). The reaction mixture was evaporated to dryness under reduced pressure. The residue was dissolved in a minimum amount of $CHCl_3$/MeOH, 5:1, and chromatographed on a silica gel column (2 cm x 15 cm) with 4% MeOH in $CHCl_3$ as the eluent. Fractions that showed the desired single spot at R_f = 0.52 were pooled and evaporated to dryness to afford **345** 50 mg, yield 57% as a pink syrup. ^{1}H NMR (DMSO-d_6) δ 1.14-1.18 (m, 6 H, 2 CH_3), 1.24-1.28 (m, 4 H, 2 CH_2), 1.46-1.49 (m, 2 H, CH_2), 1.54-1.57 (m, 2 H, CH_2), 1.78-1.83 (m, 1 H, CH_2), 1.92-1.97 (m, 1 H, CH_2), 2.08-2.11 (t, 2 H, CH_2, J = 7.5 Hz), 2.33-2.36 (t, 2 H, CH_2, J = 7.5 Hz), 2.52-2.54 (m, 2 H, CH_2), 4.02-4.10 (m, 4 H, 2 CH_2), 4.19-4.24 (m, 1 H, CH), 5.94 (s, 2 H, 2-NH_2), 6.30-6.31 (d, 1 H, CH, J = 1.0 Hz), 8.14-8.16 (d, 1 H, CONH, , J = 4.0 Hz), 10.06 (s, 1 H, 3-NH), 10.58 (s, 1H, 7-NH).

(*S*)-diethyl 2-(8-(2-amino-4-oxo-4,7-dihydro-3*H*-pyrrolo[2,3-*d*]pyrimidin-5-yl)octanamido)pentanedioate (346): Compound **346** was synthesized as described for **345**: yield 68% as a yellow syrup: R_f = 0.54 ($CHCl_3$/MeOH, 5:1). ^{1}H NMR (DMSO-d_6) δ 1.15-1.18 (m, 6 H, 2 CH_3), 1.22-1.28 (m, 6 H, 3 CH_2), 1.46-1.49 (m, 2 H, CH_2), 1.54-1.57 (m, 2 H, CH_2), 1.75-1.83 (m, 1 H, CH_2), 1.92-1.98 (m, 1 H, CH_2), 2.08-2.11 (t, 2 H, CH_2, J = 7.5 Hz), 2.33-2.36 (t, 2 H, CH_2, J = 7.5 Hz), 2.52-2.54 (m, 2 H, CH_2), 4.02-4.11 (m, 4 H, 2 CH_2), 4.20-4.24 (m, 1 H, CH), 5.94 (s, 2 H, 2-NH_2), 6.30-6.31 (d, 1 H, CH, J = 1.0 Hz), 8.14-8.16 (d, 1 H, CONH, , J = 4.0 Hz), 10.06 (s, 1 H, 3-NH), 10.57 (s, 1H, 7-NH).

(*S*)-diethyl 2-(9-(2-amino-4-oxo-4,7-dihydro-3*H*-pyrrolo[2,3-*d*]pyrimidin-5-yl)nonanamido)pentanedioate (347): Compound **347** was synthesized as described for

345: yield 64% as a yellow syrup: R_f = 0.55 ($CHCl_3$/MeOH, 5:1).^{1}H NMR (DMSO-d_6) δ 1.15-1.18 (m, 6 H, 2 CH_3), 1.22-1.28 (m, 8 H, 4 CH_2), 1.46-1.49 (m, 2 H, CH_2), 1.54-1.57 (m, 2 H, CH_2), 1.76-1.87 (m, 1 H, CH_2), 1.93-1.99 (m, 1 H, CH_2), 2.08-2.11 (t, 2 H, CH_2, J = 7.5 Hz), 2.33-2.36 (t, 2 H, CH_2, J = 7.5 Hz), 2.52-2.54 (m, 2 H, CH_2), 4.02-4.09 (m, 4 H, 2 CH_2), 4.19-4.24 (m, 1 H, CH), 5.94 (s, 2 H, 2-NH_2), 6.30-6.31 (d, 1 H, CH, J = 1.0 Hz), 8.15-8.16 (d, 1 H, CONH, , J = 4.0 Hz), 10.06 (s, 1 H, 3-NH), 10.57 (s, 1H, 7-NH).

(*S*)-2-(7-(2-amino-4-oxo-4,7-dihydro-3*H*-pyrrolo[2,3-*d*]pyrimidin-5-yl)heptanamido)pentanedioic acid (184): To a solution of the diester **345** (40 mg, 0.09 mmol) was added 1 N NaOH (5 mL), and the mixture was stirred under N_2 at room temperature for 1 h. TLC showed the disappearance of the starting material and formation of one major spot at the origin ($CHCl_3$/MeOH, 5:1). The reaction mixture was evaporated to dryness under reduced pressure. The residue was dissolved in water (5 mL), the resulting solution was cooled in an ice bath, and the pH was adjusted to 3-4 with dropwise addition of 1 N HCl. The resulting suspension was frozen in a dry ice/acetone bath, thawed in a refrigerator to 4-5 °C, and filtered. The residue was washed with a small amount of cold water and ethyl acetate and dried in vacuo using P_2O_5 to afford 35 mg (97%) **184** as a yellow powder: mp 133 °C decomposed,R_f = 0.05 ($CHCl_3$/MeOH, 5:1). ^{1}H NMR (DMSO-d_6) δ 1.24-1.28 (m, 4 H, 2 CH_2), 1.46-1.49 (m, 2 H, CH_2), 1.54-1.56 (m, 2 H, CH_2), 1.72-1.77 (m, 1 H, CH_2), 1.90-1.95 (m, 1 H, CH_2), 2.08-2.11 (t, 2 H, CH_2, J = 7.5 Hz), 2.24-2.28 (t, 2 H, CH_2, J = 7.5 Hz), 2.52-2.54 (m, 2 H, CH_2), 4.16-4.20 (m, 1 H, CH), 5.94 (s, 2 H, 2-NH_2), 6.30-6.31 (d, 1 H, CH, J = 1.0 Hz), 8.01-8.03 (d, 1 H, CONH, , J = 4.0 Hz), 10.07 (s, 1 H, 3-NH), 10.58 (s, 1H, 7-NH). Anal. ($C_{18}H_{25}N_5O_6 \cdot 0.46\ H_2O$) Cal. C: 52.00, H: 6.28, N: 16.84. Found C: 52.05, H: 6.26, N: 16.68.

(*S*)-2-(8-(2-amino-4-oxo-4,7-dihydro-3*H*-pyrrolo[2,3-*d*]pyrimidin-5-yl)octanamido)pentanedioic acid (185): Compound **185** was synthesized from **346** as described for **184**: yield 98% as a pink powder: mp 147 °C decomposed, R_f = 0.05 ($CHCl_3$/MeOH, 5:1). ^{1}H NMR (DMSO-d_6) δ 1.24-1.28 (m, 6 H, 3 CH_2), 1.46-1.49 (m, 2 H, CH_2), 1.54-1.57 (m, 2 H, CH_2), 1.72-1.77 (m, 1 H, CH_2), 1.90-1.95 (m, 1 H, CH_2), 2.08-2.11 (t, 2 H, CH_2, J = 7.5 Hz), 2.24-2.28 (t, 2 H, CH_2, J = 7.5 Hz), 2.52-2.54 (m, 2 H, CH_2), 4.16-4.20 (m, 1 H, CH), 5.95 (s, 2 H, 2-NH_2), 6.31-6.32 (d, 1 H, CH, J = 1.0 Hz), 8.02-8.04 (d, 1 H, CONH, , J = 4.0 Hz), 10.08 (s, 1 H, 3-NH), 10.57 (s, 1H, 7-NH). Anal. ($C_{19}H_{27}N_5O_6 \cdot 0.30\ CHCl_3$) Cal. C: 50.66, H: 6.01, N: 15.30. Found C: 50.77, H: 6.15, N: 14.94.

(*S*)-2-(9-(2-amino-4-oxo-4,7-dihydro-3*H*-pyrrolo[2,3-*d*]pyrimidin-5-yl)nonanamido)pentanedioic acid (186): Compound **186** was synthesized from **347** as described for **184**: yield 97% as a pink powder: mp 119 °C decomposed,R_f = 0.07 ($CHCl_3$/MeOH, 5:1). ^{1}H NMR (DMSO-d_6) δ 1.20-1.28 (m, 8 H, 4 CH_2), 1.46-1.49 (m, 2 H, CH_2), 1.54-1.57 (m, 2 H, CH_2), 1.72-1.77 (m, 1 H, CH_2), 1.90-1.95 (m, 1 H, CH_2), 2.08-2.11 (t, 2 H, CH_2, J = 7.5 Hz), 2.24-2.28 (t, 2 H, CH_2, J = 7.5 Hz), 2.52-2.54 (m, 2 H, CH_2), 4.16-4.20 (m, 1 H, CH), 5.95 (s, 2 H, 2-NH_2), 6.31-6.32 (d, 1 H, CH, J = 1.0 Hz), 8.02-8.04 (d, 1 H, CONH, , J = 4.0 Hz), 10.08 (s, 1 H, 3-NH), 10.57 (s, 1H, 7-NH). Anal. ($C_{20}H_{29}N_5O_6 \cdot 0.45\ H_2O$) Cal. C: 54.16, H: 6.79, N: 15.79. Found C: 54.24, H: 6.72, N: 15.49.

Methyl 6-(4-oxo-2-pivalamido-3*H*-pyrrolo[2,3-*d*]pyrimidin-7(4*H*)-yl)hexanoate (353): To a solution of **229** (234 mg, 1.0 mmol) in water (3 mL) and anhydrous DMF (5 mL) cooled at 0 °C was added NaH (26 mg, 1.1 mmol) The reaction mixture was stirred

at 0 °C for 0.5 hour. TLC showed the disappearance of starting materials and the formation of one major spot at R_f = 0.52 (hexane/EtOAc, 1:2). Add bromide **348** (230 mg, 1.1 mmol) to the reaction. The reaction mixture was stirred at room temperature for 5 hours. After evaporation of solvent, EtOAc (10 mL) was added followed by silica gel (3 g). Evaporation of the solvent afforded a plug, which was loaded onto a silica gel column (3.5 cm x 15 cm) and eluted hexane/EtOAc, 1:2. Fractions showing R_f = 0.52 were pooled and evaporated to afford **353** 230 mg, yield 64% as a colorless syrup: R_f = 0.52 (hexane/EtOAc, 1:2). ^{1}H NMR (DMSO-d_6) δ 1.06-1.07 (m, 4 H, 2 CH_2), 1.25 (s, 9 H, -$C(CH_3)_3$), 1.51-1.57 (m, 2 H, CH_2), 1.70-1.76 (m, 2 H, CH_2), 2.27-2.30 (t, 2 H, CH_2, J = 7.5 Hz), 3.56 (s, 3 H, CH_3), 6.41-6.42 (d, 1 H, CH, J = 1.5 Hz), 7.04-7.05 (d, 1 H, CH, J = 1.5 Hz), 10.87 (s, 1 H, 3-NH), 11.91 (s, 1H, 2-NHPiv).

Ethyl 7-(4-oxo-2-pivalamido-3*H*-pyrrolo[2,3-*d*]pyrimidin-7(4*H*)-yl)heptanoate (354): Compound **354** was synthesized from **349** as described for **353**: yield 53% as a colorless syrup: R_f = 0.56 (hexane/EtOAc, 1:2). ^{1}H NMR (DMSO-d_6) δ 1.06-1.07 (m, 4 H, 2 CH_2), 1.16-1.19 (t, 3 H, CH_3, J = 7.5 Hz), 1.25 (s, 9 H, -$C(CH_3)_3$), 1.49-1.53 (m, 2 H, CH_2), 1.76-1.80 (m, 2 H, CH_2), 2.26-2.29 (t, 2 H, CH_2, J = 7.5 Hz), 3.50-3.53 (t, 2 H, CH_2, J = 7.0 Hz), 4.02-4.07 (m, 2 H, CH_2), 6.41-6.42 (d, 1 H, CH, J = 1.5 Hz), 7.04-7.05 (d, 1 H, CH, J = 1.5 Hz), 10.84 (s, 1 H, 3-NH), 11.91 (s, 1H, 2-NHPiv).

Ethyl 8-(4-oxo-2-pivalamido-3*H*-pyrrolo[2,3-*d*]pyrimidin-7(4*H*)-yl)octanoate (355) Compound **355** was synthesized from **350** as described for **353**: yield 56% as a colorless syrup: R_f = 0.56 (hexane/EtOAc, 1:2). ^{1}H NMR (DMSO-d_6) δ 1.14-1.17 (t, 3 H, CH_3, J = 7.5 Hz), 1.20-1.24 (m, 6 H, 3 CH_2), 1.25 (s, 9 H, -$C(CH_3)_3$), 1.45-1.51 (m, 2 H, CH_2), 1.70-1.73 (m, 2 H, CH_2), 2.23-2.26 (t, 2 H, CH_2, J = 7.5 Hz), 4.00-4.07 (m, 2 H, CH_2),

6.41-6.42 (d, 1 H, CH, J = 1.5 Hz), 7.04-7.05 (d, 1 H, CH, J = 1.5 Hz), 10.85 (s, 1 H, 3-NH), 11.91 (s, 1H, 2-NHPiv).

Ethyl 9-(4-oxo-2-pivalamido-3*H*-pyrrolo[2,3-*d*]pyrimidin-7(4*H*)-yl)nonanoate (356)

Compound **356** was synthesized from **351** as described for **353**: yield 60% as a colorless syrup: R_f = 0.58 (hexane/EtOAc, 1:2). ^{1}H NMR (DMSO-d_6) δ 1.14-1.17 (t, 3 H, CH_3, J = 7.5 Hz), 1.20-1.24 (m, 8 H, 4 CH_2), 1.25 (s, 9 H, -C(CH_3)$_3$), 1.47-1.50 (m, 2 H, CH_2), 1.71-1.73 (m, 2 H, CH_2), 2.22-2.25 (t, 2 H, CH_2, J = 7.5 Hz), 4.00-4.07 (m, 2 H, CH_2), 6.41-6.42 (d, 1 H, CH, J = 1.5 Hz), 7.04-7.05 (d, 1 H, CH, J = 1.5 Hz), 10.85 (s, 1 H, 3-NH), 11.91 (s, 1H, 2-NHPiv).

(*S*)-diethyl 2-(6-(2-amino-4-oxo-3*H*-pyrrolo[2,3-*d*]pyrimidin-7(4*H*)-yl)hexanamido)pentanedioate (357)

To a suspension of **353** (70 mg, 0.27 mmol) in 3 mL CH_3OH was added 1 N NaOH (3 mL). The resulting mixture was stirred under N_2 at room temperature for 2 h. TLC indicated the disappearance of starting material and the formation of one major spot at the origin. The resulting solution was passed through Celite and washed with a minimum amount of CH_3OH. The combined filtrate was evaporated under reduced pressure to dryness. To this residue was added distilled water (10 mL). The solution was cooled in an ice bath, and the pH was adjusted 3 to 4 using 1 N HCl. The resulting suspension was chilled in a dry ice/acetone bath and thawed to 4 °C overnight in a refrigerator. The precipitate was filtered, washed with cold water, and dried in a desiccator under reduced pressure using P_2O_5 to a brown powder, which was used directly for the next step.

To a solution of this brown powder in anhydrous DMF (5 mL) was added 6-chloro-2,4-dimethoxy-1,3,5-triazine (70 mg, 0.32 mmol) and *N*-methylmorpholine (33 mg, 0.32

mmol). After the mixture was stirred at r.t. for 2 h, *N*-methylmorpholine (33 mg, 0.32 mmol) and dimethyl *L*-glutamate hydrochloride (96 mg, 0.40 mmol) were added all at once. The mixture was stirred at r.t. for 4 h. TLC showed the formation of one major spot at R_f = 0.50 ($CHCl_3$/MeOH, 5:1). The reaction mixture was evaporated to dryness under reduced pressure. The residue was dissolved in a minimum amount of $CHCl_3$/MeOH, 5:1, and chromatographed on a silica gel column (2 cm x 15 cm) with 4% MeOH in $CHCl_3$ as the eluent. Fractions that showed the desired single spot at R_f = 0.50 were pooled and evaporated to dryness to afford **357** 70 mg, yield 61% as a white syrup. ^{1}H NMR (DMSO-d_6) δ 1.15-1.18 (m, 6 H, 2 CH_3), 1.19-1.22 (m, 2 H, CH_2), 1.49-1.52 (m, 2 H, CH_2), 1.65-1.68 (m, 2 H, CH_2), 1.77-1.82 (m, 1 H, CH_2), 1.92-1.99 (m, 1 H, CH_2), 2.08-2.11 (t, 2 H, CH_2, J = 7.5 Hz), 2.33-2.36 (t, 2 H, CH_2, J = 7.5 Hz), 3.86-3.88 (t, 2 H, CH_2, J = 7.0 Hz), 4.02-4.07 (m, 4 H, 2 CH_2), 4.19-4.23 (m, 1 H, CH), 6.16 (s, 2 H, 2-NH_2), 6.19-6.20 (d, 1 H, CH, J = 1.8 Hz), 6.69-6.70 (d, 1 H, CH, J = 1.8 Hz), 8.15-8.17 (d, 1 H, CONH, , J = 4.0 Hz), 10.21 (s, 1 H, 3-NH).

(*S*)-diethyl 2-(7-(2-amino-4-oxo-3*H*-pyrrolo[2,3-*d*]pyrimidin-7(4*H*)-yl)heptanamido)pentanedioate (358): Compound **358** was synthesized as described for **357**: yield 77% as a colorless syrup: R_f = 0.51 ($CHCl_3$/MeOH, 5:1). ^{1}H NMR (DMSO-d_6) δ 1.14-1.18 (m, 6 H, 2 CH_3), 1.19-1.24 (m, 4 H, 2 CH_2), 1.43-1.48 (m, 2 H, CH_2), 1.63-1.66 (m, 2 H, CH_2), 1.77-1.82 (m, 1 H, CH_2), 1.92-1.98 (m, 1 H, CH_2), 2.07-2.10 (t, 2 H, CH_2, J = 7.5 Hz), 2.33-2.36 (t, 2 H, CH_2, J = 7.5 Hz), 3.86-3.89 (t, 2 H, CH_2, J = 7.0 Hz), 4.01-4.08 (m, 4 H, 2 CH_2), 4.19-4.23 (m, 1 H, CH), 6.16 (s, 2 H, 2-NH_2), 6.19-6.20 (d, 1 H, CH, J = 1.8 Hz), 6.69-6.70 (d, 1 H, CH, J = 1.5 Hz), 8.15-8.16 (d, 1 H, CONH, , J = 4.0 Hz), 10.21 (s, 1 H, 3-NH).

(S)-diethyl 2-(8-(2-amino-4-oxo-3*H*-pyrrolo[2,3-*d*]pyrimidin-7(4*H*)-yl)octanamido)pentanedioate (359):

Compound **359** was synthesized as described for **357**: yield 81% as a colorless syrup: R_f = 0.50 ($CHCl_3$/MeOH, 5:1). ^{1}H NMR (DMSO-d_6) δ 1.14-1.18 (m, 6 H, 2 CH_3), 1.19-1.26 (m, 6 H, 3 CH_2), 1.45-1.48 (m, 2 H, CH_2), 1.64-1.67 (m, 2 H, CH_2), 1.77-1.82 (m, 1 H, CH_2), 1.92-1.98 (m, 1 H, CH_2), 2.07-2.10 (t, 2 H, CH_2, J = 7.5 Hz), 2.33-2.36 (t, 2 H, CH_2, J = 7.5 Hz), 3.86-3.89 (t, 2 H, CH_2, J = 7.0 Hz), 4.01-4.08 (m, 4 H, 2 CH_2), 4.19-4.23 (m, 1 H, CH), 6.15 (s, 2 H, 2-NH_2), 6.19-6.20 (d, 1 H, CH, J = 1.8 Hz), 6.69-6.70 (d, 1 H, CH, J = 1.5 Hz), 8.13-8.15 (d, 1 H, CONH, , J = 4.0 Hz), 10.21 (s, 1 H, 3-NH).

(S)-diethyl 2-(9-(2-amino-4-oxo-3*H*-pyrrolo[2,3-*d*]pyrimidin-7(4*H*)-yl)nonanamido)pentanedioate (360): Compound **360** was synthesized as described for **357**: yield 71% as a colorless syrup: R_f = 0.52 ($CHCl_3$/MeOH, 5:1). ^{1}H NMR (DMSO-d_6) δ 1.14-1.18 (m, 6 H, 2 CH_3), 1.19-1.26 (m, 8 H, 4 CH_2), 1.45-1.48 (m, 2 H, CH_2), 1.64-1.67 (m, 2 H, CH_2), 1.77-1.82 (m, 1 H, CH_2), 1.94-1.99 (m, 1 H, CH_2), 2.07-2.10 (t, 2 H, CH_2, J = 7.5 Hz), 2.33-2.36 (t, 2 H, CH_2, J = 7.5 Hz), 3.86-3.89 (t, 2 H, CH_2, J = 7.0 Hz), 4.01-4.08 (m, 4 H, 2 CH_2), 4.19-4.23 (m, 1 H, CH), 6.15 (s, 2 H, 2-NH_2), 6.19-6.20 (d, 1 H, CH, J = 1.8 Hz), 6.69-6.70 (d, 1 H, CH, J = 1.5 Hz), 8.13-8.14 (d, 1 H, CONH, , J = 4.0 Hz), 10.21 (s, 1 H, 3-NH).

(*S*)-2-(6-(2-amino-4-oxo-3*H*-pyrrolo[2,3-*d*]pyrimidin-7(4*H*)-yl)hexanamido)pentanedioic acid (187): To a solution of the diester **357** (60 mg, 0.09 mmol) was added 1 N NaOH (5 mL), and the mixture was stirred under N_2 at room temperature for 1 h. TLC showed the disappearance of the starting material and formation of one major spot at the origin ($CHCl_3$/MeOH, 5:1). The reaction mixture was evaporated

to dryness under reduced pressure. The residue was dissolved in water (5 mL), the resulting solution was cooled in an ice bath, and the pH was adjusted to 3-4 with dropwise addition of 1 N HCl. The resulting suspension was frozen in a dry ice/acetone bath, thawed in a refrigerator to 4-5 °C, and filtered. The residue was washed with a small amount of cold water and ethyl acetate and dried in vacuo using P_2O_5 to afford 48 mg (92%) **187** as as a pink powder: mp 126 °C decomposed, R_f = 0.05 ($CHCl_3$/MeOH, 5:1). ^{1}H NMR (DMSO-d_6) δ 1.18-1.24 (m, 2 H, CH_2), 1.49-1.52 (m, 2 H, CH_2), 1.64-1.67 (m, 2 H, CH_2), 1.72-1.78 (m, 1 H, CH_2), 1.90-1.96 (m, 1 H, CH_2), 2.08-2.11 (t, 2 H, CH_2, J = 7.5 Hz), 2.24-2.27 (t, 2 H, CH_2, J = 7.5 Hz), 3.85-3.90 (t, 2 H, CH_2, J = 7.0 Hz), 4.16-4.21 (m, 1 H, CH), 6.18 (s, 2 H, 2-NH_2), 6.19-6.20 (d, 1 H, CH, J = 1.8 Hz), 6.69-6.70 (d, 1 H, CH, J = 1.8 Hz), 8.01-8.02 (d, 1 H, CONH, , J = 4.0 Hz), 10.22 (s, 1 H, 3-NH). Anal. ($C_{17}H_{23}N_5O_6 \cdot 0.78\ H_2O$) Cal. C: 50.10, H: 6.08, N: 17.18. Found C: 50.11, H: 5.89, N: 17.10.

(*S*)-2-(7-(2-amino-4-oxo-3*H*-pyrrolo[2,3-*d*]pyrimidin-7(4*H*)-yl)heptanamido)pentanedioic acid (188): Compound **188** was synthesized as described for **187**: yield 93% as a pink powder: mp 121 °C decomposed, R_f = 0.06 ($CHCl_3$/MeOH, 5:1). ^{1}H NMR (DMSO-d_6) δ 1.18-1.28 (m, 4 H, 2 CH_2), 1.45-1.48 (m, 2 H, CH_2), 1.63-1.66 (m, 2 H, CH_2), 1.73-1.76 (m, 1 H, CH_2), 1.91-1.96 (m, 1 H, CH_2), 2.07-2.10 (t, 2 H, CH_2, J = 7.5 Hz), 2.24-2.27 (t, 2 H, CH_2, J = 7.5 Hz), 3.86-3.89 (t, 2 H, CH_2, J = 7.0 Hz), 4.16-4.20 (m, 1 H, CH), 6.17 (s, 2 H, 2-NH_2), 6.19-6.20 (d, 1 H, CH, J = 1.8 Hz), 6.69-6.70 (d, 1 H, CH, J = 1.8 Hz), 8.02-8.03 (d, 1 H, CONH, , J = 4.0 Hz), 10.22 (s, 1 H, 3-NH). Anal. ($C_{18}H_{25}N_5O_6 \cdot 0.46\ H_2O$) Cal. C: 52.01, H: 6.28, N: 16.85. Found C: 52.08, H: 6.15, N: 16.60.

(*S*)-2-(8-(2-amino-4-oxo-3*H*-pyrrolo[2,3-*d*]pyrimidin-7(4*H*)-yl)octanamido)pentanedioic acid (189): Compound **189** was synthesized as described for **187**: yield 96% as a pink powder: mp 138 °C decomposed, R_f = 0.06 ($CHCl_3$/MeOH, 5:1). ^{1}H NMR (DMSO-d_6) δ 1.18-1.28 (m, 6 H, 3 CH_2), 1.45-1.48 (m, 2 H, CH_2), 1.64-1.67 (m, 2 H, CH_2), 1.72-1.78 (m, 1 H, CH_2), 1.91-1.96 (m, 1 H, CH_2), 2.07-2.10 (t, 2 H, CH_2, J = 7.5 Hz), 2.24-2.27 (t, 2 H, CH_2, J = 7.5 Hz), 3.86-3.89 (t, 2 H, CH_2, J = 7.0 Hz), 4.16-4.20 (m, 1 H, CH), 6.16 (s, 2 H, 2-NH_2), 6.19-6.20 (d, 1 H, CH, J = 1.8 Hz), 6.69-6.70 (d, 1 H, CH, J = 1.8 Hz), 8.00-8.02 (d, 1 H, CONH, , J = 4.0 Hz), 10.21 (s, 1 H, 3-NH). Anal. ($C_{19}H_{27}N_5O_6$) Cal. C: 54.15, H: 6.46, N: 16.62. Found C: 53.96, H: 6.49, N: 16.34.

(*S*)-2-(9-(2-amino-4-oxo-3*H*-pyrrolo[2,3-*d*]pyrimidin-7(4*H*)-yl)nonanamido)pentanedioic acid (190): Compound **190** was synthesized as described for **187**: yield 92% as a yellow powder: mp 141 °C decomposed, R_f = 0.06 ($CHCl_3$/MeOH, 5:1). ^{1}H NMR (DMSO-d_6) δ 1.18-1.28 (m, 8 H, 4 CH_2), 1.45-1.48 (m, 2 H, CH_2), 1.64-1.67 (m, 2 H, CH_2), 1.72-1.78 (m, 1 H, CH_2), 1.91-1.96 (m, 1 H, CH_2), 2.07-2.10 (t, 2 H, CH_2, J = 7.5 Hz), 2.24-2.27 (t, 2 H, CH_2, J = 7.5 Hz), 3.86-3.89 (t, 2 H, CH_2, J = 7.0 Hz), 4.16-4.20 (m, 1 H, CH), 6.16 (s, 2 H, 2-NH_2), 6.19-6.20 (d, 1 H, CH, J = 1.8 Hz), 6.69-6.70 (d, 1 H, CH, J = 1.8 Hz), 8.00-8.02 (d, 1 H, CONH, , J = 4.0 Hz), 10.21 (s, 1 H, 3-NH). Anal. ($C_{20}H_{29}N_5O_6 \cdot 0.43\ CH_3OH$) Cal. C: 54.62, H: 6.89, N: 15.59. Found C: 54.70, H: 6.78, N: 15.46.

4-(4-(2-amino-4-oxo-4,7-dihydro-3*H*-pyrrolo[2,3-*d*]pyrimidin-5-yl)butyl)benzoic acid (361): To a suspension of **291** (89 mg, 0.25 mmol) in 1 mL CH_3OH was added 3 N NaOH (3 mL). The resulting mixture was stirred under N_2 at 40-50 °C for 24 h.

TLC indicated the disappearance of starting material and the formation of one major spot at the origin. The resulting solution was passed through Celite and washed with a minimum amount of CH_3OH. The combined filtrate was evaporated under reduced pressure to dryness. To this residue was added distilled water (10 mL). The solution was cooled in an ice bath, and the pH was adjusted 3 to 4 using 3 N HCl. The resulting suspension was chilled in a dry ice/acetone bath and thawed to 4 °C overnight in a refrigerator. The precipitate was filtered, washed with cold water, and dried in a desiccator under reduced pressure using P_2O_5 to afford 70 mg (82%) of **361** as a brown powder: mp >245 °C decomposed, R_f = 0.03 ($CHCl_3$/MeOH, 5:1). Put it to next step without further purification.

(*S*)-dimethyl 2-(4-(4-(2-amino-4-oxo-4,7-dihydro-3*H*-pyrrolo[2,3-*d*]pyrimidin-5-yl)butyl)-*N*-methylbenzamido)pentanedioate (363): To a solution of **361** (316 mg, 1.0 mmol) in anhydrous DMF (10 mL) was added 6-chloro-2,4-dimethoxy-1,3,5-triazine (270 mg, 1.2 mmol) and *N*-methylmorpholine (155 mg, 1.2 mmol). After the mixture was stirred at r.t. for 2 h, *N*-methylmorpholine (155 mg, 1.2 mmol) and *N*-methyl *L*-glutamate **362** (210 mg, 1.2 mmol) were added all at once. The mixture was stirred at r.t. for 4 h. TLC showed the formation of one major spot at R_f = 0.42 ($CHCl_3$/MeOH, 5:1). The reaction mixture was evaporated to dryness under reduced pressure. The residue was dissolved in a minimum amount of $CHCl_3$/MeOH, 5:1, and chromatographed on a silica gel column (2 cm x 15 cm) with 4% MeOH in $CHCl_3$ as the eluent. Fractions that showed the desired single spot at R_f = 0.42 were pooled and evaporated to dryness to afford **363** 320 mg, yield 65% as a colorless syrup, R_f = 0.42 ($CHCl_3$/MeOH, 5:1). ^{1}H NMR (DMSO-d_6) δ 1.52-1.68 (m, 4 H, 2 CH_2), 1.97-2.03 (m, 1 H, CH_2), 2.06-2.13 (m, 1 H,

CH_2), 2.42-2.45 (m, 2 H, CH_2), 2.57-2.59 (t, 2 H, CH_2, J = 7.5 Hz), 2.64-2.67 (t, 2 H, CH_2, J = 7.5 Hz), 2.83 (s, 3 H, NCH_3), 3.60 (s, 3 H, CH_3), 3.68 (s, 3 H, CH_3), 4.88-4.91 (m, 1 H, CH), 5.95 (s, 2 H, 2-NH_2), 6.32-6.33 (d, 1 H, CH, J = 0.5 Hz), 7.23-7.28 (m, 2 H, C_6H_4), 7.29-7.34 (m, 2 H, C_6H_4), 10.09 (s, 1 H, 3-NH), 10.60 (s, 1H, 7-NH).

(*S*)-2-(4-(4-(2-amino-4-oxo-4,7-dihydro-3*H*-pyrrolo[2,3-*d*]pyrimidin-5-yl)butyl)-*N*-methylbenzamido)pentanedioic acid (191): To a solution of the diester **363** (240 mg, 0.48 mmol) was added 1 N NaOH (5 mL), and the mixture was stirred under N_2 at room temperature for 1 h. TLC showed the disappearance of the starting material and formation of one major spot at the origin ($CHCl_3$/MeOH, 5:1). The reaction mixture was evaporated to dryness under reduced pressure. The residue was dissolved in water (5 mL), the resulting solution was cooled in an ice bath, and the pH was adjusted to 3-4 with dropwise addition of 1 N HCl. The resulting suspension was frozen in a dry ice/acetone bath, thawed in a refrigerator to 4-5 °C, and filtered. The residue was washed with a small amount of cold water and ethyl acetate and dried in vacuo using P_2O_5 to afford 240 mg (89%) **191** as a yellow powder: mp 186 °C decomposed, R_f = 0.04 ($CHCl_3$/MeOH, 5:1). ^{1}H NMR (DMSO-d_6) δ 1.53-1.68 (m, 4 H, 2 CH_2), 1.97-2.03 (m, 1 H, CH_2), 2.06-2.13 (m, 1 H, CH_2), 2.42-2.45 (m, 2 H, CH_2), 2.57-2.59 (t, 2 H, CH_2, J = 7.5 Hz), 2.64-2.67 (t, 2 H, CH_2, J = 7.5 Hz), 2.81 (s, 3 H, NCH_3), 4.87-4.90 (m, 1 H, CH), 5.95 (s, 2 H, 2-NH_2), 6.33 (s, 1 H, CH), 7.23-7.28 (m, 2 H, C_6H_4), 7.29-7.34 (m, 2 H, C_6H_4), 10.09 (s, 1 H, 3-NH), 10.60 (s, 1H, 7-NH). Anal. ($C_{23}H_{27}N_5O_6 \cdot 0.44\ H_2O$) Cal. C: 57.86, H: 5.89, N: 14.67. Found C: 57.90, H: 6.03, N: 14.58.

(*S*)-dimethyl 2-(4-(4-(2-amino-4-oxo-4,7-dihydro-3*H*-pyrrolo[2,3-*d*]pyrimidin-5-yl)butyl)benzamido)succinate (366): Compound **366** was synthesized from **364** as

described for **363:** yield 75% as a colorless syrup, R_f = 0.38 ($CHCl_3$/MeOH, 5:1). ^{1}H NMR (DMSO-d_6) δ 1.54-1.63 (m, 4 H, 2 CH_2), 2.57-2.59 (t, 2 H, CH_2, J = 7.5 Hz), 2.64-2.67 (t, 2 H, CH_2, J = 7.5 Hz), 2.78-2.85 (m, 1 H, CH_2), 2.91-2.97 (m, 1 H, CH_2), 3.61 (s, 3 H, CH_3), 3.63 (s, 3 H, CH_3), 4.80-4.83 (m, 1 H, CH), 5.95 (s, 2 H, 2-NH_2), 6.32-6.33 (d, 1 H, CH, J = 1.0 Hz), 7.28-7.30 (d, 2 H, C_6H_4, J = 4.0 Hz), 7.73-7.75 (d, 2 H, C_6H_4, J = 4.0 Hz), 8.82-8.84 (d, 1 H, CONH, J = 4.0 Hz), 10.09 (s, 1 H, 3-NH), 10.61 (s, 1H, 7-NH).

(*S*)-dimethyl 2-(4-(4-(2-amino-4-oxo-4,7-dihydro-3*H*-pyrrolo[2,3-*d*]pyrimidin-5-yl)butyl)benzamido)hexanedioate (367): Compound **367** was synthesized from **365** as described for **363**: yield 74% as a colorless syrup, R_f = 0.43 ($CHCl_3$/MeOH, 5:1). ^{1}H NMR (DMSO-d_6) δ 1.54-1.63 (m, 6 H, 3 CH_2), 1.77-1.81 (m, 2 H, CH_2), 2.32-2.35 (t, 2 H, CH_2, J = 7.5 Hz), 2.57-2.60 (t, 2 H, CH_2, J = 7.5 Hz), 2.62-2.65 (t, 2 H, CH_2, J = 7.5 Hz), 3.58 (s, 3 H, CH_3), 3.63 (s, 3 H, CH_3), 4.38-4.43 (m, 1 H, CH), 5.95 (s, 2 H, 2-NH_2), 6.32 (s, 1 H, CH), 7.27-7.29 (d, 2 H, C_6H_4, J = 4.0 Hz), 7.77-7.79 (d, 2 H, C_6H_4, J = 4.0 Hz), 8.63-8.65 (d, 1 H, CONH, J = 4.0 Hz), 10.09 (s, 1 H, 3-NH), 10.59 (s, 1H, 7-NH).

(*S*)-2-(4-(4-(2-amino-4-oxo-4,7-dihydro-3*H*-pyrrolo[2,3-*d*]pyrimidin-5-yl)butyl)benzamido)succinic acid (192): Compound **192** was synthesized from **366** as described for **191**: yield 95% as a light blue powder: mp 139 °C decomposed, R_f = 0.04 ($CHCl_3$/MeOH, 5:1). ^{1}H NMR (DMSO-d_6) δ 1.52-1.66 (m, 4 H, 2 CH_2), 2.57-2.59 (t, 2 H, CH_2, J = 7.5 Hz), 2.64-2.67 (t, 2 H, CH_2, J = 7.5 Hz), 2.78-2.85 (m, 1 H, CH_2), 2.91-2.97 (m, 1 H, CH_2), 4.70-4.76 (m, 1 H, CH), 6.02 (s, 2 H, 2-NH_2), 6.33 (s, 1 H, CH), 7.27-7.29 (d, 2 H, C_6H_4, J = 4.0 Hz), 7.74-7.76 (d, 2 H, C_6H_4, J = 4.0 Hz), 8.64-8.66 (d, 1

H, CONH, J = 4.0 Hz), 10.16 (s, 1 H, 3-NH), 10.63 (s, 1H, 7-NH). Anal. ($C_{21}H_{23}N_5O_6 \cdot 1.2\ H_2O$) Cal. C: 54.47, H: 5.53, N: 15.12. Found C: 54.68, H: 5.32, N: 14.78.

(*S*)-2-(4-(4-(2-amino-4-oxo-4,7-dihydro-3*H*-pyrrolo[2,3-*d*]pyrimidin-5-yl)butyl)benzamido)hexanedioic acid (193): Compound **193** was synthesized from **367** as described for **191**: yield 93% as a blue powder: mp 126 °C decomposed, R_f = 0.05 ($CHCl_3$/MeOH, 5:1). ^{1}H NMR (DMSO-d_6) δ 1.52-1.64 (m, 6 H, 3 CH_2), 1.74-1.85 (m, 2 H, CH_2), 2.22-2.25 (t, 2 H, CH_2, J = 7.5 Hz), 2.57-2.60 (t, 2 H, CH_2, J = 7.5 Hz), 2.62-2.65 (t, 2 H, CH_2, J = 7.5 Hz), 4.32-4.37 (m, 1 H, CH), 6.09 (s, 2 H, 2-NH_2), 6.34 (s, 1 H, CH), 7.27-7.29 (d, 2 H, C_6H_4, J = 4.0 Hz), 7.77-7.79 (d, 2 H, C_6H_4, J = 4.0 Hz), 8.48-8.50 (d, 1 H, CONH, J = 4.0 Hz), 10.21 (s, 1 H, 3-NH), 10.65 (s, 1H, 7-NH). Anal. ($C_{23}H_{27}N_5O_6 \cdot 2.0\ H_2O$) Cal. C: 54.64, H: 6.18, N: 13.85. Found C: 54.86, H: 5.80, N: 13.81.

(*S*)-dimethyl 2-(8-(2-amino-4-oxo-4,7-dihydro-3*H*-pyrrolo[2,3-*d*]pyrimidin-6-yl)-*N*-methyloctanamido)pentanedioate (369): To a solution of **368** (120 mg, 0.40 mmol) in anhydrous DMF (5 mL) was added 6-chloro-2,4-dimethoxy-1,3,5-triazine (100 mg, 0.50 mmol) and *N*-methylmorpholine (60 mg, 0.50 mmol). After the mixture was stirred at r.t. for 2 h, *N*-methylmorpholine (60 mg, 0.50 mmol) and *N*-methyl *L*-glutamate **362** (90 mg, 0.50 mmol) were added all at once. The mixture was stirred at r.t. for 4 h. TLC showed the formation of one major spot at R_f = 0.48 ($CHCl_3$/MeOH, 5:1). The reaction mixture was evaporated to dryness under reduced pressure. The residue was dissolved in a minimum amount of $CHCl_3$/MeOH, 5:1, and chromatographed on a silica gel column (2 cm x 15 cm) with 4% MeOH in $CHCl_3$ as the eluent. Fractions that showed the desired single spot at R_f = 0.48 were pooled and evaporated to dryness to afford **369** 100 mg,

yield 56% as a yellow syrup, R_f = 0.48 ($CHCl_3$/MeOH, 5:1). ^{1}H NMR (DMSO-d_6) δ 1.22-1.32 (m, 6 H, 3 CH_2), 1.42-1.57 (m, 4 H, 2 CH_2), 1.76-1.82 (m, 1 H, CH), 1.92-1.99 (m, 1 H, CH), 2.26-2.37 (m, 4 H, 2 CH_2), 2.45-2.48 (m, 2 H, CH_2), 2.85 (s, 3 H, NCH_3), 3.56 (s, 3 H, CH_3), 3.60 (s, 3 H, CH_3), 4.84-4.88 (m, 1 H, CH), 5.83 (s, 1 H, CH), 5.95 (s, 2 H, 2-NH_2), 10.12 (s, 1 H, 3-NH), 10.78 (s, 1H, 7-NH).

(*S*)-2-(8-(2-amino-4-oxo-4,7-dihydro-3*H*-pyrrolo[2,3-*d*]pyrimidin-6-yl)-*N*-methyloctanamido)pentanedioic acid (194): To a solution of the diester **369** (80 mg, 0.18 mmol) was added 1 N NaOH (5 mL), and the mixture was stirred under N_2 at room temperature for 1 h. TLC showed the disappearance of the starting material and formation of one major spot at the origin ($CHCl_3$/MeOH, 5:1). The reaction mixture was evaporated to dryness under reduced pressure. The residue was dissolved in water (5 mL), the resulting solution was cooled in an ice bath, and the pH was adjusted to 3-4 with dropwise addition of 1 N HCl. The resulting suspension was frozen in a dry ice/acetone bath, thawed in a refrigerator to 4-5 °C, and filtered. The residue was washed with a small amount of cold water and ethyl acetate and dried in vacuo using P_2O_5 to afford 65 mg (87%) **194** as a yellow powder: mp 131-132 °C decomposed, R_f = 0.06 ($CHCl_3$/MeOH, 5:1). ^{1}H NMR (DMSO-d_6) δ 1.22-1.32 (m, 6 H, 3 CH_2), 1.42-1.60 (m, 4 H, 2 CH_2), 1.76-1.82 (m, 1 H, CH), 1.92-1.99 (m, 1 H, CH), 2.26-2.37 (m, 4 H, 2 CH_2), 2.45-2.48 (m, 2 H, CH_2), 2.84 (s, 3 H, NCH_3), 4.86-4.89 (m, 1 H, CH), 5.84 (s, 1 H, CH), 5.95 (s, 2 H, 2-NH_2), 10.12 (s, 1 H, 3-NH), 10.77 (s, 1H, 7-NH). Anal. ($C_{20}H_{29}N_5O_6 \cdot 0.65\ CH_3OH$) Cal. C: 54.36, H: 6.98, N: 15.36. Found C: 54.33, H: 6.85, N: 15.35.

(*S*)-dimethyl 2-(8-(2-amino-4-oxo-4,7-dihydro-3*H*-pyrrolo[2,3-*d*]pyrimidin-6-yl)octanamido)succinate (370):

Compound **370** was synthesized from **364** as described for **369**: yield 71% as a colorless syrup, R_f = 0.45 ($CHCl_3$/MeOH, 5:1). ^{1}H NMR (DMSO-d_6) δ 1.22-1.32 (m, 6 H, 3 CH_2), 1.42-1.60 (m, 4 H, 2 CH_2), 2.06-2.10 (t, 2 H, CH_2, J = 7.5 Hz), 2.30-2.43 (m, 4 H, 2 CH_2), 2.64-2.70 (m, 1 H, CH_2), 2.76-2.82 (m, 1 H, CH_2), 3.59 (s, 3 H, CH_3), 3.60 (s, 3 H, CH_3), 4.58-4.63 (m, 1 H, CH), 5.83 (s, 1 H, CH), 5.94 (s, 2 H, 2-NH_2), 8.28-8.30 (d, 1 H, CONH, J = 4.0 Hz), 10.10 (s, 1 H, 3-NH), 10.77 (s, 1H, 7-NH).

(*S*)-dimethyl 2-(8-(2-amino-4-oxo-4,7-dihydro-3*H*-pyrrolo[2,3-*d*]pyrimidin-6-yl)octanamido)hexanedioate (371):

Compound **371** was synthesized from **365** as described for **369**: yield 68% as a colorless syrup, R_f = 0.45 ($CHCl_3$/MeOH, 5:1). ^{1}H NMR (DMSO-d_6) δ 1.22-1.32 (m, 8 H, 4 CH_2), 1.42-1.60 (m, 6 H, 3 CH_2), 2.06-2.10 (t, 2 H, CH_2, J = 7.5 Hz), 2.30-2.43 (m, 4 H, 2 CH_2), 2.64-2.70 (m, 1 H, CH_2), 2.76-2.82 (m, 1 H, CH_2), 3.59 (s, 3 H, CH_3), 3.60 (s, 3 H, CH_3), 4.58-4.63 (m, 1 H, CH), 5.83 (s, 1 H, CH), 5.94 (s, 2 H, 2-NH_2), 8.16-8.18 (d, 1 H, CONH, J = 4.0 Hz), 10.11 (s, 1 H, 3-NH), 10.77 (s, 1H, 7-NH).

(*S*)-2-(8-(2-amino-4-oxo-4,7-dihydro-3*H*-pyrrolo[2,3-*d*]pyrimidin-6-yl)octanamido)succinic acid (195):

Compound **195** was synthesized from **370** as described for **194**: yield 94% as a yellow powder: mp 125 °C decomposed, R_f = 0.05 ($CHCl_3$/MeOH, 5:1). ^{1}H NMR (DMSO-d_6) δ 1.22-1.32 (m, 6 H, 3 CH_2), 1.42-1.60 (m, 4 H, 2 CH_2), 2.06-2.10 (t, 2 H, CH_2, J = 7.5 Hz), 2.30-2.43 (m, 4 H, 2 CH_2), 2.64-2.70 (m, 1 H, CH_2), 2.76-2.82 (m, 1 H, CH_2), 4.48-4.51 (m, 1 H, CH), 5.83 (s, 1 H, CH), 5.94 (s, 2 H, 2-NH_2), 8.09-8.11 (d, 1 H, CONH, J =

4.0 Hz), 10.12 (s, 1 H, 3-NH), 10.77 (s, 1H, 7-NH). Anal. ($C_{18}H_{25}N_5O_6 \cdot 0.65\ CH_3OH$) Cal. C: 52.30, H: 6.50, N: 16.34. Found C: 52.26, H: 6.31, N: 16.30.

(*S*)-2-(8-(2-amino-4-oxo-4,7-dihydro-3*H*-pyrrolo[2,3-*d*]pyrimidin-6-yl)octanamido)hexanedioic acid (196):

Compound **196** was synthesized from **371** as described for **194**: yield 92% as a yellow powder: mp 153 °C decomposed,R_f = 0.05 ($CHCl_3$/MeOH, 5:1). ^{1}H NMR (DMSO-d_6) δ 1.22-1.32 (m, 8 H, 4 CH_2), 1.42-1.66 (m, 6 H, 3 CH_2), 2.06-2.10 (t, 2 H, CH_2, J = 7.5 Hz), 2.30-2.43 (m, 4 H, 2 CH_2), 2.64-2.70 (m, 1 H, CH_2), 2.76-2.82 (m, 1 H, CH_2), 4.48-4.51 (m, 1 H, CH), 5.83 (s, 1 H, CH), 5.94 (s, 2 H, 2-NH_2), 8.09-8.11 (d, 1 H, CONH, J = 4.0 Hz), 10.11 (s, 1 H, 3-NH), 10.77 (s, 1H, 7-NH). Anal. ($C_{20}H_{29}N_5O_6 \cdot 1.0\ H_2O$) Cal. C: 52.97, H: 6.89, N: 15.44. Found C: 53.16, H: 6.81, N: 15.10.

4-(4-(2-amino-4-oxo-4,7-dihydro-3*H*-pyrrolo[2,3-*d*]pyrimidin-6-yl)butyl)-*N*-propylbenzamide (197):

To a solution of **221** (100 mg, 0.30 mmol) in anhydrous DMF (10 mL) was added 6-chloro-2,4-dimethoxy-1,3,5-triazine (64 mg, 0.36 mmol) and *N*-methylmorpholine (41 mg, 0.36 mmol). After the mixture was stirred at r.t. for 2 h, *N*-methylmorpholine (41 mg, 0.36 mmol) and **372** (46 mg, 0.30 mmol) were added all at once. The mixture was stirred at r.t. for 4 h. TLC showed the formation of one major spot at R_f = 0.56 ($CHCl_3$/MeOH, 5:1). The reaction mixture was evaporated to dryness under reduced pressure. The residue was dissolved in a minimum amount of $CHCl_3$/MeOH, 5:1, and chromatographed on a silica gel column (2 cm x 15 cm) with 4% MeOH in $CHCl_3$ as the eluent. Fractions that showed the desired single spot at R_f = 0.56 were pooled and evaporated to dryness to afford **197** 70 mg, yield 64% a colorless syrup, R_f = 0.56 ($CHCl_3$/MeOH, 5:1). ^{1}H NMR

(DMSO-d_6) δ 0.86-0.90 (t, 3 H, CH_3, J = 7.0 Hz), 1.49-1.63 (m, 6 H, 3 CH_2), 2.50-2.53 (m, 2 H, CH_2), 2.63-2.66 (t, 2 H, CH_2, J = 7.5 Hz), 3.17-3.22 (m, 2 H, CH_2), 5.83-5.84 (d, 1 H, CH, J = 1.0 Hz), 5.96 (s, 2 H, 2-NH_2), 7.25-7.27 (d, 2 H, C_6H_4, J = 4.0 Hz), 7.73-7.75 (d, 2 H, C_6H_4, J = 4.0 Hz), 8.35-8.38 (t, 1 H, CONH, J = 6.4 Hz), 10.12 (s, 1 H, 3-NH), 10.80 (s, 1H, 7-NH).

Methyl 2-(4-(4-(2-amino-4-oxo-4,7-dihydro-3*H*-pyrrolo[2,3-*d*]pyrimidin-6-yl)butyl)benzamido)butanoate (375):

Compound **375** was synthesized as described for **197**: yield 54% as a colorless syrup, R_f = 0.51 ($CHCl_3$/MeOH, 5:1). ^{1}H NMR (DMSO-d_6) δ 0.92-0.96 (t, 3 H, CH_3, J = 7.0 Hz), 1.54-1.63 (m, 4 H, 2 CH_2), 1.73-1.86 (m, 2 H, CH_2), 2.50-2.53 (m, 2 H, CH_2), 2.63-2.66 (t, 2 H, CH_2, J = 7.5 Hz), 3.84 (s, 3 H, CH_3), 4.30-4.35 (m, 1 H, CH), 5.83-5.84 (d, 1 H, CH, J = 1.0 Hz), 5.96 (s, 2 H, 2-NH_2), 7.27-7.29 (d, 2 H, C_6H_4, J = 4.0 Hz), 7.79-7.81 (d, 2 H, C_6H_4, J = 4.0 Hz), 8.60-8.62 (d, 1 H, CONH, J = 4.0 Hz), 10.12 (s, 1 H, 3-NH), 10.80 (s, 1H, 7-NH).

Ethyl 4-(4-(4-(2-amino-4-oxo-4,7-dihydro-3*H*-pyrrolo[2,3-*d*]pyrimidin-6-yl)butyl)benzamido)butanoate (376):

Compound **376** was synthesized as described for **197**: yield 46% a colorless syrup, R_f = 0.52 ($CHCl_3$/MeOH, 5:1). ^{1}H NMR (DMSO-d_6) δ 1.14-1.18 (t, 3 H, CH_3, J = 7.0 Hz), 1.52-1.62 (m, 4 H, 2 CH_2), 1.74-1.78 (m, 2 H, CH_2), 2.31-2.35 (t, 2 H, CH_2, J = 7.0 Hz), 2.59-2.66 (m, 2 H, CH_2), 3.23-3.28 (m, 2 H, CH_2), 4.01-4.06 (q, 2 H, CH_2, J = 7.0 Hz), 5.83-5.84 (d, 1 H, CH, J = 1.0 Hz), 5.96 (s, 2 H, 2-NH_2), 7.25-7.27 (d, 2 H, C_6H_4, J = 4.0 Hz), 7.73-7.75 (d, 2 H, C_6H_4, J = 4.0 Hz), 8.38-8.41 (t, 1 H, CONH, J = 6.4 Hz), 10.12 (s, 1 H, 3-NH), 10.79 (s, 1H, 7-NH).

2-(4-(4-(2-amino-4-oxo-4,7-dihydro-3*H*-pyrrolo[2,3-*d*]pyrimidin-6-yl)butyl)benzamido)butanoic acid (198):

To a solution of the ester **375** (50 mg, 0.09 mmol) was added 1 N NaOH (5 mL), and the mixture was stirred under N_2 at room temperature for 1 h. TLC showed the disappearance of the starting material and formation of one major spot at the origin ($CHCl_3$/MeOH, 5:1). The reaction mixture was evaporated to dryness under reduced pressure. The residue was dissolved in water (5 mL), the resulting solution was cooled in an ice bath, and the pH was adjusted to 3-4 with dropwise addition of 1 N HCl. The resulting suspension was frozen in a dry ice/acetone bath, thawed in a refrigerator to 4-5 °C, and filtered. The residue was washed with a small amount of cold water and ethyl acetate and dried in vacuo using P_2O_5 to afford 35 mg (86%) **198** as a grey powder: mp 162-163 °C, R_f = 0.04 ($CHCl_3$/MeOH, 5:1). ^{1}H NMR (DMSO-d_6) δ 0.92-0.96 (t, 3 H, CH_3, J = 7.0 Hz), 1.50-1.63 (m, 4 H, 2 CH_2), 1.74-1.87 (m, 2 H, CH_2), 2.50-2.53 (m, 2 H, CH_2), 2.63-2.66 (t, 2 H, CH_2, J = 7.5 Hz), 4.25-4.32 (m, 1 H, CH), 5.83-5.84 (d, 1 H, CH, J = 1.0 Hz), 5.96 (s, 2 H, 2-NH_2), 7.27-7.29 (d, 2 H, C_6H_4, J = 4.0 Hz), 7.79-7.81 (d, 2 H, C_6H_4, J = 4.0 Hz), 8.44-8.46 (d, 1 H, CONH, J = 4.0 Hz), 10.12 (s, 1 H, 3-NH), 10.79 (s, 1H, 7-NH).

4-(4-(4-(2-amino-4-oxo-4,7-dihydro-3*H*-pyrrolo[2,3-*d*]pyrimidin-6-yl)butyl)benzamido)butanoic acid (199):

Compound **199** was synthesized from **376** as described for **198**: yield 90% as a grey powder: mp 148-149 °C decomposed, R_f = 0.04 ($CHCl_3$/MeOH, 5:1). ^{1}H NMR (DMSO-d_6) δ 1.52-1.62 (m, 4 H, 2 CH_2), 1.74-1.78 (m, 2 H, CH_2), 2.31-2.35 (t, 2 H, CH_2, J = 7.0 Hz), 2.59-2.66 (m, 2 H, CH_2), 3.23-3.28 (m, 2 H, CH_2), 5.83-5.84 (d, 1 H, CH, J = 1.0

Hz), 5.96 (s, 2 H, 2-NH_2), 7.25-7.27 (d, 2 H, C_6H_4, J = 4.0 Hz), 7.73-7.75 (d, 2 H, C_6H_4, J = 4.0 Hz), 8.38-8.41 (t, 1 H, CONH, J = 6.4 Hz), 10.12 (s, 1 H, 3-NH), 10.79 (s, 1H, 7-NH).

4-(5-(2-amino-4-oxo-4,7-dihydro-3*H*-pyrrolo[2,3-*d*]pyrimidin-6-yl)pentyl)-*N*-propylbenzamide (200):

Compound **200** was synthesized from **222** and **372** as described for **197**: yield 67% a colorless syrup, R_f = 0.56 ($CHCl_3$/MeOH, 5:1). ^{1}H NMR (DMSO-d_6) δ 0.85-0.88 (t, 3 H, CH_3, J = 7.0 Hz), 1.26-1.30 (m, 2 H, CH_2), 1.49-1.63 (m, 6 H, 3 CH_2), 2.42-2.46 (m, 2 H, CH_2), 2.57-2.61 (t, 2 H, CH_2, J = 7.5 Hz), 3.15-3.20 (m, 2 H, CH_2), 5.81-5.82 (d, 1 H, CH, J = 1.0 Hz), 5.94 (s, 2 H, 2-NH_2), 7.23-7.25 (d, 2 H, C_6H_4, J = 4.0 Hz), 7.71-7.73 (d, 2 H, C_6H_4, J = 4.0 Hz), 8.33-8.35 (t, 1 H, CONH, J = 6.4 Hz), 10.10 (s, 1 H, 3-NH), 10.77 (s, 1H, 7-NH).

Ethyl 4-(4-(5-(2-amino-4-oxo-4,7-dihydro-3*H*-pyrrolo[2,3-*d*]pyrimidin-6-yl)pentyl)benzamido)butanoate (377):

Compound **377** was synthesized from **222** and **374** as described for **197**: yield 56% a colorless syrup, R_f = 0.54 ($CHCl_3$/MeOH, 5:1). ^{1}H NMR (DMSO-d_6) δ 1.15-1.19 (t, 3 H, CH_3, J = 7.0 Hz), 1.28-1.32 (m, 2 H, CH_2), 1.58-1.61 (m, 4 H, 2 CH_2), 1.75-1.79 (m, 2 H, CH_2), 2.32-2.36 (t, 2 H, CH_2, J = 7.0 Hz), 2.59-2.63 (m, 2 H, CH_2), 3.23-3.28 (m, 2 H, CH_2), 4.01-4.06 (q, 2 H, CH_2, J = 7.0 Hz), 5.83-5.84 (d, 1 H, CH, J = 1.0 Hz), 5.95 (s, 2 H, 2-NH_2), 7.25-7.27 (d, 2 H, C_6H_4, J = 4.0 Hz), 7.73-7.75 (d, 2 H, C_6H_4, J = 4.0 Hz), 8.38-8.41 (t, 1 H, CONH, J = 6.4 Hz), 10.12 (s, 1 H, 3-NH), 10.78 (s, 1H, 7-NH).

4-(4-(5-(2-amino-4-oxo-4,7-dihydro-3*H*-pyrrolo[2,3-*d*]pyrimidin-6-yl)pentyl)benzamido)butanoic acid (200a):

Compound **200a** was synthesized from **377** as described for **198**: yield 91% as a grey powder: mp mp 136 °C decomposed, R_f = 0.04 ($CHCl_3$/MeOH, 5:1). ^{1}H NMR (DMSO-d_6) δ 1.28-1.32 (m, 2 H, CH_2), 1.58-1.61 (m, 4 H, 2 CH_2), 1.75-1.79 (m, 2 H, CH_2), 2.32-2.36 (t, 2 H, CH_2, J = 7.0 Hz), 2.59-2.63 (m, 2 H, CH_2), 3.23-3.28 (m, 2 H, CH_2), 5.83-5.84 (d, 1 H, CH, J = 1.0 Hz), 5.95 (s, 2 H, 2-NH_2), 7.25-7.27 (d, 2 H, C_6H_4, J = 4.0 Hz), 7.73-7.75 (d, 2 H, C_6H_4, J = 4.0 Hz), 8.38-8.41 (t, 1 H, CONH, J = 6.4 Hz), 10.12 (s, 1 H, 3-NH), 10.79 (s, 1H, 7-NH).

VII. BIBLIOGRAPHY

1. Jae Rin Suh, A. K. H., and Patrick J Stover. New perspectives on folate catabolism. . *Annu. Rev. Nutr.* **2001,** 21, 255-282.

2. Stokstad, E. L. R. Historical perspective on key advances in the biochemistry and physiology of folates. *Contemp. Issues Clin. Nutr.* **1990,** 13, 1-21.

3. Matherly, L. H.; Goldman, I. D. Membrane transport of folates. *Vitam. Horm.* **2003,** 66, 403-456.

4. Matherly, L. H.; Hou, Z.; Deng, Y. Human reduced folate carrier: Translation of basic biology to cancer etiology and therapy. *Cancer Metastasis Rev.* **2007,** 26, 111-128.

5. Goldman, I. D.; Chattopadhyay, S.; Zhao, R.; Moran, R. The antifolates: evolution, new agents in the clinic, and how targeting delivery via specific membrane transporters is driving the development of a next generation of folate analogs. *Curr. Opin. Invest. Drugs (BioMed Cent.)* **2010,** 11, 1409-1423.

6. Hagner, N.; Joerger, M. Cancer chemotherapy: targeting folic acid synthesis. *Cancer Manage. Res.* **2010,** 2, 293-301.

7. Wright, D. L.; Anderson, A. C. Antifolate agents: a patent review (2006 - 2010). *Expert Opin. Ther. Pat.* **2011,** 21, 1293-1308.

8. Gonen, N.; Assaraf, Y. G. Antifolates in cancer therapy: Structure, activity and mechanisms of drug resistance. *Drug Resist. Updates* **2012,** 15, 183-210.

9. Visentin, M.; Zhao, R.; Goldman, I. D. The antifolates. *Hematol Oncol Clin North Am* **2012,** 26, 629-48, ix.

10. Qiu, A.; Jansen, M.; Sakaris, A.; Min, S. H.; Chattopadhyay, S.; Tsai, E.; Sandoval, C.; Zhao, R.; Akabas, M. H.; Goldman, I. D. Identification of an intestinal

folate transporter and the molecular basis for hereditary folate malabsorption. *Cell* **2006,** 127, 917-928.

11. Said, H. M.; Chatterjee, N.; Haq, R. U.; Subramanian, V. S.; Ortiz, A.; Matherly, L. H.; Sirotnak, F. M.; Halsted, C.; Rubin, S. A. Adaptive regulation of intestinal folate uptake: effect of dietary folate deficiency. *Am. J. Physiol.* **2000,** 279, C1889-C1895.

12. Subramanian, V. S.; Chatterjee, N.; Said, H. M. Folate uptake in the human intestine: Promoter activity and effect of folate deficiency. *J. Cell. Physiol.* **2003,** 196, 403-408.

13. Ashokkumar, B.; Mohammed, Z. M.; Vaziri, N. D.; Said, H. M. Effect of folate oversupplementation on folate uptake by human intestinal and renal epithelial cells. *Am. J. Clin. Nutr.* **2007,** 86, 159-166.

14. Ahmad, S. I.; Kirk, S. H.; Eisenstark, A. Thymine metabolism and thymineless death in prokaryotes and eukaryotes. *Annu. Rev. Microbiol.* **1998,** 52, 591-625.

15. Sangurdekar, D. P.; Hamann, B. L.; Smirnov, D.; Srienc, F.; Hanawalt, P. C.; Khodursky, A. B. Thymineless death is associated with loss of essential genetic information from the replication origin. *Mol. Microbiol.* **2010,** 75, 1455-1467.

16. Kompis, I. M.; Islam, K.; Then, R. L. DNA and RNA Synthesis: Antifolates. *Chem. Rev. (Washington, DC, U. S.)* **2005,** 105, 593-620.

17. Berger, F. G.; Berger, S. H. Thymidylate synthase as a chemotherapeutic drug target. Where are we after fifty years? *Cancer Biol. Ther.* **2006,** 5, 1238-1241.

18. Longley, D. B.; Harkin, D. P.; Johnston, P. G. 5-Fluorouracil: mechanisms of action and clinical strategies. *Nat Rev Cancer* **2003,** 3, 330-338.

19. Barner, H. D.; Cohen, S. S. The induction of thymine synthesis by T2 infection of

a thymine-requiring mutant of Escherichia coli. *J. Bacteriol.* **1954,** 68, 80-8.

20. Cohen, S. S.; Barner, H. D. Unbalanced growth in Escherichia coli. *Proc. Natl. Acad. Sci. U. S. A.* **1954,** 40, 885-93.

21. Barner, H. D.; Cohen, S. S. The isolation and properties of amino acid-requiring mutants of a thymineless bacterium. *J. Bacteriol.* **1957,** 74, 350-5.

22. Bazill, G. W. Lethal Unbalanced Growth in Bacteria. *Nature* **1967,** 216, 346-349.

23. Sangurdekar, D. P.; Hamann, B. L.; Smirnov, D.; Srienc, F.; Hanawalt, P. C.; Khodursky, A. B. Thymineless death is associated with loss of essential genetic information from the replication origin. *Mol. Microbiol.* **2010,** 75, 1455-67.

24. Houghton, P. J. In *Thymineless death*, 1999; Humana: 1999; pp 423-435.

25. Keszler, G.; Spasokoukotskaja, T.; Csapo, Z.; Virga, S.; Staub, M.; Sasvari-Szekely, M. Selective Increase of dATP Pools upon Activation of Deoxycytidine Kinase in Lymphocytes: Implications in Apoptosis. *Nucleosides, Nucleotides Nucleic Acids* **2004,** 23, 1335-1342.

26. Celtikci, B.; Lawrance, A. K.; Wu, Q.; Rozen, R. Methotrexate-induced apoptosis is enhanced by altered expression of methylenetetrahydrofolate reductase. *Anti-Cancer Drugs* **2009,** 20, 787-793.

27. Roth, B. Design of dihydrofolate reductase inhibitors from x-ray crystal structures. *Fed. Proc.* **1986,** 45, 2765-72.

28. Costi, M. P.; Ferrari, S. Update on antifolate drugs targets. *Curr. Drug Targets* **2001,** 2, 135-166.

29. Carreras, C. W.; Santi, D. V. The catalytic mechanism and structure of thymidylate synthase. *Annu. Rev. Biochem.* **1995,** 64, 721-62.

30. Warren, M. S.; Mattia, K. M.; Marolewski, A. E.; Benkovic, S. J. The transformylase enzymes of de novo purine biosynthesis. *Pure Appl. Chem.* **1996,** 68, 2029-2036.

31. Calvert, H. An overview of folate metabolism: features relevant to the action and toxicities of antifolate anticancer agents. *Semin. Oncol.* **1999,** 26, 3-10.

32. Jansen, G. In *Receptor- and carrier-mediated transport systems for folates and antifolates: exploitation for folate-based chemotherapy and immunotherapy*, 1999; Humana: 1999; pp 293-321.

33. Brzezinska, A.; Winska, P.; Balinska, M. Cellular aspects of folate and antifolate membrane transport. *Acta Biochim. Pol.* **2000,** 47, 735-749.

34. Moran, R. G. Roles of folylpoly-γ-glutamate synthetase in therapeutics with tetrahydrofolate antimetabolites: an overview. *Semin. Oncol.* **1999,** 26, 24-32.

35. Yao, R.; Schneider, E.; Ryan, T. J.; Galivan, J. Human γ-glutamyl hydrolase: cloning and characterization of the enzyme expressed in vitro. *Proc. Natl. Acad. Sci. U. S. A.* **1996,** 93, 10134-10138.

36. Hooijberg, J. H.; Broxterman, H. J.; Kool, M.; Assaraf, Y. G.; Peters, G. J.; Noordhuis, P.; Scheper, R. J.; Borst, P.; Pinedo, H. M.; Jansen, G. Antifolate resistance mediated by the multidrug resistance proteins MRP1 and MRP2. *Cancer Res.* **1999,** 59, 2532-2535.

37. DeGraw, J. I.; Colwell, W. T.; Piper, J. R.; Sirotnak, F. M.; Smith, R. L. New analogs of methotrexate in cancer and arthritis. *Curr. Med. Chem.* **1995,** 2, 630-53.

38. Huennekens, F. M.; Duffy, T. H.; Vitols, K. S. Folic acid metabolism and its disruption by pharmacologic agents. *NCI Monogr* **1987**, 1-8.

39. Berman, E. M.; Werbel, L. M. The renewed potential for folate antagonists in contemporary cancer chemotherapy. *J. Med. Chem.* **1991,** 34, 479-85.

40. Weinstein, G. D. Biochemical and pathophysiological rationale for amethopterin in psoriasis. *Ann. N. Y. Acad. Sci.* **1971,** 186, 452-66.

41. Gangjee, A.; Jain, H. D.; Kurup, S. Recent advances in classical and non-classical antifolates as antitumor and antiopportunistic infection agents: part I. *Anti-Cancer Agents Med. Chem.* **2007,** 7, 524-542.

42. Gangjee, A.; Jain, H. D.; Kurup, S. Recent advances in classical and non-classical antifolates as antitumor and antiopportunistic infection agents: Part II. *Anti-Cancer Agents Med. Chem.* **2008,** 8, 205-231.

43. Gangjee, A.; Dubash, N. P.; Zeng, Y.; McGuire, J. J. Recent advances in the chemistry and biology of folypoly-gamma-glutamate synthetase substrates and inhibitors. *Current medicinal chemistry. Anti-cancer agents* **2002,** 2, 331-55.

44. Gangjee, A.; Elzein, E.; Kothare, M.; Vasudevan, A. Classical and nonclassical antifolates as potential antitumor, antipneumocystis and antitoxoplasma agents. *Curr. Pharm. Des.* **1996,** 2, 263-280.

45. Jackson, R. C. In *Antifolate drugs: past and future perspectives*, 1999; Humana: 1999; pp 1-12.

46. Matherly, L. H.; Goldman, D. I. Membrane transport of folates. *Vitam. Horm.* **2003,** 66, 403-56.

47. Matherly, L. H.; Hou, Z.; Deng, Y. Human reduced folate carrier: translation of basic biology to cancer etiology and therapy. *Cancer Metastasis Rev.* **2007,** 26, 111-28.

48. Zhao, R.; Matherly, L. H.; Goldman, I. D. Membrane transporters and folate

homeostasis: intestinal absorption and transport into systemic compartments and tissues. *Expert Rev Mol Med* **2009,** 11, e4.

49. Elnakat, H.; Ratnam, M. Distribution, functionality and gene regulation of folate receptor isoforms: implications in targeted therapy. *Adv. Drug Delivery Rev.* **2004,** 56, 1067-1084.

50. Zhao, R.; Goldman, I. D. The molecular identity and characterization of a Proton-Coupled Folate Transporter-PCFT; biological ramifications and impact on the activity of pemetrexed-12 06 06. *Cancer Metastasis Rev.* **2007,** 26, 129-139.

51. Umapathy, N. S.; Gnana-Prakasam, J. P.; Martin, P. M.; Mysona, B.; Dun, Y.; Smith, S. B.; Ganapathy, V.; Prasad, P. D. Cloning and functional characterization of the proton-coupled electrogenic folate transporter and analysis of its expression in retinal cell types. *Invest. Ophthalmol. Vis. Sci.* **2007,** 48, 5299-305.

52. Nakai, Y.; Inoue, K.; Abe, N.; Hatakeyama, M.; Ohta, K.-y.; Otagiri, M.; Hayashi, Y.; Yuasa, H. Functional characterization of human proton-coupled folate transporter/heme carrier protein 1 heterologously expressed in mammalian cells as a folate transporter. *J. Pharmacol. Exp. Ther.* **2007,** 322, 469-476.

53. Goldman, I. D.; Matherly, L. H. The cellular pharmacology of methotrexate. *Pharmacol. Ther.* **1985,** 28, 77-102.

54. Goldman, I. D.; Zhao, R. Molecular, biochemical, and cellular pharmacology of pemetrexed. *Semin. Oncol.* **2002,** 29, 3-17.

55. Goldman, I. D.; Lichtenstein, N. S.; Oliverio, V. T. Carrier-mediated transport of the folic acid analog, methotrexate, in the L1210 leukemia cell. *J. Biol. Chem.* **1968,** 243, 5007-17.

56. Desmoulin, S. K.; Hou, Z.; Gangjee, A.; Matherly, L. H. The human proton-coupled folate transporter: Biology and therapeutic applications to cancer. *Cancer Biology & Therapy* **2012,** 13, 1355-1373.

57. Cao, W.; Matherly, L. H. Analysis of the membrane topology for transmembrane domains 7-12 of the human reduced folate carrier by scanning cysteine accessibility methods. *Biochem. J.* **2004,** 378, 201-206.

58. Ferguson, P. L.; Flintoff, W. F. Topological and functional analysis of the human reduced folate carrier by hemagglutinin epitope insertion. *J. Biol. Chem.* **1999,** 274, 16269-16278.

59. Liu, X. Y.; Matherly, L. H. Analysis of membrane topology of the human reduced folate carrier protein by hemagglutinin epitope insertion and scanning glycosylation insertion mutagenesis. *Biochim. Biophys. Acta, Biomembr.* **2002,** 1564, 333-342.

60. Wong, S. C.; Zhang, L.; Proefke, S. A.; Matherly, L. H. Effects of the loss of capacity for N-glycosylation on the transport activity and cellular localization of the human reduced folate carrier. *Biochim. Biophys. Acta, Biomembr.* **1998,** 1375, 6-12.

61. Liu, X. Y.; Witt, T. L.; Matherly, L. H. Restoration of high-level transport activity by human reduced folate carrier/ThTr1 thiamine transporter chimaeras: role of the transmembrane domain 6/7 linker region in reduced folate carrier function. *Biochem. J.* **2003,** 369, 31-37.

62. Zhao, R.; Diop-Bove, N.; Visentin, M.; Goldman, I. D. Mechanisms of membrane transport of folates into cells and across epithelia. *Annu. Rev. Nutr.* **2011,** 31, 177-201, 5 plates.

63. Whetstine, J. R.; Flatley, R. M.; Matherly, L. H. The human reduced folate carrier

gene is ubiquitously and differentially expressed in normal human tissues: identification of seven non-coding exons and characterization of a novel promoter. *Biochem. J.* **2002,** 367, 629-640.

64. Zhao, R.; Russell, R. G.; Wang, Y.; Liu, L.; Gao, F.; Kneitz, B.; Edelmann, W.; Goldman, I. D. Rescue of embryonic lethality in reduced folate carrier-deficient mice by maternal folic acid supplementation reveals early neonatal failure of hematopoietic organs. *J. Biol. Chem.* **2001,** 276, 10224-10228.

65. Liu, M.; Ge, Y.; Cabelof, D. C.; Aboukameel, A.; Heydari, A. R.; Mohammad, R.; Matherly, L. H. Structure and Regulation of the Murine Reduced Folate Carrier Gene: identification of four noncoding exons and promoters and regulation by dietary folates. *J. Biol. Chem.* **2005,** 280, 5588-5597.

66. Henderson, G. B.; Zevely, E. M. Structural requirements for anion substrates of the methotrexate transport system in L1210 cells. *Arch. Biochem. Biophys.* **1983,** 221, 438-46.

67. Goldman, I. D. Characteristics of the membrane transportof amethopterin and the naturally occurring folates. *Ann. N. Y. Acad. Sci.* **1971,** 186, 400-22.

68. Goldman, I. D.; Matherly, L. H. The cellular pharmacology of methotrexate. *Pharmacol. Ther.* **1985,** 28, 77-102.

69. Fischer, G. A. Defective transport of amethopterin (methotrexate) as a mechanism of resistance to the antimetabolite in L 5178 Y leukemic cells. *Biochem. Pharmacol.* **1962,** 11, 1233-4.

70. Zhao, R.; Goldman, I. D. Resistance to antifolates. *Oncogene* **2003,** 22, 7431-7457.

71. Zhao, R.; Chattopadhyay, S.; Hanscom, M.; Goldman, I. D. Antifolate Resistance in a HeLa Cell Line Associated With Impaired Transport Independent of the Reduced Folate Carrier. *Clin. Cancer Res.* **2004,** 10, 8735-8742.

72. Ragoussis, J.; Senger, G.; Trowsdale, J.; Campbell, I. G. Genomic organization of the human folate receptor genes on chromosome 11q13. *Genomics* **1992,** 14, 423-30.

73. Salazar, M. D. A.; Ratnam, M. The folate receptor: What does it promise in tissue-targeted therapeutics? *Cancer Metastasis Rev.* **2007,** 26, 141-152.

74. Chancy, C. D.; Kekuda, R.; Huang, W.; Prasad, P. D.; Kuhnel, J.-M.; Sirotnak, F. M.; Roon, P.; Ganapathy, V.; Smith, S. B. Expression and differential polarization of the reduced-folate transporter-1 and the folate receptor α in mammalian retinal pigment epithelium. *J. Biol. Chem.* **2000,** 275, 20676-20684.

75. Weitman, S. D.; Weinberg, A. G.; Coney, L. R.; Zurawski, V. R.; Jennings, D. S.; Kamen, B. A. Cellular localization of the folate receptor: potential role in drug toxicity and folate homeostasis. *Cancer Res.* **1992,** 52, 6708-11.

76. Ratnam, M.; Marquardt, H.; Duhring, J. L.; Freisheim, J. H. Homologous membrane folate binding proteins in human placenta: cloning and sequence of a cDNA. *Biochemistry* **1989,** 28, 8249-54.

77. Wang, H.; Zheng, X.; Behm, F. G.; Ratnam, M. Differentiation-independent retinoid induction of folate receptor type β, a potential tumor target in myeloid leukemia. *Blood* **2000,** 96, 3529-3536.

78. Reddy, J. A.; Haneline, L. S.; Srour, E. F.; Antony, A. C.; Clapp, D. W.; Low, P. S. Expression and functional characterization of the β-isoform of the folate receptor on CD34+ cells. *Blood* **1999,** 93, 3940-3948.

79. Ross, J. F.; Wang, H.; Behm, F. G.; Mathew, P.; Wu, M.; Booth, R.; Ratnam, M. Folate receptor type β is a neutrophilic lineage marker and is differentially expressed in myeloid leukemia. *Cancer* **1999,** 85, 348-357.

80. Pan, X. Q.; Zheng, X.; Shi, G.; Wang, H.; Ratnam, M.; Lee, R. J. Strategy for the treatment of acute myelogenous leukemia based on folate receptor β-targeted liposomal doxorubicin combined with receptor induction by all-trans-retinoic acid. *Blood* **2002,** 100, 594-602.

81. Wu, M.; Gunning, W.; Ratnam, M. Expression of folate receptor type alpha in relation to cell type, malignancy, and differentiation in ovary, uterus, and cervix. *Cancer Epidemiol Biomarkers Prev* **1999,** 8, 775-82.

82. Ross, J. F.; Chaudhuri, P. K.; Ratnam, M. Differential regulation of folate receptor isoforms in normal and malignant tissues in vivo and in established cell lines. Physiologic and clinical implications. *Cancer* **1994,** 73, 2432-43.

83. Yang, J.; Vlashi, E.; Low, P. Folate-linked drugs for the treatment of cancer and inflammatory diseases. *Subcell. Biochem.* **2012,** 56, 163-179.

84. Kamen, B. A.; Smith, A. K. A review of folate receptor alpha cycling and 5-methyltetrahydrofolate accumulation with an emphasis on cell models in vitro. *Adv. Drug Delivery Rev.* **2004,** 56, 1085-1097.

85. Lu, Y.; Low, P. S. Folate-mediated delivery of macromolecular anticancer therapeutic agents. *Adv. Drug Delivery Rev.* **2002,** 54, 675-693.

86. Kamen, B. A.; Wang, M. T.; Streckfuss, A. J.; Peryea, X.; Anderson, R. G. W. Delivery of folates to the cytoplasm of MA104 cells is mediated by a surface membrane receptor that recycles. *J. Biol. Chem.* **1988,** 263, 13602-9.

87. Rothberg, K. G.; Ying, Y.; Kolhouse, J. F.; Kamen, B. A.; Anderson, R. G. W. The glycophospholipid-linked folate receptor internalizes folate without entering the clathrin-coated pit endocytic pathway. *J. Cell Biol.* **1990,** 110, 637-49.

88. Yang, J.; Chen, H.; Vlahov, I. R.; Cheng, J.-X.; Low, P. S. Characterization of the pH of folate receptor-containing endosomes and the rate of hydrolysis of internalized acid-labile folate-drug conjugates. *J. Pharmacol. Exp. Ther.* **2007,** 321, 462-468.

89. Kamen, B. A.; Smith, A. K.; Anderson, R. G. W. The folate receptor works in tandem with a probenecid-sensitive carrier in MA104 cells in vitro. *J. Clin. Invest.* **1991,** 87, 1442-9.

90. Prasad, P. D.; Mahesh, V. B.; Leibach, F. H.; Ganapathy, V. Functional coupling between a bafilomycin A1-sensitive proton pump and a probenecid-sensitive folate transporter in human placental choriocarcinoma cells. *Biochim. Biophys. Acta, Mol. Cell Res.* **1994,** 1222, 309-14.

91. Toffoli, G.; Cernigoi, C.; Russo, A.; Gallo, A.; Bagnoli, M.; Boiocchi, M. Overexpression of folate binding protein in ovarian cancers. *Int. J. Cancer* **1997,** 74, 193-198.

92. Inoue, K.; Nakai, Y.; Ueda, S.; Kamigaso, S.; Ohta, K.-y.; Hatakeyama, M.; Hayashi, Y.; Otagiri, M.; Yuasa, H. Functional characterization of PCFT/HCP1 as the molecular entity of the carrier-mediated intestinal folate transport system in the rat model. *Am. J. Physiol.* **2008,** 294, G660-G668.

93. Qiu, A.; Min, S. H.; Jansen, M.; Malhotra, U.; Tsai, E.; Cabelof, D. C.; Matherly, L. H.; Zhao, R.; Akabas, M. H.; Goldman, I. D. Rodent intestinal folate transporters (SLC46A1): secondary structure, functional properties, and response to dietary folate

restriction. *Am. J. Physiol.* **2007,** 293, C1669-C1678.

94. Unal, E. S.; Zhao, R.; Qiu, A.; Goldman, I. D. N-linked glycosylation and its impact on the electrophoretic mobility and function of the human proton-coupled folate transporter (HsPCFT). *Biochim Biophys Acta* **2008,** 1778, 1407-14.

95. Zhao, R.; Unal, E. S.; Shin, D. S.; Goldman, I. D. Membrane Topological Analysis of the Proton-Coupled Folate Transporter (PCFT-SLC46A1) by the Substituted Cysteine Accessibility Method. *Biochemistry* **2010,** 49, 2925-2931.

96. Wollack, J. B.; Makori, B.; Ahlawat, S.; Koneru, R.; Picinich, S. C.; Smith, A.; Goldman, I. D.; Qiu, A.; Cole, P. D.; Glod, J.; Kamen, B. Characterization of folate uptake by choroid plexus epithelial cells in a rat primary culture model. *J. Neurochem.* **2008,** 104, 1494-1503.

97. Zhao, R.; Qiu, A.; Tsai, E.; Jansen, M.; Akabas, M. H.; Goldman, I. D. The proton-coupled folate transporter: impact on pemetrexed transport and on antifolates activities compared with the reduced folate carrier. *Mol. Pharmacol.* **2008,** 74, 854-862.

98. Qiu, A.; Jansen, M.; Sakaris, A.; Min, S. H.; Chattopadhyay, S.; Tsai, E.; Sandoval, C.; Zhao, R.; Akabas, M. H.; Goldman, I. D. Identification of an intestinal folate transporter and the molecular basis for hereditary folate malabsorption. *Cell* **2006,** 127, 917-28.

99. Qiu, A.; Min, S. H.; Jansen, M.; Malhotra, U.; Tsai, E.; Cabelof, D. C.; Matherly, L. H.; Zhao, R.; Akabas, M. H.; Goldman, I. D. Rodent intestinal folate transporters (SLC46A1): secondary structure, functional properties, and response to dietary folate restriction. *Am. J. Physiol. Cell Physiol.* **2007,** 293, C1669-78.

100. Zhao, R.; Qiu, A.; Tsai, E.; Jansen, M.; Akabas, M. H.; Goldman, I. D. The

proton-coupled folate transporter: impact on pemetrexed transport and on antifolates activities compared with the reduced folate carrier. *Mol. Pharmacol.* **2008,** 74, 854-62.

101. Schron, C. M.; Washington, C., Jr.; Blitzer, B. L. The transmembrane pH gradient drives uphill folate transport in rabbit jejunum. Direct evidence for folate/hydroxyl exchange in brush border membrane vesicles. *J. Clin. Invest.* **1985,** 76, 2030-3.

102. Helmlinger, G.; Yuan, F.; Dellian, M.; Jain, R. K. Interstitial pH and pO2 gradients in solid tumors in vivo: High-resolution measurements reveal a lack of correlation. *Nat. Med. (N. Y.)* **1997,** 3, 177-182.

103. Raghunand, N.; Altbach, M. I.; Van, S. R.; Baggett, B.; Taylor, C. W.; Bhujwalla, Z. M.; Gillies, R. J. Plasmalemmal pH-gradients in drug-sensitive and drug-resistant MCF-7 human breast carcinoma xenografts measured by 31P magnetic resonance spectroscopy. *Biochem. Pharmacol.* **1999,** 57, 309-312.

104. Zhao, R.; Gao, F.; Hanscom, M.; Goldman, I. D. A prominent low-pH methotrexate transport activity in human solid tumors: contribution to the preservation of methotrexate pharmacologic activity in HeLa cells lacking the reduced folate carrier. *Clin. Cancer Res.* **2004,** 10, 718-727.

105. Salazar, M. D.; Ratnam, M. The folate receptor: what does it promise in tissue-targeted therapeutics? *Cancer Metastasis Rev.* **2007,** 26, 141-52.

106. Hilgenbrink, A. R.; Low, P. S. Folate receptor-mediated drug targeting: from therapeutics to diagnostics. *J. Pharm. Sci.* **2005,** 94, 2135-46.

107. Jansen, G. Receptor- and Carrier-Mediated Transport Systems for Folates and Antifolates. Exploitation for Folate Chemotherapy and Immunotherapy. In *Anticancer Development Guide: Antifolate Drugs in Cancer Therapy*, Jackman, A. L., Ed. Humana

Press Inc.: Totowa, NJ, 1999; pp 293-321.

108. Jackman, A. L.; Theti, D. S.; Gibbs, D. D. Antifolates targeted specifically to the folate receptor. *Adv. Drug Deliv. Rev.* **2004,** 56, 1111-25.

109. Deng, Y.; Wang, Y.; Cherian, C.; Hou, Z.; Buck, S. A.; Matherly, L. H.; Gangjee, A. Synthesis and Discovery of High Affinity Folate Receptor-Specific Glycinamide Ribonucleotide Formyltransferase Inhibitors with Antitumor Activity. *J. Med. Chem.* **2008,** 51, 5052-5063.

110. Gibbs, D. D.; Theti, D. S.; Wood, N.; Green, M.; Raynaud, F.; Valenti, M.; Forster, M. D.; Mitchell, F.; Bavetsias, V.; Henderson, E.; Jackman, A. L. BGC 945, a Novel Tumor-Selective Thymidylate Synthase Inhibitor Targeted to α-Folate Receptor-Overexpressing Tumors. *Cancer Res.* **2005,** 65, 11721-11728.

111. Theti, D. S.; Bavetsias, V.; Skelton, L. A.; Titley, J.; Gibbs, D.; Jansen, G.; Jackman, A. L. Selective Delivery of CB300638, a Cyclopenta[g]quinazoline-based Thymidylate Synthase Inhibitor into Human Tumor Cell Lines Overexpressing the α-Isoform of the Folate Receptor. *Cancer Res.* **2003,** 63, 3612-3618.

112. Deng, Y.; Zhou, X.; Desmoulin, S. K.; Wu, J.; Cherian, C.; Hou, Z.; Matherly, L. H.; Gangjee, A. Synthesis and Biological Activity of a Novel Series of 6-Substituted Thieno[2,3-d]pyrimidine Antifolate Inhibitors of Purine Biosynthesis with Selectivity for High Affinity Folate Receptors over the Reduced Folate Carrier and Proton-Coupled Folate Transporter for Cellular Entry. *J. Med. Chem.* **2009,** 52, 2940-2951.

113. Wang, L.; Cherian, C.; Desmoulin, S. K.; Polin, L.; Deng, Y.; Wu, J.; Hou, Z.; White, K.; Kushner, J.; Matherly, L. H.; Gangjee, A. Synthesis and Antitumor Activity of a Novel Series of 6-Substituted Pyrrolo[2,3-d]pyrimidine Thienoyl Antifolate Inhibitors

of Purine Biosynthesis with Selectivity for High Affinity Folate Receptors and the Proton-Coupled Folate Transporter over the Reduced Folate Carrier for Cellular Entry. *J. Med. Chem.* **2010,** 53, 1306-1318.

114. Desmoulin, S. K.; Wang, Y.; Wu, J.; Stout, M.; Hou, Z.; Fulterer, A.; Chang, M.-H.; Romero, M. F.; Cherian, C.; Gangjee, A.; Matherly, L. H. Targeting the proton-coupled folate transporter for selective delivery of 6-substituted pyrrolo[2,3-d]pyrimidine antifolate inhibitors of de novo purine biosynthesis in the chemotherapy of solid tumors. *Mol. Pharmacol.* **2010,** 78, 577-587.

115. Wang, L. Ph.D. dissertation. Duquesne University, **2010**, 352-353.

116. Wang, L.; Cherian, C.; Desmoulin, S. K.; Mitchell-Ryan, S.; Hou, Z.; Matherly, L. H.; Gangjee, A. Synthesis and biological activity of 6-substituted pyrrolo[2,3-d]pyrimidine thienoyl regioisomers as inhibitors of de novo purine biosynthesis with selectivity for cellular uptake by high affinity folate receptors and the proton-coupled folate transporter over the reduced folate carrier. *J. Med. Chem.* **2012,** 55, 1758-1770.

117. Warren, L.; Buchanan, J. M. Biosynthesis of the purines. XIX. 2-Amino-N-ribosylacetamide 5'-phosphate (glycinamide ribotide) transformylase. *J Biol Chem* **1957,** 229, 613-26.

118. Moran, R. G. In *Folate antimetabolites inhibitory to de novo purine synthesis*, 1991; Kluwer: **1991**; pp 65-87.

119. Beardsley, G. P.; Moroson, B. A.; Taylor, E. C.; Moran, R. G. A new folate antimetabolite, 5,10-dideaza-5,6,7,8-tetrahydrofolate is a potent inhibitor of de novo purine synthesis. *J. Biol. Chem.* **1989,** 264, 328-33.

120. Shim, J. H.; Benkovic, S. J. Evaluation of the Kinetic Mechanism of Escherichia

coli Glycinamide Ribonucleotide Transformylase. *Biochemistry* **1998,** 37, 8776-8782.

121. Shim, J. H.; Benkovic, S. J. Catalytic Mechanism of Escherichia coli Glycinamide Ribonucleotide Transformylase Probed by Site-Directed Mutagenesis and pH-Dependent Studies. *Biochemistry* **1999,** 38, 10024-10031.

122. Poch, M. T.; Qin, W.; Caperelli, C. A. The human trifunctional enzyme of de novo purine biosynthesis: heterologous expression, purification, and preliminary characterization. *Protein Expression Purif.* **1998,** 12, 17-24.

123. Klein, C.; Chen, P.; Arevalo, J. H.; Stura, E. A.; Marolewski, A.; Warren, M. S.; Benkovic, S. J.; Wilson, I. A. Towards structure-based drug design: crystal structure of a multisubstrate adduct complex of glycinamide ribonucleotide transformylase at 1.96 Å resolution. *J. Mol. Biol.* **1995,** 249, 153-75.

124. Almassy, R. J.; Janson, C. A.; Kan, C. C.; Hostomska, Z. Structures of apo and complexed Escherichia coli glycinamide ribonucleotide transformylase. *Proc. Natl. Acad. Sci. U. S. A.* **1992,** 89, 6114-18.

125. Greasley, S. E.; Yamashita, M. M.; Cai, H.; Benkovic, S. J.; Boger, D. L.; Wilson, I. A. New Insights into Inhibitor Design from the Crystal Structure and NMR Studies of Escherichia coli GAR Transformylase in Complex with β-GAR and 10-Formyl-5,8,10-trideazafolic Acid. *Biochemistry* **1999,** 38, 16783-16793.

126. Zhang, Y.; Desharnais, J.; Greasley, S. E.; Beardsley, G. P.; Boger, D. L.; Wilson, I. A. Crystal Structures of Human GAR Tfase at Low and High pH and with Substrate β-GAR. *Biochemistry* **2002,** 41, 14206-14215.

127. Taylor, E. C.; Harrington, P. J.; Fletcher, S. R.; Beardsley, G. P.; Moran, R. G. Synthesis of the antileukemic agents 5,10-dideazaaminopterin and 5,10-dideaza-5,6,7,8-

tetrahydroaminopterin. *J. Med. Chem.* **1985,** 28, 914-21.

128. Boger, D. L.; Haynes, N. E.; Kitos, P. A.; Warren, M. S.; Ramcharan, J.; Marolewski, A. E.; Benkovic, S. J. 10-Formyl-5,8,10-trideazafolic acid (10-formyl-TDAF): a potent inhibitor of glycinamide ribonucleotide transformylase. *Bioorg. Med. Chem.* **1997,** 5, 1817-30.

129. Boger, D. L.; Haynes, N. E.; Warren, M. S.; Gooljarsingh, L. T.; Ramcharan, J.; Kitos, P. A.; Benkovic, S. J. Functionalized analogues of 5,8,10-trideazafolate as potential inhibitors of GAR Tfase or AICAR Tfase. *Bioorg. Med. Chem.* **1997,** 5, 1831-8.

130. Boger, D. L.; Haynes, N. E.; Warren, M. S.; Ramcharan, J.; Kitos, P. A.; Benkovic, S. J. Multisubstrate analogue based on 5,8,10-trideazafolate. *Bioorg. Med. Chem.* **1997,** 5, 1853-7.

131. Boger, D. L.; Haynes, N. E.; Warren, M. S.; Ramcharan, J.; Kitos, P. A.; Benkovic, S. J. Functionalized analogues of 5,8,10-trideazafolate: development of an enzyme-assembled tight binding inhibitor of GAR Tfase and a potential irreversible inhibitor of AICAR Tfase. *Bioorg. Med. Chem.* **1997,** 5, 1839-46.

132. Boger, D. L.; Haynes, N. E.; Warren, M. S.; Ramcharan, J.; Marolewski, A. E.; Kitos, P. A.; Benkovic, S. J. Abenzyl 10-formyl-trideazafolic acid (abenzyl 10-formyl-TDAF): an effective inhibitor of glycinamide ribonucleotide transformylase. *Bioorg. Med. Chem.* **1997,** 5, 1847-52.

133. Varney, M. D.; Palmer, C. L.; Romines, W. H., 3rd; Boritzki, T.; Margosiak, S. A.; Almassy, R.; Janson, C. A.; Bartlett, C.; Howland, E. J.; Ferre, R. Protein structure-based design, synthesis, and biological evaluation of 5-thia-2,6-diamino-4(3H)-oxopyrimidines: potent inhibitors of glycinamide ribonucleotide transformylase with

potent cell growth inhibition. *J. Med. Chem.* **1997,** 40, 2502-24.

134. Marsilje, T. H.; Labroli, M. A.; Hedrick, M. P.; Jin, Q.; Desharnais, J.; Baker, S. J.; Gooljarsingh, L. T.; Ramcharan, J.; Tavassoli, A.; Zhang, Y.; Wilson, I. A.; Beardsley, G. P.; Benkovic, S. J.; Boger, D. L. 10-Formyl-5,10-dideaza-acyclic-5,6,7,8-tetrahydrofolic acid (10-formyl-DDACTHF): a potent cytotoxic agent acting by selective inhibition of human GAR Tfase and the de novo purine biosynthetic pathway. *Bioorg. Med. Chem.* **2002,** 10, 2739-49.

135. Deng, Y.; Wang, Y.; Cherian, C.; Hou, Z.; Buck, S. A.; Matherly, L. H.; Gangjee, A. Synthesis and discovery of high affinity folate receptor-specific glycinamide ribonucleotide formyltransferase inhibitors with antitumor activity. *J. Med. Chem.* **2008,** 51, 5052-63.

136. Deng, Y.; Zhou, X.; Kugel Desmoulin, S.; Wu, J.; Cherian, C.; Hou, Z.; Matherly, L. H.; Gangjee, A. Synthesis and biological activity of a novel series of 6-substituted thieno[2,3-*d*]pyrimidine antifolate inhibitors of purine biosynthesis with selectivity for high affinity folate receptors over the reduced folate carrier and proton-coupled folate transporter for cellular entry. *J. Med. Chem.* **2009,** 52, 2940-51.

137. Wang, L.; Cherian, C.; Desmoulin, S. K.; Polin, L.; Deng, Y.; Wu, J.; Hou, Z.; White, K.; Kushner, J.; Matherly, L. H.; Gangjee, A. Synthesis and antitumor activity of a novel series of 6-substituted pyrrolo[2,3-*d*]pyrimidine thienoyl antifolate inhibitors of purine biosynthesis with selectivity for high affinity folate receptors and the proton-coupled folate transporter over the reduced folate carrier for cellular entry. *J. Med. Chem.* **2010,** 53, 1306-18.

138. Aimi, J.; Qiu, H.; Williams, J.; Zalkin, H.; Dixon, J. E. De novo purine nucleotide

biosynthesis: cloning of human and avian cDNAs encoding the trifunctional glycinamide ribonucleotide synthetase-aminoimidazole ribonucleotide synthetase-glycinamide ribonucleotide transformylase by functional complementation in E.coli. *Nucleic Acids Res.* **1990,** 18, 6665-72.

139. Zhang, Y.; Desharnais, J.; Marsilje, T. H.; Li, C.; Hedrick, M. P.; Gooljarsingh, L. T.; Tavassoli, A.; Benkovic, S. J.; Olson, A. J.; Boger, D. L.; Wilson, I. A. Rational Design, Synthesis, Evaluation, and Crystal Structure of a Potent Inhibitor of Human GAR Tfase: 10-(Trifluoroacetyl)-5,10-dideazaacyclic-5,6,7,8-tetrahydrofolic Acid. *Biochemistry* **2003,** 42, 6043-6056.

140. Caperelli, C. A.; Giroux, E. L. The human glycinamide ribonucleotide transformylase domain: purification, characterization, and kinetic mechanism. *Arch. Biochem. Biophys.* **1997,** 341, 98-103.

141. Sanghani, S. P.; Moran, R. G. Tight Binding of Folate Substrates and Inhibitors to Recombinant Mouse Glycinamide Ribonucleotide Formyltransferase. *Biochemistry* **1997,** 36, 10506-10516.

142. Moran, R. G.; Baldwin, S. W.; Taylor, E. C.; Shih, C. The 6*S*- and 6*R*-diastereomers of 5, 10-dideaza-5, 6, 7, 8-tetrahydrofolate are equiactive inhibitors of *de novo* purine synthesis. *J. Biol. Chem.* **1989,** 264, 21047-51.

143. Habeck, L. L.; Leitner, T. A.; Shackelford, K. A.; Gossett, L. S.; Schultz, R. M.; Andis, S. L.; Shih, C.; Grindey, G. B.; Mendelsohn, L. G. A novel class of monoglutamated antifolates exhibits tight-binding inhibition of human glycinamide ribonucleotide formyltransferase and potent activity against solid tumors. *Cancer Res.* **1994,** 54, 1021-6.

144. Mendelsohn, L. G.; Shih, C.; Schultz, R. M.; Worzalla, J. F. Biochemistry and pharmacology of glycinamide ribonucleotide formyltransferase inhibitors: LY309887 and lometrexol. *Invest. New Drugs* **1996,** 14, 287-94.

145. Boritzki, T. J.; Barlett, C. A.; Zhang, C.; Howland, E. F. AG2034: a novel inhibitor of glycinamide ribonucleotide formyltransferase. *Invest. New Drugs* **1996,** 14, 295-303.

146. Neuferm, H. B.; Boritzki, T. J. Drug interactions between AG2037 and a panel of standard chemotherapeutic agents against cancer cells *in vitro*. *Proc. Am. Assoc. Cancer Res. (AACR)* **2001,** 42, Abst 1579.

147. Taylor, E. C.; Harrington, P. J.; Fletcher, S. R.; Beardsley, G. P.; Moran, R. G. Synthesis of the antileukemic agents 5,10-dideazaaminopterin and 5,10-dideaza-5,6,7,8-tetrahydroaminopterin. *J. Med. Chem.* **1985,** 28, 914-21.

148. Moran, R. G.; Baldwin, S. W.; Taylor, E. C.; Shih, C. The 6S- and 6R-diastereomers of 5,10-dideaza-5,6,7,8-tetrahydrofolate are equiactive inhibitors of de novo purine synthesis. *J. Biol. Chem.* **1989,** 264, 21047-51.

149. Matherly, L. H.; Angeles, S. M.; McGuire, J. J. Determinants of the disparate antitumor activities of (6R)-5,10-dideaza-5,6,7,8-tetrahydrofolate and methotrexate toward human lymphoblastic leukemia cells, characterized by severely impaired antifolate membrane transport. *Biochem. Pharmacol.* **1993,** 46, 2185-95.

150. Ray, M. S.; Muggia, F. M.; Leichman, C. G.; Grunberg, S. M.; Nelson, R. L.; Dyke, R. W.; Moran, R. G. Phase I study of (6R)-5,10-dideazatetrahydrofolate: a folate antimetabolite inhibitory to de novo purine synthesis. *J Natl Cancer Inst* **1993,** 85, 1154-9.

151. Grindey, G. B. A., T., Shih, C. Reversal of the toxicity but not the antitumor activity of lometrexol by folic acid. *Proc. Am. Assoc. Cancer Res.* **1991,** 32, 324.

152. Roberts, J. D.; Poplin, E. A.; Tombes, M. B.; Kyle, B.; Spicer, D. V.; Grant, S.; Synold, T.; Moran, R. Weekly lometrexol with daily oral folic acid is appropriate for phase II evaluation. *Cancer Chemother. Pharmacol.* **2000,** 45, 103-110.

153. Mendelsohn, L. G.; Worzalla, J. F.; Walling, J. M. In *Preclinical and clinical evaluation of the glycinamide ribonucleotide formyltransferase inhibitors lometrexol and LY309887*, 1999; Humana: **1999**; pp 261-280.

154. Aylesworth, C. B., S. D.; Stephenson, J. Phase I and pharmacokinetic study of the glycinamide ribonucleotide formyltransferase inhibitor LY309887 as a bolus every 3 weeks with folic acid (FA). *Proc. Am. Soc. Clin. Oncol. (ASCO)* **1998,** 17, 865.

155. Budman, D. R. B., B.; Johnson, R. Phase I trial of LY309887: A specific inhibitor of purine biosynthesis. *Proc. Am. Soc. Clin. Oncol. (ASCO)* **1998,** 17, 864.

156. Mader, M. M.; Henry, J. R. In *Antimetabolites*, 2006; Elsevier Ltd.: **2006**; pp 55-79.

157. Neuferm, H. B. B., T. J. Drug interactions between AG2037 and a panel of standard chemotherapeutic agents against cancer cells in vitro. *Proc. Am. Assoc. Cancer Res. (AACR)* **2001,** 42, 1579.

158. Kisliuk, R. L. Deaza analogs of folic acid as antitumor agents. *Curr. Pharm. Des.* **2003,** 9, 2615-2625.

159. Shih, C.; Gossett, L. S.; Worzalla, J. F.; Rinzel, S. M.; Grindey, G. B.; Harrington, P. M.; Taylor, E. C. Synthesis and biological activity of acyclic analogues of 5,10-dideaza-5,6,7,8-tetrahydrofolic acid. *J. Med. Chem.* **1992,** 35, 1109-16.

160. Kelley, J. L.; McLean, E. W.; Cohn, N. K.; Edelstein, M. P.; Duch, D. S.; Smith, G. K.; Hanlon, M. H.; Ferone, R. Synthesis and biological activity of an acyclic analogue of 5,6,7,8-tetrahydrofolic acid, *N*-[4-[[3-(2,4-diamino-1,6-dihydro-6-oxo-5-pyrimidinyl)propyl]amino]-benzoyl]-*L*-glutamic acid. *J. Med. Chem.* **1990,** 33, 561-7.

161. Hodson, S. J.; Bigham, E. C.; Duch, D. S.; Smith, G. K.; Ferone, R. Thienyl and thiazolyl acyclic analogues of 5-deazatetrahydrofolic acid. *J. Med. Chem.* **1994,** 37, 2112-5.

162. Zhang, Y.; Desharnais, J.; Marsilje, T. H.; Li, C.; Hedrick, M. P.; Gooljarsingh, L. T.; Tavassoli, A.; Benkovic, S. J.; Olson, A. J.; Boger, D. L.; Wilson, I. A. Rational design, synthesis, evaluation, and crystal structure of a potent inhibitor of human GAR Tfase: 10-(trifluoroacetyl)-5,10-dideazaacyclic-5,6,7,8-tetrahydrofolic acid. *Biochemistry* **2003,** 42, 6043-56.

163. DeMartino, J. K.; Hwang, I.; Connelly, S.; Wilson, I. A.; Boger, D. L. Asymmetric synthesis of inhibitors of glycinamide ribonucleotide transformylase. *J. Med. Chem.* **2008,** 51, 5441-8.

164. Chong, Y.; Hwang, I.; Tavassoli, A.; Zhang, Y.; Wilson, I. A.; Benkovic, S. J.; Boger, D. L. Synthesis and biological evaluation of alpha- and gamma-carboxamide derivatives of 10-CF_3CO-DDACTHF. *Bioorg. Med. Chem.* **2005,** 13, 3587-92.

165. DeMartino, J. K.; Hwang, I.; Xu, L.; Wilson, I. A.; Boger, D. L. Discovery of a potent, nonpolyglutamatable inhibitor of glycinamide ribonucleotide transformylase. *J. Med. Chem.* **2006,** 49, 2998-3002.

166. Taylor, E. C.; Harrington, P. M.; Shih, C. A facile route to "open chain" analogs of 5,10-dideaza-5,6,7,8-tetrahydrofolic acid (DDATHF). *Heterocycles* **1989,** 28, 1169-78.

167. Kelley, J. L.; McLean, E. W.; Cohn, N. K.; Edelstein, M. P.; Duch, D. S.; Smith, G. K.; Hanlon, M. H.; Ferone, R. Synthesis and biological activity of an acyclic analog of 5,6,7,8-tetrahydrofolic acid, N-[4-[[3-(2,4-diamino-1,6-dihydro-6-oxo-5-pyrimidinyl)propyl]amino]benzoyl]-L-glutamic acid. *J. Med. Chem.* **1990,** 33, 561-7.

168. Marsilje, T. H.; Labroli, M. A.; Hedrick, M. P.; Jin, Q.; Desharnais, J.; Baker, S. J.; Gooljarsingh, L. T.; Ramcharan, J.; Tavassoli, A.; Zhang, Y.; Wilson, I. A.; Beardsley, G. P.; Benkovic, S. J.; Boger, D. L. 10-Formyl-5,10-dideaza-acyclic-5,6,7,8-tetrahydrofolic acid (10-Formyl-DDACTHF) A potent cytotoxic agent acting by selective inhibition of human GAR Tfase and the de novo purine biosynthetic pathway. *Bioorg. Med. Chem.* **2002,** 10, 2739-2749.

169. Cheng, H.; Chong, Y.; Hwang, I.; Tavassoli, A.; Zhang, Y.; Wilson, I. A.; Benkovic, S. J.; Boger, D. L. Design, synthesis, and biological evaluation of 10-methanesulfonyl-DDACTHF, 10-methanesulfonyl-5-DACTHF, and 10-methylthio-DDACTHF as potent inhibitors of GAR Tfase and the de novo purine biosynthetic pathway. *Bioorg Med Chem* **2005,** 13, 3577-85.

170. DeMartino, J. K.; Hwang, I.; Connelly, S.; Wilson, I. A.; Boger, D. L. Asymmetric synthesis of inhibitors of glycinamide ribonucleotide transformylase. *J. Med. Chem.* **2008,** 51, 5441-5448.

171. Chong, Y.; Hwang, I.; Tavassoli, A.; Zhang, Y.; Wilson, I. A.; Benkovic, S. J.; Boger, D. L. Synthesis and biological evaluation of alpha- and gamma-carboxamide derivatives of 10-CF3CO-DDACTHF. *Bioorg Med Chem* **2005,** 13, 3587-92.

172. DeMartino, J. K.; Hwang, I.; Xu, L.; Wilson, I. A.; Boger, D. L. Discovery of a Potent, Nonpolyglutamatable Inhibitor of Glycinamide Ribonucleotide Transformylase. *J.*

Med. Chem. **2006,** 49, 2998-3002.

173. Shim, J. H.; Wall, M.; Benkovic, S. J.; Diaz, N.; Suarez, D.; Merz, K. M., Jr. Evaluation of the Catalytic Mechanism of AICAR Transformylase by pH-Dependent Kinetics, Mutagenesis, and Quantum Chemical Calculations. *J. Am. Chem. Soc.* **2001,** 123, 4687-4696.

174. Greasley, S. E.; Horton, P.; Ramcharan, J.; Beardsley, G. P.; Benkovic, S. J.; Wilson, I. A. Crystal structure of a bifunctional transformylase and cyclohydrolase enzyme in purine biosynthesis. *Nat Struct Biol* **2001,** 8, 402-6.

175. Cheong, C. G.; Wolan, D. W.; Greasley, S. E.; Horton, P. A.; Beardsley, G. P.; Wilson, I. A. Crystal structures of human bifunctional enzyme aminoimidazole-4-carboxamide ribonucleotide transformylase/IMP cyclohydrolase in complex with potent sulfonyl-containing antifolates. *J Biol Chem* **2004,** 279, 18034-45.

176. Wolan, D. W.; Greasley, S. E.; Wall, M. J.; Benkovic, S. J.; Wilson, I. A. Structure of Avian AICAR Transformylase with a Multisubstrate Adduct Inhibitor β-DADF Identifies the Folate Binding Site. *Biochemistry* **2003,** 42, 10904-10914.

177. Erba, E.; Sen, S.; Sessa, C.; Vikhanskaya, F. L.; D'Incalci, M. Mechanism of cytotoxicity of 5,10-dideazatetrahydrofolic acid in human ovarian carcinoma cells in vitro and modulation of the drug activity by folic or folinic acid. *Br. J. Cancer* **1994,** 69, 205-11.

178. Xu, L.; Chong, Y.; Hwang, I.; D'Onofrio, A.; Amore, K.; Beardsley, G. P.; Li, C.; Olson, A. J.; Boger, D. L.; Wilson, I. A. Structure-based Design, Synthesis, Evaluation, and Crystal Structures of Transition State Analogue Inhibitors of Inosine Monophosphate Cyclohydrolase. *J. Biol. Chem.* **2007,** 282, 13033-13046.

179. Wolan, D. W.; Greasley, S. E.; Beardsley, G. P.; Wilson, I. A. Structural Insights into the Avian AICAR Transformylase Mechanism. *Biochemistry* **2002,** 41, 15505-15513.

180. Wolan, D. W.; Cheong, C.-G.; Greasley, S. E.; Wilson, I. A. Structural Insights into the Human and Avian IMP Cyclohydrolase Mechanism via Crystal Structures with the Bound XMP Inhibitor. *Biochemistry* **2004,** 43, 1171-1183.

181. Rayl, E. A.; Moroson, B. A.; Beardsley, G. P. The human purH gene product, 5-aminoimidazole-4-carboxamide ribonucleotide formyltransferase/IMP cyclohydrolase. Cloning, sequencing, expression, purification, kinetic analysis, and domain mapping. *J. Biol. Chem.* **1996,** 271, 2225-33.

182. Wall, M.; Shim, J. H.; Benkovic, S. J. Human AICAR Transformylase: Role of the 4-Carboxamide of AICAR in Binding and Catalysis. *Biochemistry* **2000,** 39, 11303-11311.

183. Beardsley, G. P.; Rayl, E. A.; Gunn, K.; Moroson, B. A.; Seow, H.; Anderson, K. S.; Vergis, J.; Fleming, K.; Worland, S.; Condon, B.; Davies, J. Structure and functional relationships in human pur H. *Adv Exp Med Biol* **1998,** 431, 221-6.

184. Li, C.; Xu, L.; Wolan, D. W.; Wilson, I. A.; Olson, A. J. Virtual Screening of Human 5-Aminoimidazole-4-carboxamide Ribonucleotide Transformylase against the NCI Diversity Set by Use of AutoDock to Identify Novel Nonfolate Inhibitors. *J. Med. Chem.* **2004,** 47, 6681-6690.

185. Bulock, K. G.; Beardsley, G. P.; Anderson, K. S. The kinetic mechanism of the human bifunctional enzyme ATIC (5-amino-4-imidazolecarboxamide ribonucleotide transformylase/inosine 5'-monophosphate cyclohydrolase): A surprising lack of substrate channeling. *J. Biol. Chem.* **2002,** 277, 22168-22174.

186. Itoh, F.; Russello, O.; Akimoto, H.; Beardsley, G. P. Novel pyrrolo[2,3-d]pyrimidine antifolate TNP-351: cytotoxic effect on methotrexate-resistant CCRF-CEM cells and inhibition of transformylases of de novo purine biosynthesis. *Cancer Chemother. Pharmacol.* **1994,** 34, 273-9.

187. Chattopadhyay, S.; Moran, R. G.; Goldman, I. D. Pemetrexed: Biochemical and cellular pharmacology, mechanisms, and clinical applications. *Mol. Cancer Ther.* **2007,** 6, 404-417.

188. Ricciardi, S.; Tomao, S.; de, M. F. Pemetrexed as first-line therapy for non-squamous non-small cell lung cancer. *Ther. Clin. Risk Manage.* **2009,** 5, 781-787.

189. Taylor, E. C.; Kuhnt, D.; Shih, C.; Rinzel, S. M.; Grindey, G. B.; Barredo, J.; Jannatipour, M.; Moran, R. G. A dideazatetrahydrofolate analog lacking a chiral center at C-6: N-[4-[2-(2-amino-3,4-dihydro-4-oxo-7H-pyrrolo[2,3-d]pyrimidin-5yl)ethyl[benzoyl]-L-glutamic acid is an inhibitor of thymidylate synthase. *J. Med. Chem.* **1992,** 35, 4450-4.

190. Racanelli, A. C.; Rothbart, S. B.; Heyer, C. L.; Moran, R. G. Therapeutics by Cytotoxic Metabolite Accumulation: Pemetrexed Causes ZMP Accumulation, AMPK Activation, and Mammalian Target of Rapamycin Inhibition. *Cancer Res.* **2009,** 69, 5467-5474.

191. Rothbart, S. B.; Racanelli, A. C.; Moran, R. G. Pemetrexed Indirectly Activates the Metabolic Kinase AMPK in Human Carcinomas. *Cancer Res.* **2010,** 70, 10299-10309.

192. Gridelli, C.; Rossi, A.; Morgillo, F.; Bareschino, M. A.; Maione, P.; Di, M. M.; Ciardiello, F. A randomized phase II study of pemetrexed or RAD001 as second-line treatment of advanced non-small-cell lung cancer in elderly patients: treatment rationale

and protocol dynamics. *Clin. Lung Cancer* **2007,** 8, 568-571.

193. Pandya, K. J.; Dahlberg, S.; Hidalgo, M.; Cohen, R. B.; Lee, M. W.; Schiller, J. H.; Johnson, D. H. A randomized, phase II trial of two dose levels of temsirolimus (CCI-779) in patients with extensive-stage small-cell lung cancer who have responding or stable disease after induction chemotherapy: a trial of the Eastern Cooperative Oncology Group (E1500). *J Thorac Oncol* **2007,** 2, 1036-41.

194. Gorlick, R.; Goker, E.; Trippett, T.; Waltham, M.; Banerjee, D.; Bertino, J. R. Intrinsic and acquired resistance to methotrexate in acute leukemia. *N. Engl. J. Med.* **1996,** 335, 1041-8.

195. Werkheiser, W. C. Specific Binding of 4-Amino Folic Acid Analogs by Folic Acid Reductase. *J. Biol. Chem.* **1961,** 236, 888-893.

196. Trippett, T.; Schlemmer, S.; Elisseyeff, Y.; Goker, E.; Wachter, M.; Steinherz, P.; Tan, C.; Berman, E.; Wright, J. E.; Rosowsky, A.; et al. Defective transport as a mechanism of acquired resistance to methotrexate in patients with acute lymphocytic leukemia. *Blood* **1992,** 80, 1158-62.

197. Assaraf, Y. G. Characterization by flow cytometry and fluorescein-methotrexate labeling of hydrophilic and lipophilic antifolate resistance in cultured mammalian cells. *Anticancer Drugs* **1993,** 4, 535-44.

198. Matherly, L. H.; Taub, J. W.; Ravindranath, Y.; Proefke, S. A.; Wong, S. C.; Gimotty, P.; Buck, S.; Wright, J. E.; Rosowsky, A. Elevated dihydrofolate reductase and impaired methotrexate transport as elements in methotrexate resistance in childhood acute lymphoblastic leukemia. *Blood* **1995,** 85, 500-9.

199. Goker, E.; Waltham, M.; Kheradpour, A.; Trippett, T.; Mazumdar, M.; Elisseyeff,

Y.; Schnieders, B.; Steinherz, P.; Tan, C.; Berman, E.; et al. Amplification of the dihydrofolate reductase gene is a mechanism of acquired resistance to methotrexate in patients with acute lymphoblastic leukemia and is correlated with p53 gene mutations. *Blood* **1995,** 86, 677-84.

200. Lin, J. T.; Tong, W. P.; Trippett, T. M.; Niedzwiecki, D.; Tao, Y.; Tan, C.; Steinherz, P.; Schweitzer, B. I.; Bertino, J. R. Basis for natural resistance to methotrexate in human acute non-lymphocytic leukemia. *Leuk. Res.* **1991,** 15, 1191-6.

201. Hryniuk, W. M.; Bertino, J. R. Treatment of leukemia with large doses of methotrexate and folinic acid: clinical-biochemical correlates. *J. Clin. Invest.* **1969,** 48, 2140-55.

202. Rodenhuis, S.; McGuire, J. J.; Narayanan, R.; Bertino, J. R. Development of an assay system for the detection and classification of methotrexate resistance in fresh human leukemic cells. *Cancer Res.* **1986,** 46, 6513-9.

203. Li, W. W.; Waltham, M.; Tong, W.; Schweitzer, B. I.; Bertino, J. R. Increased activity of gamma-glutamyl hydrolase in human sarcoma cell lines: a novel mechanism of intrinsic resistance to methotrexate (MTX). *Adv. Exp. Med. Biol.* **1993,** 338, 635-8.

204. Waltham, M. C.; Li, W. W.; Gritsman, H.; Tong, W. P.; Bertino, J. R. gamma-Glutamyl hydrolase from human sarcoma HT-1080 cells: characterization and inhibition by glutamine antagonists. *Mol. Pharmacol.* **1997,** 51, 825-32.

205. Matthews, D. A.; Alden, R. A.; Bolin, J. T.; Freer, S. T.; Hamlin, R.; Xuong, N.; Kraut, J.; Poe, M.; Williams, M.; Hoogsteen, K. Dihydrofolate reductase: x-ray structure of the binary complex with methotrexate. *Science* **1977,** 197, 452-5.

206. Blakeley, R. L.; Appleman, J. R. Recent Advances in the Study of Dihydrofolate

Reductase. In *Chemistry and Biology of Pteridines*, Walter de Gruyter Berlin N.Y.: **1986**; pp 769-772.

207. Freisham, J. H.; Matthews, D. A. The Comparative Biochemistry of DHFR. In *Folate as Therapeutic Agents*, Sirotnak; Burchall; Ensminger; Montgomery, Eds. Academic Press, Inc., Orlando: **1984**; Vol. 1, pp 69-131.

208. Davies, J. F., 2nd; Delcamp, T. J.; Prendergast, N. J.; Ashford, V. A.; Freisheim, J. H.; Kraut, J. Crystal structures of recombinant human dihydrofolate reductase complexed with folate and 5-deazafolate. *Biochemistry* **1990,** 29, 9467-79.

209. Ferrer, S.; Silla, E.; Tunon, I. Catalytic Mechanism of Dihydrofolate Reductase Enzyme. A Combined Quantum-Mechanical/Molecular-Mechanical Characterization of the N5 Protonation Step. *J. Phys. Chem. B* **2003,** 107, 14036-14041.

210. Schnell, J. R.; Dyson, H. J.; Wright, P. E. STRUCTURE, DYNAMICS, AND CATALYTIC FUNCTION OF DIHYDROFOLATE REDUCTASE. *Annual Review of Biophysics and Biomolecular Structure* **2004,** 33, 119-140.

211. Oefner, C.; D'Arcy, A.; Winkler, F. K. Crystal structure of human dihydrofolate reductase complexed with folate. *Eur. J. Biochem.* **1988,** 174, 377-85.

212. Gready, J. E. Dihydrofolate reductase: binding of substrates and inhibitors and catalytic mechanism. *Adv. Pharmacol. Chemother.* **1980,** 17, 37-102.

213. Subramanian, S.; Kaufman, B. T. Interaction of methotrexate, folates, and pyridine nucleotides with dihydrofolate reductase: calorimetric and spectroscopic binding studies. *Proc. Natl. Acad. Sci. U S A* **1978,** 75, 3201-5.

214. Stockman, B. J.; Nirmala, N. R.; Wagner, G.; Delcamp, T. J.; DeYarman, M. T.; Freisheim, J. H. Methotrexate binds in a non-productive orientation to human

dihydrofolate reductase in solution, based on NMR spectroscopy. *FEBS Lett.* **1991,** 283, 267-9.

215. Fry, D. W.; Jackson, R. C. Biological and biochemical properties of new anticancer folate antagonists. *Cancer Metastasis Rev.* **1987,** 5, 251-70.

216. Roth, B.; Cheng, C. C. Recent progress in the medicinal chemistry of 2,4-diaminopyrimidines. *Prog. Med. Chem.* **1982,** 19, 269-331.

217. Seeger, D. R.; Cosulich, D. B.; Smith, J. M., Jr.; Hultquist, M. E. Analogs of pteroylglutamic acid. III. 4-Amino derivatives. *J. Am. Chem. Soc.* **1949,** 71, 1753-1758.

218. Deng, Y.; Hou, Z.; Wang, L.; Cherian, C.; Wu, J.; Gangjee, A.; Matherly, L. H. Role of lysine 411 in substrate carboxyl group binding to the human reduced folate carrier, as determined by site-directed mutagenesis and affinity inhibition. *Mol. Pharmacol.* **2008,** 73, 1274-81.

219. Jolivet, J.; Cowan, K. H.; Curt, G. A.; Clendeninn, N. J.; Chabner, B. A. The pharmacology and clinical use of methotrexate. *N. Engl. J. Med.* **1983,** 309, 1094-104.

220. Bertino, J. R.; Mini, E.; Sobrero, A.; Moroson, B. A.; Love, T.; Jastreboff, M.; Carmen, M.; Srimatkandada, S.; Dube, S. K. In *Advances in Enzyme Regulation. 24*, Weber, G., Ed. Pergamon: New York, **1985**; pp 3-12.

221. Bertino, J. R.; Srimatkandada, S.; Carman, M. D.; Mini, E.; Jastreboff, M.; Moroson, B. A.; Dube, S. K. In *Modern Trends in Human Leukemia VI*, Neth, R.; Gallo, R. C.; Greaves, M. F.; Janka, G., Eds. Springer-Verlag: Berlin, **1985**.

222. Flombaum, C. D.; Meyers, P. A. High-dose leucovorin as sole therapy for methotrexate toxicity. *J. Clin. Oncol.* **1999,** 17, 1589-1594.

223. Widemann, B. C.; Adamson, P. C. Understanding and managing methotrexate

nephrotoxicity. *Oncologist* **2006,** 11, 694-703.

224. Zain, J. M.; Marchi, E. Pralatrexate - from bench to bedside. *Drugs Today (Barc)* **2010,** 46, 91-9.

225. Malik, S. M.; Liu, K.; Qiang, X.; Sridhara, R.; Tang, S.; McGuinn, W. D., Jr.; Verbois, S. L.; Marathe, A.; Williams, G. M.; Bullock, J.; Tornoe, C.; Lin, S. C.; Ocheltree, T.; Vialpando, M.; Kacuba, A.; Justice, R.; Pazdur, R. Folotyn (pralatrexate injection) for the treatment of patients with relapsed or refractory peripheral T-cell lymphoma: u.s. Food and drug administration drug approval summary. *Clin. Cancer Res.* **2010,** 16, 4921-7.

226. Harrison, P. T.; Scott, J. E.; Hutchinson, M. J.; Thompson, R. Site-directed mutagenesis of varicella-zoster virus thymidylate synthase. Analysis of two highly conserved regions of the enzyme. *Eur. J. Biochem.* **1995,** 230, 511-6.

227. Douglas, K. T. The thymidylate synthesis cycle and anticancer drugs. *Med. Res. Rev.* **1987,** 7, 441-75.

228. Cisneros, R. J.; Silks, L. A.; Dunlap, R. B. Mechanistic aspects of thymidylate synthase: molecular basis for drug design. *Drugs Fut.* **1988,** 13, 859.

229. Pogolotti, A. L., Jr.; Santi, D. V. The Catalytic Activity of Thymidylate Synthase. In *Bioorganic Chemistry*, van Tamelen, E. E., Ed. Academic Press: Orlando, FL, **1977**; Vol. 1, pp 277-311.

230. Phan, J.; Koli, S.; Minor, W.; Dunlap, R. B.; Berger, S. H.; Lebioda, L. Human thymidylate synthase is in the closed conformation when complexed with dUMP and raltitrexed, an antifolate drug. *Biochemistry* **2001,** 40, 1897-902.

231. Sayre, P. H.; Finer-Moore, J. S.; Fritz, T. A.; Biermann, D.; Gates, S. B.;

MacKellar, W. C.; Patel, V. F.; Stroud, R. M. Multi-targeted antifolates aimed at avoiding drug resistance form covalent closed inhibitory complexes with human and *Escherichia coli* thymidylate synthases. *J. Mol. Biol.* **2001,** 313, 813-29.

232. Kamb, A.; Finer-Moore, J. S.; Stroud, R. M. Cofactor triggers the conformational change in thymidylate synthase: implications for an ordered binding mechanism. *Biochemistry* **1992,** 31, 12876-84.

233. Kamb, A.; Finer-Moore, J.; Calvert, A. H.; Stroud, R. M. Structural basis for recognition of polyglutamyl folates by thymidylate synthase. *Biochemistry* **1992,** 31, 9883-90.

234. Matthews, D. A.; Appelt, K.; Oatley, S. J.; Xuong, N. H. Crystal structure of Escherichia coli thymidylate synthase containing bound 5-fluoro-2'-deoxyuridylate and 10-propargyl-5,8-dideazafolate. *J. Mol. Biol.* **1990,** 214, 923-36.

235. Matthews, D. A.; Villafranca, J. E.; Janson, C. A.; Smith, W. W.; Welsh, K.; Freer, S. Stereochemical mechanism of action for thymidylate synthase based on the X-ray structure of the covalent inhibitory ternary complex with 5-fluoro-2'-deoxyuridylate and 5,10-methylenetetrahydrofolate. *J. Mol. Biol.* **1990,** 214, 937-48.

236. Finer-Moore, J. S.; Montfort, W. R.; Stroud, R. M. Pairwise specificity and sequential binding in enzyme catalysis: thymidylate synthase. *Biochemistry* **1990,** 29, 6977-86.

237. Carreras, C. W.; Santi, D. V. The catalytic mechanism and structure of thymidylate synthase. *Annu. Rev. Biochem.* **1995,** 64, 721-62.

238. Jackman, A. L.; Calvert, A. H. Folate-based thymidylate synthase inhibitors as anticancer drugs. *Ann. Oncol.* **1995,** 6, 871-81.

239. Jones, T. R.; Calvert, A. H.; Jackman, A. L.; Brown, S. J.; Jones, M.; Harrap, K. R. A potent antitumour quinazoline inhibitor of thymidylate synthetase: synthesis, biological properties and therapeutic results in mice. *Eur. J. Cancer* **1981,** 17, 11-9.

240. Jackman, A. L.; Taylor, G. A.; Gibson, W.; Kimbell, R.; Brown, M.; Calvert, A. H.; Judson, I. R.; Hughes, L. R. ICI D1694, a quinazoline antifolate thymidylate synthase inhibitor that is a potent inhibitor of L1210 tumor cell growth *in vitro* and *in vivo*: a new agent for clinical study. *Cancer Res.* **1991,** 51, 5579-86.

241. Taylor, E. C.; Kuhnt, D.; Shih, C.; Rinzel, S. M.; Grindey, G. B.; Barredo, J.; Jannatipour, M.; Moran, R. G. A dideazatetrahydrofolate analogue lacking a chiral center at C-6, *N*-[4-[2-(2-amino-3,4-dihydro-4-oxo-7H-pyrrolo[2,3-*d*]pyrimidin-5-yl)ethyl]benzoyl]-L-glutamic acid, is an inhibitor of thymidylate synthase. *J. Med. Chem.* **1992,** 35, 4450-4.

242. Shih, C.; Thornton, D. E. Preclinical Pharmacology Studies and the Clinical Development of a Novel Multitargeted Antifolate, MTA (LY231514). In *Antifolate Drugs in Cancer Therapy*, Jackman, A. L., Ed. Humana Press: Totowa, NJ, 1999; pp 183-201.

243. Boyle, F. T.; Stephens, T. C.; Averbuch, S. D.; Jackman, A. L. ZD9331: Preclinical and Clinical Studies. In *Antifolate Drugs in Cancer Therapy*, Jackman, A. L., Ed. Humana Press: Totowa, NJ, **1999**; pp 243-260.

244. Paz-Ares, L.; Bezares, S.; Tabernero, J. M.; Castellanos, D.; Cortes-Funes, H. Review of a promising new agent - pemetrexed disodium. *Cancer* **2003,** 97, 2056-2063.

245. Nowak, A. K.; Byrne, M. J.; Millward, M. J.; Alvarez, J. M.; Robinson, B. W. S. Current chemotherapeutic treatment of malignant pleural mesothelioma. *Expert Opin.*

Pharmacother. **2004,** 5, 2441-2449.

246. Gangjee, A.; Zaware, N.; Raghavan, S.; Ihnat, M.; Shenoy, S.; Kisliuk, R. L. Single agents with designed combination chemotherapy potential: synthesis and evaluation of substituted pyrimido[4,5-b]indoles as receptor tyrosine kinase and thymidylate synthase inhibitors and as antitumor agents. *J. Med. Chem.* **2010,** 53, 1563-1578.

247. Gangjee, A.; Zaware, N.; Raghavan, S.; Yang, J.; Thorpe, J. E.; Ihnat, M. A. N4-(3-Bromophenyl)-7-(substituted benzyl) pyrrolo[2,3-d]pyrimidines as potent multiple receptor tyrosine kinase inhibitors: Design, synthesis, and in vivo evaluation. *Bioorg. Med. Chem.* **2012,** 20, 2444-2454.

248. Gangjee, A.; Qiu, Y.; Li, W.; Kisliuk, R. L. Potent Dual Thymidylate Synthase and Dihydrofolate Reductase Inhibitors: Classical and Nonclassical 2-Amino-4-oxo-5-arylthio-substituted-6-methylthieno[2,3-d]pyrimidine Antifolates. *J. Med. Chem.* **2008,** 51, 5789-5797.

249. Zhao, R.; Babani, S.; Gao, F.; Liu, L.; Goldman, I. D. The mechanism of transport of the multitargeted antifolate (MTA) and its cross-resistance pattern in cells with markedly impaired transport of methotrexate. *Clin. Cancer Res.* **2000,** 6, 3687-3695.

250. Teicher, B. A.; Chen, V.; Shih, C.; Menon, K.; Forler, P. A.; Phares, V. G.; Amsrud, T. Treatment Regimens Including the Multitargeted Antifolate LY231514 in Human Tumor Xenografts. *Clinical Cancer Research* **2000,** 6, 1016-1023.

251. Taylor, E. C.; Patel, H. H.; Jun, J. G. A One-Step Ring Transformation/Ring Annulation Approach to Pyrrolo[2,3- *d*]pyrimidines. A New Synthesis of the Potent Dihydrofolate Reductase Inhibitor TNP-351. *J. Org. Chem.* **1995,** 60, 6684-6687.

252. Noell, C. W.; Robins, R. K. Aromaticity in Heterocyclic Systems. II. The Application of NMR in a Study of the Synthesis and Structure of Certain Imidazo[1,2-*c*]pyrimidines and Related Pyrrolo[2,3-*d*]pyrimidines. *J. Heterocycl. Chem.* **1964,** 1, 34-41.

253. Gibson, C. L.; Ohta, K.; Paulini, K.; Suckling, C. J. Specific Inhibitors in Vitamin Biosynthesis. Part 10. Synthesis of 7- and 8-Substituted 7-Deazaguanines. *J. Chem. Soc., Perkin Trans. 1* **1998,** 1998, 3025-3032.

254. Fumio, Y.; Masatsugu, H.; Keitaro, S.; Michiko, K.; Dadao, N. Synthesis and Properties of Some Pyrrolo[2,3-*d*]pyrimidine Derivatives. *Chem. Pharm. Bull.* **1973,** 21, 473-477.

255. Secrist, J. A.; Liu, P. S. Studies directed toward a total synthesis of nucleoside Q. Annulation of 2,6-diaminopyrimidin-4-one with .alpha.-halo carbonyls to form pyrrolo[2,3-*d*]pyrimidines and furo[2,3-*d*]pyrimidines. *J. Org. Chem.* **1978,** 43, 3937-3941.

256. Davoll, J. Pyrrolo[2,3-*d*]pyrimidines. *J. Chem. Soc.* **1960**, 131-138.

257. Gangjee, A.; Yu, J.; McGuire, J. J.; Cody, V.; Galitsky, N.; Kisliuk, R. L.; Queener, S. F. Design, synthesis, and X-ray crystal structure of a potent dual inhibitor of thymidylate synthase and dihydrofolate reductase as an antitumor agent. *J. Med. Chem.* **2000,** 43, 3837-51.

258. Gangjee, A.; Dubash, N. P.; Kisliuk, R. L. Synthesis of novel, nonclassical 2-amino-4-oxo-6-(arylthio)ethylpyrrolo[2,3-d]pyrimidines as potential inhibitors of thymidylate synthase. *J. Heterocycl. Chem.* **2001,** 38, 349-354.

259. Gangjee, A.; Vidwans, A.; Elzein, E.; McGuire, J. J.; Queener, S. F.; Kisliuk, R. L.

Synthesis, Antifolate, and Antitumor Activities of Classical and Nonclassical 2-Amino-4-oxo-5-substituted-pyrrolo[2,3-d]pyrimidines. *J. Med. Chem.* **2001,** 44, 1993-2003.

260. Miwa, T.; Hitaka, T.; Akirnoto, H. A Novel Synthetic Approach to Pyrrolo[2,3-*d*]pyrimidine Antifolates. *J. Org. Chem.* **1993,** 58, 1696-1701.

261. Taylor, E. C.; Liu, B. A Simple and Concise Synthesis of LY231514 (MTA). *Tetrahedron Lett.* **1999,** 40, 4023-4026.

262. Taylor, E. C.; Dowling, J. E.; Schrader, T.; Bhatia, B. Unexpected and Facile Bridgehead Substitution in 5,6,7,8,9,10-Hexahydro-5,9-methanopyrimido[4,5-*b*]azocin-4(3*H*)-ones. *Tetrahedron Lett.* **1998,** 54, 9507-9518.

263. Anderson, G. L. Regioselective Synthesis of Pyrido[2,3-*d*]pyrimidines. *J. Heterocycl. Chem.* **1985,** 22, 1469-1470.

264. Bennett, G. B.; Mason, R. B. The Regioselective Behavior of Unsaturated Keto Esters toward Vinylogous Amides. *J. Org. Chem.* **1977,** 42, 1919-1922.

265. Broom, A. D.; Shim, J. L.; Anderson, G. L. Pyrido[2,3-*d*]pyrimidines. IV. Synthetic Studies Leading to Various Oxopyrido[2,3-*d*]pyrimidines. *J. Org. Chem.* **1976,** 41, 1095-1099.

266. Koen, M. J.; Gready, J. E. Preparation of 8-Substituted Pyrido[2,3-*d*]pyrimidines (N5-Deazapterins). *J. Org. Chem.* **1993,** 58, 1104-1108.

267. Taylor, E. C.; Gillespie, P.; Patel, M. Novel 5-Desmethylene Analogs of 5,10-Dideaza-5,6,7,8-tetrahydrofolic Acid as Potential Anticancer Agents. *J. Org. Chem.* **1992,** 57, 3218-3225.

268. Melton, J.; McMurry, J. E. New Method for the Dehydration of Nitro Alcohols. *J. Org. Chem.* **1975,** 40, 2138-2319.

269. Barnett, C. J.; Wilson, T. M.; Kobierski, M. E. A Practical Synthesis of Multitargeted Antifolate LY231514. *Organic Process Research & Development* **1999,** 3, 184-188.

270. Legraverend, M.; Ngongo-Tekam, R. M.; Bisagni, E.; Zerial, A. (+/-)-2-Amino-3,4-dihydro-7-[2,3-dihydroxy-4-(hydroxymethyl)-1- cyclopentyl]-7*H*-pyrrolo[2,3-*d*]pyrimidin-4-ones: new carbocyclic analogues of 7-deazaguanosine with antiviral activity. *J. Med. Chem.* **1985,** 28, 1477-80.

271. Sakamoto, T.; Satoh, C.; Kondo, Y.; Yamanaka, H. Condensed Heteroaromatic Ring Systems. XXI. Synthesis of Pyrrolo[2,3-*d*]pyrimidines and Pyrrolo[3,2-*d*]pyrimidines. *Chem. Pharm. Bull.* **1993,** 41, 81-86.

272. Kondo, Y.; Watanabe, R.; Sakamoto, T.; Yamanaka, H. Condensed Heteroaromatic Ring Systems. XVI. Synthesis of Pyrrolo[2,3-*d*]pyrimidine Derivatives. *Chem. Pharm. Bull.* **1989,** 37, 2933-2936.

273. Crooks, P. A.; Robinson, B. Thermal Indolization of 4-Pyrimidinylhydrazones and 4-Pyridylhydrazones. *Chem. Ind.* **1967**, 547-548.

274. Senda, S.; Hirota, K. Pyrimidine Derivatives and Related Compounds. XXII. Synthesis and Parmacological Properties of 7-Deazaxanthine Derivatives. *Chem. Pharm. Bull.* **1974,** 22, 1459-1467.

275. Senda, S.; Hirota, K. Novel Synthesis of 2,4-Dioxo-1,2,3,4-tetrahydropyrrolo[2,3-*d*]pyrimidine Derivatives. *Chem. Lett.* **1972,** 5, 367-368.

276. Wright, G. E. 9*H*-Pyrimido[4,5-*b*]indole-2,4-diones. The Acid-catalyzed Cyclization of 6-(Phenylhydrazino)uracils. *J. Heterocycl. Chem.* **1976,** 13, 539-544.

277. Duffy, T. D.; Wibberley, D. G. Pyrrolo[2,3-*d*]pyrimidines. Synthesis from 4-

Pyrimidylhydrazones, A 2-Bis(ethylthio)methyleneaminopyrrolo-3-carbonitrile and a Pyrrolo[2,3-*d*][1,3]thiazine-2(1*H*)-thione. *J. Chem. Soc., Perkin Trans. 1* **1974,** 16, 1921-1929.

278. Taylor, E. C.; Hendess, R. W. Synthesis of Pyrrolo(2,3-*D*)Pyrimidines. The Aglycone of Toyocamycin. *J. Am. Chem. Soc.* **1965,** 87, 1995-2003.

279. Middleton, W. J.; Engelhardt, V. A.; Fisher, B. S. Cyanocarbon Chemistry. VIII. Heterocyclic Compounds from Tetracyanoethylene. *J. Am. Chem. Soc.* **1958,** 80, 2822-2829.

280. Tolman, R. L.; Robins, R. K.; Townsend, L. B. Pyrrolopyrimidine nucleosides. 3. The total synthesis of toyocamycin, sangivamycin, tubercidin, and related derivatives. *J. Am. Chem. Soc.* **1969,** 91, 2102-8.

281. Ramasamy, K.; Robins, R. K.; Revankar, G. R. Total Synthesis of 2'-Deoxytoyocamycin, 2'-Deoxysangivamycin and Related 7-(*b*-D-Arabinofuranosylpyrrolo[2,3-*d*]pyrimidines Via Ring Closure of Pyrrole Precursors Prepared by the Stereospecific Sodium Salt Glycosylation Procedure. *Tetrahedron* **1986,** 42, 5869-5878.

282. Swayze, E. E.; Hinkley, J. M.; Townsend, L. B. 2-Amino-5-bromo-3,4-dicyanopyrrole. The Improved Preperation of a Versatile Synthon for the Synthesis of Pyrrolo[2,3-*d*]pyrimidines. *Nucleic Acid Chem.* **1991**, 16-18.

283. Pichler, H.; Folkers, G.; Roth, H. J.; Eger, K. Synthesis of 7-Unsubstituted 7*H*-pyrrolo[2,3-*d*]pyrimidines. *Liebigs Ann. Chem.* **1986,** 9, 1485-1505.

284. Eger, K.; Pfahl, J. G.; Folkers, G.; Roth, H. J. Selected Reactions on the o-Aminonitrile System of Substituted Pyrroles. *J. Heterocycl. Chem.* **1987,** 24, 425-430.

285. Chen, Y. L.; Mansbach, R. S.; Winter, S. M.; Brooks, E.; Collins, J.; Corman, M. L.; Dunaiskis, A. R.; Faraci, W. S.; Gallaschun, R. J.; Schmidt, A.; Schulz, D. W. Synthesis and oral efficacy of a 4-(butylethylamino)pyrrolo[2,3-*d*]pyrimidine: a centrally active corticotropin-releasing factor1 receptor antagonist. *J. Med. Chem.* **1997,** 40, 1749-54.

286. Girgis, N. S.; Joergensen, A.; Pedersen, E. B. Phosphorus Pentoxide in Organic Synthesis; XI. A New Synthetic Approach to 7-Deazahypoxanthines. *Synthesis* **1985**, 101-104.

287. Wamhoff, H.; Wehling, B. Heterocyclic *b*-Enamino Esters; 18. Synthesis of 2-Aminopyrrole-3-carboxylic Acid Derivatives. *Synthesis* **1976**, 51-52.

288. Yumoto, M.; Kawabuchi, T.; Sato, K.; Takashima, M. 2-Aminopyrrole Derivatives and Method for Their Preparation. JP 10316654 A2 19981202 Heisei CAN 130:66386, 1998.

289. Taylor, E. C.; Liu, B. A New Route to 7-Substituted Derivatives of *N*-{4-[2-(2-Amino-3,4-dihydro-4-oxo-7*H*-pyrrolo[2,3-*d*]pyrimidin-5-yl)-ethyl]benzoyl}-*L*-glutamic Acid [ALIMTA (LY231514, MTA)] *J. Org. Chem.* **2001,** 66, 3726-3738.

290. Galeazzi, R.; Mobbili, G.; Orena, M. A Convenient Approach to Diastereomerically Pure 1,3,4-Trisubstituted Pyrrolidin-2-ones by Intramolecular Cyclization of N-(2-Alken-1-yl)amides Mediated by Mn(III). An Entry to Both (*R*)- and (*S*)-3-Pyrrolidineacetic Acid. *Tetrahedron* **1996,** 52, 1069-1084.

291. Barnett, C. J.; Wilson, T. M.; Grindley, G. B. Synthesis and Antitumor Activity of LY288601, the 5,6 Dihydro analog of LY231514. *Adv. Exp. Med Biol.* **1993,** 338, 409-412.

292. Dave, K. G.; Shishoo, C. J.; Devani, M. B.; Kalyanaraman, R.; Ananthan, S.; Ullas, G. V.; Bhadti, V. S. Reaction of nitriles under acidic conditions. Part I. A general method of synthesis of condensed pyrimidines. *J. Heterocycl. Chem.* **1980,** 17, 1497-500.

293. Bookser, B. C.; Ugarkar, B. G.; Matelich, M. C.; Lemus, R. H.; Allan, M.; Tsuchiya, M.; Nakane, M.; Nagahisa, A.; Wiesner, J. B.; Erion, M. D. Adenosine Kinase Inhibitors. 6. Synthesis, Water Solubility, and Antinociceptive Activity of 5-Phenyl-7-(5-deoxy-β-D-ribofuranosyl)pyrrolo[2,3-d]pyrimidines Substituted at C4 with Glycinamides and Related Compounds. *J. Med. Chem.* **2005,** 48, 7808-7820.

294. Chinchilla, R.; Najera, C. Recent advances in Sonogashira reactions. *Chemical Society Reviews* **2011,** 40, 5084-5121.

295. Chinchilla, R.; Nájera, C. The Sonogashira Reaction: A Booming Methodology in Synthetic Organic Chemistry†. *Chemical Reviews* **2007,** 107, 874-922.

296. Sonogashira, K.; Tohda, Y.; Hagihara, N. Convenient synthesis of acetylenes. Catalytic substitutions of acetylenic hydrogen with bromo alkenes, iodo arenes, and bromopyridines. *Tetrahedron Lett.* **1975**, 4467-70.

297. Liang, B.; Dai, M.; Chen, J.; Yang, Z. Copper-Free Sonogashira Coupling Reaction with PdCl2 in Water under Aerobic Conditions. *The Journal of organic chemistry* **2004,** 70, 391-393.

298. Soheili, A.; Albaneze-Walker, J.; Murry, J. A.; Dormer, P. G.; Hughes, D. L. Efficient and General Protocol for the Copper-Free Sonogashira Coupling of Aryl Bromides at Room Temperature. *Organic letters* **2003,** 5, 4191-4194.

299. Chandra, A.; Singh, B.; Khanna, R. S.; Singh, R. M. Copper-Free Palladium-Catalyzed Sonogashira Coupling−Annulation: Efficient One-Pot Synthesis of

Functionalized Pyrano[4,3-b]quinolines from 2-Chloro-3-formylquinolines. *The Journal of organic chemistry* **2009,** 74, 5664-5666.

300. Fukuyama, T.; Shinmen, M.; Nishitani, S.; Sato, M.; Ryu, I. A Copper-Free Sonogashira Coupling Reaction in Ionic Liquids and Its Application to a Microflow System for Efficient Catalyst Recycling. *Organic letters* **2002,** 4, 1691-1694.

301. Negishi, E.-i.; Anastasia, L. Palladium-Catalyzed Alkynylation. *Chemical Reviews* **2003,** 103, 1979-2018.

302. Gangjee, A.; Yu, J.; Copper, J. E.; Smith, C. D. Discovery of Novel Antitumor Antimitotic Agents That Also Reverse Tumor Resistance. *J. Med. Chem.* **2007,** 50, 3290-3301.

303. Heck, R. F.; Nolley, J. P. Palladium-catalyzed vinylic hydrogen substitution reactions with aryl, benzyl, and styryl halides. *The Journal of organic chemistry* **1972,** 37, 2320-2322.

304. Mizoroki, T.; Mori, K.; Ozaki, A. Arylation of Olefin with Aryl Iodide Catalyzed by Palladium. *Bulletin of the Chemical Society of Japan* **1971,** 44, 581-581.

305. de Meijere, A.; Meyer, F. E. Fine Feathers Make Fine Birds: The Heck Reaction in Modern Garb. *Angewandte Chemie International Edition in English* **1995,** 33, 2379-2411.

306. Beletskaya, I. P.; Cheprakov, A. V. The Heck Reaction as a Sharpening Stone of Palladium Catalysis. *Chemical Reviews* **2000,** 100, 3009-3066.

307. Muzart, J. Palladium-catalyzed reactions of alcohols. Part B: Formation of C-C and C-N bonds from unsaturated alcohols. *Tetrahedron* **2005,** 61, 4179-4212.

308. Heck, R. F. The arylation of allylic alcohols with organopalladium compounds. A

new synthesis of 3-aryl aldehydes and ketones. *Journal of the American Chemical Society* **1968,** 90, 5526-5531.

309. Melpolder, J. B.; Heck, R. F. Palladium-catalyzed arylation of allylic alcohols with aryl halides. *The Journal of organic chemistry* **1976,** 41, 265-272.

310. Chalk, A. J.; Magennis, S. A. Palladium-catalyzed vinyl substitution reactions. I. New synthesis of 2- and 3-phenyl-substituted allylic alcohols, aldehydes, and ketones from allylic alcohols. *The Journal of organic chemistry* **1976,** 41, 273-278.

311. Larock, R. C.; Leung, W.-Y.; Stolz-Dunn, S. Synthesis of aryl-substituted aldehydes and ketones via palladium-catalyzed coupling of aryl halides and non-allylic unsaturated alcohols. *Tetrahedron Letters* **1989,** 30, 6629-6632.

312. Taylor, E. C.; Wang, Y. Synthesis of 7-methyl derivatives of 5,10-dideaza-5,6,7,8-tetrahydrofolic acid (DDATHF), 5,10-dideaza-5,6,7,8-tetrahydrohomofolic acid (HDDATHF), and LY254155. *Heterocycles* **1998,** 48, 1537-1554.

313. Belley, M.; Gallant, M.; Roy, B.; Houde, K.; Lachance, N.; Labelle, M.; Trimble, L. A.; Chauret, N.; Li, C.; Sawyer, N.; Tremblay, N.; Lamontagne, S.; Carriere, M.-C.; Denis, D.; Greig, G. M.; Slipetz, D.; Metters, K. M.; Gordon, R.; Chan, C. C.; Zamboni, R. J. Structure-activity relationship studies on ortho-substituted cinnamic acids, a new class of selective EP3 antagonists. *Bioorg. Med. Chem. Lett.* **2005,** 15, 527-530.

314. Kim, H.-Y.; Sohn, J.; Wijewickrama, G. T.; Edirisinghe, P.; Gherezghiher, T.; Hemachandra, M.; Lu, P.-Y.; Chandrasena, R. E.; Molloy, M. E.; Tonetti, D. A.; Thatcher, G. R. J. Click synthesis of estradiol-cyclodextrin conjugates as cell compartment selective estrogens. *Bioorg. Med. Chem.* **2010,** 18, 809-821.

315. Tamaru, Y.; Yamada, Y.; Yoshida, Z. I. Palladium catalyzed thienylation of

allylic alcohols with 3-bromothiophene. *Tetrahedron Lett.* **1977**, 3365-8.

316. Yoshida, Z.; Yamada, Y.; Tamaru, Y. Palladium-catalyzed thienylation of allylic alcohols. *Chem. Lett.* **1977**, 423-4.

317. Marsham, P. R.; Hughes, L. R.; Jackman, A. L.; Hayter, A. J.; Oldfield, J.; Wardleworth, J. M.; Bishop, J. A.; O'Connor, B. M.; Calvert, A. H. Quinazoline antifolate thymidylate synthase inhibitors: heterocyclic benzoyl ring modifications. *J Med Chem* **1991,** 34, 1594-605.

318. Hilgenbrink, A. R.; Low, P. S. Folate receptor-mediated drug targeting: From therapeutics to diagnostics. *J. Pharm. Sci.* **2005,** 94, 2135-2146.

319. Jackman, A. L.; Theti, D. S.; Gibbs, D. D. Antifolates targeted specifically to the folate receptor. *Adv. Drug Delivery Rev.* **2004,** 56, 1111-1125.

320. Gibbs, D. D.; Theti, D. S.; Wood, N.; Green, M.; Raynaud, F.; Valenti, M.; Forster, M. D.; Mitchell, F.; Bavetsias, V.; Henderson, E.; Jackman, A. L. BGC 945, a novel tumor-selective thymidylate synthase inhibitor targeted to alpha-folate receptor-overexpressing tumors. *Cancer Res* **2005,** 65, 11721-8.

321. Shih, C.; Grindey, G. B.; Taylor, E. C.; Harrington, P. M. Synthesis and biological activity of nor- and homo-5,10-dideazatetrahydrofolic acid. *Bioorg. Med. Chem. Lett.* **1992,** 2, 339-42.

322. Gangjee, A.; Zeng, Y.; McGuire, J. J.; Mehraein, F.; Kisliuk, R. L. Synthesis of Classical, Three-Carbon-Bridged 5-Substituted Furo[2,3-*d*]pyrimidine and 6-Substituted Pyrrolo[2,3-d]pyrimidine Analogues as Antifolates. *J. Med. Chem.* **2004,** 47, 6893-6901.

323. Gangjee, A.; Zeng, Y.; McGuire, J. J.; Kisliuk, R. L. Synthesis of Classical, Four-Carbon Bridged 5-Substituted Furo[2,3-d]pyrimidine and 6-Substituted Pyrrolo[2,3-

d]pyrimidine Analogues as Antifolates. *J. Med. Chem.* **2005,** 48, 5329-5336.

324. Baldwin, S. W.; Tse, A.; Gossett, L. S.; Taylor, E. C.; Rosowsky, A.; Shih, C.; Moran, R. G. Structural features of 5,10-dideaza-5,6,7,8-tetrahydrofolate that determine inhibition of mammalian glycinamide ribonucleotide formyltransferase. *Biochemistry* **1991,** 30, 1997-2006.

325. Yiqiang Wang, S. R., Larry H. Matherly, Aleem Gangjee Design, Synthesis and Biological Evaluation of 6-Substituted Straight Side Chain Pyrrolo[2,3-*d*]pyrimidines as High Affinity Folate Receptor (FR)-Specific β-Glycinamide Ribonucleotide Formyltransferase (GARFTase) Inhibitors with Antitumor Activity. *J. Med. Chem.* **2013**, in press.

326. Habeck, L. L.; Mendelsohn, L. G.; Shih, C.; Taylor, E. C.; Colman, P. D.; Gossett, L. S.; Leitner, T. A.; Schultz, R. M.; Andis, S. L.; Moran, R. G. Substrate specificity of mammalian folylpolyglutamate synthetase for 5,10-dideazatetrahydrofolate analogs. *Mol. Pharmacol.* **1995,** 48, 326-33.

327. Yiqiang Wang, S. R., Larry H. Matherly, Aleem Gangjee. Design, Synthesis and Biological Evaluation of Pemetrexed (PMX) Homologs as Potent Inhibitors of Tumors Expressing Folate Receptors via 5-Aminoimidazole-4-carboxamide Ribonucleotide Formyl Transferase (AICARFTase) Inhibition. *J. Med. Chem.* **2013**, in press.

328. Chattopadhyay, S.; Zhao, R.; Krupenko, S. A.; Krupenko, N.; Goldman, I. D. The inverse relationship between reduced folate carrier function and Pemetrexed activity in a human colon cancer cell line. *Mol. Cancer Ther.* **2006,** 5, 438-449.

329. Wang, L.; Desmoulin, S. K.; Cherian, C.; Polin, L.; White, K.; Kushner, J.; Fulterer, A.; Chang, M.-H.; Mitchell-Ryan, S.; Stout, M.; Romero, M. F.; Hou, Z.-J.;

Matherly, L. H.; Gangjee, A. Synthesis, Biological, and Antitumor Activity of a Highly Potent 6-Substituted Pyrrolo[2,3-*d*]pyrimidine Thienoyl Antifolate Inhibitor with Proton-Coupled Folate Transporter and Folate Receptor Selectivity over the Reduced Folate Carrier That Inhibits β-Glycinamide Ribonucleotide Formyltransferase. *J. Med. Chem.* **2011,** 54, 7150-7164.

330. Deng, Y.; Hou, Z.; Wang, L.; Cherian, C.; Wu, J.; Gangjee, A.; Matherly, L. H. Role of lysine 411 in substrate carboxyl group binding to the human reduced folate carrier, as determined by site-directed mutagenesis and affinity inhibition. *Mol. Pharmacol.* **2008,** 73, 1274-1281.

331. Salley, J. J., Jr.; Glennon, R. A. Studies on simplified ergoline derivatives. A general six-step synthesis of phenyl-substituted 4-methyl-3,4,4a,5,6,10b-hexahydrobenzo[f]quinolin-1(2*H*)-one analogs. *J. Heterocycl. Chem.* **1982,** 19, 545-50.

332. Gangjee, A.; Yang, J.; Ihnat, M. A.; Kamat, S. Antiangiogenic and antitumor agents. Design, synthesis, and evaluation of novel 2-amino-4-(3-bromoanilino)-6-benzylsubstituted pyrrolo[2,3-*d*]pyrimidines as inhibitors of receptor tyrosine kinases. *Bioorg. Med. Chem.* **2003,** 11, 5155-5170.

333. Taylor, E. C.; Young, W. B.; Chaudhari, R.; Patel, H. H. Syntheses of a Regioisomer of *N*-[4-[2-(2-Amino-4(3*H*)-Oxo-7h-Pyrrolo[2,3-*d*]Pyrimidin-5-Yl)Ethyl]Benzoyl)-L-Glutamic Acid (Ly231514), an Active Thymidylate Synthase Inhibitor and Antitumor Agent. *Heterocycles* **1993,** 36, 1897-1908.

334. Secrist, J. A., III; Liu, P. S. Studies directed toward a total synthesis of nucleoside Q. Annulation of 2,6-diaminopyrimidin-4-one with α-halo carbonyls to form pyrrolo[2,3-d]pyrimidines and furo[2,3-*d*]pyrimidines. *J. Org. Chem.* **1978,** 43, 3937-41.

335. Larock, R. C.; Leung, W. Y.; Stolzdunn, S. Synthesis of Aryl-Substituted Aldehydes and Ketones Via Palladium-Catalyzed Coupling of Aryl Halides and Non-Allylic Unsaturated Alcohols. *Tetrahedron Letters* **1989,** 30, 6629-6632.

336. Bloch, R. 5,5-Dibromo-2,2-Dimethyl-4,6-Dioxo-1,3-Dioxane - New Brominating Agent for Saturated and Alpha,Beta-Unsaturated Carbonyl-Compounds. *Synthesis-Stuttgart* **1978**, 140-142.

337. Kisliuk, R. L.; Strumpf, D.; Gaumont, Y.; Leary, R. P.; Plante, L. Diastereoisomers of 5,10-methylene-5,6,7,8-tetrahydropteroyl-D-glutamic acid. *J Med Chem* **1977,** 20, 1531-1533.

338. Wahba, A. J.; Friedkin, M. Enzymic synthesis of thymidylate. I. Early steps in the purification of thymidylate synthetase of Escherichia coli. *J. Biol. Chem.* **1962,** 237, 3794-3801.

339. Davisson, V. J.; Sirawaraporn, W.; Santi, D. V. Expression of human thymidylate synthase in Escherichia coli. *J. Biol. Chem.* **1989,** 264, 9145-8.

340. Yiqiang Wang, S. R., Larry H. Matherly, Aleem Gangjee. Design, Synthesis and Biological Evaluation of 2-amino-4-oxo-5-substituted-pyrrolo[2,3-*d*]pyrimidines with a thiophenyl ring in the side chain as Potent Inhibitors of Tumors Expressing Folate Receptors via 5-Aminoimidazole-4-carboxamide Ribonucleotide Formyl Transferase (AICARFTase) Inhibition *J. Med. Chem.* **2013** in press.

APPENDIX 1

The biological evaluations of the analogs listed in the following tables were performed by Dr. Larry H. Matherly's group (Developmental Therapeutics Program, Barbara Ann Karmanos Cancer Institute and the Cancer Biology Program and the Department of Pharmacology, Wayne State University School of Medicine) against GARFTase, RFC-expressing PC43-10 cells, FRα-expressing RT16 cells, FRβ-expressing D4 cells and hPCFT-expressing R2/hPCFT4 cells; Dr. Roy L. Kisliuk's group (Department of Biochemistry, Tufts University School of Medicine) against rhTS, rhDHFR, *E. coli* TS and *E. coli* DHFR.

Cell Lines and Assays of Antitumor Activities

RFC- and FR-null MTXRIIOuaR2-4 (R2) CHO cells were gifts from Dr. Wayne Flintoff (University of Western Ontario, London, ON, Canada) and were cultured in R-minimal essential medium (MEM) supplemented with 10% bovine calf serum (Invitrogen, Carlsbad, CA), penicillin- streptomycin solution and *L*-glutamine at 37 °C with 5% CO_2. PC43-10 cells are R2 cells transfected with hRFC. RT16 cells are R2 cells transfected with human FRα and D4 cells are R2 cells transfected with human FRβ. R2/hPCFT4 cells were prepared by transfection of R2 cells with hPCFT cDNA, epitope tagged at the C-terminus with Myc-His6 ($hPCFT^{Myc\text{-}His6}$) and cloned in pCDNA3.1. All the R2 transfected cells (PC43- 10, RT16, D4 and R2/hPCFT4) were routinely cultured in R-MEM plus 1.5 mg/mL G418. Prior to the cytotoxicity assays, RT16 and D4 cells were

cultured in complete folate-free RPMI1640 (without added folate) for 3 days. KB human cervical cancer cells were purchased from the American Type Culture Collection (Manassas, VA) and IGROV1 ovarian carcinoma cells were a gift of Dr. Manohar Ratnam (Medical University of Ohio). Cells were routinely cultured in folate-free RPMI1640 medium, supplemented with 10% fetal bovine serum, penicillin-streptomycin solution, and 2 mM *L*-glutamine with 5% CO_2 at 37 °C.

For growth inhibition assays, cells (CHO, KB, and IGROV1) were plated in 96 well dishes (~2500-5000 cells/well, total volume of 200 μL medium) with a broad range of antifolate concentrations. The medium was RPMI1640 (contains 2.3 μM folic acid) with 10% dialyzed serum and antibiotics for experiments with R2 and PC43-10 cell lines. For RT16, D4, KB, and IGROV1 cells, they were cultured in folate-free RPMI media with 10% dialyzed fetal bovine serum (Invitrogen) and antibiotics supplemented with 2 nM LCV. The requirement for FR mediated drug uptake in these assays was established by a parallel incubation including 200 nM folic acid.

For R2/hPCFT4 cells, the medium was folate-free RPMI1640 (pH = 7.2) containing 25 nM LCV, supplemented with 10% dialyzed fetal bovine serum (Invitrogen) and antibiotics. Cells were routinely incubated for up to 96 h during which the medium pH decreased to ~6.8-6.9 and metabolically active cells (a measure of cell viability) were assayed with Cell Titer-blue cell viability assay (Promega, Madison, WI), with fluorescence measured (590 nm emission, 560 nm excitation) using a fluorescence plate reader. Raw data were exported from Softmax Pro software to an Excel spreadsheet for analysis and determinations of IC_{50} values, corresponding to the drug concentrations that

result in 50% loss of cell growth.

For some of the *in vitro* growth inhibition studies, the inhibitory effects of the antifolates on *de novo* thymidylate biosynthesis (i.e., TS) and *de novo* purine biosynthesis (GARFTase and AICARFTase) were tested by coincubations with thymidine (10 μM) and adenosine (60 μM), respectively. For *de novo* purine biosynthesis, additional protection experiments used AICA (320 μM) as a way of distinguishing inhibitory effects at GARFTase from those at AICARFTase.

For assays of colony formation in the presence of the drugs, KB cells were harvested and diluted, and 200 cells were plated into 60mmdishes in folate-free RPMI1640 medium supplemented with 2 nM LCV, 10% dialyzed fetal bovine serum, penicillin-streptomycin, and 2 mM L-glutamine in the presence of antifolate drugs. The dishes were incubated with 5% CO_2 at 37 °C for 10-14 days. At the end of the incubations, the dishes were rinsed with Dulbecco's phosphate-buffered saline (DPBS), 5% trichloroacetic acid and borate buffer (10 mM, pH= 8.8), followed by 30 min incubation in 1% methylene blue in the borate buffer. The dishes were rinsed with the borate buffer, and colonies were counted for calculating percent colony-forming efficiency normalized to control.

Compound solution preparation

The compound to be tested was dissolved in DMSO to achieve a final concentration of 1 mM and added so that the DMSO concentration in the media with the

cells did not exceed 0.5%. The culture conditions are standard media, RPMI1640/10% dialyzed fetal bovine serum, penicillin/streptomycin solution and 2mM glutamine. pH was adjusted for the RPMI to 7.4 and cells were grown under 5% CO2 to maintain pH balance. In spite of this, the pH of the media decreases accompanying cell growth to pH 6.8-6.9. The cell culture solution composition has been described in the Cell Lines and Assays of Antitumor Activities section above.

FR Binding Assay

[^{3}H]Folic acid binding was used to assess levels of surface folate receptors (FRs). Briefly, cells (e.g., RT16 or D4; ∼1.6 × 106) were rinsed twice with Dulbecco's phosphate-buffered saline (DPBS) followed by two washes in acidic buffer (10 mM sodium acetate, 150 mM NaCl, pH = 3.5) to remove FR-bound folates. Cells were washed twice with ice-cold HEPES-buffered saline (20 mM HEPES, 140 mM NaCl, 5 mM KCl, 2 mM MgCl2, 5 mM glucose, pH = 7.4; HBS), then incubated in HBS with [^{3}H]folic acid (50 nM, specific activity 0.5 Ci/mmol) in the presence and absence of a range of concentrations of unlabeled folic acid or antifolate for 15 min at 0 °C. The dishes were rinsed 3 times with ice-cold HBS, after which the cells were solubilized with 0.5 N sodium hydroxide and aliquots measured for radioactivity and protein contents. Protein concentrations were measured by Folin phenol reagent. Bound [^{3}H]folic acid concentration was calculated as pmol/mg protein. Relative binding affinities for tested folate/antifolate substrates were calculated as the inverse molar ratios of unlabeled ligands required to inhibit [^{3}H]folic acid binding by 50%. By definition, the relative

binding affinity of folic acid is 1.

Transport Assays

For transport assays, R2/hPCFT4, PC43-10 and R2(VC) CHO cells grown as monolayers were used to seed spinner flasks. For experiments to determine the inhibitions of transport by antifolate substrates, cells were collected and washed with DPBS and resuspended in 2 mL of physiologic Hank's balanced salts solution (HBSS) for PC43-10 cells and in HBS adjusted to pH = 7.2 or 6.8 or 4-morpholinepropanesulfonic acid (MES)-buffered saline (20 mM MES, 140 mM NaCl, 5 mM KCl, 2 mM MgCl2, and 5 mM glucose) adjusted to pH 6.5, 6.0, or 5.5 for R2/hPCFT4 cells. In either case, uptakes of [^{3}H]MTX (0.5 μM) were measured at 37 °C over 2 min in the presence and absence of unlabeled antifolates (10 μM). Uptakes of [^{3}H]MTX were quenched by ice-cold DPBS. Cells were washed with ice-cold DPBS 3 times and solubilized with 0.5 N NaOH. Intracellular radioactivity Levels were expressed as pmol/mg protein, calculated from direct measurements of radioactivity and protein contents of cell homogenates. Protein concentrations were measured by Folin phenol reagent. Percentage of MTX transport inhibition was calculated by comparing level of [^{3}H]MTX uptake in the presence and absence of the inhibitors. Kinetic constants (K_t, V_{max}, and K_is) were calculated from Lineweaver-Burke and Dixon plots, respectively.

In Vitro GARFTase Enzyme Inhibition Assay

Purified recombinant mouse GARFTase enzyme was a gift of Dr. Richard Moran (Virginia Commonwealth University, Richmond, VA). Briefly, enzyme activity was assayed spectrophotometrically at 37 °C using GARFTase (0.75 nM), α,β-GAR (11 μM) and coenzyme 10-formyl-5,8-dideazafolic acid (10 μM) in HEPES buffer (75 mM, pH = 7.5) with or without antifolate inhibitor (10-30 000 nM). The absorbance of the reaction product, 5,8-dideazafolic acid, was monitored at 295 nM by UV over the first minute as a measure of the initial rate of enzyme activity. IC_{50} values were calculated as the concentrations of inhibitors that resulted in a 50% decrease in the initial velocity of the GARFTase reaction.

In Situ GARFT Enzyme Inhibition Assay

Incorporation of [^{14}C]glycine into [^{14}C]FGAR was used as an in situ measure of endogenous GARFTase activity. For these experiments, KB cells were seeded in 4 mL of complete folate acid-free RPMI1640 plus 2 nM LCVin 60 mm dishes at a density of 2 × 106 cells per dish. On the next day, the medium was replaced with 2 mL of fresh complete folate acid-free RPMI1640 plus 2 nM LCV (without supplementing glutamine). Azaserine (4 μM) was added in the presence and absence of the antifolate inhibitors (0.1, 1, 10, 100, or 1000 nM). After 30 min, *L*-glutamine (2 mM) and [^{14}C]glycine (tracer amounts; final specific activity 0.1 mCi/L) were added. Incubations were at 37 °C for 15 h, at which time cells were washed with ice-cold folate-free RPMI1640 plus serum. Cell

pellets were dissolved at 0 °C in 2mL of 5% trichloroacetic acid. Cell debris was removed by centrifugation (the cell protein contents in the pellets were measured) and the supernatants were extracted with 2 mL of ice-cold ether twice. The aqueous layer was passed through a 1 cm column of AG1 × 8 (chloride form), 100-200 mesh (Bio-Rad), washed with 10 mL of 0.5 N formic acid and then 10 mL of 4 N formic acid, and eluted with 8 mL of 1 N HCl. The elutants were collected and measured for radioactivity. The accumulation of radioactive FGAR was calculated as pmol per mg protein over a range of inhibitor concentrations. IC_{50} values were calculated as the concentrations of inhibitors that resulted in a 50% decrease in FGAR synthesis.

Dihydrofolate Reductase (DHFR) Assay[246, 337]

Human DHFR enzyme was kindly provided by Dr. Andre Rosowsky, Dana-Farber Cancer Institute, Harvard Medical School, Boston, MA. All enzymes were assayed spectrophotometrically in a solution containing 80 μM NADPH, 50 μM dihydrofolate, 50 mM Tris-HCl, 0.001 M 2-mercaptoethanol, and 0.001 M EDTA at pH 7.4 at 30 °C.The reaction was initiated by an amount of enzymes yielding a change in optical density at 340 nm of 0.015 units/min.

Thymidylate Synthase (TS) Assay.

Human TS enzyme was kindly provided by Dr. Andre Rosowsky, Dana-Farber Cancer Institute, Harvard Medical School, Boston, MA. TS was assayed spectrophotometrically at pH 7.4 at 30 °C in a mixture containing 0.1 M 2-

mercaptoethanol, 0.0003 M(6*R*,*S*)-tetrahydrofolate, 0.012 M formaldehyde, 0.02 M $MgCl_2$, 0.001 M dUMP, 0.04 M Tris-HCl, and 0.00075 M NaEDTA. This was the assay described by Wahba and coworkers[338] except that the dUMP concentration was increased 25-fold according to the method of Davisson and coworkers.[339] The reaction was initiated with the addition of an amount of enzyme yielding a change in absorbance at 340 nm of 0.016 units/min in the absence of inhibitor.

APPENDIX 2

The molecular modeling and computational studies of the analogs listed in dissertation were performed by Dr. Sudhir Raghavan in Dr. Aleem Gangjee's group with hGARFTase and hAICARFTase.

Molecular Modeling and Computational Studies

The X-ray crystal structures of hGARFTase at 1.98Å resolution (PDB ID: 1NJS)[139] and AICARFTase at 2.55 Å resolution (PDB ID: 1P4R)[175] were obtained from the protein database. The hGARFTase crystal structure contains hGARFTase complexed with the hydrolyzed form of 10-trifluoroacetyl-5,10-dideaza-acyclic-5,6,7,8-tetrahydrofolic acid (10-CF_3CO-DDACTHF) while the AICARFTase crystal structure contains human AICARFTase with the sulfamido-bridged 5,8-dideazafolate analog BW1540.

General docking procedure:

Docking studies were performed using Lead IT 1.3 (BioSolveIT GmbH Sankt Augustin, Germany, 2011). The protonation state of the proteins and the ligands were calculated using the default settings. Water molecules in the active site were permitted to rotate freely. The active site was defined by a sphere of 6.5 Å from the native ligand in the crystal structure. Ligands for docking were prepared using MOE 2010.10 (Chemical Computing Group: Montreal, Quebec, Canada) and energy minimized using the MMF94X forcefield to a constant of 0.05 kcal/mol. Triangle matching was used as the placement method and the docked poses were scored using default settings. The docked poses were exported and visualized in MOE.

Validation of docking software:

Molecules used for the docking experiments were constructed in MOE 2010.11 and minimized using the MMFF94x forcefield to a constant of 0.05 kcal/mol.In order to validate the docking software for docking the proposed compounds, the native ligands, 10-CF_3CO-DDACTHF for hGARFTase and BW1540 for AICARFTase were built using the molecule builder function in MOE, energy minimized and docked as described above. RMSD of the docked poses were calculated using an SVL code obtained from the MOE website (www.chemcomp.com) and compared to the conformation of the crystal structure ligands.

The best docked pose for 10-CF_3CO-DDACTHF in the hGARFTase crystal structure had an RMSD of 1.0368 Å and the best docked pose for BW1540 had an RMSD of 1.0995 Å in the AICARFTase crystal structure. Thus LeadIT 1.3. was validated for our docking purposes in hGARFTase and AICARFTase.

APPENDIX 3

1. SAR of 2-amino-4-oxo-6-substituted-pyrrolo[2,3-*d*]pyrimidines with a phenyl ring in the side chain in whole cell assay as GARFTase inhibitors with selectivity for FRs and/or PCFT over RFC (carbon bridge optimization).[109]

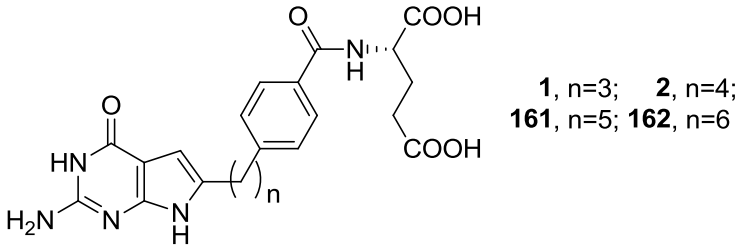

Figure A1 Structures of 2-amino-4-oxo-6-substituted-pyrrolo[2,3-d]pyrimidines.[109]

The series of 6-substituted pyrrolo[2,3-*d*]pyrimidine antifolates with a phenyl ring in the side chain (Figure A1) was screened in the CHO cell sublines by in vitro drug sensitivity assays as measures of their capacities for cellular uptake by RFC versus FRs (Table 1).[109] Only analog **1** showed significant (low level) growth inhibitory activity (IC_{50} = 304 nM) toward RFC-expressing PC43-10 cells; however, the level was nearly identical for R2 cells which do not express RFC or FRs, suggesting the additional involvement of an unidentified non-RFC mechanism of cellular uptake. All the compounds in this series (3- to 6-carbon bridge, respectively) showed potent inhibition against the FR-expressing sublines (RT-16 and D4) with IC_{50}s in the low to moderate nM range. Analogs **1** and **2** with 3- and 4-methylene groups in the bridge, respectively, were the most potent of this series and there were no obvious differences in their activities toward FRα (RT16) versus FRβ (D4) -expressing cells. For both RT-16 and D4 cells, the growth inhibitory effects of all these compounds were completely abolished in the

presence of excess (200 nM) folic acid, indicating the specific utilization of FRs by these analogs.

Table A1 IC_{50}s (nM) for compounds 6-substituted-pyrrolo[2,3-*d*]pyrimidines with a phenyl ring in cell proliferation inhibition of RFC- and FR-expressing cell lines.[109]

Antifolate	hRFC		hFRα		hFRβ		hRFC/ FRα		hRFC/ FRα	
	PC43-10	R2	RT16	RT16 (+FA)	D4	D4 (+FA)	KB	KB (+FA)	IGROV1	IGROV 1 (+FA)
1	304(89)	448(78)	4.1(1.6)	>1000	5.6(1.2)	>1000	1.7(0.4)	>1000	2.2(0.8)	>1000
2	>1000	>1000	6.3(1.6)	>1000	10(2.0)	>1000	1.9(0.7)	>1000	3.6(0.9)	>1000
161	>1000	>1000	54(21)	>1000	80(9)	>1000	13(7.2)	>1000	40(12)	>1000
162	>1000	>1000	162(18)	>1000	198(34)	>1000	23(12)	>1000	309(77)	>1000
Methotrexate	12(1.1)	216(8.7)	114(31)	461(62)	106(11)	211(43)	6.0(0.6)	20(2.4)	21(3.4)	22(2.1)
Pemetrexed	14(2.5)	258(44)	42(9)	388(68)	60(8)	254(78)	68(12)	327(103)	102(25)	200(18)
Raltitrexed	6.3(1.3)	>1000	15(5)	>1000	22(10)	746(138)	5.9(2.2)	22(5)	12.6(3.3)	20(4.3)
Lometrexol	12(2.3)	>1000	12(8)	188(41)	2.6(1.0)	275(101)	1.2(0.6)	31(7)	3.1(0.9)	16(6)
Trimetrexate	25(7.3)	6.7(1.3)	13(1)	4.1(1)	11(4.2)	6.1(1.9)	58(18)	155(38)	12(4)	8.6(1.9)
GW1843U89	11(3.3)	>1000	277(81)	>1000	52(12)	>1000	5.8(3.5)	32(15)	5.2(1.7)	6.9(1.6)

a)For the FR experiments, cytotoxicity assays were performed in the absence and presence of 200 nM folic acid (FA). The data shown are mean values from three experiments (plus/minus SEM in parentheses).b) Compound **1** was synthesized by Dr. Yibin Zeng.

Analogous patterns of drug sensitivity and protection by folic acid were seen with KB and IGROV1 human tumor cells (**Table A1**). In order to assess the effects of increasing levels of extracellular reduced folate on the activity of **2**, KB cells were treated in complete folate-free media including 2-100 nM leucovorin (LCV).

Table A2 IC_{50}s for 6-substituted pyrrolo[2,3-*d*]pyrimidine compounds in *in vitro* (mouse GARFTase) and *in situ* GARFTase inhibition assays.[109]

Antifolate	IC_{50}	
	***In vitro* (μM)**	***In situ* (nM)**
1	2.44 (0.12)	18(2.0)
2	0.15 (0.01)	6.8(0.9)
161	2.26 (0.16)	7.2(1.8)
162	2.51 (0.25)	8.6(0.7)
Pemetrexed	>20	30(7.7)
Lometrexol	0.78 (0.08)	14(5.6)

The IC_{50} data shown are mean values from 3 (*in vitro*; SEM in parentheses) or 2 (*in situ*; range in parentheses) experiments.

The compounds were also evaluated as inhibitors of isolated mouse GARFTase and compared with in situ assay (KB cells) against GARFTase (Table 2). The most potent compound in isolated mouse GARFTase was **2** and compounds **1**, **161** and **162** were equipotent. However this difference in potency is absent in the in situ assays and all of the analogs are almost equipotent nanomolar inhibitors. The equalization and increased inhibition in situ of GARFTase could reflect the result of polyglutamylation in situ that would be absent in the isolated GARFTase assays.

2. SAR of 6-substituted straight chain compounds as folate receptor transport and GARFTase enzyme Inhibition[325]

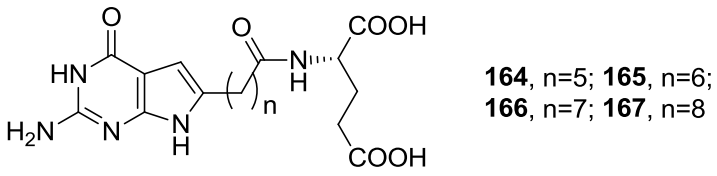

164, n=5; **165**, n=6;
166, n=7; **167**, n=8

Figure A2 Structures of 2-amino-4-oxo-6-substituted straight chain pyrrolo[2,3-d]pyrimidines.[325]

No compound in the new straight chain series showed any growth inhibitory activity toward RFC-expressing PC43-10 cells, which is similar to the lead compound **2** indicating absolute selectivity for FR transport and hence tumor selectivity.

Table A3 IC_{50}s (nM) for compound 164-167 (n=5-8) **in cell proliferation inhibition of RFC-, FR- and PCFT-expressing cell lines.**[325]

Antifolate	hRFC		hFRα	hPCFT	hRFC/ FRα/hPCFT
	PC43-10	R2	RT16	R2/hPCFT4	KB
164 (n=5)	>1000	>1000	>1000	>1000	181.1 (49.9)
165 (n=6)	>1000	>1000	153.7 (79.8)	>1000	6.8 (0.7)
166 (n=7)	>1000	>1000	9.32 (2.69)	>1000	1.3 (0.58)
167 (n=8)	>1000	>1000	12.31 (3.14)	>1000	1.48 (0.04)
Pemetrexed (n=2)	138(13)	894(93)	42(9)	13.2(2.4)	68(12)
Raltitrexed	6.3(1.3)	>1000	15(5)	99.5(11.4)	5.9(2.2)
Methotrexate	12(1.1)	216(8.7)	114(31)	120.5(16.8)	6.0(0.6)
Lometrexol	12(2.3)	>1000	12(8)	38.0(5.3)	1.2(0.6)
GW1843U	11(3.3)	>1000	277(81)	>1000	5.8(3.5)

The data shown are mean values from three experiments (plus/minus SEM in parentheses).

While the analogue with a five-carbon bridge (**164**, n=5) was also inactive toward both FRα-expressing RT-16, compounds **165-167** (six- to eight-carbon bridge, respectively) showed potent inhibition against RT-16 with IC_{50} values in the moderate to low nanomolar range. Analogues **166-167** with 7- and 8-methylene groups in the bridge, respectively, were the most potent of this series, and there were no obvious differences in their activities toward FRα (RT16) expressing cells. For RT-16 cells, the growth inhibitory effects of compounds **165-167** were completely abolished in the presence of excess (200 nM) folic acid, indicating the specific utilization of FRs by these analogues. Analogous patterns of drug sensitivity and protection by folic acid were seen with KB and IGROV1 human tumor cells (**Table** A**2**). Compared with lead compound **2** showed moderate inhibition toward PCFT-expressing cells, it is very interesting to note that there is no growth inhibitory activity toward PCFT-expressing cells for any of the new straight chain series. Thus, the in vitro cytotoxicity results establish that the growth inhibitory effects of compounds **165-167** are dependent on their cellular accumulation via FRs rather than RFC and/or PCFT indicating the FR targeted specificity of these straight chain compounds. Against KB tumor cells in culture, the 7-carbon atom chain analog (**166**) showed an IC_{50} value of 1.3 nM, similar to the most potent phenyl analog **2** (1.9 nM). In the CHO sublines, both **166** and **2** inhibited growth of RT-16 cells (IC_{50} = 9.3 nM and 6.3 nM respectively). The most potent compound **166** (n=7) has been selected for antitumor activity in tumor xenograft models in animals.

The present work is, to our knowledge, the first study on the impact of a modulation (replacement of the aromatic ring by methylene units) on the side chain of classical antifolates for transport specificity to FRs. A novel series of classical 6-substituted

straight chain pyrrolo[2,3-*d*]pyrimidine antifolate **164-167** (n=5-8) were designed and synthesized as **2** analogs with the replacement of the phenyl ring by methylene units. We have identified distinct structure-activity relationship for this series involving the length of the methylene "bridge" region between the pyrrolo[2,3-*d*]pyrimidine and the *L*-glutamate with corresponding FR binding and optimal inhibition of GARFTase. Compounds with 7- and 8-carbon chain lengths, **166** and **167** (n=7-8), proved to be the most potent for the KB tumor cell inhibition (IC_{50}=1.3 nM and IC_{50}=1.48 nM, respectively). Compounds had excellent FR specificity over RFC and PCFT. In conclusion, the aromatic ring in the side chain of the lead **2** was demonstrated not necessary for either FR specificity or potent tumor cell inhibition. It was also concluded that the spatial requirements for the bridge region/phenyl ring region are highly compatible that analogs with a more flexible side chain **164-167** (n=5-8) were equal or more potent to GARFTase and selective to FRs than their rigid analogs. The structure simplicity and extraordinary antitumor activities of these 6-substituted straight chain compounds provide a good starting point for further study including in vivo antitumor activities and the design of additional analogs to optimize cellular folate uptake by FRs and GARFTase inhibition to discover potent antitumor agents with high tumor-targeting capability.

3. SAR of 2-amino-4-oxo-5-substituted-pyrrolo[2,3-*d*]pyrimidines with a phenyl ring in the side chain as GARFTase inhibitors with selectivity for FRs and/or PCFT over RFC.[327]

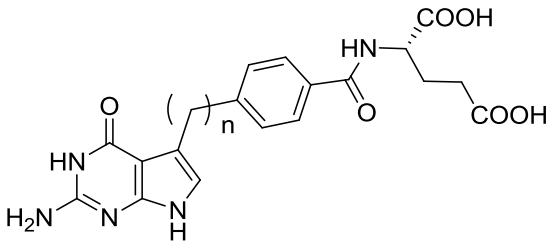

172, n=1; **173**, (PMX), n=2; **174**, n=3;
175, n=4; **176**, n=5; **177**, n=6

Figure A3 Structures of 2-amino-4-oxo-5-substituted pyrrolo[2,3-d]pyrimidines **172-177 (n=1-6).**[327]

Table A4 IC_{50}s (nM) for compound 172-177 (n=1-6) in cell proliferation inhibition of RFC-, FR- and PCFT-expressing cell lines.[327]

Antifolate	hRFC		hFRα	hPCFT	hRFC/ FRα/hPCFT
	PC43-10	R2	RT16	R2/hPCFT4	KB
172 (n=1)	>1000	>1000	N	>1000	N
174 (n=3)	81.6	>1000	54.67	328.5	38.5
175 (n=4)	53.9	>1000	8.2	733	3.6
176 (n=5)	194.6	>1000	33.5	>1000	20.1
177 (n=6)	>1000	>1000	>1000	>1000	N
Pemetrexed (n=2)	138(13)	894(93)	42(9)	13.2(2.4)	68(12)
Raltitrexed	6.3(1.3)	>1000	15(5)	99.5(11.4)	5.9(2.2)
Methotrexate	12(1.1)	216(8.7)	114(31)	120.5(16.8)	6.0(0.6)
Lometrexol	12(2.3)	>1000	12(8)	38.0(5.3)	1.2(0.6)
GW1843U	11(3.3)	>1000	277(81)	>1000	5.8(3.5)

The data shown are mean values from three experiments (plus/minus SEM in parentheses). N = No activity

Compound **174-176**, the 3-5 carbon chain homologs of PMX, could be transported by all three folate uptake systems just like PMX. More importantly, **174-176** have better KB cell inhibition potency than PMX. Compound **175** inhibits KB cells at 3.6 nM, about 20-fold greater than PMX. Thus increasing the side chain length of PMX improves tumor cell inhibitory activity. It is also interesting to note that this series of compounds **172-177** (n=1-6) do not have selectivity for FR or PCFT over RFC as we have reported for their 6-substituted regioisomers.

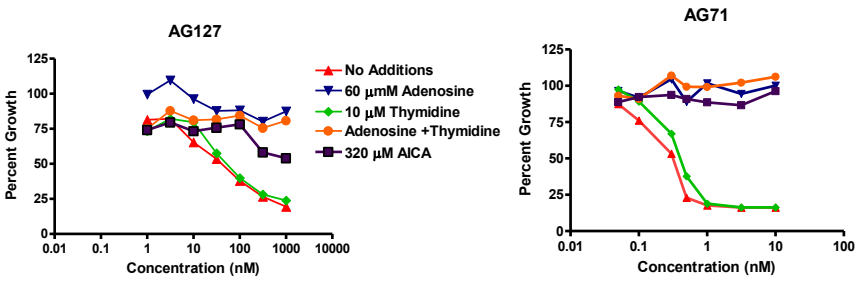

Nucleoside Protection From Growth Inhibition of Novel Antifolates. Cell proliferation inhibition was measured on 96-well plates with 4000 KB cells per well initially and a range of antifolate concentrations (1-1000 nM), in the presence or absence of: adenosine (60 µM), thymidine (10 µM), or AICA (320 µM). Cell densities were measured with CellTiter BlueTM fluorescence dye and a fluorescence plate reader. Results were normalized to cell density in the absence of drug. Results shown are representative data of experiments performed in triplicate.

Figure A4 3 (AG71) and **175** (**AG127**) KB Protections.[327]

The **3** and **175** KB tumor cell nucleoside protection assays were employed to determine the targeted pathway and folate-dependent enzyme (Figure A4). These data show that KB cells treated with **3** are completely protected from the growth inhibitory effects by adenosine but not thymidine, establishing *de novo* as the targeted pathway. 5-Amino-4-imidazolecarboxamide (AICA), a precursor of 5-amino-4-imidazolecarboxamide ribonucleotide (ZMP) is also protective, establishing that

GARFTase is the major intracellular target.[11] Inhibition of KB cell proliferation by **175** was abolished by excess adenosine, but not thymidine or AICA, suggesting that AICARFTase was the principle intracellular target. Collectively, our results show that the side chain two carbon homologated analog of PMX, **175**, exhibits nanomolar inhibition of proliferation of KB tumor cells in culture. The unique and specific AICARFTase inhibition of **175** makes it a promising lead for further preclinical development as an agent for cancer chemotherapy.

It was also determined that **172-177** (n=1-6)**,** like PMX**,** inhibit human TS and DHFR at 1-20 μM range (Table A5). The GARFTase inhibitory effects are currently being evaluated. It is highly probable that **172-177** (n=1-6) have multiple enzyme inhibition including TS, DHFR and GARFTase similar to PMX.

Table A5 hDHFR and hTS inhibitory activity of 172-177 (n=1-6).[327]

Antifolate	**IC_{50} (μM, hDHFR)**	**IC_{50} (μM, hTS)**
MTX	0.022	-
PDDF	-	0.037
PMX(n=2)	2.2	11
172 (n=1)	0.45	7.6
174 (n=3)	3.3	9
175 (n=4)	21	15
176 (n=5)	20	15
177 (n=6)	3	14

The most potent compound **175** (n=4) was further selected by NCI (National Cancer Institute) for evaluation in their preclinical 60 tumor cell line panel. Compound **175** shows excellent growth inhibition (GI_{50} < 100 nM) on 16 different cancer cell lines(**Table A6**).

Table A6 Tumor cell inhibitory activity (NCI) GI_{50} (M) of 175 (n=4).[327]

Panel/ Cell line	GI_{50} (M)	Panel/ Cell line	GI_{50} (M)	Panel/ Cell line	GI_{50} (M)
Leukemia		**Colon Cancer**		**Melanoma**	
CCRF-CEM	6.51×10^{-8}	COLO 205	$>1.00\times10^{-4}$	LOX IMVI	5.58×10^{-5}
HL-60(TB)	-	HCT-116	3.76×10^{-8}	MALME-3M	$>1.00\times10^{-4}$
K-562	$< 1.00\times10^{-8}$	HCT-15	$>1.00\times10^{-4}$	M14	$>1.00\times10^{-4}$
MOLT-4	8.10×10^{-8}	HT29	3.84×10^{-8}	MDA-MB-435	6.98×10^{-8}
SR	5.23×10^{-7}	KM12	8.60×10^{-7}	SK-MEL-2	$>1.00\times10^{-4}$
		SW-620	2.96×10^{-8}	SK-MEL-28	9.27×10^{-5}
Prostate Cancer				SK-MEL-5	$>1.00\times10^{-4}$
PC-3	6.37×10^{-8}	**NSCLC**		UACC-257	$>1.00\times10^{-4}$
DU-145	$>1.00\times10^{-4}$	A549/ATCC	2.19×10^{-7}	UACC-62	$>1.00\times10^{-4}$
		EKVX	3.25×10^{-7}		
CNS Cancer		HOP-62	$>1.00\times10^{-4}$	**Breast Cancer**	
SF-268	8.84×10^{-5}	HOP-92	$>1.00\times10^{-4}$	MCF7	4.24×10^{-8}
SF-295	5.28×10^{-8}	NCI-H226	$>1.00\times10^{-4}$	MDA-MB-231/ATCC	$>1.00\times10^{-4}$
SF-539	$>1.00\times10^{-4}$	NCI-H23	$>1.00\times10^{-4}$	HS 578T	$>1.00\times10^{-4}$
SNB-19	$>1.00\times10^{-4}$	NCI-H322M	$>1.00\times10^{-4}$	BT-549	$>1.00\times10^{-4}$
SNB-75	$>1.00\times10^{-4}$	NCI-H460	6.16×10^{-8}	T-47D	$>1.00\times10^{-4}$
U251	6.15×10^{-8}	NCI-H522	$>1.00\times10^{-4}$	MDA-MB-468	$>1.00\times10^{-4}$
Renal Cancer		**Ovarian cancer**			
786 - 0	1.60×10^{-8}	IGROVI	1.60×10^{-6}		
A498	$>1.00\times10^{-4}$	OVCAR-3	$>1.00\times10^{-4}$		
ACHN	1.78×10^{-6}	OVCAR-4	$>1.00\times10^{-4}$		
CAKI-1	5.75×10^{-8}	OVCAR-5	$>1.00\times10^{-4}$		
RXF 393	$>1.00\times10^{-4}$	OVCAR-8	$>1.00\times10^{-4}$		
SN12C	7.87×10^{-7}	NCI/ADR-RES	$>1.00\times10^{-4}$		
TK10	$>1.00\times10^{-4}$	SK-OV-3	9.00×10^{-5}		
UO-31	3.60×10^{-7}				

4. SAR of 2-amino-4-oxo-5-substituted-pyrrolo[2,3-*d*]pyrimidines with a thiophenyl ring in the side chain as GARFTase inhibitors with selectivity for FRs and/or PCFT over RFC.[340]

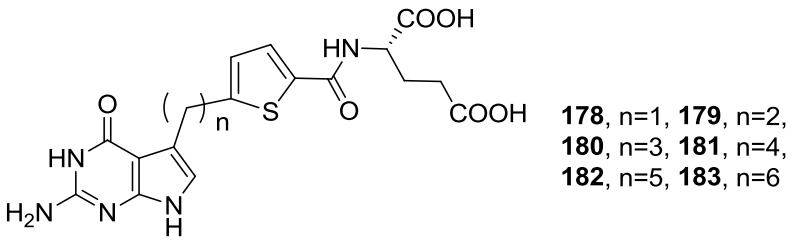

178, n=1, **179**, n=2,
180, n=3, **181**, n=4,
182, n=5, **183**, n=6

Figure A5 Structures of 2-amino-4-oxo-5-substituted pyrrolo[2,3-d]pyrimidines **178-183 (n=1-6)**.[340]

Table A7 IC_{50}s (nM) for compound 178-183 in cell proliferation inhibition of RFC-, FR- and PCFT-expressing cell lines.[340]

Antifolate	hRFC		hFRα	hPCFT	hRFC/ FRα/hPCFT
	PC43-10	R2	RT16	R2/hPCFT4	KB
178 (n=1)	>1000	>1000	>1000	552	N
179 (n=2)	43.1	>1000	500	86.7	500
180 (n=3)	110	>1000	109	396	215
181 (n=4)	26.15	>1000	25	103	17.1
182 (n=5)	220	>1000	46	362	32.4
183 (n=6)	>1000	>1000	>1000	>1000	>1000
3 (n=4)	>1000	>1000	2	43.4	0.25
Pemetrexed (n=2)	138(13)	894(93)	42(9)	13.2(2.4)	68(12)
Raltitrexed	6.3(1.3)	>1000	15(5)	99.5(11.4)	5.9(2.2)

Methotrexate	12(1.1)	216(8.7)	114(31)	120.5(16.8)	6.0(0.6)
Lometrexol	12(2.3)	>1000	12(8)	38.0(5.3)	1.2(0.6)
GW1843U	11(3.3)	>1000	277(81)	>1000	5.8(3.5)

The data shown are mean values from three experiments (plus/minus SEM in parentheses). N = No activity

Analogs with 4 and 5-carbon atom chains (**181** and **182**) showed IC_{50} values of 17.9 nM and 16.4 nM, respectively, against KB tumor cells in culture; other analogs of this series were 13- to >58-fold less active. Drug effects were completely abolished by excess folic acid establishing FR-mediated uptake. In the CHO sublines, **181** and **182** were growth inhibitory in the order RT-16 = PC43-10 > R2/PCFT4 and RT-16 >> PC43-10 = R2/PCFT4, respectively. Thus, at least for **181** unlike **3**, significant RFC activity is preserved. Whereas PMX is a multi-targeted agent with inhibitory effects on both *de novo* thymidylate and purine nucleotide biosynthetic pathways, the anti-proliferative effects of **181** and **182** were abolished by adenosine but not thymidine, establishing exclusive inhibition of purine biosynthesis. Our results suggest that 6-subtitution of the pyrrolo[2,3-*d*]pyrimidine scaffold is more effective in conferring selective transport of FRα over RFC, although inhibition of *de novo* purine biosynthesis is preserved in the 5-substituted compounds.

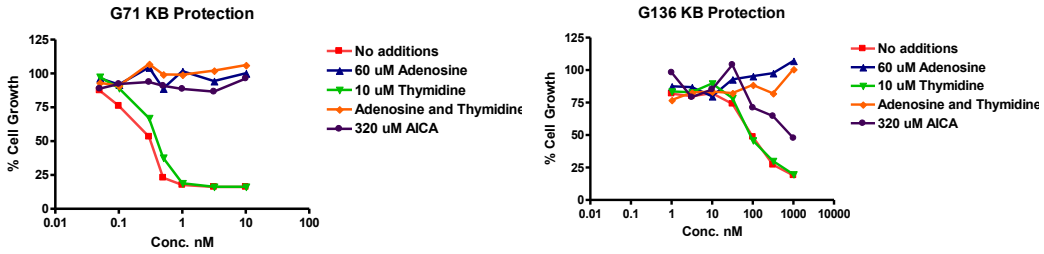

Figure A6 3 (**G71**) and **181** (**G136**) KB Protections.[340]

These data (Figure A6) show that KB cells treated with **3** are completely protected from the growth inhibitory effects by adenosine but not thymidine. Aminoimidazolecarboxamide a precursor of aminoimidazolecarboxamide ribonucleotide is also protective, establishing that GARFTase is the major intracellular target. These results were previously reported.[113]

For **181**, adenosine was again protective whereas thymidine is not. AICA is protective at G136 concentrations up to 32 uM but not at higher concentrations suggesting an alternate enzyme target, likely 5-amino-4-imidazolecarboxamide ribonucleotide formyltransferase (AICARFTase).

Table A8 hDHFR and hTS inhibitory activity of 178-183.[340]

Antifolate	IC_{50} (μM, hDHFR)	IC_{50} (μM, hTS)
MTX	0.022	-
PDDF	-	0.037
PMX(n=2)	2.2	11
178 (n=1)	11	0.36
179 (n=2)	23	3.8
180 (n=3)	11	2.7
181 (n=4)	19	16
182 (n=5)	22	1.9
183 (n=6)	18	2.6

It was also determined that **178-183**, like PMX**,** inhibit human TS and DHFR at 1-23 μM range (**Table A8**). The GARFTase inhibitory effects are currently being evaluated. It is highly probable that **178-183** have multiple enzyme inhibition including TS, DHFR and GARFTase similar to PMX.

Table A9 Tumor cell inhibitory activity (NCI) GI_{50} (M) of 181 (n=4).[340]

Panel/ Cell line	GI_{50} (M)	Panel/Cell line	GI_{50} (M)	Panel/ Cell line	GI_{50} (M)
Leukemia		**Colon Cancer**		**Melanoma**	
CCRF-CEM	**8.96×10^{-8}**	COLO 205	7.20×10^{-5}	LOX IMVI	**1.50×10^{-8}**
HL-60(TB)	-	HCT-116	**< 1.00×10^{-8}**	MALME-3M	$>1.00\times10^{-4}$
K-562	**< 1.00×10^{-8}**	HCT-15	$>1.00\times10^{-4}$	M14	$>1.00\times10^{-4}$
MOLT-4	1.22×10^{-7}	HT29	**3.10×10^{-8}**	MDA-MB-435	**7.09×10^{-8}**
SR	2.86×10^{-7}	KM12	5.10×10^{-5}	SK-MEL-2	$>1.00\times10^{-4}$
		SW-620	**1.91×10^{-8}**	SK-MEL-28	$>1.00\times10^{-4}$
Prostate Cancer				SK-MEL-5	$>1.00\times10^{-4}$
PC-3	1.88×10^{-7}	**NSCLC**		UACC-257	$>1.00\times10^{-4}$
DU-145	$>1.00\times10^{-4}$	A549/ATCC	1.38×10^{-7}	UACC-62	$>1.00\times10^{-4}$
		EKVX	2.14×10^{-7}		
CNS Cancer		HOP-62	$>1.00\times10^{-4}$	**Breast Cancer**	
SF-268	$>1.00\times10^{-4}$	HOP-92	$>1.00\times10^{-4}$	MCF7	**5.87×10^{-8}**
SF-295	**2.56×10^{-8}**	NCI-H226	-	MDA-MB-231/ATCC	$>1.00\times10^{-4}$
SF-539	$>1.00\times10^{-4}$	NCI-H23	$>1.00\times10^{-4}$	HS 578T	$>1.00\times10^{-4}$
SNB-19	$>1.00\times10^{-4}$	NCI-H322M	$>1.00\times10^{-4}$	BT-549	$>1.00\times10^{-4}$
SNB-75	$>1.00\times10^{-4}$	NCI-H460	**8.82×10^{-8}**	T-47D	$>1.00\times10^{-4}$
U251	**4.02×10^{-8}**	NCI-H522	$>1.00\times10^{-4}$	MDA-MB-468	$>1.00\times10^{-4}$
Renal Cancer		**Ovarian cancer**			
786 - 0	**2.56×10^{-8}**	IGROVI	$>1.00\times10^{-4}$		
A498	$>1.00\times10^{-4}$	OVCAR-3	$>1.00\times10^{-4}$		
ACHN	-	OVCAR-4	$>1.00\times10^{-4}$		
CAKI-1	**2.09×10^{-8}**	OVCAR-5	$>1.00\times10^{-4}$		
RXF 393	$>1.00\times10^{-4}$	OVCAR-8	$>1.00\times10^{-4}$		
SN12C	-	NCI/ADR-RES	$>1.00\times10^{-4}$		
TK10	$>1.00\times10^{-4}$	SK-OV-3	$>1.00\times10^{-4}$		
UO-31	-				

One of the most potent compounds against KB tumor cells in culture, **181** (n=4), was further selected by NCI (National Cancer Institute) for evaluation in their preclinical 60 tumor cell line panel. Compound **181** shows excellent growth inhibition against 12 different cancer cell lines (**Table A9**). It is important to note that **181** was not a general tumor poison but showed GI_{50} values in a range of 10,000-fold demonstrating selectivity for certain tumor types.

APPENDIX 4

GARFTase inhibitors **2**, **161**, **166** and **194** had showed potent antitumor activity in the nanomolar range against KB and IGROV1 tumor cells. For further evaluation in animal models, gram quantities of these analogs were synthesized using the same synthetic procedures as described in the experimental section.

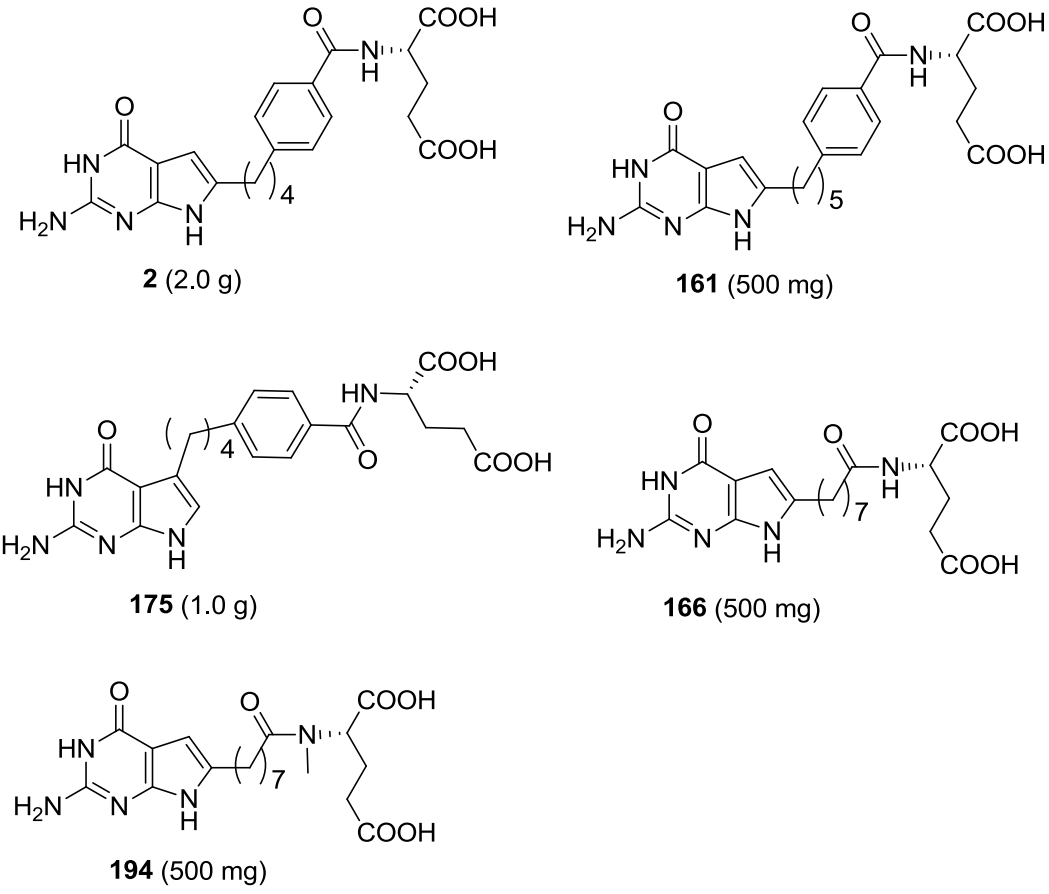

Figure A7 Bulk synthesis for animal study.

AICARFTase inhibitors **175** had showed potent antitumor activity in the nanomolar range against KB and IGROV1 tumor cells. For further evaluation of this analog in animal models, gram quantities were synthesized.

APPENDIX 5

The physico-chemical properties of the market drug, pemetrexed (PMX) and the most potent compound **2**, **161**, **166**, **175** and **194** were predicted by calculating the tPSA and ClogP values with ChemBioDraw Ultra 12.0.2.

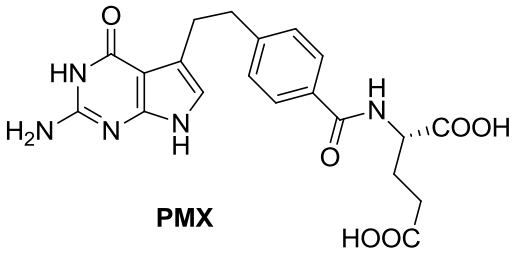

PMX

Log P: 0.25
tPSA: 183.21
CLogP: -0.217401

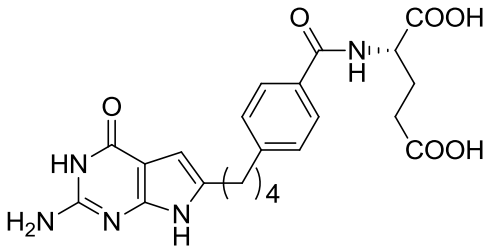

2

Log P: 1
tPSA: 183.21
CLogP: 0.840599

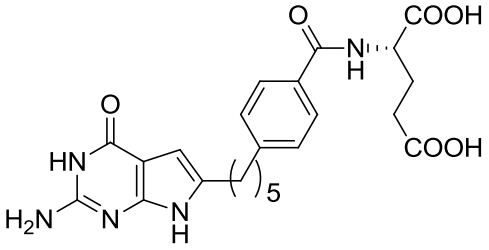

161

Log P: 1.42
tPSA: 183.21
CLogP: 1.3696

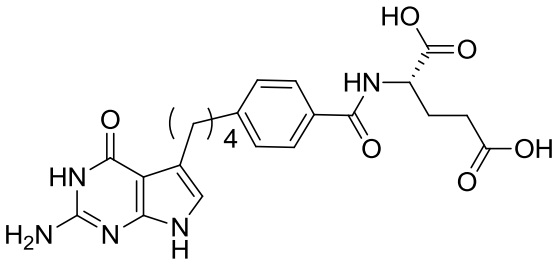

175

Log P: 1.08
tPSA: 183.21
CLogP: 0.840599

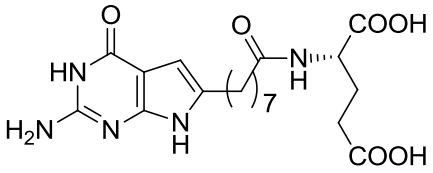

166

Log P: 0.11
tPSA: 183.21
CLogP: 0.3676

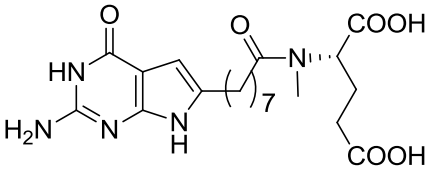

194

Log P: 0.34
tPSA: 174.42
CLogP: 0.845199

Figure A8 Calculated tPSA and ClogP values of PMX and selected compounds by ChemBioDraw Ultra 12.0.2..